HIGH-RATE CENTRELESS GRINDING OF FERROUS COMPONENTS

By

William Francis Bell. B.Sc.

A thesis submitted as partial requirements for the degree of Doctor of Philosophy (C.N.A.A.) following work carried out in the Department of Mechanical, Marine and Production Engineering, Liverpool Polytechnic. The work was conducted in collaboration with Associated Engineering Ltd., Leamington Spa, Warwickshire.

October, 1983.

RELEVANT PUBLICATIONS NOT SCANNED ON INSTRUCTION FROM THE UNIVERSITY

W.F. Bell

High-Rate Centreless Grinding of Ferrous Components

Synopsis

A prototype centreless grinding machine was modified extensively to operate satisfactorily at high grinding wheel speeds and in the high rate centreless grinding regime. The principal modifications included the provision of a 75 k.W. d.c., variable speed, main drive motor which enables grinding wheel speeds upto 120 m/s to be employed and a coolant supply manifold was designed and manufactured.which was capable of delivering a high velocity coolant stream to the grinding zone. In addition, a measurement system was developed which allowed the grinding forces to be monitored and recorded in process.

Two solutions for the accepted kinematic model of plunge feed cylindrical grinding are proposed. The general and more accurate solution takes account of the variable grit height and separation of the grinding wheel, whilst the particular and approximate analytical solution makes provision for variable grit separation only. The particular solution enabled parametric studies to be undertaken and allowed comparisons with the solutions proposed by other workers.

The trends of theoretical grinding forces were predicted from analysis of the undeformed chip dimensions. The trends indicated two methods of achieving high stock removal rates, firstly, for a constant force value, higher stock removal rates are possible by increasing the grinding wheel speed and infeed-rate. Secondly, at a constant grinding wheel speed, and force level, reducing the workpiece speed and increasing the infeed-rate will yield higher stock removal rates. Experimental results were in agreement with these predictions.

An extensive experimental programme investigating plunge feed centreless grinding of ferrous components was undertaken. Results from approximately 300 grinding experiments were used to establish a data bank of grinding parameters for a range of grinding conditions.

High-rate centreless grinding has been shown to be a feasible first machining process. It has also been shown that the choice of kinematic conditions is important in achieving high stock removal rate grinding. Incorrect choice of kinematic conditions can cause problems of workpiece burn, grinding vibrations and excessive power demands. Limit charts have been constructed which outline the boundaries to the process in terms of burn, grinding vibration and power limit. Operation between the boundaries is best achieved if the ratio of grinding wheel to workpiece speeds is in the range 90 - 200.

The results enable a data based control strategy to be formulated and it is proposed that in process variable kinematics will allow a single cycle roughing and finishing operation on a suitably adapted centreless grinding machine.

Acknowledgements

The author is deeply indebted to both his research supervisors, Professor W.B. Rowe and Dr. D. Brough who have been constant sources of guidance and encouragement. Their assistance was invaluable in the preparation of the thesis and development of the analytical aspects of the work.

Many thanks are extended to the Directors of R & H Injection Mould Tools who allowed much of the transmission system and coolant manifolds to be manufactured on their premises. I am particularly grateful to my father, W.W. Bell, who was responsible for the manufacture of these items.

Thanks are also extended to Mr. M. Jackson (Research Technician) who assisted with the preparation of materials and the experimental programme. In addition, the author is grateful for the technical assistance and manufacturing facilities provided by the Department of Mechanical, Marine and Production Engineering, Liverpool Polytechnic.

The author is indebted to the Science and Engineering Research Council which provided the funding which enabled the work to be conducted.

Finally, to my wife Rosie, for her support and understanding during the writing up period.

The Author

William Francis Bell, commenced his engineering career at the age of sixteen as an apprentice with T.W. Forms Limited, Maghull. After two years part-time study at Bootle College of Further Education, he gained an Ordinary National Certificate in Mechanical Engineering.

After a further four years study at Liverpool Polytechnic, the author was awarded, by the Council for National Academic Awards, the degree of Bachelor of Science in Mechanical Engineering. During this period of study, industrial training was undertaken with the Ocean Transport and Trading Company and the United Kingdom Atomic Energy Authority.

In 1977, he was appointed a Research Assistant in the Department of Mechanical, Marine and Production Engineering, Liverpool Polytechnic, and now holds the position of Research Fellow.

He was elected a Graduate of the Institution of Mechanical Engineers in 1978, and a Graduate of the Institution of Production Engineers in 1982.

List of Publications

1) Brough, D., W.B. Rowe, W. Weston, and W.F. Bell, "Diaphragm Compensated Hydrostatic Bearings for Achieving and Monitoring High-Speed Centreless Grinding", 2nd. Joint Polytechnic Symposium on Manufacturing Engineering, Lanchester Polytechnic, 1978.

2) Brough, D., W.F. Bell, and W.B. Rowe, "Achieving and Monitoring High-Rate Centreless Grinding", 21st. M.T.D.R. Conf., Swansea University, 1980.

3) Bell, W.F., D. Brough, and W.B. Rowe, "Calculation of Undeformed Chip Parameters for High Grinding Rates", 3rd. Joint Polytechnic Symposium on Manufacturing Engineering, Wolverhampton Polytechnic, 1982.

4) Vukasojevic, R.S., D. Brough, and W.F. Bell, "New Parameters for Specifying the Cutting Quality of Grinding Wheels", 3rd. Joint Polytechnic Symposium on Manufacturing Engineering, Wolverhampton Polytechnic, 1982.

5) Bell, W.F., "Practical Achievement of High-Rate Centreless Grinding", B.A. Williams Award Winning Paper, Institution of Production Engineers, Merseyside and North Wales Section, 1982.

6) Brough, D., W.F. Bell, and W.B. Rowe, "Re-examination of the Uncut Chip Model of Grinding and its Practical Implications", 24th. M.T.D.R. Conf., U.M.I.S.T., 1983.

7) Bell, W.F., D. Brough, and W.B. Rowe, "High-Rate Centreless Grinding of Ferrous Components", 24th. M.T.D.R. Conf., U.M.I.S.T., 1983.

Additional Studies Undertaken

The author attended final year lecture courses for Manufacturing Systems Technology, Manufacturing Processes, and Instrumentation and Control.

In addition, computer courses covering programming, and hardware interfacing were attended. Regular attendance at conferences and seminars has also been part of the additional studies undertaken.

Contents

List of Appendices

List of Figures

List of Plates

List of Tables

Nomenclature

Symbol	Units	Definition
ad	mm	Dressing depth of cut
A_j	mm	U.v. oscillograph trace amplitude
b	mm	Grinding wheel face width
d	mm/rev	Depth of cut per revolution of the workpiece (π .Dw.vi/vw)
Dc	mm	Control wheel diameter
De	mm	Equivalent diameter (Dw.Dg/(Dw+Dg))
Dg	mm	Grinding wheel diameter
Dw	mm	Workpiece diameter
F'_g	N/mm	Specific resulting grinding force
F_i	N	Bearing reaction to grinding force
F'_n	N/mm	Specific normal grinding force
F'_t	N/mm	Specific tangential grinding force
G	-	Grinding ratio ($G = V'/G'_w$)
G'_w	mm^3/mm	Specific volume of grinding wheel removed
h'	mm	Height variation between workpiece and wheel centres
heq	μm	Equivalent chip thickness (Z'/vg)
$\Delta I'$	amps	Specific grinding current
Imax	amps	Maximum current sipplied whilst grinding
Inl	amps	Motor idling current
K_i	N/mm	Scale factor
$\overline{K}$	N/mm	Average scale factor
$\overline{lc}$	mm	Undeformed chip length
ld	mm	Dynamic grit spacing
lg	mm	Static grit spacing
mp	kg	Calibrating mass
mq	kg	Calibrating mass
mu	kg	Mass equivalent
Ng	r/sec	Rotational speed of the grinding wheel

Symbol	Units	Definition
Nw	r/sec	Rotational speed of the workpiece
P'	W/mm	Specific power to grind (F'_t x vg)
P'_s	W/mm	Specific electrical power supplied
q-ratio	-	Ratio of vg to vw
r	mm	Radius on wheel flange where calibration mass is placed
Ra	µm	Centre line average surface roughness
Rz	µm	Peak to valley height average
R_i	mm	Deflection of u.v. oscillograph traces at maximum point
Sd	mm/rev	Dressing lead
$\overline{tc}$	µm	Average undeformed chip thickness
$\overline{tf}$	µsec	Average chip formation time
U	J/mm^3	Specific energy to grind (P'/Z')
vc	m/s	Control wheel speed
vg	m/s	Grinding wheel speed
vi	mm/s	Infeed-rate
vw	m/s	Workpiece speed
V	volts	Motor supply voltage
V'	mm^3/mm	Specific volume of metal removed
Z'	$mm^3/mm/s$	Specific maximum metal removal rate ($Z' = \pi . Dw . vi$)
β	rad	Angle of rotation of workpiece between contact with two acitive grits
θ	degrees	The angular position of the mass equivalent from position a towards b
λ	$mm^3/N/s$	Workpiece removal parameter (Z'/F'_n)
	rad/s	Angular velocity
φ_k , φ_n	degrees	Contact angles between wheel and workpiece
α	mm^2/s	Thermal diffusivity
c1	mm^{-3}	Number of cutting edges per unit volume of the wheel
c11	mm^{-3}	Total number of cutting edges at one mm depth under surface

Symbol	Units	Definition
cp	mm^{-2}	Number of cutting edges per unit wheel surface
D	-	+1 for external grinding
A	-	$1/(1 + vw/vg)^2$
B	-	$1 - D.vw/vg.rg/vw.(2 + vw/vg)$
γ_{eq}	-	$b.g.\cos(D/A.B.(rw + D.a)/rg.(-1 + D\ 1 + x))$
x	-	$(A.B)^2.(rw + D.a)^2/rg.2.D.rw/rg.A.B$
g	-	Exponent relating grinding ratio to equivalent grinding thickness
k	$J/m.s.^{\circ}C$	Heat conductivity
n	mm^{-1}	Number of cutting particles per unit length of wheel circumference

1.0 INTRODUCTION

1.0 INTRODUCTION

1.1 Brief History of Centreless Grinding

Although man has been grinding basic tools since the Neolithic period, the grinding of tools (stone initially and later metals) remained a sharpening and polishing process until the latter part of the eighteenth century [1] .

The process of grinding machine development was a product of the demands initiated by the industrial revolution which required the manufacture of high precision components for the new technology. The origins of the first form of centreless grinding machine (single wheel) can be dated to about 1820, in the shape of Wilkinson's spindle grinder. Other forms of centreless grinding machines were Schleicher's self-feeding needle grinding machine of 1853, and Poole's roll grinder of 1870 [1] . It was not until 1915 that the centreless grinding machine appeared in its present form. This was due to the invention of the control wheel and workplate by Heim [1] .

In the early 1920's, it became apparent that it was possible to achieve high production rates and obtain high precision from centreless grinding machines. It was found also, that the process was particularly well suited to the mass production of automobile components where continued operation could be obtained with minimal requirements of operator intervention. From the 1920's very few changes have been made to the basic machine form. Various refinements have enabled screw-thread grinding and other forms of specialist grinding to be achieved. In latter years there has been a trend towards the use of higher grinding wheel speeds, particularly by European Companies e.g. Lidkoping, and Ghiringhelli. Attempts to optimise machining processes have led to the

development of adaptive control systems and no doubt centreless grinding will be the focus of attention for such a system in the near future.

1.2 The Centreless Grinding Process

The basic geometry is illustrated in Figure 1. The component is supported on a workplate situated between the control wheel and the grinding wheel. Stock removal is achieved by advancing one or more of the machine elements. A common arrangement is for the control wheel (and sometimes the workplate too) to advance towards the grinding wheel.

The relative directions of rotation of the component and machine rotational elements are also indicated in Figure 1. These directions of rotation were adopted by the author throughout the experimental investigations. With the directions of rotation indicated, the resulting grinding force pushes the workpiece downwards onto the workplate and against the control wheel. Rowe [2] has shown that for normal grinding, the component has a surface speed equal (within 5 %) to that of the control wheel.

Throughout the experimental programme, plunge feeding of the workpiece was adopted. The workpiece was held against an end stop by an axial force created by the control wheel speed and tilt. A control wheel tilt of $\frac{1}{2}^{o}$ was employed [3] . Through-feeding of the workpiece was not attempted, although it is accepted that this form of workpiece feeding is also important as an aspect of centreless grinding.

1.3 Process Suitability for High-Rate Grinding

The grinding process evolved as a second operation, finishing process. However, in recent years, there has been an interest in developing the grinding process towards a first-operation machining role [4,5,6] .

An anticipated trend toward heavy duty grinding is based on considerations of optimal utilisation of materials and cost-effective production of components. Rough-and-finish grinding could in some cases replace first-operation processes such as turning. Increased use of precision castings and pre-formed components would accelerate this trend.

The centreless grinding process readily lends itself toward the high-rate grinding concept. It is known that the support afforded by the workplate and control wheel enables heavier cuts to be taken, without giving rise to serious workpiece inaccuracy, than would be possible with a component held between centres. The component loading time in centreless grinding is very low (seconds) compared to other machining processes and loading can be automated. In addition the process is suitable for use with semi-skilled labour.

1.4 Choice of Materials for Investigation

The centreless grinding process is capable of grinding a wide range of materials. Currently little is known about which materials are best suited to high-rate grinding. En 9 steel is a common material and has been adopted by the Science and Engineering Research Council in a co-ordinated grinding research programme as a standard for comparison between the various researchers. Hence, this became one of the materials to be investigated. The choice of other materials arose as follows:-

In the project conducted by Brough [7] a request was received from industry to examine the feasibility of grinding (with high-stock removal rates) cast iron cylinder liners. A series of preliminary grinding trials were conducted and he concluded that a full scale investigation would yield valuable grinding performance data. However, problems within the Company concerned prevented the continuing supply of the requested

materials. The encouraging results obtained with the cast iron [7] prompted a Polytechnic based investigation to examine high-rate centreless grinding of solid grey cast iron bars (readily available) and to compare the results obtained with those of En 9 steel bar. The specifications of both materials are contained in Appendix 1.

A further request to produce plain cylindrical bar from rough sintered iron powder compacts was received. Again preliminary grinding trials showed that high grinding rates were possible, hence, this material was included in the investigative programme. However, the supply of sintered iron powder compact components was insufficient for the investigation to be as comprehensive as that for cast iron and steel.

1.5 Need for the Research

Grinding is not generally regarded as a stock removal process competitive with the conventional first machining processes such as milling and turning. Research at several establishments has been undertaken recently to determine the performance characteristics of particular grinding processes in a first machining role [8, 9, 10] . This research has been concentrated mainly on surface grinding and cylindrical grinding, and to a lesser extent on centreless grinding. Nevertheless, it is considered by the author for reasons discussed in section 1.3, that the centreless grinding process has the greatest potential for achieving high productivity.

It was decided therefore, to examine the feasibility of centreless grinding as a first machining process, and to compare its production capabilities with other forms of cylindrical grinding which have been investigated more extensively.

1.6 Objectives of the Project

i) To make the necessary machine modifications and adjustments to an existing research machine available in the laboratory in order to achieve reasonably controlled grinding conditions and thus reduce experimental scatter, improve repeatability of results from grinding trials, and extend the machine's performance capabilities.

ii) To investigate the high-rate grinding performance of a range of ferrous materials (cast iron, sintered iron compacts, and En 9 steel) in terms of grinding forces, specific energy, surface roughness, maximum metal removal rate and workpiece removal parameter, for a range of kinematic conditions.

iii) To analyse the kinematic relationships of the process from an idealised undeformed chip model and attempt to correlate theoretical parameters with experimental parameters.

iv) To establish the conditions which limit the metal removal rate in centreless grinding.

v) To compare the results obtained from centreless grinding with those from centretype grinding.

vi) To discuss the implications of the results for optimisation of the centreless grinding process and application to improvement of industrial operations.

1.7 Scope of the Project

The scope of the project can be divided into two broad parts. Part 1 (section 2.0) indicates the refinements made to the modified grinding machine to extend its performance capabilities - which also enabled consistent and repeatable results to be obtained. Some experiments were conducted to establish the effect the improvements had on the

performance of the machine.

Part 2 (sections 3.0, 4.0, and 5.0) describes an experimental programme to investigate the effect of the principal variables on grinding performance when grinding En 9 steel, cast iron, and sintered iron powder compacts. In addition an experimental programme is described which outlines the grinding conditions which limit the metal removal rate. An analysis of an idealised undeformed chip model is presented and the theoretical parameters are correlated with experimental parameters.

2.0 MACHINE DEVELOPMENT

2.0 MACHINE DEVELOPMENT

2.1 Critical Features of the Existing Machine

The centreless grinding machine was purchased as a prototype general purpose production machine tool manufactured by Wickman-Scrivener Limited, and designated a model 2K. The principal features of the machine, as purchased, and the projected characteristics of the modified machine are listed in Figure 2. The main departure from most conventional machine tool designs was the use of oil hydrostatic bearings for the grinding wheel and control wheel spindles rather than rolling element or hydrodynamic bearings.

Several modifications had been conceived and implemented prior to the author's involvement with the project; these were at various levels of completion, and are discussed briefly below.

The 15 kW a.c. fixed speed grinding wheel drive motor supplied with the machine had been replaced with a variable speed 75 kW d.c. motor. A KTK Thyristor Control Unit provided steplessly variable motor speeds within the range 0 - 2225 r.p.m.

The oil hydrostatic system had previously been uprated to withstand oil pressures upto 7 MPa. In addition to the replacement of existing flexible piping with heavy duty flexible hose, an accumulator and pressure switch had been included in the hydraulic circuit to protect the bearings against accidental shutdown of the power pack.

Grinding forces were monitored by utilising three differential pressure transducers, each connected across a pair of diametrically opposed recesses. Output signals from the transducers were fed via a carrier frequency amplifier to an u.v. oscillograph to give an output in the form

of a series of traces.

Additional grinding wheel-head guarding had been designed, manufactured and placed in position, such that it shrouded the previously existing guard. The additional guard was constructed of 25 mm thick steel plate and was designed in compliance with the recommendations of the D.S.A. document 00615. The guard design allowed for physical movement (lift and rotation) as a further energy dissipation possibility.

A powerful air extraction system had been installed above the machine tool to remove any vapours created whilst grinding.

2.2 Some Limitations of the Existing Machine

Although the existing machine had been developed previously by other workers so that it was capable of high-rate grinding (<10 cu.mm/mm/s) [11] , it was found that the following elements of the system created restrictions on the machining and monitoring capabilities:-

i) The Hydraulic System

Grinding problems occured when the temperature of the hydraulic oil in the oil reservoir exceeded 38° C. The calibration curve for the force measuring system and stability whilst grinding were both dependent on the temperature of the hydraulic oil. Attempts to grind with the oil temperature above 38° C almost always resulted in chatter marks being produced on the components. A further problem with the hydraulic system was that air tended to accumulate in the differential pressure transducer supply lines. This caused inconsistency in the force measurements.

ii) The Coolant System

The coolant system provided with the machine tool was a light duty type

(0 - 34 litres/min); filtration was by settlement and the tank capacity was 220 litres. Coolant application to the grinding zone was by the flood technique. The coolant pump by-pass line (in-built) prevented the possibility of throttling the coolant. With a grinding wheel peripheral speed of 60 m/s, deflection of the full flood coolant stream by the grinding wheel air belt was apparent.

Dimensional variations in component size were attributed not only to grinding wheel wear but also (to a more limited extent) to the rise in the coolant temperature. The relatively low capacity tank could not dissipate the heat extracted from the grinding zone and temperatures varied by upto 20° C above ambient. The filtration facilities were considered unsatisfactory for a heavy stock removal application [12] ; undoubtedly there would be some recirculation of foreign matter to the grinding zone.

iii) The Main Drive System

The main motor/drive conversion had been constrained by the physical features of the machine which dictated the degree of access and installation space available. Calculations based on data from a power transmission design book [13] , suggested that of the available 75 kW of power, the new transmission system could transmit only 45 kW. The constraints imposed by the machine and the further constraint of cost prevented the transmission system being modified at this time. Unbalance within the transmission system was detected by the force monitoring system. This effect was minimised as far as possible by adjustment and machining of the elements responsible for unbalance.

2.3 Literature Survey of Mechanical Requirements

Before any modifications to the machine were attempted a review of

coolant supply techniques, design of grinding wheels for use at high speeds, dressing techniques and the design of wheel guards was made. This is presented below:-

2.3.1 Coolant Function and Supply

i) Coolant Function

The primary function of a cutting fluid is to improve the efficiency of a metal-cutting operation [14]. This may be measured in terms of the fraction by which grinding forces are reduced. The secondary functions of the cutting fluid are to cool the workpiece, remove the swarf, and protect the workpiece from corrosion [14].

ii) Coolant Application at High Wheel-Speeds

It has been found [15] that a rotating boundary layer of air exists at the periphery of a revolving grinding wheel. The extent of the boundary layer increases with an increase in grinding wheel speed. Coolant applied at low velocity cannot penetrate the air layer and consequently the primary role of the coolant is defeated [14]; conventional flood cooling techniques are therefore ineffective at high grinding wheel speeds. The coolant supply techniques which have the potential to overcome the air layer effects are:- a) Mist Cooling [16], b) Treated wheels [17], c) Nozzle and scraper plate coolant applicator [18], d) The shoe coolant applicator [19], and e) Through-wheel coolant supply [20].

Investigation of Mist Cooling [16] has shown that it offers some benefits. Mist cooling involves the spraying of a metered jet of coolant into the work area by compressed air. Cooling is effected by evaporation and air expansion. Penetration of the air layer is possible with this cooling

technique and a completely unobstructed view of the grinding zone is provided.

Impregnated wheels [17] [21] are attractive for use at higher wheel speeds because the air layer has no effect. Colloidal graphite, and fat with additives of molybdenum disulphide, sulphur, chlorine and lead sulphide are claimed to be effective solid lubricants. But paraffin, carnauba wax and P.T.F.E. are said to be unsatisfactory. P.T.F.E. severely loads the wheel, whilst paraffin and carnauba wax reduce the removal rate by 3-5% compared with a non-treated wheel. To maintain component dimensional stability a conventional coolant supply may also be necessary to ensure adequate heat convection and swarf clearance.

The hydrodynamic shoe applicator [19, 22, 23] design for high wheel speed coolant application involves pumping coolant into the grinding wheel by hydrodynamic action. The shoe is placed at a calculated distance from the grinding zone. The grinding wheel then delivers the coolant to the cutting zone by boundary layer action, the coolant delivery rate being controlled to suit the wheel speed. The grinding wheel is flushed from within by the coolant under centrifugal action in the wheel voids. This requires an efficient filtration unit otherwise internal wheel loading and wheel unbalance problems may ensue. Flushing the wheel from within should prevent or minimise wheel loading when grinding, thus it may be possible to increase removal rates, and grinding wheel life.

The air layer effects can be minimised by use of a scraper-plate combination [18, 24]. The nozzle throttles the fluid increasing its velocity whilst the scraper-plate deflects the air belt. It is necessary to establish the optimum angle of inclination for the nozzle and the required scraper-plate gap width.

Coolant can be supplied radially outwards to the grinding zone by making use of the 35 - 45 percent void (present in the majority of grinding wheels) as the delivery network [20]. Reported benefits include reductions in workpiece burn and distortion; increased wheel life and the prevention of wheel loading.

All the described coolant application techniques have merits but are, each suited only to specific applications. Secondary coolant supplies may be necessary for swarf clearance if either treated wheels or mist cooling are employed as cooling techniques during high stock removal. To avoid workpiece thermal distortion and structural damage it may also be necessary to provide conventional flood cooling.

The combination of a wide wheel (200 mm) and restricted access prevents the shoe design and nozzle techniques being used for the present application in the form described in the references [18, 19] . However, the nozzle could be developed to suit a wide wheel application. Supplying coolant via the voids in the grinding wheel could cause internal loading of the grinding wheel leading to grinding wheel unbalance. In addition with this method uniform coolant distribution to the grinding zone across the grinding wheel face width cannot be guaranteed.

2.3.2 Designs for High-Speed Grinding Wheels

A significant improvement in grinding performance can be achieved by increasing the grinding wheel speed from the traditional range of 20 - 33 m/s [8] . However, increasing the grinding wheel speed presents technical problems of wheel design. If the grinding wheel speed is doubled, the stresses are increased four-fold; the Lamé Equations express the variation of the stresses across the wheel section [25] :

The bursting speed of the grinding wheel is dependent on the physical strength of the grinding wheel; and is therefore influenced by the grinding wheel design [26] .

Grinding wheels operated at high peripheral speeds should preferably contain fine grain abrasive set in a matrix of adequate plasticity and have a high hardness [27] . To achieve high-rates of metal removal it is usual to employ a vitrified bond, a coarse grain with open structure, and a soft grade. High-speed grinding wheel design involves achieving a workable compromise.

Two principal grinding wheel designs have evolved which enable the grinding wheel to be run at speeds in excess of 120 m/s (four times greater than conventional grinding wheel speeds).

i) Segmented Grinding Wheels

Segmented grinding wheels prevent the development of large circumferential tensile stresses which can cause failure of conventional wheels. In a design published by Shaw [28] , the segments have tapered faces which engage against substantial steel restraining flanges. Hence, the internal grinding wheel stresses are compressive rather than tensile. It may be possible to manufacture segments of high strength rather than whole grinding wheels.

ii) Annular Reinforcement of the Wheel

The large tensile stresses which occur at the grinding wheel inner diameter may be accommodated by reinforcing this region with an annular section [29] . Materials such as aluminium alloys are suitable, since they have sufficient strength to withstand the rotational stresses without adding cumbersome mass to the grinding wheel assembly.

2.3.3 Wheel Dressing Conditions

A comparative study between single point and rotary dressing of grinding wheels indicated that both dressing methods gave very similar grinding performance [30] . The results obtained suggested that rotary dressing was marginally superior insofar as a better surface finish tends to be obtained at the same grinding energy level.

Crush dressing of grinding wheels (with light crush loads) is basically a similar process to coarse single point dressing [31] . Improved surface finish from crush dressing can be achieved by allowing "crush-out" (similar to "spark-out"). Crush dressing enables a coarsely dressed grinding wheel to be obtained which is desirable for high rates of stock removal in that the wheel is less likely to become loaded.

Thus the grinding performance obtained by rotary and crush dressing can almost be matched by single point dressing. Because of this and since an investigation of grinding wheel dressing was not part of the experimental programme, the single point dressing unit was retained.

2.3.4 Wheel Guarding

The provision of adequate containment of grinding wheel fragments in the event of a grinding wheel burst is an essential safety requirement regardless of the grinding wheel speed. The D.S.A. document 00615 provides information for designing grinding wheel guards capable of withstanding the impact of a fragmenting wheel. The main limitation of the document is that it provides experimental data for grinding wheel speeds not exceeding 80 m/s; for grinding wheel speeds greater than the limit, extrapolation of the published data would be required. An experimental guard for a cylindrical grinding machine designed according to the above guidelines has been constructed at M.T.I.R.A. [32].

2.4 Refinements to the Modified Machine - Design Discussion

2.4.1 The Hydraulic System

Temperature control of the hydraulic oil was achieved by introducing a counter-flow heat-exchanger into the hydraulic circuit. The measured temperature rise across the system from the inlet to the return lines was 15° C before installation of the heat-exchanger. The maximum oil flow was 0.63 litres/second and it was therefore calculated that a heat-exchanger with a maximum heat dissipation capacity of 16 KJ would be adequate. The heat-exchanger fitted was capable of this heat dissipation. The coolant used was water; a flowrate of 26 litres per minute was sufficient to maintain a steady bulk temperature of 27° C, $\pm \frac{1}{2}$° C. In addition, the oil cooler was used as a pre-heater by passing hot water (instead of cold) through the water pipes. This meant that the period of at least one hour normally allowed to achieve thermal stability was no longer necessary.

The modified hydraulic system is illustrated schematically in Figure 3. The elements of the hydraulic circuit associated with temperature control are the return pump, header tank for the return pump, micro-switches for the return pump operation, and the oil cooler. The oil return lines were fed to the header tank. Oil returned to the header tank at a flow rate of 41 litres per minute and was pumped from there into the oil cooler at a flow rate of 45 litres per minute. The level of oil in the header tank was controlled by the two microswitches. The electrical circuit which controls the header tank oil level is shown in Figure 4.

Controlling the oil temperature improved the machine performance by increasing the stability and accuracy during grinding and by ensuring

the machine operated at the temperature at which the transducers were calibrated.

Air was extracted from the hydraulic system via air-bleed valves. An automatic air-bleed valve was inserted into the output line from the hydraulic pump to minimise air intake, but it was still necessary to remove air from the differential pressure transducer circuits. A separate air-bleed valve was manufactured for each line. Figure 5 illustrates the design. The air-bleed valve was designed to ensure that any air in the line would enter the air trap instead of the transducer. It was a simple matter to bleed the valves prior to each experimental session.

2.4.2 The Replacement Coolant System

i) Coolant Tank

A commercial coolant system was installed (see specification, Appendix 2). The tank capacity was 750 litres, with a pump delivery of approximately 2 litres per second, at the maximum pumping pressure of 0.85 MPa. The tank was supplied with a hydrocyclone filtration unit capable of filtering debris 10 microns or more in size. It was found necessary to connect a by-pass line and an adjustable pressure relief valve to the delivery pump output so that the coolant supply lines to the grinding wheel nozzles could be closed if required. The valve allowed the supply pressure to be varied.

ii) Coolant Nozzle

The coolant supply problem (wide wheel and restricted access) was solved by designing and making use of a manifold with an unrestricted discharge [33] . The main design requirements were uniformity of flow

at the discharge from the manifold, and a discharge velocity capable of penetrating the air belt generated by the rotating grinding wheel.

Preliminary tests using a pitot-static tube and manometer revealed a maximum indicated air belt velocity of 22 m/s (at a distance of 3 mm from the periphery of the grinding wheel) when the surface speed of the grinding wheel was 60 m/s. A grinding wheel type WA 60 MV-RC with reinforcing annulus was used for the test. The existing flood nozzle was adjustable and was positioned to act as a scraper-plate. This had the effect of reducing the air velocity by half.

iii) Determination of Manifold Dimensions

Two methods were considered suitable for machining the discharge ports, i) to drill a sucession of holes with an overlapping configuration, and ii) to machine a continuous slot. For a uniform discharge from a slot type manifold, Keller [34] indicated that it was necessary to vary the discharge width along the discharge length; greater at the inlet end with a taper reducing towards the closed end of the manifold.

It was decided that it would be simpler technically to drill an arrangement of holes along the discharge length as illustrated in Figure 6. The largest practicable manifold outside diameter that could be accommodated between the grinding and regulating wheels for the range of component sizes that would be machined, was 12½ mm. The corresponding bore size for brass pipe of this outside diameter was 8 mm.

For manifold stability during discharge [34], the area ratio (the ratio of the total exit areas divided by the cross-sectional area of the manifold bore) must be unity. The drill size was chosen as ½ mm, for stability of the shorter manifold (most high-speed grinding wheels have narrow face widths) 250 holes were drilled along the discharge length

(110 mm long). The corresponding number of holes for the longer manifold (210 mm long) was 460.

The variation in the discharge by pitching the holes equidistant and maintaining the same bore size for the longer manifold as the shorter one was expected to be approximately 16 percent [33, 34] . However, when tested with ignited natural gas, the flame appeared everywhere uniform for both manifolds. When they were tested with water, there was again no apparent variation, except at very low fluid flow-rates. The maximum exit velocities for the short manifold and long manifold (when used during grinding) were calculated to be 28 m/s and 56 m/s respectively.

It was found that the coolant could penetrate the air belt regardless of whether the flood nozzle was used as a scraper-plate. Plates 1 and 2 illustrate the uniform discharge across a wide wheel. It can be seen that the air belt does not deflect the coolant sheet which adheres to the wheel periphery. The coolant flow-rate was set at 0.001cu.m/s.

Retaining the flood system and introducing the manifold system for coolant supply, enabled various combinations of supply techniques to be used.

2.4.3 Force Measurement, Instrumentation Calibration and Dynamic Wheel Balancing

i) Force Measurement

The system for measuring the grinding forces was based on differential pressure transducers introduced into the bearing system. The scheme is illustrated in Figure 7. The oil hydrostatic bearing had six equi-spaced recesses around its periphery. The oil supply to the recesses

was restricted by a diaphragm valve [35] . The diaphragm was a form of pressure sensing valve and each diaphragm was connected across diametrically opposed recesses as shown. The effect of an applied load to the grinding wheel was to cause a differential pressure between opposed recesses, the differential pressure being proportional to the applied load. The differential pressures were monitored by the use of frequency modulated inductive pressure transducers, Type S.E. 180/N/L/ 02/BB/100 P.S.I.D., manufactured by S.E. (EMI) Labs. Limited. The transducers were supplied with a 3 KHz excitation signal. The output from each transducer was fed to an u.v. oscillograph. Three traces were obtained for the bearing bearing reactions to each load.

Figure 8 and 9 illustrate the relationship between the reactions F_1, F_2 and F_3 and an applied load, F_g . Resolving the forces into normal and tangential directions yields:-

$$F_n = F_1 + \tfrac{1}{2} \cdot [\, F_2 - F_3 \,] \quad \ldots\ldots\ldots\ldots\ldots\ldots\ldots\ldots \quad (2.1)$$

$$F_t = (3/2)^{\frac{1}{2}} \cdot [\, F_2 + F_3 \,] \quad \ldots\ldots\ldots\ldots\ldots\ldots\ldots\ldots \quad (2.2)$$

$$F_g = (\, (F_t)^2 + (F_n)^2 \,)^{\frac{1}{2}} \quad \ldots\ldots\ldots\ldots\ldots\ldots\ldots\ldots \quad (2.3)$$

ii) Instrumentation Calibration

The forces F_1, F_2 and F_3 and hence the grinding forces may be obtained by calibrating the u.v. oscillograph traces. The calibration was achieved by adding known masses to the grinding wheel flange at a pre-determined radius so as to generate known centrifugal forces. A mass was placed sequentially at three different positions, a, b, and c on the flange, at the same radius but with a 120^{o} angular separation, thus the effect of any out-of balance mass in the grinding wheel was obviated. By repeating this with two masses m_p and m_q a calibration

graph was drawn. The scale factor (K_i) for each of the traces (i=1, 2, 3) was defined as the reciprocal of sensitivity and was expressed in units of Newtons/millimetre of trace deflection.

The variations in the three u.v. oscillograph traces obtained during a calibration exercise correspond to pressure fluctuations in the three opposed pairs of recesses in the bearing caused by the out of balance mass, and the grinding wheel speed. The grinding wheel speed (revs/sec) can be found accurately from the resultant sinusoidal traces, the peaks correspond to the passage of the out of balance mass past the line of a given pair of recesses. Figure 10 shows a section of a typical u.v. oscillograph trace obtained during a force calibration run.

For any trace i the scale factor K_i is :-

$$K_i = \frac{\bar{K} . \bar{A}}{A_i} \quad \ldots\ldots\ldots\ldots\ldots\ldots\ldots\ldots\ldots \quad (2.4)$$

where $\bar{K}$ is the average scale factor of the three traces, A_i the amplitude of trace i, and $\bar{A}$ the average amplitude for the three traces. $\bar{K}$ is found from all the trace amplitudes, for the three traces i, for both masses in the three positions j (j=a, b, c), from the relationship:-

$$\bar{K} = (8/(3)^{\frac{1}{2}}).\pi^2.n^2.r.((m_p^2 - m_q^2)/((\Sigma \bar{A}_j^2)_p - (\Sigma \bar{A}_j^2)_q))^{\frac{1}{2}} \ldots \quad (2.5)$$

Appendix 3 provides the derivation of this expression.

A graph of calibration values versus grinding wheel speed (Figure 11) shows that they are dependent on grinding wheel speed. Thus the grinding wheel speed must be taken into account when measuring grinding forces.

<u>iii) Dynamic Balancing of the Grinding Wheel</u>

The output traces obtained from the calibration technique were also

used to improve the dynamic balance of the grinding wheel [36] .
The amplitudes of a selected trace with just one of the calibrating masses, m, in the three positions j (j=a, b, c) along with the amplitude A_o, (no extra mass added to the wheel flange), enables the mass equivalent m_u of the grinding wheel unbalance at the chosen radius (r) to be calculated. The angular position of the mass equivalent from position a towards position b (with a, b, c such that $A_a > A_b > A_c$) can also be determined. The relationships required are :-

$$m_u = m \cdot ((\Sigma A_j^2)/(3.A_o^2) - 1)^{-\frac{1}{2}} \quad \ldots\ldots\ldots\ldots\ldots\ldots\ldots\ldots \quad (2.6)$$

$$\theta = \cot^{-1} \cdot ((2/(3)^{\frac{1}{2}}) \cdot (((A_a^2 - A_b^2)/(A_b^2 - A_c^2)) + \tfrac{1}{2})) \quad \ldots\ldots\ldots \quad (2.7)$$

A compensating mass m_u can then be added to the wheel flange at an angle of $(60 - \theta)^o$ from direction c to b to obtain an improvement in the dynamic grinding wheel balance. Figure 12 illustrates the vector diagram associated with this analysis.

2.5 Performance Trials Using the Modified Machine

2.5.1 Objectives

i) To establish the effect of machine modifications on the machine performance.

ii) To conduct a simple grinding experiment and produce some first-order trends.

iii) To compare the experimental results with those of previously published work.

2.5.2 Nature of the Trials

i) Calibration of the force measuring system.

ii) Examination of the influence of the coolant supply technique on grinding performance.

iii)Investigation of the effects of varying grinding wheel speeds for constant control wheel speed and infeed rate.

2.5.3 Experimental Procedure

Plate 3 shows the centreless grinding machine used in the experimental programme. The experimental procedures for the trials are described below.

i) Calibrating the Force Measuring System

a) The hydraulic oil temperature was preheated to the calibration temperature of 27° C and maintained at this value.

b) The calibration procedure described in section 2.4.3 was followed.

c) The amplitudes of traces obtained from the u.v. oscillograph were measured and recorded, Table 1 contains a typical set of values.

d) The scale factors were subsequently calculated and the calibration graphs were drawn (Figure 11).

e) The procedure was then repeated twice more for constant oil temperatures of 25° C and 29° C.

ii) To Determine the Effect of the Coolant Supply Method

a) The grinding wheel was dressed by traversing a single point diamond across the wheel face. The grinding wheel speed was 60 m/s and the dressing lead was 0.8 mm/s; the coarsest practicable at this wheel speed (see section 4.5 for a full explanation). It was not redressed

during the experiment.

b) Several components (10 off, En 9 steel) were ground at a removal rate of 12 cu.mm/mm/s with a grinding wheel speed of 60 m/s, and a q-ratio (v_g/v_w) of 120.

c) The coolant flow-rate through the flood nozzle was increased until on grinding no burn marks appeared on the components, and the components were cool to touch immediately afterwards.

d) With this condition established, the wheel was redressed and the first batch of eight component groups (3 components per group) were ground. Components initially were ground with the coolant supplied via the flood nozzle. The procedure was repeated for another batch of eight components but the coolant was then supplied via the manifold instead.

e) Machine settings, component dimensions and other relevant data were entered in the standard data sheet shown in Table 2.

f) Computed results for the experiment are shown in Table 3.

The only experimental variable per batch of components was the infeed-rate. The coolant manifold position was adjusted to provide maximum coolant delivery to the grinding zone.

iii) The Effect of Grinding Wheel Speed on Grinding Forces and Surface Finish

a) The grinding wheel was dressed as in section 2.5.3 (ii) above, however, the grinding wheel was dressed at a wheel speed of 45 m/s.

b) Components were grouped in threes so that average grinding performance values for each set value of the process variable could be obtained.

c) The grinding wheel speed was set at 30 m/s and the first group of components were ground.

d) Force measurements were taken and all other relevant data were recorded.

e) The procedure (operations (b), (c), and (d)) was then repeated for each increment of 5 m/s between 30 and 60 m/s. Each time the control wheel speed was adjusted to maintain the same speed ratio, and a further group of components was ground.

f) The remaining groups of components were used to repeat conditions within the experiment.

Throughout the experiment, the infeed-rate, dressing lead and coolant flow-rate were maintained constant. All pertinent machine setting data and component information were recorded, see Table 4. A "spark-out" period of four seconds was used, this period of time allowed a complete grinding cycle (force build-up, plateau and force decay) to be obtained.

2.5.4 Results and Discussion

Elimination of air from the oil hydraulic system and the ability to control the oil temperature enabled repeatable grinding force results to be obtained (within 5 %). The inclusion of the oil cooler in the hydraulic circuit helped avoid the vibrations previously experienced whilst grinding. By maintaining a constant running temperature, it became possible to avoid the conditions at which instability was known to occur. Also, constant temperature conditions enabled the number of calibration graphs required for the force measuring system to be limited to one, rather than several. The machine could be operated within 2° C of the calibration temperature (27° C) without there being significant changes in the calibration values. The calibration values obtained for the three oil temperatures investigated were almost identical at any given value of grinding wheel speed for a specific

differential pressure transducer.

The effect of the coolant supply technique on the grinding forces is shown in Table 3. A maximum reduction of 13 % in the grinding forces was obtained when the manifold was used at a grinding wheel speed of 60 m/s. The coolant used was 98.75 % water with 1.25 % by volume of Fina Purfisol 2006/A (a chemical type, oil-less grinding fluid). It is not known how far grinding forces could be reduced by the manifold supply technique with a different concentration or choice of coolant type. Although trials were not conducted at other grinding wheel speeds at this time, it is possible that the benefits gained by using the manifold instead of the flood nozzle would increase as the grinding wheel speed increases. There was no apparent deflection of the coolant sheet by the air belt when the coolant was supplied via the manifold even when the scraper-plate (flood nozzle) was removed. This effect was not tested at wheel speeds in excessof 60 m/s; a scraper-plate may be necessary to reduce the air belt velocity at higher wheel speeds.

Due to a lack of published data on grinding forces for centreless grinding, it was decided to compare the experimental results obtained, with those previously published for surface and cylindrical (centre-type) grinding. The results obtained from the investigation of the grinding wheel speed effect are shown in Table 5. Figures 13 and 14 indicate trends consistent with those obtained by the investigators of surface and cylindrical grinding [8, 9, 37] . The results revealed that a decrease in grinding forces and surface roughness was obtained when the grinding wheel speed was increased. The maximum rate of reduction is obtained at grinding wheel speeds below 50 m/s and it appears that increasing the grinding wheel speed above 60 m/s would invoke the law of diminishing returns.

The forces obtained, when compared with those obtained from previously published work were 40 percent larger. This variation was attributable to the coolant type used (water compared to oil), wheel type, dressing lead and different direction of workpiece rotation. The values of surface roughness are not comparable (wheel type, dressing lead, coolant application and grinding force all influence surface roughness) in magnitude with previously published work, but follow similar trends.

The last three groups of components ground were used for repeat runs at lower grinding wheel speeds. No significant differences were observed in the values of grinding force and surface roughness for the initial and repeat runs. Thus, the variation in the results obtained was linked directly with the variation in the grinding wheel speed rather than changes in grinding wheel topography.

2.5.5 Conclusions

i) The machine development stage of the project ensured that the initial problems encountered whilst grinding were overcome. Satisfactory research into the grinding process could now be conducted at grinding wheel speeds upto 60 m/s as a result of improvements in the coolant system and force measuring sytem.

ii) Further increases in grinding wheel speed would require additional modifications to the transmission system.

iii) Initial results when grinding En 9 steel produced trends for grinding forces and surface roughness comparable with those published previously by workers who investigated other grinding operations (surface and cylindrical grinding).

3.0 THEORETICAL MODEL - GEOMETRY OF THE UNDEFORMED CHIP

3.0 THEORETICAL MODEL - GEOMETRY OF THE UNDEFORMED CHIP

3.1 Introduction

Different grinding operations which are kinematically similar can be represented by a single kinematic model, such operations are directly comparable in terms of the undeformed chip dimensions. A kinematic model of the grinding process does not take into consideration the physical process of material removal. It is merely associated with the idealised shape and size of the undeformed workpiece material which obstructs the passage of an active grain [38] .

Changes in the undeformed chip dimensions can and do result in significant changes in the grinding forces and the energy dissipated at active grits. Hence, the metal removal rates which can be achieved are affected significantly by the values of the undeformed chip thickness, chip length and cutting edge contact time. It is therefore important to be able to describe the kinematic conditions of grinding.

The chip thickness tc, is the predominant parameter determining the force on an individual grit, and is a parameter governing surface texture. Depending on the magnitude of the force on a grit, wear of the grit and eventual dislodgement will occur. The chip length lc, is a further parameter affecting wear according to Archards Law, i.e. wear is proportional to force x distance. The chip formation time tf, (in addition to tc and lc) is a parameter affecting the heat flux at a grit and hence the temperature rise at a grit.

The normal and tangential components of grinding force, specific energy and temperature will depend on the net contribution of all grits and the number of grits which can be brought into contact, which may be treated by a statistical approach.

The statistical treatment ideally takes into account wheel topography based on grinding wheel specification, dressing conditions, and subsequent wear of the grinding wheel.

3.2 Objectives

i) To examine the basic undeformed chip geometry and derive equations which yield the undeformed chip dimensions.

ii) To determine the influence of process variables on the undeformed chip thickness and undeformed chip length and compare the trends produced with those from other models.

iii) To use the developed analysis as a basis for predicting experimental trends in grinding trials.

3.3 Literature Survey

Equations which yield idealised undeformed chip dimensions have been proposed by many investigators [37, 39 - 46] . Table 6 lists a selection of these equations. The main criticism of such equations is that they rely on parameters which lack clear definitions and measuring techniques [47] . The principal parameters that fall into the above categories are the number of active cutting edges per unit area of wheel surface (c), the mean undeformed chip width ($\bar{b}$), and the theoretical chip length (lc). Consequently, the extent of the variation in the undeformed chip dimensions due to changes in process variables may be disguised or suppressed.

Examination of the equations contained in Table 6 reveal that equations (1, 2, 4, 5, and 9) predict a strong workpiece speed dependence for the dimension of the undeformed chip thickness. Other equations (3, 6, 7, and 8) suggest that the dependence is weak and even the possibility that

the undeformed chip thickness is independent of workpiece speed. Equations (4) and (5) proposed by Peklenik [42] and Opitz, Ernst, and Meyer [37] are identical. Calculated values of the undeformed chip thickness using these equations are smaller by a factor of two than the values obtained from other equations contained in the table. Opitz, Ernst and Meyer [37] suggested that the undeformed chip thickness is independent of workpiece speed, however, the published graph which is the basis of the arguement cannot be reproduced from the information presented.

An accurate solution for determining undeformed chip dimensions has been proposed by Brough and Rowe [27] . The solution is based on an exact equation for the locus of a cutting-edge through the workpiece and allows a realistic distribution of cutting edges to be applied for predicting chip dimensions. By using an iteration technique, they were able to provide dimensions for the maximum undeformed chip thickness. This solution requires the use of a computer to undertake the calculations but the variables used are clearly defined and measurable.

The author decided that a simpler solution than Brough's [27] was required; but one sufficiently accurate to form the basis for discussion of the experimental grinding results. Additionally, the form of the equation should allow its comparison with the equations of others. Hence, the following cases are presented:-

Case 1 - Variable grit height and separation.

Case 2 - Simplified analysis for constant grit height and separation.

For Case 1 it is shown that it is possible to take account of the

variations in the depth and separation of cutting-edges at the surface of the grinding wheel. Hence, a range of chip sizes and shapes are produced. It is necessary, therefore, to determine the distribution of a population of chips in order that the appropriate average chip can be determined. The solution also allows for variation in the wheel topography with grinding conditions. The expression obtained from Case 2 (variation of separation) enables comparisons to be made with the expressions of other workers, the significance of individual terms is discussed.

3.4 Development of the Solution

3.4.1 Assumptions

i) The chip shape is described by the loci of two active grits passing through the workpiece during the relative rotation of the grinding wheel and workpiece.

ii) The amount of workpiece rotation during the time for an active grit to achieve maximum penetration into the workpiece is negligible.

3.4.4 The Undeformed Chip Geometry

i) Introduction

The accepted basis of the undeformed chip model is modified slightly by the effect of some cutting-edges becoming inactive. This situation arises when one grit is shielded from contact with the workpiece by the action of the preceding grit. The basic geometry is illustrated in Figure 15a. Position A corresponds to a point on the workpiece which first comes into contact with the leading active grit on the grinding wheel. The relative rotations of the grinding wheel and workpiece result in a second point A' on the workpiece being presented to the next active grit.

Figure 15b illustrates the situation at the instant of contact between the second active grit and point A'. It is assumed that the arc A'B on the surface of the grinding wheel represents the average contact length of each active grit on the workpiece. The arc A'B, based on this assumption, is the average length of the undeformed chip, $\bar{l}c$.

Circumferential separation A'A on the workpiece is dependent on the relative speeds of the grinding wheel and workpiece, the height variation of the active grits and the dynamic grit spacing. The dynamic cutting-edge separation is the distance between two adjacent active cutting-edges, (ld). The average undeformed chip thickness $\bar{t}c$, is defined as the difference between the radius of the second active cutting-edge from the centre of the grinding wheel OA' and the length OA (termed Rg). The chip cross-section corresponds approximately to the shaded area in Figure 15a and the undeformed chip is characterised by the parameters $\bar{t}c$ and $\bar{l}c$. The vertical separation between the two active cutting-edges is represented by the parameter hg.

ii) Determination of the Undeformed Chip Dimensions

a) General Solution for the Average Idealised Undeformed Chip Thickness

From triangle OAC, Figure 16,

$$(Rd)^2 = (Rg + Rwn)^2 + (Rw)^2 - 2.(Rg + Rwn).Rw.\cos\phi d \quad \ldots\ldots\ldots\ldots \quad (3.1)$$

$$\text{and } \theta_1 = \cos^{-1}.\left[\frac{(Rg + Rwn)^2 + (Rg + hg)^2 - (Rw)^2}{2.(Rg + Rwn).(Rg + hg)}\right] \quad \ldots\ldots\ldots\ldots \quad (3.2)$$

Similarly, θ_o and ϕ_o can be found (Appendix 4 provides the derivation).

$$\text{Now } \theta_2 = \theta_o + ld/Rg \quad \ldots\ldots\ldots\ldots\ldots\ldots\ldots\ldots\ldots\ldots \quad (3.3)$$

The angle $\phi_o - \phi_d$ is the rotation of the workpiece between contact with the two adjacent active grits on the grinding wheel,

but $\phi_o - \phi_d = (\theta_2 - \theta_1) \cdot \omega_w/\omega_g$ ..... (3.4)

hence, $\phi_d = \phi_o - (\theta_2 - \theta_1) \cdot \omega_w/\omega_g$ ..... (3.5)

Thus Rd can be determined, and since the radius of the second active grit is Rg + hg, then from Figure 15a, the average undeformed chip thickness ($\overline{tc}$) is represented by :-

$$tc = Rg + hg - Rd \quad \text{..... (3.6)}$$

The various terms can be expressed to sufficient accuracy to give a value of $\overline{tc}$ accurate to 3 significant figures for angles of $\phi_d < 5^\circ$. Equation (3.6) is a general equation employed for the more accurate Case 1 solution with variable grit height and separation. Putting hg = 0 in equation (3.6) leads to the simplified analytical solution which is applicable only for the case of constant grit height. This solution is useful for comparison with the results of other workers and also for parametric studies.

b) Simplification of the Solution

Direct comparison between the solution proposed with those contained in Table 6 is impossible with equation (3.6) in its presented form. An expression must be substituted for Rd in equation (3.6), and the term cosØd from equation (3.1) must be expressed in terms of measurable properties. This is the Case 2 particular model which now conforms to the format used by other investigators, except that here an average dynamic cutting-edge separation may be used.

The value of Rd is given by,

$$Rd = ((Rg + Rwn)^2 + (Rw)^2 - 2.(Rg + Rwn).Rw.\cos\phi_d)^{\frac{1}{2}} \text{..... (3.7)}$$

and $\phi_d = \phi_o - B$ ..... (3.8)

where B is the angle whose arc is given by A'A on the workpiece.

And, $B = \frac{ld.vw}{Rw.vg}$ ..... (3.9)

Also, $\sin\phi_o = h/Rw \approx \sqrt{\frac{4.d.Dg}{Dw.(Dg+Dw)}} \approx \phi_o$ ..... (3.10)

where $d = Dw.vi.\pi/vw$ ..... (3.11)

Substituting (3.11) in (3.10) and (3.10) and (3.9) in (3.8) yields,

$$\phi_d = \sqrt{\frac{4.\pi.De.vi}{vw.Dw}} - \frac{2.ld.vw}{Dw.vg} \quad \text{..... (3.12)}$$

For $\phi_d < 5^o$, this expression is accurate to better than 0.1 %.

From equations (3.7) and (3.12) it can be shown that an expression for the average undeformed chip thickness ($\bar{t}c$) is given by :-

$$\bar{t}c = \left(1 - \frac{2.\pi.vi.De}{vw.Dg}\right).\left[\frac{ld.vw}{vg}.\sqrt{\frac{4.De.\pi.vi}{vw.Dw}} - \frac{\pi.vi.De}{vw} - \left(\frac{ld.vw}{vg}\right)^2.\frac{1}{Dw}\right] + \frac{\pi.Dw.vi.}{vw}.\left(1 + \frac{Dw.\pi.vi}{vw.Dg}\right) \quad \text{... (3.13)}$$

See Appendix 4 for the full development of the solution.

Expression (3.13) can be reduced further since the terms $(ld.vw/vg)^2/Dw$ and $(1 - 2.\pi.vi.De/(vw.Dg))$ have negligible affect on the magnitude of $\bar{t}c$ for the range of grinding conditions considered.

Thus equation (3.13) reduces to,

$$\bar{t}c = \frac{ld.vw}{vg}.\sqrt{\frac{4.De.\pi.vi}{vw.Dw}} - \frac{\pi.vi.De}{vw} + \frac{\pi.Dw.vi.}{vw}.\left(1 + \frac{Dw.\pi.vi}{vw.Dg}\right) \quad \text{..... (3.14)}$$

iii) Determination of the Average Undeformed Chip Length

The general solution for the average undeformed chip length ($\bar{l}c$) is

given by the expression,

$$\bar{l}c = (Rg + hg) \cdot \theta_o = Rg \cdot (1 + hg/Rg) \cdot \theta_o \quad \ldots\ldots\ldots\ldots\ldots\ldots (3.15)$$

From Figure 15a,

$$\sin\theta_o = h/Rg \approx \sqrt{\frac{4.\pi.vi.Dw^2}{Dw + Dg}} \quad \ldots\ldots\ldots\ldots\ldots\ldots\ldots\ldots\ldots\ldots (3.16)$$

however, for $\theta_o < 5^o$, $\sin\theta_o \approx \theta_o$

Hence the general solution is given by,

$$\bar{l}c = (1 + hg/Rg).\sqrt{\frac{\pi.vi.Dg.Dw^2}{Dw + Dg}} = (1 + hg/Rg).\sqrt{\frac{\pi.Dw.vi.De}{vw}}$$

$\ldots\ldots\ldots\ldots\ldots\ldots\ldots\ldots\ldots\ldots\ldots\ldots$ (3.17)

For the particular solution where hg is zero, equation (3.17) reduces to,

$$\bar{l}c = \sqrt{\frac{\pi.Dw.vi.De}{vw}} \quad \ldots\ldots\ldots\ldots\ldots\ldots\ldots\ldots\ldots\ldots\ldots\ldots\ldots\ldots (3.18)$$

iv) Average Chip Formation Time

The time taken ($\bar{t}f$) for the active grit loci to describe the average undeformed chip shape for the general solution is given by the expression,

$$\bar{t}f = \bar{l}c/vg = (1 + hg/Rg) \cdot \sqrt{\frac{\pi.Dw.vi.De}{vw.vg^2}} \quad \ldots\ldots\ldots\ldots (3.19)$$

And for the particular solution with hg equal to zero,

$$\bar{t}f = \sqrt{\frac{\pi.Dw.vi.De}{vw.vg^2}} \quad \ldots\ldots\ldots\ldots\ldots\ldots\ldots\ldots\ldots\ldots\ldots\ldots\ldots\ldots (3.20)$$

A comparison between the simplified expression for the undeformed chip thickness and those proposed previously by other workers (Table 6) shows that it contains some additional terms. The first term in equation (3.14) for the undeformed chip thickness is almost identical to the expressions of Pahlitzsch and Helmerdig [40] , Rowe and Stout [46] and Reichenbach, Mayer, Kalpakcioglu and Shaw [41] . The remaining expressions in the table tend to be single term expressions which bear no resemblance to the simplified proposal in equation (3.14).

High stock removal rates are obtained by optimising grinding parameters in conjunction with increasing the infeed-rate. At low infeed-rates (say 0.001 mm/sec) the predominant term in equations (3.13) and (3.14) is $(ld.vw/vg).(4.\pi.De.vi/(vw.Dw))^{\frac{1}{2}}$, the remaining terms tend to cancel each other out. However, at a higher infeed-rate (say 0.01 mm/sec) the effect of these terms on the undeformed chip thickness becomes increasingly significant, and could be of importance for correlating trends with experiments conducted at high infeed-rates. As such equation (3.13) should be used.

The expressions proposed for the idealised chip lengths are very similar to those proposed by other investigators. The majority of the authors propose one of two expressions for the undeformed chip length. These are :- i) $\bar{l}c = lg.vw.vg^{-1} + (\pi.Dw.vi.De/vw)^{\frac{1}{2}}$ and ii) $\bar{l}c = (\pi.Dw.vi.De/vw)^{\frac{1}{2}}$. For most purposes $lg.vw.vg^{-1}$ is very small and so expression i) reduces to expression ii). This is true of term $(1 + hg/Rg)$ in equation (3.17), and equation (3.17) reduces to equation (3.18). Thus the expression for the idealised undeformed chip length is identical to one of the two most popularly publicised.

A comparison of expressions for the chip formation time could not be

made, since none of the papers reviewed provided such expressions.

The term vg/vw has been designated by C.I.R.P. [47] as the q-ratio. The inverse of this ratio is found in two principal terms of equation (3.13) and in one term of equation (3.14). However, it could not be inferred that the q-ratio was a fundamental parameter because vw appears as an independent parameter in the expressions also.

3.4.3 Correlation of Theoretical Parameters with Experimental Results

It is possible to have a positive or negative correlation between the undeformed chip data and measured grinding parameters. Positive correlation implies that a proportional relationship exists between parameters, whilst a negative correlation indicates an inverse proportionality. In section 1.6 the principal grinding performance parameters were listed. Their correlation with theoretical chip data allows the trends of some graphs drawn from experimental data to be predicted.

i) Grinding Forces

Normal and tangential grinding forces are dependent upon the average force per chip and the average number of chips at any time. An expression for the normal grinding force is given by:-

$F'_n = f'_c . N_c$ .... (3.21)

The term N_c represents the number of chips being formed at any time per millimetre of grinding wheel width. f'_c is dependent on the depth of penetration of the cutting-edge i.e. the chip thickness, and represents the average force per chip. It is proposed that f'_c is proportional to the shear area and will depend therefore upon the square of the chip thickness [81].

Hence, F'_n is proportional to $N_c . \overline{tc}^2$ .... (3.22)

Now, the volume of each chip is approximately $1/6.(\frac{1}{2}.\overline{tc} + 4.\overline{tc}^2).\overline{lc}$ after Thompson and Malkin [82] , and the volume of material removed per second is therefore given by - $1/6.(\frac{1}{2}.\overline{tc} + 4.\overline{tc}^2).\overline{lc}.\overline{tf}^{-1}$. The total volume removed per unit grinding wheel width is:-

$$Z' = 1/6.(\tfrac{1}{2}.\overline{tc} + 4.\overline{tc}^2).\overline{lc}.\overline{tf}^{-1}.N_c \quad \ldots\ldots\ldots\ldots\ldots\ldots\ldots (3.23)$$

$$\text{Hence, } N_c = 6.Z'.\overline{tf}/((\tfrac{1}{2}.\overline{tc} + 4.\overline{tc}^2).\overline{lc}) \quad \ldots\ldots\ldots\ldots\ldots\ldots\ldots (3.24)$$

Thus N_c can be estimated from the theoretical undeformed chip data. If F_n' is proportional to $N_c.\overline{tc}^2$ then it is possible to predict the influence of infeed-rate, workpiece speed and grinding wheel speed on F_n' . Figure 38a which is a graph of experimentally determined values of F_n' versus $N_c.\overline{tc}^2$ demonstrates that F_n' is proportional to $N_c.\overline{tc}^2$. This result applies reasonably for both Case 1 and Case 2 solutions of $\overline{tc}$.

The case for F_t' can be argued in a similar manner, again a positive correlation exists. Figure 38a shows F_t' plotted against $N_c.\overline{tc}^2$. It is therefore possible to predict the trend for F_t' from undeformed chip data and hence the trends for power and specific energy using the relationships:-

$$\text{Power, } P' = F_t'.vg \quad \ldots\ldots\ldots\ldots\ldots\ldots\ldots\ldots\ldots\ldots\ldots\ldots\ldots\ldots (3.25)$$

$$\text{Specific energy, } U = P'/Z' \quad \ldots\ldots\ldots\ldots\ldots\ldots\ldots\ldots\ldots\ldots (3.26)$$

ii) Workpiece Surface Roughness

The workpiece surface roughness is by definition associated with the irregularities which are an inevitable consequence of the grinding process and should be remote from the imperfections in the machine geometry [52, 53] . Ideally the surface roughness is dependent on the depth of penetration of each active grit and can be represented by the

expression $Rz = \Sigma \Delta t/(\frac{1}{2}.N)$, where N is the number of coordinates and Δt is the peak to valley variation caused by the action of two adjacent active cutting-edges. Hence, as the chip thickness increases then a corresponding increase in the surface roughness is predicted. Figure 38c is a graph of surface roughness versus undeformed chip thickness, and demonstrates that the surface roughness value increases with an increase in the undeformed chip thickness. In practice, the surface texture may also be correlated with dressing lead particularly in the period shortly after dressing the wheel [48] .

iii) Equivalent Chip Thickness

The equivalent chip thickness (heq); the sum effect of all the instantaneous chip thicknesses in an arbitrary longitudinal section of the contact area [47] , is represented by the expression heq = Z'/vg. Now, the maximum metal removal rate Z', increases with an increase in the value of the undeformed chip thickness. From equation (3.14) for the undeformed chip thickness it may be shown that at low infeed-rates $\bar{t}c$ is proportional to $vi^{\frac{1}{2}}$, and at higher infeed-rates $\bar{t}c$ becomes aproximately proportional to vi. Since heq is proportional to vi, then increasing Z' for constant vg will result in a positive correlation between heq and $\bar{t}c$. Increasing vg for constant Z' will result quite closely in a direct proportionality between heq and $\bar{t}c$ since both heq and $\bar{t}c$ are proportional to 1/vg, again a positive correlation exists. This must be viewed as a criticism of the use of heq as a parameter in view of the varying functional relationship with the fundamental parameter $\bar{t}c$ depending whether vi or vg is varied.

iv) Wheel Cutting Ability

The wheel cutting ability λ , is defined as Z'/F'_n [83]. With this parameter

it is possible to have either positive or zero correlation with $\overline{tc}$ depending upon which grinding variables predominate. A positive correlation will exist if the normal force is varied with the maximum metal removal rate held constant. The wheel cutting ability can be increased by reducing the workpiece speed, by increasing the grinding wheel speed or by a combination of both. From equation (3.14) it may be deduced that if the infeed-rate is varied then both the normal force and the metal removal rate will vary approximately proportionately with infeed-rate and the wheel cutting ability will be unaffected. In this case there will be no correlation between λ and $\overline{tc}$, since $\overline{tc}$ has an approximately proportional relationship with $vi^{\frac{1}{2}}$ at low infeed-rates and vi at much higher infeed-rates.

v) Specific Grinding Energy

The specific grinding energy is defined as,

$$U = \frac{P'}{Z'} = \frac{F_t'.vg}{\pi.Dw.vi} \quad \ldots\ldots\ldots\ldots\ldots\ldots\ldots\ldots\ldots\ldots\ldots\ldots \quad (3.27)$$

A theory, to account for the specific energy in grinding, states that the total grinding energy consists of chip formation, ploughing, and sliding energies. The specific ploughing and sliding energies decrease at larger metal removal rates, but the specific chip formation energy remains constant. The specific chip formation energy is the minimum energy required to grind away a unit volume of material [54]. From equation (3.14) and equation (3.27) it would be expected that specific energy would be independent of $\overline{tc}$. However, this is not found to be the case experimentally at low removal rates [50]. It is closer to the expectation at higher removal rates. Thus, at higher removal rates a low correlation with undeformed chip thickness will be found, with a larger correlation predominating the lower infeed-rate range.

3.4.4 Discussion of Theoretical Results

i) Introduction

A large number of results for $\bar{t}c$, $\bar{l}c$ and $\bar{t}f$ were obtained directly from the solutions based on constant grit spacing (Case 2). A set of graphs has been compiled for this case (Figures 17 - 37). Using a numerical procedure it is possible to obtain a solution for variable grit height and separation (Case 1). This procedure is laborious (the technique for obtaining values for the grit height and separation is described in Appendix 7) due to the requirement for an extensive programme to cover the experimental range of grinding conditions. However, a limited set of results for variable grit height and separation have been computed and are presented in Figure 37 for comparison with constant grit spacing, Figure 36.

ii) Principal Parameters Affecting Chip Dimensions

The three principal operator set parameters are grinding wheel speed, workpiece speed and infeed-rate. Increasing the grinding wheel speed with the other operator set parameters held constant has the effect of increasing the number of active cutting-edges coming into contact with the workpiece. This should result in a reduction in grinding forces (each grit does less work), and surface roughness, with an increase in grinding wheel life due to reduced grit forces, contact time per contact and a reduced number of grinding wheel redressings. Producing chips of smaller dimensions will result in less efficient machining and as a consequence the net energy input to remove a unit volume of material will increase, with a possible increase in workpiece temperature.

Increasing the workpiece speed causes the amount of material presented to the grinding wheel in the interval between two active cutting-edges

contacting the workpiece, to be increased. The net result is an increase in the magnitude of the undeformed chip thickness with consequent higher forces, increased surface roughness and reduced wheel life. Increasing the infeed-rate has a similar effect.

Work conducted at Aachen T.H. [8, 9, 15] has highlighted two important effects of increasing the grinding wheel speed a) higher stock removal rates are possible if the infeed-rate is increased appropriately within the capacity of the machine and b) the workpiece speed must be of sufficient magnitude for a given grinding wheel speed if burn is to be avoided. Whilst research workers at Aachen T.H. were aware of the importance of the choice of workpiece speed for the avoidance of burn, they were not aware apparently of the importance of the choice of workpiece speed to avoid chatter.

The centreless grinding process, by virtue of the method of workpiece support is particularly vulnerable to grinding vibration. For centreless grinding it will be demonstrated in section 5.0 that chatter is an inevitable consequence of too high a workpiece speed just as burn is a consequence of too low a workpiece speed. Thus it would appear that for a given grinding wheel speed, that the choice of workpiece speed is important. Grinding wheel speed and workpiece speed are two independent parameters which have opposite effects on the trends of the undeformed chip thickness. A convenient parameter for describing the relationship between the grinding wheel and workpiece speeds for a given grinding wheel speed is the q-ratio (vg/vw).

The graphs (Figures 17 - 37) drawn from the theoretical results, samples of which are contained in Table 8, exhibit trends which are dependent on the relative values of grinding wheel speed, workpiece speed and infeed-rate. Graphs containing the parameter q-ratio are presented also.

This parameter allows the influence of workpiece speed on the idealised undeformed chip dimensions for a given grinding wheel speed to be examined.

iii) Practical Implications of the Theoretical Analysis

The solutions for the undeformed chip thickness proposed are of no practical value unless they can be manipulated or transformed so that experimental trends can be predicted. For high removal rate centreless grinding it is desirable to be able to predict the influence of grinding wheel speed, workpiece speed, and infeed-rate on the trends of force, power and metal removal rate so that it is possible to optimise on selected performance parameters.

It has been postulated previously that F_n' is proportional to $N_c.\bar{t}c^2$, and Figure 38a has shown that F_n' is directly proportional to $N_c.\bar{t}c^2$. Therefore, from (3.22),

$$F_n' = A.N_c.f_1^2(vg,vw,vi) \quad \ldots\ldots\ldots\ldots\ldots\ldots\ldots\ldots\ldots\ldots \quad (3.28)$$

A can be considered constant. If either an assumption is made for the value of A, or a value is taken from an experimental measurement of F_n', it is possible to construct the graphs shown in Figure 38b. Three graphs of infeed-rate versus workpiece speed are presented, each graph representing the results for a constant grinding wheel speed. Lines of constant force as predicted from the undeformed chip thickness and removal rate are drawn on the graphs. The direction of increasing force and power level (force and power are directly related by the constant vg) are also indicated.

The implications from a given graph i.e. constant grinding wheel speed are as follows:-

a) For a selected stock removal rate (or infeed-rate) increasing the workpiece speed increases the grinding forces.

b) Similarly increasing the infeed-rate (or stock removal rate) for a given workpiece speed also increases the force level.

c) Higher stock removal rates are possible at lower workpiece speeds - the force limit is shifted appreciably to enable higher infeed-rates to be employed.

As a group, the graphs demonstrate the grinding wheel speed effect on grinding forces. The effect of increasing the grinding wheel speed is to reduce the grinding force level for a given removal rate at a constant value of workpiece speed. For example, at a constant value for workpiece speed of 1 m/s and a metal removal rate of 62.8 cu.mm/mm/s, at 30 m/s the grinding force level is greater than 60 N/mm. Increasing the grinding wheel speed to 60 m/s, the grinding force level for the same stock removal rate reduces to a value less than 20 N/mm. The figure demonstrates two important features:-

a) Higher stock removal rates are possible at any given value of grinding wheel speed by reducing the workpiece speed for the same limiting force level.

b) Higher stock removal rates are possible at the same limiting force level by increasing the grinding wheel speed.

The graphs are not completely representative of practical grinding situations since they do not contain the boundaries known to exist which represent burn and chatter. Insufficient information at this time has prevented such lines from being constructed, however, this area of work will be the subject of further consideration.

iv) Undeformed Chip Thickness

Figures 17 and 18 illustrate the variation of the undeformed chip thickness with grinding wheel speed and infeed-rate for constant q-ratios of 180 and 60. There is an inverse relationship between $\bar{t}c$ and vg as indicated by equation (3.14). The largest undeformed chip thicknesses are obtained at the highest infeed-rate, at the lowest grinding wheel speed and q-ratio (high workpiece speed). From Figure 38b it can be inferred that the large undeformed chip thicknesses obtained with the conditions described above will be accompanied by large grinding forces. Such conditions are detrimental for achieving high stock removal rates. In addition to large forces, large undeformed chip thicknesses are also associated with large surface roughness values. Thus for increased stock removal rates with acceptable force levels and surface roughness values, higher grinding wheel speeds should be used for a given workpiece speed.

Graphs of undeformed chip thickness versus workpiece speed for various infeed-rates and grinding wheel speeds are presented in Figures 19 and 20a. Increasing the workpiece speed results in an increase in the undeformed chip thickness - the opposite effect to increasing the grinding wheel speed. Larger undeformed chip thickness values are obtained at large values of infeed-rate and low values of grinding wheel speed. The trend of chip thickness increases with increasing workpiece speed, thus these parameters by increasing the force level reach a limiting value. The lowest possible workpiece speed is necessary to obtain the maximum metal removal rate. However, the workpiece speed should not be so low as to give rise to burn [8] , and in section 5.0 it will be shown that vw should not be so high as to give rise to chatter.

Figures 20b and 20c, are graphs of undeformed chip thickness versus

grinding wheel speed which illustrate the influence of workpiece speed and infeed-rate on the magnitude of $\bar{t}c$. The trends are similar to those obtained in Figures 17 and 18 i.e. $\bar{t}c$ decreases in value as vg is increased. The convergence of the lines on the graphs at the higher grinding wheel speed suggests that the choice of workpiece speed for avoiding burn and chatter which it is suggested are dependent on $\bar{t}c$ becomes more restrictive. Workpiece regenerative chatter tends to be associated with large grinding forces [82] and it will be shown that it is also associated with high workpiece speeds. Since the large total forces are associated with large undeformed chip thicknesses, it is reasonable to assume that the choice of workpiece speed would be important to avoid this type of chatter. A second reason for this expectation is the increased number of regenerative cycles during the period of grinding at high workpiece speeds.

The graphs (Figures 21 and 22) of undeformed chip thickness versus grinding wheel speed for constant infeed-rate indicate that q-ratio has a significant effect on the magnitude of the chip thickness. The largest values of $\bar{t}c$ are found at low values of q-ratio (high vw) and grinding wheel speed. Because chatter and burn are workpiece speed related, the q-ratio parameter might be useful for describing a range of workpiece speeds, for any given grinding wheel speed, which can be used without the possibility of encountering burn or chatter.

Figures 23a to 24b illustrate the variation of the undeformed chip thickness with infeed-rate for a range of grinding wheel and workpiece speeds. The figures indicate generally that the largest valuse of $\bar{t}c$ are obtained at the highest infeed-rate when the values of the grinding wheel speed and workpiece speed are their lowest. Hence, the rate of increase of $\bar{t}c$ with infeed-rate is reduced with increasing grinding

wheel speed. The stock removal rate and undeformed chip thickness are proportional to infeed-rate, therefore, as stock removal rate increases so does chip thickness with a corresponding increase in the grinding force level. If the rate of increase of $\bar{t}c$ with infeed-rate is reduced with increasing grinding wheel speed as Figures 23a to 24b demonstrate, then increasingly higher stock removal rates will be possible at higher grinding wheel speeds.

The graph of the undeformed chip thickness versus q-ratio (Figure 25) for various grinding wheel speeds and infeed-rates illustrates that increasing q-ratio (decreasing vw) has a similar effect on the magnitudes of $\bar{t}c$ to that of increasing the grinding wheel speed. The largest values of $\bar{t}c$ are found at the highest infeed-rate and the lowest grinding wheel speed and q-ratio. All the graphs presented which have grinding wheel speed, or q-ratio as an abscissa parameter demonstrated that, increasing either grinding wheel speed or q-ratio reduces the undeformed chip thickness value. However, the graphs demonstrate that diminishing returns are obtained if vg or q is increased further. Although increasing stock removal rates may be achieved with increasing grinding wheel speed or q-ratio, the optimum stock removal rate may be achieved at some value below the maximum if the product quality becomes unreliable.

Figure 26a is a composite graph and summarises the most important aspects of the previous set of graphs. The points discussed previously are highlighted on this graph by constructing surfaces and allowing development into a third dimension [49] .

v) Comparison with the Solutions of Other Researchers

Numerical comparison of the values for the undeformed chip thickness obtained from equations (3.6) and (3.14) i.e. variable grit height and

separation and constant grit separation solutions respectively, with those obtained from the equations of others can be made by examining Table 7. Two values of the undeformed chip thickness for the variable grit height and separation solution are presented. The larger of the two values was obtained by using dynamic grinding wheel surface parameters (grit height and separation) in the equation. In fact, the value of the undeformed chip thickness obtained with this solution is the largest at both infeed-rates given. The value of $\bar{t}c$ obtained from the variable grit height and separation solution without the grit height being included, approximates closely, at the lower infeed-rate, the values obtained from the solution for constant grit separation and those of Pahlitzsch, and Rowe. The values obtained using the solutions of Peklenik and Opitz were almost half those obtained from the other expressions. At the higher infeed-rate, the solution for variable grit height and separation presents a value of $\bar{t}c$ which is again significantly different from all other values tabulated. The same solution without values for the variable grit height also produced a value for $\bar{t}c$ which was marginally larger than others in the table. The constant grit separation solution fails since $\sin\phi_o$ exceeds 5^o. The values from the solutions of Pahlitzsch [40] and Rowe [46] are identical, and again the solutions of Opitz [37] and Peklenik [42] provide values of $\bar{t}c$ less than half the largest value.

Figures 27a and 27b provide a comparison between trends of several undeformed chip thickness expressions. The results in Figure 27a were obtained using a constant infeed-rate of 0.4 mm/s, whilst Figure 27b was constructed using an infeed-rate of 1 mm/s. In both figures the two curves produced from the equation of Rowe [46] could equally well have been produced from the equation of Pahlitzsch [40] . Similarly, the results obtained from the expression of Opitz [37] are identical to

those obtained from the expressions of Peklenik [42] .

In Figure 27a all the curves indicate a reduction in the undeformed chip thickness as the q-ratio is increased. The curves which exhibit the largest rate of decrease in the undeformed chip thickness with increasing q-ratio (reducing vw) are those of Rowe and Bell. Both figures demonstrate the wide variation in the magnitude of the undeformed chip thickness that can be obtained depending which solution is used.

vi) Undeformed Chip Length and Chip Formation Time

Table 9 contains the undeformed chip length expressions of those authors whose corresponding undeformed chip thickness expressions appear in Table 6. As discussed previously, most authors propose one of two expressions for this parameter. Table 10 illustrates the difference in the dimensions of the undeformed chip length for these two expressions at two infeed-rates. At an infeed-rate of 1 mm/s the difference between the dimensions is less than 2 % . This difference reduces to less than $\frac{1}{2}$ % at the increased infeed-rate of 10 mm/s.

The undeformed chip length is independent of grinding wheel speed ($\bar{l}c = \sqrt{\pi.Dw.vi.De/vw}$), but its magnitude can be reduced effectively by either reducing the infeed-rate or by increasing the workpiece speed. Figure 28 illustrates the trends of the undeformed chip length versus workpiece speed for various infeed-rates. The trend of $\bar{l}c$ varying with vw is the inverse of the trend for $\bar{t}c$ varying with vw, i.e. $\bar{l}c$ decreases, as $\bar{t}c$ increases with increasing vw. Long chip lengths are a disadvantage, the grit contact time is high which causes undue wear, reducing wheel life and increasing the number of dressings per unit number of components.

The graphs of undeformed chip formation time versus grinding wheel speed, Figures 29a to 30b, indicate that the chip formation time reduces rapidly

with an increase in grinding wheel speed. Figures 31a and 31b indicate that increasing the workpiece speed decreases the grit contact time also. The ability to reduce the grit contact time could be an important aspect for minimising the specific grinding energy and total heat flux into the workpiece. Figures 32a to 34 show the chip formation time versus infeed-rate for various wheel speeds and q-ratios. The graphs are similar in shape to those obtained for chip thickness i.e. the chip formation time increases with increasing infeed-rate. Chip formation time is directly associated with grit contact length. The chip dimensions influence many parameters, some ratio between chip thickness and chip length may coincide with the conditions for optimum grinding performance.

Figure 35 shows the trend of the curve for the aspect ratio ($\bar{t}c/\bar{l}c$) in addition to the trends of chip formation time versus q-ratio, which vary in a similar manner to those of $\bar{t}f$ versus infeed-rate. The curve for $\bar{t}c/\bar{l}c$ indicates that the aspect ratio is inversely proportional to q-ratio [49] . The curve is independent of infeed-rate and grinding wheel speed. It is known that chatter is found at high workpiece speeds irrespective of the grinding wheel speed. Now, the graph indicates that the value of the aspect ratio increases sharply for q-ratios below 80 approximately. Therefore, it may be possible that for centreless grinding operations using kinematic conditions which yield aspect ratios in the range 1.3 and larger will take the operation into a region where chatter is highly probable.

From the results contained in Table 8, Figures 19 and 28, it can be seen that for constant removal rate, the undeformed chip thickness decreases with workpiece speed. Hence, associated with small undeformed chip thicknesses are large chip formation times, high specific cutting energies and

burn [50, 51] . Also, if the grit contact time is high then the sharpness of the cutting-edges will suffer. Hence, the results suggest that, for reduced specific energy and longer wheel life, a high value of workpiece speed (not too high to cause chatter) should be deployed.

vii) Effect of Variable Grit Height and Separation on Undeformed Chip Dimensions

The influence of variable grit height and separation on the undeformed chip thickness can be seen by comparing Figure 36 with Figure 37. The results indicate that the undeformed chip thickness is not only related to infeed-rate, grinding wheel speed and workpiece speed, but is related to the grinding wheel grit height and separation also. Comparison of these figures reveals the significance of these grinding wheel topographical parameters. They influence the trend of the curves and alter the magnitudes of the undeformed chip thickness appreciably. This implies that previous solutions by other workers not only fail to provide an accurate picture of high-rate grinding but provide dimensions for the undeformed chip thickness which are subject to considerable error. It is clearly important that any solution proposed for the accepted kinematic model of cylindrical grinding be able to take account of the effect of grinding conditions.

The increase in the magnitude of $\bar{t}c$ when the solution for variable grit height and separation is implemented can be explained as follows. The variable grit height and separation solution increases the number of grits with increasing infeed-rate which would tend to reduce the rate of increase of $\bar{t}c$ with infeed-rate. Thus, the slope of graph 37 would be expected to be lower than the slope of graph 36 which represents the solution for constant grit separation only. However, the number of active cutting-edges in the variable grit height and separation

solution is smaller than in the constant grit separation solution which has the opposite effect of making $\bar{t}c$ larger for the variable grit spacing solution. Apparently the reduction in the number of active cutting-edges is the predominant effect since the slope is greater for the variable grit spacing solution than the constant grit separation solution particularly at higher values of stock removal rate.

The effect of grit height and separation on the magnitude of the undeformed chip length and chip formation time is negligible. Therefore, they can be omitted from solutions suggested for these theoretical parameters.

3.4.5 Conclusions

i) Operator set parameters (vg, vw and vi) have significant influence on the magnitude of the undeformed chip thickness. The largest values of undeformed chip thickness are found when the values of workpiece speed, and infeed-rate are largest, and the value of grinding wheel speed is smallest.

ii) The q-ratio has been shown not to be a fundamental parameter but it is a convenient parameter for relating vg and vw for a given vg. q-ratio may prove to be a useful experimental parameter providing the conditions which limit grinding can be related to it - thus undesirable workpiece speed ranges and effects can be avoided.

iii) The expressions for the undeformed chip thickness proposed by the author, enable theoretical grinding performance graphs to be constructed (Figure 38b).

iv) The theoretical grinding performance graphs have shown that for a given force or power level it is possible to increase the stock removal rate by increasing the grinding wheel speed.

v) It is apparent also from the theoretical grinding performance graphs that for a given grinding wheel speed, and force level, higher stock removal rates are possible by decreasing the workpiece speed.

vi) The theoretical trends drawn for grinding forces varying with vg, vw and vi require one experiment to determine the value of A , from this one experiment however, grinding performance for a range of conditions can be predicted and the experimental results obtained will corroborate the predictions.

vii) Increasing the grinding wheel speed reduces the magnitude of the undeformed chip thickness. However, there are diminishing returns after a grinding wheel speed of approximately 60 m/s. Therefore, any benefits such as reduced force level and surface roughness for a given stock removal rate will be less significant.

viii) The grit height and separation affect the dimensions of the undeformed chip thickness appreciably, hence, the solution which accommodates these parameters (Case 1) should be used as the basis of any correlation between idealised parameters and actual grinding results.

ix) As the grinding wheel speed is increased the undeformed chip lengths and undeformed chip formation times are reduced markedly, which will reduce the heat transferred to the workpiece material at each grit position.

x) To reduce the specific grinding energy and the grit/workpiece contact time high workpiece speeds should be used.

xi) The accurate solution presented by the author for the undeformed chip model reveals the importance of infeed-rate, workpiece speed and grinding wheel topography at high removal rates. The solutions of most other workers fail to provide an accurate representation for the trends of the undeformed chip thickness in the high stock removal rate regime.

3.4.6 Predictions

i) Increasing the grinding wheel speed for constant vw and vi, will result in a reduction in the value of $\overline{tc}$. This will cause a reduction in the values of grinding force and surface roughness.

ii) Reducing the workpiece speed for constant vg and vi results in a decrease in the value of the undeformed chip thickness, thus a reduction in the values of the grinding forces and surface roughness will be obtained.

iii) Reducing the workpiece speed or increasing the grinding wheel speed will allow higher stock removal rates to be achieved for a given force/power level.

iv) Reducing the chip thickness for constant removal rate causes an increase in the grit contact time, thus the heat influx to the workpiece increases, this will increase the probability of burn.

4.0 INVESTIGATION OF THE HIGH-RATE GRINDING REGIME

4.0 INVESTIGATION OF THE HIGH-RATE GRINDING REGIME

4.1 Objectives

i) To investigate the high-rate grinding performance of selected ferrous materials in terms of grinding forces, specific energy, surface roughness, maximum metal removal rate and wheel cutting ability for a range of kinematic conditions.

ii) To compare the experimental trends with variations in relevant parameters derived from the analysis of undeformed chip dimensions.

4.2 Literature Survey

In order to investigate the high-rate grinding regime with some foresight, a review of available literature reporting the findings of others who have explored this regime was undertaken; this is presented below.

4.2.1 Review

The primary idea of increasing the grinding wheel speed in order to increase the metal removal rates was expressed by Krug in 1925 [72] . The effect of the grinding wheel speed on grinding performance has been reported subsequently by many researchers, however, the principal investigators of this parameter were Ernst [15] , Opitz and Guhring [8] , [55] .

Ernst [15] provided the first useful and systematic investigation of high wheel speed precision cylindrical grinding (employing centres). Grinding wheel speeds of up to 60 m/s were used. Opitz and Guhring [8] investigated the effects of grinding wheel speed (in the range 20 - 90 m/s) in the cylindrical grinding process (i.e. employing centres) whilst maintaining a constant q-ratio (vg/vw) of 60.

It was decided by these investigators, that increasing the grinding wheel speed for the same stock removal rate, regardless of the grinding process, resulted in reductions in the grinding forces, and surface roughness values. Associated with these two effects were an increased grinding wheel life and an increase in the interval between required grinding wheel re-dressings. It was deduced that the reduction in grinding forces lowers workpiece and machine tool deflections and enables greater workpiece dimensional accuracy to be obtained. It was suggested that, alternatively greater removal rates are possible within the capacity of the machine.

Hahn and Lindsay [56] agreed with the results of Opitz [8] and Guhring [55] on the effects of grinding wheel speed on grinding performance. However, they suggested that the surface roughness was a function of the interface force intensity, dressing conditions and conformity and not, as Opitz and Guhring [8] suggested, a function of grinding wheel speed. This conclusion was reached by plotting surface roughness versus normal force intensity for various grinding wheel speeds. It was argued that surface roughness was proportional to normal force since the results for the three grinding wheel speeds used, fell on the same curve. The grinding forces were reduced due to the use of higher grinding wheel speeds (for constant removal rates) and this was reflected in a reduced surface roughness.

Konig and Dederichs [9] investigated the effect of workpiece speed in the surface grinding process by varying the workpiece speed in the range 8 - 500 mm/s whilst using a constant grinding wheel speed of 60 m/s. Konig and Dederichs claimed that the workpiece suffers thermal damage when ground at low workpiece speeds with high stock removal rates and that this effect is influenced by the coolant type used. They found that

significant structural changes occurred when grinding heat-treated 50 Cr V4 (alloy steel) regardless of whether coolant was an emulsion or neat oil. However, neat oil had a beneficial influence on reducing the extent of the thermal damage. The improvement was attributed to the greater wetting and lubricating properties of the oil.

Ernst [15] diminished the heating in the grinding zone by deflecting the air layer, which accompanies the wheel at its circumference, in order to ensure adequate coolant reached the grinding zone. He also showed that a further method of decreasing the thermal effect in grinding was to increase the workpiece speed.

Opitz and Guhring [8] also found that it was possible to decrease the thermal effects associated with grinding by increasing the workpiece speed. They produced a series of micrographs illustrating the changes in structure due to variation in q-ratio on a C45 steel and a high speed steel (6 % tungsten, 5 % molybdenum, 2 % vanadium). Using a low workpiece speed (5 m/min) and no coolant, a change in structure was observed which extended to a depth of 150 μm, in both steels. The grinding wheel speed was 80 m/s and the removal rate was 10 cu.mm/mm/s. Repeating this experiment for the same conditions, except for an increase in workpiece speed to 80 m/min, resulted in no observable damage. The structures were examined with an electron microscope. Guhring [55] claimed that according to temperature measurement during grinding, the optimum speed ratio (q-ratio = vg/vw) was 60. A further increase in workpiece speed did not yield any noticeable advantage.

Surface and subsurface damage in hardened and tempered En 31 steel has been examined by El-Helieby and Rowe [57] . It is claimed that three forms of mechanical and metallurgical damage can be detected beneath the surface of ground components. These are:- a network of practicably

invisible cracks, microstructural modifications and hardness changes. The latter tempering is caused by the considerable heat generated during the grinding process, which is responsible for the occurrence of high residual tensile stress. It is suggested that an improvement in the grinding technique may just be sufficient to eliminate cracking, but the surface will remain highly stressed. The avoidance of long contact times for cutting-edges and large numbers of grits simultaneously contacting the workpiece per unit area is recommended.

Opitz and Guhring [8] examined the effect of grinding wheel speed on grinding wheel life. A range of wheel speeds from 20 - 90 m/s (q-ratio constant at 60) were investigated, the grinding wheel type was EK60 J0T 7VX, the coolant was neat oil and the removal rate was 10 cu.mm/mm/s. It was found that the grinding wheel life was greatly improved by increasing the speed. A graph of grinding ratio versus stock removal at various grinding wheel speeds revealed that the curves followed an exponential law of the type $y = 1 - e^{-kx}$, where y and x correspond to the grinding ratio and stock removal respectively. After a total stock removal of 3000 cu.mm/mm, the grinding ratio levelled off at 70 (for a grinding wheel speed of 40 m/s). For the same total stock removal, at a grinding wheel speed of 80 m/s, the grinding ratio was increased to 290, a four-fold improvement by doubling the grinding wheel speed.

Konig and Dederichs [9] investigated the wear behaviour of both resinoid and vitrified bonded grinding wheels. The grinding ratio of the resinoid bonded grinding wheels of various grain sizes compared favourably with the performance of vitrified bonded grinding wheels. However, once the grain size of the resinoid bonded grinding wheel was reduced (grit sizes 100 and finer) loading of the grinding wheel became apparent, this

was reflected in an increase in the workpiece surface roughness.

Kobayashi, Takazawa, Harada, and Horike [10] , conducted a series of experiments, initially to establish the maximum infeed-rate for rough cylindrical grinding when grinding between centres at high grinding wheel speeds. The limit for the maximum removal rate was defined as the onset of chatter at each grinding wheel speed. The purpose of these experiments was to obtain design data so that a new high-speed, high efficiency, centreless grinding machine could be designed and manufactured. The results obtained suggested that if the maximum grinding wheel speed of the designed machine was 50 m/s, then a maximum metal removal rate of 19 cu.mm/mm/s would be possible. An implication of the paper was that the maximum metal removal rates for centreless grinding would be similar to those of centretype grinding.

Further experiments concerned with the effects of grinding wheel grade on the total metal removed (before dressing was required) revealed that a hard grade grinding wheel should be used for high-speed grinding [10] . It was discovered that the total metal removed, increased as the grinding wheel grade became harder at the same grinding wheel speed. No information was provided on such important parameters as grinding forces, specific grinding energy and grinding efficiency.

A review of other papers on the centreless grinding process [58, 59], provided a very limited amount of performance data which was generally limited to surface roughness and removal rate values, for grinding wheel speeds in the range 30 m/s to 60 m/s. This is undoubtedly due to the difficulty of measuring forces and other such parameters for the centreless grinding process.

4.3 Design of Experiments

Design formats of scientific experiments have been categorised as either classical or factorial [60] . The classical design of experiments requires examination of the fundamental relationship between cause and effect, and from an understanding of the nature of this relationship, predicts the effect of controlled causes on a given situation. Factorial experiments help dtermine the optimum method for operating a system without the provision of causal relationships [60] .

The grinding process is complicated in nature due to the very large number of associated variables, and invariably there are continuous variations in many of the operating and machining conditions. A scientific study of the grinding process requires accurate control of the process variables, because of this, a classical design of experiments was considered to be preferable for an initial study of the effects of a limited number of process variables.

It was attempted to design classical experiments which would yield the maximum information from the minimum number of experiments. Because of the acknowledged variability experienced in grinding experiments, at least three components must be ground for each grinding condition so that reasonable confidence can be placed in the results obtained. Seventy individual experiments were conducted. The grinding wheel and workpiece speeds were held constant within a given experiment, the infeed-rate was the only parameter varied. Grinding wheel speeds in the range 30 to 70 m/s were investigated. For convenience the workpiece speed was related to the grinding wheel by q-ratio, and a range of q-ratios (60 - 200) were examined.

4.4 Specimen Preparation

Three materials were used for the experimental programme:- grey cast

iron bar, En 9 steel bar, and sintered compacted iron powder bar (P.M). However, less P.M. components were available than the other materials.

Preliminary grinding trials indicated that, to achieve high stock removal rates with the facilities available, the length of the components used could be up to 70 mm. High removal rate grinding (Z'max $>$ 2 cu.mm/mm/s) with long components ($>$100 mm) could result in excessive current demands beyond the capacity of the supply. The initial component diameter was dictated by the standard diameters available from material supply sources.

The En 9 bars were supplied as bright bar, in 2 metre lengths which were approximately 50 mm in diameter. The bars were cut to 65 mm lengths and were end-faced for smooth contact with the endstop during grinding. They were then ground on a centreless grinding machine to a common diameter.

The grey cast iron bars (BS 1452) were supplied in 300 mm lengths, 45 mm in diameter, and in the as-cast condition. The bars were cut to 65 mm lengths, end-faced, and ground (for removal of scale) to a common diameter of 42.5 mm. A further two millimetres were removed from the diameter to eliminate the presence of any hard casting "skin". The eventual diameter was 40.5 mm.

The sintered iron material was produced and supplied by Liverpool University, in bar form of 200 mm length, approximately 27 mm in diameter, and irregular in shape. The components had been isostatically formed under a compacting pressure of 333 MPa. The bars were cut to 50 mm lengths and ground to a common diameter (approximately 27 mm).

The components required no further preparation.

4.5 Experimental Procedure

i) Prior to each experimental session the force measuring equipment and the oil hydraulic system were brought to normal operating temperatures.

ii) The workblade height was set to give a β angle of 7° after Rowe [2] and the other chosen experimental conditions were detailed on specially designed data sheets.

iii) With the system at the normal operating temperature the wheels were dressed. The grinding wheel was dressed with a single point diamond using a dressing lead of 0.8 mm/rev at the speed to be employed during the experiment. This lead was maintained for all experiments; it was the coarsest lead practicable when dressing the grinding wheel at 60 m/s. (Pande and Lal [61] recommend a dressing lead in the range 0.5 - 1 mm/rev for maximum economic usage of the grinding wheel). A dressing depth of cut of 40 μm was used (Pacitti and Rubenstein [62] and Pande and Lal [61] recommend that from considerations of grinding wheel life, the dressing depth of cut should be the largest practicable). The control wheel was dressed with a dressing lead of 0.04 mm/rev. A copious supply of coolant was delivered to the dressing diamonds during the dressing operation. The diamonds were rotated after grinding three batches of twenty-four components. The wheels were dressed once per batch of twenty-four components.

iv) Three workpieces were ground for each condition. After each group of workpieces had been ground, the infeed-rate was changed (normally increased).

The raw data recorded included bearing reactions (from which grinding forces could be calculated), current and voltage increases during grinding (from which power consumption and specific grinding energy could be

determined), surface roughness values, ground diameter and several components were tested for roughness. Standard measurement techniques were applied. A "spark-out" period of 4 seconds was used.

4.6 Metallurgical Examination of Specimens

Several components from the steel and cast iron batches were examined metallurgically to determine whether high removal rate grinding had caused thermal damage. The selection of components for metallurgical examination was limited to those ground at a high q-ratio (200), at a high grinding wheel speed, and stock removal rate - the conditions most likely to cause burn and damage. Segments were removed from the selected components. These were mounted in a cold-mounting resin and positioned so that the ground edge could be examined in addition to the bulk material. After polishing, the specimens were etched with a 2 % nital solution for approximately 10 seconds.

A Vickers M41 Photoplan microscope, complete with a 35 mm camera and microhardness testing attachment was used in the metallurgical examination. A series of micrographs were taken to show the structure at the edge in addition to the bulk structure. The microhardness survey was conducted in a similar manner. The results are shown in Plates 4 - 7.

4.7 Data Processing

The data obtained during experimentation was recorded on data sheets specifically developed to assist with systematic data recording. A typical set of completed data sheets is contained in Table 11.

Data was processed using a microcomputer. The pertinent data required to determine the various performance parameters were extracted from experimental data recording sheets and u.v. oscillograph traces.

Manipulation of these data by the microcomputer resulted in a printed output which contained the majority of performance data normally associated with the grinding process. The output data included, grinding forces, metal removal rates, specific energy, grinding power, and wheel cutting ability.

Calculated performance data for the experimental programme were recorded in printed outputs of the form contained in Appendix 5. Graphs (Figures 39 - 69) were drawn using data extracted from the printouts. Sample data analyses are contained in Appendix 6.

4.8 Discussion

4.8.1 Introduction

A selection of results illustrating the variation of normal and tangential components of grinding force, maximum metal removal rate, specific grinding energy, wheel cutting ability, equivalent chip thickness and surface roughness from seventy experiments are presented below. All three component materials used in the experimental programme are represented in the results considered. The results are shown in Figures 39 - 69, and are representative of the general trends observed. Comments in the discussion that follows, relate to observations made from all seventy experiments.

4.8.2 Grinding Wheel and Workpiece Speed Effects

i) Effect on Grinding Forces

Approximately linear trends were obtained when the thrust force (F'_n - the normal component of grinding force per mm width of workpiece) and cutting force (F'_t - the tangential component of grinding force per mm

width of workpiece) were plotted against maximum metal removal rate (Z'max). Such graphs are illustrated in Figures 39 - 41. The graphs also illustrate the effect of grinding wheel speed and q-ratio on the slopes of the curves. The graphs presented are characteristic of many "easy-to-grind" metals; they are approximately linear with intercepts close to the origin [63, 64] . Thus all three materials ground can be categorised as "easy-to-grind" metals.

The graphs illustrate the effect of increasing the grinding wheel speed from 30 m/s to 60 m/s on the values of the grinding forces. An increase in the value of grinding wheel speed, for a given metal removal rate, results in a decrease in the values of the normal and tangential grinding forces. The effect of q-ratio on the trends of the grinding forces is also demonstrated. Except for a region of removal rates <2.5 cu.mm/mm/s for En 9 steel where there is some interception of the trends, the general trend for the effect of q-ratio on grinding forces is to decrease the value of force as q-ratio is increased. Thus the combined effect of increasing q-ratio and grinding wheel speed, for a given removal rate (in general), is to reduce significantly the grinding forces. The normal force is larger than the tangential force, the ratio F'_n/F'_t varies in the range 1.2 - 4 depending on the material (typically for the P.M.s, the range is 1.2 - 2.33, for En 9 it varies between 1.54 - 3.33, and for cast iron, F'_n/F'_n is in the range 2.22 - 4). The curves become divergent as the metal removal rate is increased. For En 9 steel, at very low metal removal rates below 2.5 cu.mm/mm/s, there is considerable scatter in the experimental points; trends are difficult to distinguish, and the influence of q-ratio is not very clear. Generally, from experience, the results for the normal force are less prone to scatter than those of the tangential force. Thus this parameter was chosen to exemplify grinding

performance for the remaining graphs.

The easiest to grind material was the cast iron, followed by the sintered iron powder compacts, with the En 9 steel requiring the highest power provision per unit volume of metal removed. Although, a coaser grade grinding wheel was used to grind the cast iron, the comparative ease with which this particular material was ground must also be attributable to the material properties. The maximum metal removal rate achieved when grinding cast iron was 80 cu.mm/mm/s. The maximum metal removal rate for the En 9 steel was 50 cu.mm/mm/s, with a corresponding value of 8 cu.mm/mm/s for the sintered iron powder compacts. There was no obvious evidence of workpiece burn at these metal removal rates.

Figures 42 - 44 illustrate that the normal grinding force varies approximately linearly with infeed-rate throughout the range of infeed-rates investigated for all three materials. The effect of grinding wheel speed, and q-ratio in reducing normal force is also evident on these graphs. Again the influence of speed ratio is not clear at the low infeed-rate end of the range investigated. Its effect is more pronounced as the infeed-rate is increased. The rate of increase of normal force is reduced with an increase in q-ratio [65] .

Data from several different ground batches were used to compile Figures 45 and 46 which illustrate the influence of grinding wheel speed on the normal grinding force (the tangential force varies in a similar manner). The graphs show (the now well known effect [15, 27, 55, 66] that, F'_n decreases with increase in grinding wheel surface speed, vg. Increasing vg from 30 m/s to 50 m/s results in a worthwhile reduction in F'_n, this would result in attractive reductions in wheel wear, surface roughness and possibly power consumption. Beyond approximately 50 m/s there are diminishing returns and the reduction in F'_n is barely measurable.

A comparison of Figure 46 with Figure 45 reveals that the results for the cast iron and En 9 steel are similar, however, the reduction in the force level is less pronounced for the cast iron. The number of pure iron P.M. components available for grinding trials was very limited but similar trends were observed. The figures also show that increasing either the infeed-rate or q-ratio increases the normal force.

The effect q-ratio has on the magnitude of the grinding forces would appear to have received little attention from other workers. In fact some previous workers most notably Opitz, Ernst and Meyer [37] have concluded that chip thickness (which can be related to grinding force) and the surface roughness are insensitive to variations in q-ratio. Examination of Figures 47 and 48, graphs of F'_n versus q-ratio for En 9 steel and cast iron reveals that F'_n is affected quite appreciably by the value of q-ratio. The graphs provide a range of q-ratios from approximately 70 to 200. At q-ratios below 90 there is a tendency to encounter grinding vibrations particularly at high grinding wheel speeds and stock removal rates. At q-ratios above 200 burn becomes a problem. Vibration and burn are discussed more fully in section 5.0 - Conditions Which Limit High-Rate Centreless Grinding. The graphs demonstrate quite clearly that increasing the value of q-ratio, within the range presented, reduces the value of F'_n, e.g. for En 9 steel with a Z'max = 15 cu.mm/mm/s, vg = 40 m/s, an increase of q-ratio from 70 to 200 can result in more than a 14 % reduction in F'_n . As with grinding wheel speed effects, there are diminishing returns as q-ratio is increased. An optimum working range for q-ratio appears to be between 100 to 200.

ii) Effect on Surface Roughness

As the metal removal rate is increased, the surface roughness of cast iron increases to a level which thereafter remains approximately constant.

Figures 49 and 50 illustrate this effect, two wheel speeds and several q-ratios are presented. The q-ratios for the two wheel speeds do not correspond exactly due to the problem of "chatter", but they provide an overall view of the trends.

In the case of the En 9 steel (Figure 49) the increase in surface roughness with increasing metal removal rate is more gradual than for the cast iron. Larger values of surface roughness are found at lower grinding wheel speeds and higher workpiece speeds. It may be that the initial build up in surface roughness is related to the size and strength of the abrasive grit, and the tenacity of the bond, in addition to the increased chip thickness as the removal rate is increased. When a grinding wheel has been dressed the surface becomes keen and it contains some loose abrasive grits and bond material. It normally requires 2 or 3 components to be ground to remove these loose particles and this initial keenness. Figure 51 is a graph of grinding forces versus volume ground at high removal rate for cast iron. The wheel achieves steady state grinding conditions after removing less than 100 cu.mm of metal per mm width of wheel. Thus it normally requires several components to be ground to condition the wheel. Once this has been done the condition of the wheel does not change considerably within a particular wear state [67] (after Fletcher). Thus, with the low batch sizes used (typically 24) the effects of wheel wear and loading would not be demonstrated. Hence a gradual increase in the surface roughness value may be anticipated once the wheel has been conditioned.

Fletcher [67] has shown that a rise in grinding force ratio to a new level is indicative of the change from primary grinding wheel wear to some secondary grinding wheel wear state. It was not possible to establish from the grinding force ratios obtained whether or not a transition between grinding wheel wear states had occurred; the results possessed scatter.

Comparison of previously published results on the effects of grinding wheel speed on grinding forces and grinding wheel wear have been discussed in section 3.4, grinding ratio will receive attention in section 5.0.

Figures 52 - 55 indicate that increasing q-ratio or the grinding wheel speed, with all other conditions remaining constant reduces the surface roughness. The trends are similar to those obtained for grinding forces and the comments made previously apply here also. The maximum surface roughness value measured was 4.5 μm Ra (0.25) Lay perpendicular. The surface roughness values obtained experimentally, were similar in magnitude to those obtained by other workers for similar grinding conditions [58, 68] . No surface roughness values are presented for the P.M. components as they tend to reflect the porosity rather than the surface finish of the metal.

iii) Effect on Wheel Cutting Ability

By definition the wheel cutting ability, $\lambda = Z'/F_n'$. Figures 56 and 57 illustrate the variation of the wheel cutting ability with infeed-rate for various q-ratios and two grinding wheel speeds. Irrespective of the material ground, the wheel cutting ability increased with an increase in infeed-rate, q-ratio and grinding wheel speed. In section 3.4 it was proposed that λ would be unaffected by varying infeed-rate, however, this was found not to be the case. F_n' can be expressed in terms of heq, i.e. from section 4.8.3, $F_n' = k.(heq)^p$, and $heq = Z'/vg$, therefore, $F_n' = k.(Z'/vg)^p$. Thus λ , for constant vg, is proportional to $Z'/(Z')^p$, and $p < 1$. Thus λ is dependent on vi, and will increase with increasing vi. From the graphs it is clear that for a given value of normal force a greater stock removal rate is possible by increasing the grinding wheel speed or q-ratio. Increasing both grinding wheel speed and q-ratio results

in a net increase in wheel cutting ability. Wheel cutting ability has been suggested as a measure of grinding efficiency [83].

The variation of wheel cutting ability with grinding wheel speed is shown in Figures 58 and 59. Two infeed-rates and q-ratios are presented. For the cast iron, linear trends are observed. The trends for the En 9 steel have a linear region for vg < 50 m/s with a positive gradient, afterwhich the gradient becomes zero suggesting that any further increase in wheel speed at these particular infeed-rates and q-ratios would yield little benefit, and the process is therefore at its optimum efficiency for these conditions.

Figures 60 and 61 illustrate the variation of wheel cutting ability with q-ratio for two grinding wheel speeds and infeed-rates. The general trend of the graphs is for the wheel cutting ability to increase with an increase in q-ratio. In the case of the cast iron the trends suggest that increasing the q-ratio beyond 200 will result in diminishing returns.

The wheel cutting ability values for the cast iron specimens were almost twice those of the En 9 steel. Inspite of the fact that each material was ground with a different grade grinding wheel, it is considered by the author, that the cast iron would be expected to have the higher wheel cutting ability value. Thus for a given grinding wheel and dressed condition, λ can be used as a measure of the "grindability" of the workpiece material.

iv) Effect on Specific Grinding Energy

The graphs of specific grinding energy versus infeed-rate are shown in Figures 62 - 64. Two grinding wheel speeds and q-ratios are demonstrated. Curves of the form $y = 1 - e^{-kx}$ are obtained, there is a rapid initial decrease in the value of specific grinding energy as the infeed-rate is

increased, afterwhich the curve flattens out and remains constant. The shape of the curves are similar to those obtained by Malkin [50] for grinding, and by Boothroyd [51] for horizontal milling.

Grinding energy consists of three components [50, 63, 69] , chip formation energy, ploughing energy, and sliding energy. The existence of the ploughing and sliding energies result in some important effects and provide an explanation for the so called "size effect". This term refers to the increase in specific grinding energy at low values of undeformed chip thickness. Figures 62 - 64 show that at low infeed-rates (which can be related to small chip thicknesses), the specific grinding energy increases rapidly with decreasing infeed-rate (i.e. chip thickness). It is thought that the sliding and ploughing energies are constant and therefore become a greater proportion of the total cutting energy as the chip thickness decreases. The specific grinding energy can vary considerably for a given material and it is affected by changes in infeed-rate, grinding wheel grade, grinding wheel speed, workpiece speed and coolant type.

The graphs of specific grinding energy versus grinding wheel speed (Figures 65 and 66) and specific grinding energy versus q-ratio (Figures 67 and 68) illustrate the "size effect". In Figures 65 and 66 the lower infeed-rate yields the highest specific grinding energy values. The trend of the curves is one of gradual decrease as vg inreases upto 50 m/s afterwhich there is a rapid rise in the value of the specific grinding energy. This is an anticipated trend, it has been shown previously that F_t' versus vg decreases rapidly initially (a curve to the law $y = 1 - e^{-kx}$ is obtained) becoming constant and remaining so. A plot of vg versus vg would be a straight line passing through the origin at 45°. Now the specific grinding energy is by definition $F_t'.vg$. Hence, the trend from

the product of two such curves (F_t' versus vg, and vg versus vg) would be the same as that obtained in Figures 65 and 66. Figures 67 and 68 (specific grinding energy versus q-ratio) illustrate the variation of $F_t'.vg$ with q-ratio. Since vg is constant the graphs portray the variation of F_t' versus q-ratio. The significance of this type of result has been discussed in section 4.8.2, (i).

4.8.3 The Significance of Equivalent Chip Thickness

The three parameters, normal grinding force, specific grinding energy, and surface roughness are generally regarded as the most important grinding parameters. Snoeys and Peters [47] have shown that the influence of grinding wheel speed and infeed-rate on these parameters to be simple power functions of the equivalent chip thickness (Z'max/vg). By plotting logarithms of values of these three parameters against the logarithm of equivalent chip thickness, straight line graphs are obtained. Figure 69 illustrates this result. Thus these parameters are simple power functions of equivalent chip thickness, i.e. $F_n' = k.he^p$ where p is the slope, and k is the intercept at log he equal to zero. For the surface roughness the index is small and positive, for the specific energy it is small and negative, and for the normal force it is positive and close to unity. The value of the index varies with q-ratio. In the case of surface roughness and normal force an increase in q-ratio will reduce the index p, for specific grinding energy increasing q-ratio increases the negative index.

Hence the equivalent chip concept is useful for the high-rate grinding regime and may allow a vast amount of data on the grinding behaviour of particular materials with paricular grinding wheels to be summarized by a few empirical equations.

4.8.4 Roundness Errors

Although an examination of the effects of high-rate centreless grinding on the roundness error was not part of the investigation, some Talyrond traces were taken. For both materials the values of roundness error varied between 4 - 10 μm. There appeared to be no correlation between roundness error and wheel speed or infeed-rate for the ranges of these parameters investigated. This was possibly due to the fact that a 4 second "spark-out" period was employed. The parameter q-ratio appeared to influence roundness and as such it was decided to investigate this effect more thoroughly when establishing the conditions which limit the centreless grinding process when grinding at high removal rates (section 5.0).

4.8.5 Some Characteristics of the Grinding Forces

Grinding force ratios (F'_n/F'_t) for cast iron varied from 2.22 to 4, whilst for the En 9 steel and sintered iron powder compacts the ranges were 1.54 to 3.33 and 1.2 to 2.33 respectively. There was no apparent trend of grinding force ratio with any particular parameter.

Plate 8 illustrates typical force traces for the three materials. It is possible to identify which material has been ground from the force traces. The force traces for the En 9 steel normally comprised two equal force components F_1 and F_2 ($F_3 = 0$). However, at high infeed-rates (> 0.25 mm/s) a value of F_3 could be detected; even so, the trace deflection was very small. The bearing configuration dictates that if F_3 is zero, then F_1 must equal F_2 and the subsequent force ratio must equal 1.73, this was found to be the case. The influence of a negative force component F_3 was to increase the grinding force ratio.

The directions of the grinding force traces for cast iron (F_1 and F_2

positive with F_3 negative) indicate a positive deflection of all force components. Even at low infeed-rates (0.025 mm/s), the value of F_3 was substantial. The grinding force ratios tended to be larger than the corresponding values (for similar experimental conditions) for the other two materials. In the case of the sintered iron powder compacts, a positive deflection of the trace for F_3 was apparent. Consequently, the grinding force ratios are less than those obtained for the other two materials for similar grinding conditions.

The inverse force ratio is representative of the friction between the workpiece and the grinding wheel. The value of this ratio, F'_t/F'_n shows that the cast iron has less associated friction than En 9 steel whilst the P.M. components have more. The resultant friction coefficients are characteristic of each type of ferrous material. For En 9 steel the range of values of F'_t/F'_n is 0.3 - 0.65. For cast iron, containing large amounts of graphite, the value is lower being in the range 0.25 - 0.45. For pure iron P.M. components F'_t/F'_n is 0.43 - 0.83, the more ductile pure iron has a higher associated friction.

A resinoid bonded grinding wheel was used to grind the cast iron specimens, whilst a vitrified bonded grinding wheel was used for the steel workpieces. The difference between the grinding force traces for the three material types may be partly due to the different stiffnesses of the two grinding wheels, in addition to the metallurgical differences of the components.

4.8.6 Average Grinding Stiffness of the Machine Tool

A measure of the average grinding stiffness of the machine including the grinding wheels was made by grinding two components of identical initial diameters at a high-rate. One was ground with "spark-out", the other was not. The difference in final diameters (ΔD) represents the total

elastic deflection of the machine elements during grinding at the maximum rate. By determining the grinding force (Fmax) whilst grinding at the maximum rate, the stiffness λ av can be determined. The grinding stiffness can be expressed by λ av = Fmax/ D, this was calculated to be 10 MN/m. It is possible to change the stiffness of the machine by changing the hydraulic oil pressure, or by changing the thickness of the Rowe [35] diaphragm valve. Most authors quote the static stiffness of the machine hence it was not possible to make a machine stiffness comparison but the figure indicates that for the modified machine a very high grinding stiffness is obtained.

4.8.7 Vibration Types Encountered During Grinding

Two types of vibration were encountered during grinding. The first type (Type 1) involved violent vibration of the workpiece and required the run to be abandoned. Plate 9 illustrates the grinding force traces of such a run. The force trace indicates no build-up, and in fact this type of vibration always set in abruptly, in every case the component surface was wavy. The normal frequency (based on the number of workpiece waves) varied between 86 and 263 Hz. It was necessary to redress the grinding wheel and control wheel after this type of vibration had been encountered; the surface of the wheels became damaged.

The second type of vibration (Type 2) was barely audible, and manifested itself chiefly in the grinding force traces. The frequency of the vibration corresponded to the grinding wheel frequency. The trace thickness obtained normally without vibrations of this nature is a function of the wheel dynamic balance, however, once this vibration type is established the amplitude of the traces increases upto twice its previous value. Plate 9 illustrates this type of vibration which can appear anywhere on the force trace within the grinding cycle. It was found that this type of vibration

could be "driven" through by increasing the infeed-rate. Unlike the previous type of grinding vibration, this type of vibration did not always affect the surface of the component, although marks were observed occasionally.

Accurate values of surface roughness and roundness error can not be presented for vibration Type 1 because the run was inevitably aborted. However, both the surface roughness and roundness error increased significantly once vibration was encountered. The final values were never established for vibration Type 1, but the roundness error was in excess of 20 μm and the surface roughness was in excess of 2 μm Ra (0.25) Lay perpendicular. For vibration Type 2 the surface roughness value was generally in excess of 1.5 μm Ra (0.25) Lay perpendicular with a roundness error in excess of 14 μm.

Grinding vibrations were detected in fourteen experiments from a total of seventy. Five of the grinding trials were aborted because the vibration was extremely violent. Grinding vibrations were encountered on six occasions when the q-ratio was 60, the grinding wheel speed on these occasions was always in excess of 40 m/s. At a q-ratio of 90, five instances of vibration were recorded, again the grinding wheel speed was always in excess of 40 m/s. The remaining three records of grinding vibration were made at a q-ratio of 100, one of these was for a grinding wheel speed of 30 m/s; the others were at grinding wheel speeds in excess of 45 m/s. Type 2 vibration was associated principally with En 9 steel, cast iron normally experienced Type 1 vibration.

The violent nature of the Type 1 vibration was such that it warranted further investigation. Previous workers have shown the critical importance of the geometric configuration on the ability to produce round workpieces. Geometric stability charts have been proposed by Rowe and Richards [73],

the charts enable the frequency of geometric instability to be predicted and an assessment of the severity of the instability can be made.

Figure 70 is a chart which represents the geometric stability situation for the configuration used experimentally. Rowe [2] has shown that for optimum workpiece roundness, values of β should be in the range 6 - 8°. An experimental value of 7° for β was chosen. Practical difficulties prevented setting the exact value of β, it was however, set as close as possible to 7°, and was always in the range 6 - 8°. Hence the chart was constructed for the three β values thus providing a limiting range.

Interpretation of the chart according to Rowe and Richards [73] is that serious instability will occur when there is coincidence between an integer number of waves, and a negative trough on the stability chart. Also, if the frequency of the trough coincides with a machine natural frequency or that of a forced vibration, then irrespective of whether the trough is positive or negative serious waviness is probable.

Table 12 contains all the pertinent data corresponding to the trials that were aborted due to Type 1 grinding vibration. The number of workpiece waves were 22, 24 and 26 (3 incidences of 26 waves). If Figure 70 is consulted it can be seen that these integer values of workpiece waves all coincide with troughs on the chart. Hence, the instability could have been predicted. In addition, Table 12 contains values of the machines natural frequencies, after Rowe, Weston and Xu [74], and the frequency of the grinding vibration. The frequencies of the waves are close to the natural frequencies of the machine except for vg = 60 m/s with a q-ratio of 60. The natural frequencies presented in Table 12 are for the machine fitted with the new transmission system. The method of connecting the drive shaft (flexible coupling) is identical to the original arrangement, and since no structural alterations were

made, the natural frequencies should not have been affected. The occurrence of vibration at high workpiece rotational speeds and the coincidence of integer numbers of waves and negative troughs on the stability charts suggests that workpiece regenerative vibrations were obtained. The relative stability found at low workpiece speeds is due possibly to the reduced number of rotations giving rise to the workpiece regenerative effect. There appears to be no correlation between grinding wheel rotational frequency or the ratio of grinding wheel to workpiece rotational frequencies and the frequency of workpiece waves.

The results demonstrate two important points a) that by judicious choice of q-ratio, preferably above 100, grinding vibrations can be avoided, and b) a small change in the workpiece speed may be sufficient to change a geometrically unstable grinding configuration into a stable one (this can be deduced from the geometric stability chart).

Other workers [10, 55] have reported high specific stock removal rates (100 cu.mm/mm/s) at low q-ratios with centretype grinding machines and apparently no grinding vibrations were encountered. To achieve comparable specific stock removal rates with the centreless grinding process, slower workpiece speeds i.e. higher q-ratios have to be used if vibrations are to be avoided. Schreitmuller [70] does however report high removal rates (up to 15 cu.mm/mm/s) for centreless grinding at very low speed ratios (q-ratio = 8 approximately) without noticeable chatter but this could not be reproduced in the present project.

When discussing chatter and relating it to stock removal rates it is important to quote maximum metal removal rates and not specific removal rates. To discuss specific removal rates can be misleading since chatter is dependent on the total force level and not the specific force level encountered. It is difficult to make comparisons between centretype

and centreless grinding regarding chatter. This is chiefly due to the differences in the methods of workpiece support and the mechanism of workpiece rotation, which can be contributing factors affecting the onset of chatter.

4.8.8 Correlation of Theoretical Parameters with Experimental Results

A strong correlation exists between the undeformed chip thicknesses calculated in section 3.4 and measured grinding parameters particularly F_n' and F_t' . The results obtained in this section indicated that the undeformed chip thickness can be reduced by either reducing the workspeed or increasing the grinding wheel speed. In addition, reducing the infeed-rate reduces the value of the undeformed chip thickness. It was predicted in section 3.4 that increasing the grinding wheel speed with all other conditions remaining constant would result in reduced grinding forces, reduced surface roughness values and an increase in specific grinding energy, this was found to occur.

Figures 21 & 22, the graphs of chip thickness versus grinding wheel speed compares favourably with Figures 45 & 46, graphs of specific normal force versus grinding wheel speed. The effects of infeed-rate, q-ratio and grinding wheel speed on the magnitude and trends of the undeformed chip thickness and specific normal force are consistent. The trends for undeformed chip thickness varying with q-ratio (Figure 25) are also consistent with those for F_n' versus q-ratio (Figures 47 and 48). Whilst it was proposed that the specific normal force was proportional to $N_c.\bar{t}c^2$, there is clearly a relationship between F_n' and $\bar{t}c$.

The theoretical trends of grinding force for varying vw,vg and vi obtained in section 3.4, Figure 38b, are supported by the results obtained in the experimental programme. It was found experimentally that higher

stock removal rates were possible at low values of workpiece speed and at high values of grinding wheel speed. It was also shown experimentally, that higher stock removal rates were possible for any given grinding wheel speed by reducing the workpiece speed and increasing the infeed-rate. The theoretical predictions of grinding performance derived from Figure 38b did not account for the practical limitations of burn and chatter. Recommendations for establishing expressions which predict burn and chatter so that boundary limits can be constructed are made in section 7.0.

In the case of the wheel cutting ability, it was found that for the grinding conditions employed, an increase in its value coincided with increases in grinding wheel speed, infeed-rate, and q-ratio. This may not be the case always, λ for constant vg, is proportional to $Z'/(Z')^p$ and the value of p can vary depending on grinding parameters and workpiece material. Hence an increase in infeed-rate could result in a reduction or constant values for λ in addition to the afore mentioned increase.

Reducing the grinding wheel speed, increasing the workpiece speed and increasing the infeed-rate results in larger undeformed chip thicknesses. Associated with large undeformed chip thickness values are large forces on the grits, low specific grinding energy and increased surface roughness - again these results were realised. In addition large values of wheel cutting ability were obtained.

Grinding forces, surface roughness and specific grinding energy can be expressed in terms of equivalent chip thickness in the form of a simple power law. The grinding forces and surface roughness correlate with equivalent chip thickness in a positive manner when expressed in this form. The specific grinding energy has a negative correlation.

Components ground with large values of q-ratio (say 200) are considerably warmer (to touch) than those ground at lower q-ratios. Thus the choice of q-ratio is important to avoid possible workpiece burn.

The undeformed chip thicknesses calculated from equation (3.17), section 3.4, have been shown to correlate with experimental grinding parameters.

4.8.9 Microstructures of Ground Components

A metallurgical examination of several components was undertaken to establish the extent, if any, of thermal damage caused to the components through high-rate centreless grinding. The examination consisted of a microhardness survey and photographs of the microstructure at the ground edge. The micrographs for En 9 steel and cast iron are shown in Plates 4 and 5 and Plates 6 and 7 respectively. The grinding wheel speed was 60 m/s and the q-ratio was set at 200, these conditions represented the extreme of the range of conditions investigated i.e. the conditions most conducive to burn. Guhring [55] has shown that structural damage is most likely to occur whilst grinding at low workpiece speeds. One component was ground for each material with and without spark-out. The stock removal rate was 50 cu.mm/mm/s so that comparison between the materials could be made at the current metal removal rate limit of the En 9 steel. The components were prepared before the test by removing 1 mm from the diameter at a very low removal rate.

Micrographs for the grey cast iron components are shown in Plates 6 and 7. The structure at the ground edge is consistent with the bulk structure for both components ground. The microhardness survey did not indicate any change in the hardness value at the ground edge when compared with other values taken from the sample cross-section. A Vickers pyramid hardness number of 220 was obtained.

Plate 4 for the En 9 steel component ground with spark-out illustrates a typical En 9 steel microstructure. There is no structural change at the ground edge, and again no variation in microhardness number could be found for this component. A Vickers pyramid hardness number of 300 was obtained.

The micrograph for the En 9 steel component ground without spark-out is shown in Plate 5. The micrograph reveals that this component suffered severe plastic deformation at the ground edge. The deformation layer extends 30 microns into the workpiece, radially. A microhardness survey provided a Vickers pyramid number of 300 for the bulk material and a value of 500 in the deformation zone. The "burnt" colour of the component was blue, suggesting a surface temperature of approximately 400° C - too low to anneal the work hardened surface layer. The change in colour of the pearlite grains from dark to light within the same grain (the light region being in the deformation layer) suggests the possibility of incipient spheroidisation. For this to occur the sub-surface temperature of the component would need to be greater than the temperature of the surface itself.

The burnt En 9 steel component was cut in to half. One half was tested for surface cracks by using the Magnaflux method, and by etching with a 10 percent nital solution. None could be found. The other half was tested for stress cracks by immersing the component in a 15 percent sulphuric acid solution for approximately 30 minutes [71] . Again no cracks could be found.

The results for the En 9 steel are very important. They indicate the need to employ a spark-out period of sufficient duration to remove layers of surface damage. The spark-out period used was 4 seconds which resulted in a diametrial variation of 84 µm between the En 9 steel

component ground with spark-out and that without. Thus any deformation layer present on the component ground with spark-out would have been removed. An alternative to employing spark-out would be to reduce the infeed-rate just prior to reaching the limit of the infeed stroke. The experimental conditions used were the extremes, chosen because they were the most likely to cause burn. It must be concluded therefore, that when grinding with the conditions used during the high-rate grinding trials, that the spark-out period was sufficient to remove the deformation layer and that the deformation layer was smaller in thickness.

4.9 Conclusions

i) Maximum metal removal rates of 80 cu.mm/mm/s for cast iron and 50 cu.mm/mm/s for En 9 steel have been achieved when plunge feed centreless grinding.

ii) These very high removal rates have been achieved despite the limitations of single point diamond wheel dressing and the use of a water based coolant.

iii) The experimental trends of the grinding forces substantiated the theoretical trends and predictions for grinding forces made in section 3.0 . The experimental results indicated that higher stock removal rates are possible at a given grinding wheel speed, with a constant force level, by reducing the workpiece speed and increasing the infeed-rate.

iv) Further-more correlation between theoretical predictions and practical achievements has shown that by increasing the grinding wheel speed and the removal rate simultaneously, it is possible to achieve high-rate centreless grinding with no reduction in the quality of the finished component.

v) The graphs of grinding forces versus infeed-rate indicated that

the materials ground experimentally were in the "easy-to-grind" category.

vi) The magnitudes of the grinding forces and the surface roughness can be reduced by increasing the grinding wheel speed, reducing the workpiece speed or by altering both, for constant removal rates.

vii)The results suggest an optimum speed ratio range for high-rate centreless grinding outside which grinding vibrations or burn are likely to be encountered.

viii) Increasing the grinding wheel speed from 30 m/s to 50 m/s results in worthwhile reductions in the grinding forces, attractive reductions in surface roughness and wheel wear ensue. Beyond 50 m/s there are diminishing returns and going beyond 60 m/s the reduction in forces is barely measurable.

ix) Wheel cutting ability increases with increasing infeed-rate and grinding wheel speed, and reduces with reducing workpiece speed.

x) Specific grinding energy is dependent on the grinding wheel speed, the dressing lead of the grinding wheel, the workpiece speed and the infeed-rate. It can be decreased by increasing the workpiece speed, the infeed-rate and the dynamic cutting-edge separation. Reducing the grinding wheel speed reduces the value also. These parameters can be varied separately or in combination.

xi) Vibrations obtained whilst grinding with the present system are most likely to occur at q-ratios below 100 (higher workpiece speeds).

xii) Grinding vibrations are more severe at higher grinding wheel speeds.

xiii) The cases of violent vibration experienced during grinding could have been predicted had geometric stability charts been constructed.

xiv) Once a geometrically unstable grinding configuration has been encountered, a marginal change in the workpiece speed may be sufficient

to re-establish stability.

xv) The measured experimental parameters correlate with the theoretical parameters discussed in section 3.4.

xvi) Severe plastic deformation layers can be found in normalised En 9 steel components when grinding with very high stock removal rates, high grinding wheel speeds and low workpiece speeds. No corresponding deformation was found to occur in cast iron for similar conditions.

xvii) The Vickers pyramid hardness number of the deformation layer is larger than the bulk material value indicating that considerable work hardening had taken place.

xviii) A spark-out period of 4 - 5 seconds is sufficient to remove all evidence of the plastically deformed layer.

xix) The main grinding parameters appear to be simple power functions of equivalent chip thickness. The constants in the empirical equations are dependent on q-ratio.

5.0 CONDITIONS WHICH LIMIT HIGH-RATE CENTRELESS GRINDING

5.0 CONDITIONS WHICH LIMIT HIGH-RATE CENTRELESS GRINDING

5.1 Introduction

All manufacturing systems have operating limits which are governed by the process efficiency and machining capabilities of the system. To exploit a manufacturing process fully it is necessary to know what these limiting conditions are so that they can be avoided. Only then can the quality of the component and the efficient utilisation of the material be ensured.

High-rate centreless grinding has shown itself to be a feasible first machining process. However, the investigation detailed in section 4.0 indicated that some kinematic conditions can cause undesirable degradation of the workpiece, and in extreme circumstances, can jeopardise personnel safety. The principal forms of degradation are vibration marks, errors in roundness, excessive surface roughness, burn and possible surface cracking. Personnel safety is jeopardised when violent grinding vibrations are encountered, if grinding is continued, it would be probable that either the workpiece would be ejected or that the grinding wheel would burst. Normally the infeed rapid retract is operated once this regime has been entered, re-establishing control over the system.

At the onset of the programme of work to establish the conditions which limit high-rate centreless grinding, it was assumed that the principal parameters to be examined included, grinding vibrations, burn, machine power capacity, roundness, maximum and minimum operating speeds of the grinding wheel and surface roughness. Grinding vibrations, roundness and burn have been examined extensively by many other workers too numerous to mention. However, whilst the mechanisms which govern the parameters have been the subject of consideration, no one has amalgamated

the results to construct limit charts. No research papers could be used for comparison of the experimental results obtained. Rowe and Richards [73], and Rowe, Richards and Koenigsberger [75] did however suggest geometric stability charts for the centreless grinding process.

It is not the intention of this section to examine thoroughly all aspects of the conditions which limit grinding but merely to establish them. An extensive investigation of every phenomenon which can limit the rate of grinding would go beyond the scope of this thesis.

5.2 Objectives

i) To establish the conditions which limit high-rate centreless grinding.

ii) To construct limit charts.

5.3 Additional Machine Modifications

The transmission system fitted to the grinding machine transmitted sufficient vibration to limit the accuracy of grinding force measurements and also the dynamic wheel balancing. The vibration level transmitted had become unacceptable for the sensitive measurement equipment used. This system was superseded by the one shown in Plate 10. The grinding wheel spindle is connected to a final drive shaft via a flexible coupling. The shaft is supported by two bearing blocks mounted on stanchions braced by lengths of box section. A drive pulley is mounted between the two bearings (rolling element), thus the grinding wheel spindle receives a pure torque and does not experience the effects of variation in the dynamic belt tension or unbalance in the drive system. A layshaft is mounted on the base plate. It is possible to interchange the pulleys throughout the system, this ensures that the drive motor may always be run at its optimum speed and power level. The maximum design speed of

the final drive shaft is 4440 r.p.m., giving a maximum surface speed for the grinding wheel of 120 m/s. No further modifications were deemed necessary.

5.4 Materials for the Investigation

The choice of materials for the investigation was explained previously (section 1.4), for consistency of the theme En 9 steel and cast iron were used again. Unfortunately the supply of sintered iron powder compacts was exhausted.

5.5 Specimen Preparation and Experimental Procedure

The specimens were prepared in the manner described in section 4.4 . A similar experimental procedure to that described in section 4.5 was used. However, there were two principal differences, a) the components used in the burn trials were pre-ground to remove traces of previous burn, and b) the q-ratio range was extended to cover values from 20 to 600. Some components were ground with spark-out and some were ground without. Incipient burning was revealed by swabbing the components with a 2 % nital solution.

5.6 Technique for Obtaining the Grinding Ratio

To obtain a measure of the grinding ratio (G-ratio) a fixture was designed to accept thin pieces of aluminium plate. The fixture was accommodated in the diamond locating hole in the dressing attchment after the diamond had been removed. By careful infeeding, the aluminium plate was plunged into the rotating grinding wheel. The dressing attachment was positioned over the boundary between worn and unworn areas of the grinding wheel. The step obtained after "replication" of the worn and unworn sections was a direct measure of the radial grinding wheel wear. By knowing the

total stock removed and the magnitudes of the radial wheel wear a value for the grinding ratio could be determined. The magnitude of the step was measured using a shadow graph.

5.7 Experimental Results

i) Effect of Grinding Wheel Speed on the Onset of Grinding Vibrations

In section 4.8.7 it was shown that grinding vibrations are likely to occur at high workpiece speeds (q-ratios $<\approx 90$) depending upon other conditions. Figures 71 and 71a are graphs of q-ratio versus grinding wheel speed for various infeed-rates. The graphs demonstrate the effect of grinding wheel speed on the trend of grinding vibrations. The graph is split into three regions. The upper region is a safe grinding region (indicated on the graph) where grinding vibrations will not normally be encountered. A second region is indicated which is a transition zone where grinding can be conducted but the probability of chatter is high. The third region is where violent vibrations are encountered, and pronounced workpiece waves are obtained. An interesting feature of the graphs, is the trend of grinding vibration with grinding wheel speed. Increasing the grinding wheel speed has the effect of increasing the value of the q-ratio at which the vibrations will be found. For cast iron the trend is steeper.

Plate 11a and 11b contain Talyrond traces for components ground with and without chatter. The roundness error of a component ground with chatter is significantly larger than one ground without. The trace emphasises the workpiece waves on the chattered component.

Plate 12 illustrates the workpiece waves that are found on components which have been ground in the "chatter region" of the graphs in Figures 71 and 71a. The workpiece material was En 9 steel, but similar results

are obtained for cast iron. The component was ground with a grinding wheel speed of 60 m/s, with an infeed-rate of 0.055 mm/s and a q-ratio of 50, the number of workpiece waves was 32. It was found that components ground at high grinding wheel speeds had more pronounced workpiece waves than components ground at lower grinding wheel speeds.

Plate 13 illustrates a phenomenon peculiar to En 9 steel; just prior to the onset of chatter, a ring which became recognised as a characteristic indicator of the onset of chatter appeared on the surface of the workpiece. The ring stood proud and its position along the workpiece length was variable and independent apparently of set grinding conditions. The ring was thicker and wider on components ground at lower grinding wheel speeds. Roundness and surface roughness degrade appreciably once this condition occurs. The surface of the grinding wheel was damaged also and required redressing.

For En 9 steel the number of workpiece waves caused by violent grinding vibrations when experimenting with high values of workpiece speed varied in the range 14 to 20, but the predominant number of waves was 20. At low workpiece speeds (q-ratios above 250) some workpiece waviness was indicated on the Talyrond traces and occasionally, it was observed on the workpiece surface. This type of vibration normally manifest as a "rumble" during grinding, it was non-violent in nature. The range of the numbers of workpiece waves was 18 to 56 and often accompanied burn. In the case of cast iron workpieces, waviness was observed only at high workpiece speeds (q-ratio < 100). The range of values for the number of waves was 16 to 26, no particular value being dominant, but the trend was such that more workpiece waves were found on components ground at lower workpiece speeds with chatter.

Table 13 details the incidences of vibration for both materials and the

grinding conditions used. The frequencies of the workpiece waves are somewhat higher than those reported in section 4.0 (this may be due to the change in the transmission system since all other conditions remained the same), and tended in the main, to be larger than the nearest machine natural frequencies. For En 9 steel, Table 13a, there were four instances from a total of twelve where the frequency of workpiece waves approximates a natural frequency of the machine. For cast iron, Table 13b, there were eleven instances from a total of nineteen where the natural frequencies of the machine approximate the frequencies of workpiece waviness. In only two instances (for both materials) the number of workpiece waves does not correspond with an integer number coincident with a trough on the stability chart, and there is no apparent relationship between the wheel and workpiece rotational frequencies or ratios thereof and the number of workpiece waves. Workpiece regenerative chatter was the probable cause of the workpiece waviness.

Table 13c presents the results for En 9 steel ground at low workpiece speed, q-ratio > 248, and the records of non-violent vibrations which marked the workpiece surface. The principal difference between the results obtained at these q-ratios to those discussed previously was the very low values for the frequencies of workpiece waviness. Again no apparent relationship existed between the grinding wheel and workpiece speeds and the frequencies of workpiece waves. The number of waves tended to be consistent with integer values coincident with troughs on the geometric stability charts suggesting workpiece regenerative chatter.

ii) Effect of Workpiece Speed and q-ratio on Surface Roughness

The graphs of surface roughness versus q-ratio for various infeed-rates and grinding wheel speeds are shown in Figures 72 to 75. The first two figures are for En 9 steel and the remainder are for cast iron. For

q-ratios below 80 approximately, the trend of the surface roughness increases with a decrease in q-ratio, this is the case for both materials. The graphs include the results obtained from components ground with chatter, which appears to influence the surface roughness value considerably, increasing it beyond the anticipated trend shown dotted. The effects of grinding wheel speed and infeed-rate are the same as discussed previously in section 4.8.

The graphs in Figures 76 and 77 show the effect of low workpiece speeds, q-ratios > 250, on the trends of surface roughness. The previous graphs, Figures 72 to 75, indicated that the trend of surface roughness increased with workpiece speed or decreased with increased q-ratio but with diminishing returns above a value of approximately 80. At low workpiece speeds (q-ratio > 200), the trend of surface roughness is to start increasing once more. If burn is encountered the finish tends to deteriorate even faster.

iii) Effect of q-ratio on Roundness Error

Figures 78 to 81 present the graphs of roundness error versus q-ratio for both cast iron and En 9 steel. The dominant parameter influencing roundness error in the experimental programme, as suggested by the results, was workpiece speed as expressed by q-ratio. Little difference was obtained in the values of roundness error for the various infeed-rates and grinding wheel speeds investigated.

The hard-line drawn as a boundary to the points on the graphs represents the overall trend of the results and indicates as might be anticipated a range of workpiece speeds (low values of q-ratio) where the workpiece roundness deteriorates as a result of chatter. There is also a region of low workpiece speeds, at high q-ratios, where the roundness deteriorates

once more. This region corresponds to the conditions for burn and occasionally some chatter. The deterioration in roundness at low workpiece speeds may be attributed to the reduced number of revolutions in which to achieve a rounding action [76].

The trend of the broken-line shows that at certain workpiece speeds there are peaks in the roundness error which can be interpreted as being decidedly unfavourable grinding conditions. Figures 82 to 85 allow comparison between the results obtained experimentally and those of Spraggett [77]. The roundness errors obtained by the author are considerably larger than those of Spraggett. Spraggett was able to correlate the number of workpiece waves with the value of Ng/Nw, this was not possible with the present results. Spraggett attributed his result to a disturbance related to grinding wheel speed i.e. possible wheel unbalance.

5.8 Grinding Ratio

The grinding ratio (volume of metal removed/volume of grinding wheel worn away) was plotted against stock removed, the results are shown in Figure 86. The trends obtained are similar to those obtained by Opitz and Guhring [8]. The trend is one of increasing grinding ratio with increased stock removal upto a plateau value, afterwhich it remains constant. The graph indicates that some wheel conditioning takes place initially and the comments made regarding Figure 51, section 4.8 are applicable here also. Higher grinding wheel speeds and lower infeed-rates yield higher grinding ratios. The initial wear rate of the wheel used to grind the cast iron components is similar to that of the wheel used to grind the steels except that it reaches its plateau value earlier. This implies that it has a higher wear rate and as such a lower wheel life. Although the influence of workpiece speed was not investigated it is very probable that low workpiece speeds will result in higher

grinding ratios and therefore longer wheel life. It is assumed that wheel wear is likely to depend upon the magnitude of the normal force which in turn is dependent on workpiece speed.

5.9 Boundary Conditions

i) Introduction

From purely kinematic considerations, the prediction of chatter and burn is not directly possible. However, it was possible to predict the theoretical power limitation trends in section 3.4.4, and these were illustrated in Figure 38b. Figures 87 and 88 illustrate experimentally-determined power limitation trends for cast iron and En 9 steel ground at two grinding wheel speeds. The experimental chatter and burn boundaries are shown also. The shape of the theoretical and experimental trends for power limitation correlate, and the influence of grinding wheel speed on the trends is consistent. The experimental results confirm the prediction that higher stock removal rates are possible, for the same power limit, by increasing the grinding wheel speed or by reducing the workpiece speed.

ii) Limits to High-Rate Centreless Grinding

Construction of limit charts of significance and in which the important parameters were displayed was not a simple matter. The charts in Figures 89 to 92 are the most informative and are complementary.

The speed ratio has been established by the author as a useful kinematic parameter which allows the effect of varying workpiece speed to be related to the magnitude of the idealised chip dimensions and grinding performance parameters. It is also a significant parameter influencing the limiting boundaries in centreless grinding and as such is used as

a coordinate in both sets of graphs presented.

Figures 89 and 90 demonstrate the chatter, burn and power limit lines drawn as boundaries to regions where chatter, burn and power limitations have been determined experimentally. Figure 89 is for cast iron and Figure 90 is for En 9 steel. The power limit was set at a value just below the maximum power supply available to the constant speed d.c. main drive motor. The figures indicate that in practice a narrow band of q-ratios are available to the operator in which machining can take place without encountering chatter or burn. It is clear also that at higher grinding wheel speeds the power limit is shifted allowing higher infeed-rates to be employed, thus higher stock removal rates are possible at the higher grinding wheel speed. A wider range of infeed-rates within the power limit lines are available when machining cast iron than for En 9 steel.

Figures 91 and 92 illustrate the limitations of workpiece speed as expressed by q-ratio and grinding wheel speed. The upper limit on grinding wheel speed is the maximum operating speed limit of the grinding wheel set by the wheel manufacturer. There is no lower limit, but low speed grinding is characterised by high surface roughness values, very low grinding ratio and low removal rate at the maximum permissible torque on the grinding wheel. Stable grinding conditions are limited by the workpiece speed. The burn boundaries move up and down according to the infeed-rate used. The chatter boundary is almost independent of the infeed-rate, it consists of two lines, a broken-line and a hard-line. Below the broken-line exists a transition zone where it is possible to grind but it is probable that some grinding vibrations will be encountered. Below the hard-line chatter is inevitable. At low and high grinding wheel speeds the burn and chatter boundaries converge. The

boundaries are at their widest at a grinding wheel speed of approximately 40 m/s which provides the largest range of permissible workpiece speeds. The graphs are similar for cast iron and En 9 steel. The charts presented are for specific grinding conditions, wheel types, dressing technique, coolant type, coolant supply technique, and workpiece material, and will be affected by variations in these parameters. An exhaustive investigation was not practicable.

iii) Optimisation for High-Rate Centreless Grinding

The graphs presented in this section show the importance of q-ratio on surface roughness, roundness error, burn limits, chatter limits and power limits. Quite clearly, the information obtained could be used as a data base from which an adaptive control strategy could be formulated. By monitoring and controlling grinding forces, power supplied to the machine, infeed-rate, grinding wheel and workpiece speeds, operation between the boundaries could be effected. With such a system it may be feasible to insert a component between the wheels without specifying all the grinding conditions, and allowing the system to hunt the optimum conditions.

Having established the limits to achieve satisfactory grinding performance, high rate centreless grinding can be exploited. By judicious choice of operator controlled grinding parameters it is also possible to combine required finish with high infeed-rate and stable grinding conditions. The possibility of rough grinding a component and finish grinding a component within a single grinding cycle is now feasible. Such a cycle would require inprocess variable kinematics to present a component of desired roundness, surface roughness and dimensional accuracy without thermal damage or loss of surface integrity.

5.10 Conclusions

i) The parameter defined as the q-ratio is a useful parameter that expresses the relationship between the grinding wheel and workpiece speeds. For a given grinding wheel speed, the workpiece speed as expressed by q-ratio has an appreciable influence on surface roughness, roundness error, burn limit, chatter limit and power limit.

ii) The correct choice of workpiece speed and hence q-ratio is important to avoid chatter and burn. Too high a workpiece speed (q-ratio too low) results in chatter and too low a workpiece speed (q-ratio too high) results in burn with the further possibility of chatter.

iii) The stable range for workpiece speed and hence q-ratio is dependent on grinding wheel speed. The range is greatest for a grinding wheel speed of 40 m/s.

iv) The boundaries are not strictly deterministic. There is a range in which it is possible to grind some workpieces satisfactorily but the frequency of unsatisfactory operation increases. This was particularly evident with the incidence of chatter.

v) The boundaries may be moved by selecting different operator controlled parameters such as dressing lead or wheel grade.

vi) The workpiece waves are more pronounced on components ground at higher grinding wheel speeds with chatter and the vibrations are more violent than those obtained at lower grinding wheel speeds.

vii) The results contained in the limit charts provide the basis for a data based adaptive control strategy to be formulated.

6.0 PRACTICAL IMPLICATIONS OF THE WORK

6.0 PRACTICAL IMPLICATIONS OF THE WORK

Experimental investigations using the developed machine have demonstrated that the plunge feed centreless grinding process is capable of achieving high stock removal rates an order of magnitude or more higher than current industrial practice. This is possible even with a single point diamond wheel dressing technique and water based cutting fluid. Enquiries into industrial practices undertaken by the author [78] showed that in the case of the cast iron components, the removal rate achieved when centreless grinding plain cylindrical components was more than four-fold that obtained by turning similar components on the centrelathe.

To achieve high stock removal rates by the grinding process, it is necessary to supply considerably more power to the machine than would be required by a centrelathe to achieve the same stock removal. Grinding wheel life and the frequency of grinding wheel redressings are very much dependent on the grindability of the materials being ground. Thus, economic high-rate grinding may be restricted to materials with which high grinding ratios are associated. Such materials fall into the "easy-to-grind" material category. Practical utilisation of grinding as a first machining process may influence subsequently the choice of workpiece material.

In order to use the dependence of the idealised undeformed chip data upon grinding conditions to select optimum grinding conditions for given requirements of surface roughness and production rate, it is helpful to employ an accurate solution for the kinematic model of grinding. This also helps to provide an understanding of the relationship between idealised chip data and actual grinding performance parameters. From the solutions proposed, grinding force and power trends can be predicted

in terms of the operator set parameters of grinding wheel and workpiece speeds and infeed-rate. It has been shown that a limited number of experiments can be employed to extrapolate grinding trends using kinematic relationships. Predictions of grinding trends have been substantiated by grinding experiments. A few carefully chosen grinding trials in conjunction with the appropriate uncut chip data could be invaluable in selecting suitable grinding conditions for given grinding performance requirements.

The ability to achieve high stock removal rates with the centreless grinding process whilst plunge feeding, suggests that form grinding becomes an increasingly practicable proposition. Here the use of precision castings and forgings could be exploited fully. The use of wide wheels and the low loading/unloading times associated with centreless grinding make it more attractive high production rate grinding process than the centretype grinding process.

In order to exploit high-rate centreless grinding, whilst avoiding chatter and burn, a suitable choice of stable grinding conditions must be made. Grinding results presented indicate the safe region of stable grinding conditions in terms of infeed-rate, grinding wheel speed and workpiece speed. For the centreless grinding process, where actual metal cutting is taking place throughout most of the operating time, a small increase in infeed-rate can be worthwhile.

To-date the choice of grinding wheels and coolant has been restricted. It may be possible to increase further the maximum metal removal rate obtained by improving the coolant type and grinding wheel grade used.

The sensitivity of the force measuring system to changes in the process may enable it to be used as the basis for adaptive control. Force level

which increases during the infeed period could provide the basis for control of the infeed-rate. Such a control system would monitor the geometric and kinematic stability of the process and keep power requirements within the supply capacity. The force level during dwell could control the spark-out period so as to achieve satisfactory accuracy and surface texture with improved production rates. It would also be possible to implement inprocess variable kinematics as a further strategy to improve production rates and achieve satisfactory accuracy. With this approach a component can be brought through a roughing operation to a finished state within a single grinding cycle. During the first part of the cycle, the workpiece speed would be held low to maximise the infeed-rate and to condition the grinding wheel also. Near the end of the cycle, the workpiece speed and/or the grinding wheel speed would be adjusted to values appropriate to achieving the required roundness accuracy and surface finish while the infeed-rate is necessarily adjusted.

7.0 RECOMMENDATIONS FOR FUTURE WORK

7.0 RECOMMENDATIONS FOR FUTURE WORK

i) Investigation of Difficult to Grind Materials

The present investigation was limited to plunge feed grinding of easy-to-grind materials. Future experiments should examine the favourable conditions for centreless grinding of more difficult to grind materials such as titanium, hardened steels and ceramics.

ii) Sintered Iron Powder Compacts

The limited availability of the P.M. components restricted a thorough investigation. Results obtained were however, most encouraging and indicated that P.M. materials were ideally suited to high-rate centreless grinding. Iron P.M. components can be hardened effectively by surface hardening processes such as austenitic nitriding [79] and can be used as impregnated bearing surfaces [80]. As such they could become an important manufacturing medium.

iii) Improvements to the Machine

a) Some means for determining the grinding wheel wear needs to be devised and incorporated in the machine set-up so that this is a more readily available parameter for future use.

b) The present infeed device has a total stroke of $\frac{1}{2}$ mm, this would be inadequate for large stock removal applications which include formed work and grinding of poor quality castings and forgings.

iv) In Process Variable Kinematics

By changing the grinding conditions during the grinding cycle it should be possible to maximise the metal removal rate for the main part of the grinding cycle and the alter the conditions to achieve the required

finish and roundness for the end of the grinding cycle. A preliminary investigation of in process variable kinematics is necessary to establish whether such a technique is feasible pracically. A manual adjustment of wheel speeds may be sufficient to establish an initial feel for the process.

v) Control Strategy and Optimisation

The boundary conditions determined experimentally can be used as the basis of a control strategy, one which is data based. Linear programming may be able to provide a mathematical solution to achieve optimum grinding performance within the experimentally determined constraints. A microcomputer control system fed from the transducers on the machine could determine whether the optimum machining conditions were being implemented, adjusting parameters as necessary.

vi) Investigation of Presently Fixed Parameters

The experimental programme was intentionally restricted to investigate the influence of variation of kinematic conditions only, with other parameters such as dressing lead, dressing technique, wheel grade, coolant type (dilution and supply technique) and set-up geometry chosen and maintained constant as optimum values quoted by other workers. It may be possible to improve high-rate centreless grinding further by examining the influence of variations in these parameters which were maintained constant.

vii) Formed Work

The experimental work undertaken was limited to plain cylindrical components. Future work should incorporate the grinding of formed components particularly in the high-rate grinding regime. Points of

interest arising from such studies would include grinding ratios, grinding forces, and the cost effectiveness of producing formed components by grinding.

viii) Through Feed Centreless Grinding

Plunge feed centreless grinding was investigated only, an investigation of high-rate through feed centreless grinding is currently of interest to industry and would in itself be an interesting academic exercise.

ix) Idealised Undeformed Chip Model

The uncut chip solutions for the accepted kinematic model of plunge feed cylindrical grinding proposed in this thesis were used to predict the trends of grinding forces and power for various values of infeed-rate, workpiece speed and grinding wheel speed. The theoretical trends obtained were substantiated by experimental results.

Presently no theoretical expressions exist for burn and chatter prediction. However, attempts to establish such expressions will be made by the author and hopefully it will be shown that the theoretical and experimental results describing boundary conditions in centreless grinding will be in full agreement.

x) Ring on En 9 Steel Components

The ring found on En 9 steel components just prior to encountering chatter was an interesting phenomenon which has not been disclosed by other workers - further investigation is necessary.

8.0 BROAD CONCLUSIONS

8.0 Broad Conclusions

1) The practicability of utilising centreless grinding as a first machining operation in the plunge feed mode, when grinding materials in the easy-to-grind category, has been demonstrated.

2) Large gains in stock removal rates can be obtained by using higher grinding wheel speeds, higher infeed-rates, and by judicious choice of workpiece speed to avoid chatter and burn.

3) A substantial data bank has been established from the results obtained in the experimental programmes allowing a thorough examination of the influence of operator control parameters on grinding performance to be made.

4) The results of the grinding trials for ferrous materials can be understood in terms of the uncut chip model. The analysis of the uncut chip dimensions along with appropriate grinding trials can be used as a basis for selecting optimum grinding conditions for given requirements of finish and production rate.

5) Predictions of the trends of theoretical grinding forces are substantiated by experimental results.

6) If the theoretical predictions of boundary conditions in centreless grinding can be formulated, it will be possible to develop a control strategy for C.N.C. centreless grinding.

7) Very high stock removal rate grinding may cause loss of surface/subsurface integrity of the components. This can be avoided by using in process variable kinematics to achieve roughing and finishing operations within a single grinding cycle.

References

References

[1] Woodbury, R.S., "History of the Grinding Machine", 1964, M.I.T. Press, Massachusettes.

[2] Rowe, W.B., "Some Studies of the Centreless Grinding Process with Particular Reference to the Roundness Accuracy", Ph.D. Thesis, U.M.I.S.T., 1964

[3] Anon, "Machine Tool Manual", Wickman-Scrivener, circa 1975.

[4] Gough, T., and G. Sweeney, "Grinding Research in Relation to the Likely Developments of Grinding Technology in the United Kingdom Over the Next Five-To-Ten Years", Survey Commissioned by the Science and Engineering Research Council, 1974.

[5] Sweeney, G., "Trends in Grinding", Conference at the Polytechnic of Central London, 1977.

[6] Hinderwell, F.B., "Introduction", One-Day Seminar on High-Speed Grinding, M.T.I.R.A., 1972.

[7] Brough, D., "Feasibility Study on the Grinding of Cast Iron Cylinder Liners", Interim Report, Liverpool Polytechnic, 1977.

[8] Opitz, H., and K. Guhring, "High-Speed Grinding", C.I.R.P. Annals, Vol. 16, 1968.

[9] Konig, W., and M. Dederichs, "Surface Grinding with High Wheel Speeds and Metal Removal Rates", 13th Int.M.T.D.R. Conf., 1972.

[10] Kobayashi, A., K. Takazawa, M. Harada, and M. Horike, "Study of High-Speed Centreless Grinding", Proc. Int. Grinding Conf., 1972.

[11] Discussion with Machine Tool Manufacturer - Wickman-Scrivener, circa, 1976.

[12] Various Trade Literature.

[13] Fenner Power Transmission Design Manuals, 110/77.

[14] Cookson, J.O., "An Introduction to Cutting Fluids", Tribology International, February, 1977.

[15] Ernst, W., "Erhohte Schnittgeschwindigkeit beim Außenrund - Einstechschleifen und ihr Einfluß auf das Schleifergebnis und die Wirkschaftlichkeit", Diss., T.H. Aachen, 1964

[16] Hauser, H., "Mist Cooling", Microtechnic, Vol. 18, 1964.

[17] Furuichi, R., and M. Nakayama, " On the Grinding Performance of Treated Wheels", Memoirs of the Faculty of Engineering, Osaka University, Vol. 7, 1965.

[18] Trmal, G., and H. Kaliszer, "Delivery of Cutting Fluid in Grinding", 16th Int. M.T.D.R. Conf., 1975.

[19] Palmer-Lewis, I., and R.M. Baul, "Coolant Supply for High-Speed Grinding", Metal Working Production, December, 1968.

[20] Graham, W., and M.G. Whiston, "Some Observations of Through-Wheel-Coolant Application in Grinding", Int. J. Mach. Tool. Des. Res., Vol. 18, 1978.

[21] Anon, " On the Grinding Action of Grinding Wheels Containing Solid Lubricants", J. Soc. Mech. Engrs., Japan, Vol. 26, 1960.

[22] Shafto, G.R., T.D. Howes, and C. Andrews, "Thermal Aspects of Creep Feed Grinding", 16th Int. M.T.D.R. Conf., 1975.

[23] Powell, J.W., "Coolant Applications in Creep Feed Grinding : An Interim Report on Shoe Design", Bristol University, 1976.

[24] Furuichi, R., M. Nakayama, T. Doi, and H. Tamura, "Influence of Supply Conditions of Grinding Fluids on Grinding Performance on Free-Infeed Plunge Grinding", Bull. J.S.E.E., Vol. 9, 1966.

[25] Den Hartog, J.P., "Strength of Materials", Dover Edition, Published by Constable, 1961.

[26] Barlow, N., and W.B. Rowe, " Discussion of Stresses in Plain and Reinforced Cylindrical Grinding Wheels", Int. J.M.T.D.R. Agreed for Publication, 1983.

[27] Brough, D., and W.B. Rowe, "Aspects of High-Speed Centreless Grinding", 1st Joint Polytechnic Symposium on Manufacturing Engineering, Leicester Polytechnic, 1977.

[28] Shaw, M.C., "A New Wheel Concept for High-Speeds", Abrasive Engineering, January, 1971.

[29] Southwell, K.B., "Vitrified Wheels for High-Speed Use", One Day Seminar on High-Speed Grinding, M.T.I.R.A., 1972.

[30] Malkin, S., and T. Murray, "Comparison of Single Point and Rotary Dressing of Grinding Wheels", Proc. 5th North American Metal Working Res. Conf., 1977.

[31] Pattison, E.J., and A.W.J. Chisholm, "The Effect of Dressing Techniques on Grinding Wheel Wear", University of Salford.

[32] Sweeney, G., and A.R. Thorn, "Safety in Grinding", Proc. 16th Int. M.T.D.R. Conf., 1975.

[33] Anon, "Manifolds and Side-Inlets", General Electric Data Books (Heat Transfer and Fluid Flow), 1974.

[34] Keller, J.D., "Design of Manifolds and Pipe Burners", Industrial Heating, January, 1952.

[35] Rowe, W.B., and J.P. O'Donoghue, "Diaphragm Valves for Controlling Opposed Pad Hydrostatic Bearings", I. Mech. E., Tribology Convention, 1970.

[36] Brough, D., W.B. Rowe, W. Weston, and W.F. Bell, "Diaphragm Compensated Hydrostatic Bearings for Achieving and Monitoring High-Speed Centreless Grinding", 2nd Joint Polytechnic Symposium on Manufacturing Engineering, Lancaster Polytechnic, 1978.

[37] Opitz, H., W. Ernst, and K.F. Meyer, "Grinding at High Cutting Speeds", 6th Int. M.T.D.R. Conf., 1965.

[38] Bell, W.F., D. Brough, and W.B. Rowe, "Calculation of Undeformed Chip Parameters for High Grinding Rates", 3rd Joint Polytechnic Symposium on Manufacturing Engineering, May, 1982.

[39] Alden, G.I., "Operation of Grinding Wheels in Machine Grinding", Trans. A.S.M.E., December, 1914.

[40] Pahlitzsch, G., and H. Helmerdig, "Einfluss des Abriehtens mit diamantbestuckten Rollen auf die Feingestalt der Schleifscheibenschneidflache", Werkstattstechnik 58 J.g., Helf 1, Jan., 1968.

[41] Reichenbach, G.S., J.E. Mayer, S. Kalpakcioglu, and M.C. Shaw, "The Role of Chip Thickness in Grinding", Trans. A.S.M.E., Vol. 78, 1956.

[42] Peklenik, J., "Ermittlung von geometrischen und physikalischen Kenngrossen fur die Grundlagenforschung des Schleifens", Diss., T. H. Aachen, 1957.

[43] Okamura, K., and L. Lemon, "Study of Grinding Process as Applied to High Strength Thermal Resistant Alloys", Interim Engineering Report, 1966.

[44] Kassen, G., "Beschreibung der elementaren Kinematic des Schleifvorganges", Diss., T.H. Aachen, 1969.

[45] Werner, G., "Kinematic und Mechanik des Schleifprozesses", Diss., T.H. Aachen, 1971.

[46] Rowe, W.B., and K. Stout, "Review of Grinding Process Parameters", Engineers Digest, Vol. 32, 1971.

[47] Snoeys, R., and J. Peters, " The Significance of Chip Thickness in Grinding", C.I.R.P. ANN(Swit), Vol. 23, 1975.

[48] Vukasojevic, R.S., D. Brough, and W.F. Bell, "New Parameters for Specifying the Cutting Quality of Grinding Wheels", 3rd Joint Polytechnic Symposium on Manufacturing Engineering, May, 1982.

[49] Brough, D., W.F. Bell, and W.B. Rowe, "A Re-examination of the Uncut Chip Model of Grinding and its Practical Implications", 24th M.T.D.R. Conf., 1983.

[50] Malkin, S., and N. Joseph, "Minimum Energy in Abrasive Processes", Wear, Vol. 32, 1975.

[51] Boothroyd, G., "Fundamentals of Metal Machining and Machine Tools", Mc Graw - Hill, 1975.

[52] B.S. 1134, "Method for the Assessment of Surface Texture", Parts 1 and 2, 1961.

[53] Galyer, J., and C. Shotbolt, "Metrology for Engineers", Published by Cassell, 4th Edition, 1981.

[54] Konig, W., and W. Lortz, "Properties of Cutting Edges Related to Chip Formation in Grinding", C.I.R.P. ANN., Vol. 24, 1975.

[55] Guhring, K., "Hochleistungsschleifen - Ein Methode zur Leistungssteigerung der Schleifverfahren durch hohe Schnittgeschwindigkeiten", Diss., T.H. Aachen, 1967.

[56] Hahn, R.S., and R.P. Lindsay, "The Influence of Process Variables on Material Removal, Surface Integrity, Surface Finish and Vibration in Grinding", 10th Int. M.T.D.R. Conf., 1969.

[57] El-Helieby, S.O.A., and G. Rowe, "Grinding Cracks and Microstructural Changes in Ground Steel Surfaces", Metal Technology, Feb., 1981.

[58] Anon, "What is Gained by High-Speed Grinding", Metal Working Production, November, 1968.

[59] Wick, C., "Switch to Centreless Grinding Boosts Productivity", Manufacturing Engineering, June, 1978.

[60] Duckworth, W.E., "Statistical Techniques in Technological Research", Methuen, 1967.

[61] Pande, S.J., and G.K. Lal, "Effect of Dressing on Grinding Wheel Performance", Int. J.M.T.D.R., Vol. 19, 1979.

[62] Pacitti, V., and C. Rubenstein, "Influence of Dressing Depth of Cut on the Performance of a Single Point Diamond Dressed Alumina Grinding Wheel", Int. J.M.T.D.R. , Vol. 12, 1972.

[63] Hahn, R.S., "On the Mechanics of the Grinding Process Under Plunge Cut Conditions", Trans. A.S.M.E., Feb., 1966.

[64] Lindsay, R.P., and R.S. Hahn, "On the Basic Relationships Between Grinding Parameters", C.I.R.P. ANN., Vol. 19, 1971.

[65] Bell, W.F., D. Brough, and W.B. Rowe, "High-Rate Centreless Grinding of Ferrous Components", 24th M.T.D.R. Conf., 1983.

[66] Salje, "Gesetzmaßigkeiten and Kennzahlen beim Schleifen", Diss., T.H. Aachen, 1952.

[67] Fletcher, N.P., "Single Point Diamond Dressing of Aluminium Oxide Grinding Wheels and its Influence in Cylindrical Traverse Grinding", Int. J.M.T.D.R., Vol. 20, 1978.

[68] Willmore, J.J., "Plunge Grinding and the Accuracy of the Workpiece Geometry", 6th Int. M.T.D.R. Conf., 1965.

[69] Lortz, W., "A Model of the Cutting Mechanism in Grinding", Wear, Vol. 53, 1979.

[70] Schreitmuller, H., "Kinematic Basis for the Practical Application of Centreless High Performance Grinding", Diss., T.H. Aachen.

[71] Tarasov, L.P., "Detection, Causes and Prevention of Injury in Ground Surfaces", Trans. Am. Soc. Met., Vol. 36, 1946.

[72] Krug, C., "Beitrage zur Kenntnis des Schleifens", Machinenbau, No. 4, 1925.

[73] Rowe, W.B., and D.L. Richards, "Research Note : Geometric Stability Charts for the Centreless Grinding Process", Journal Mech. Eng. Sciences, Vol. 14, No. 2, 1972.

[74] Rowe, W.B., W. Weston, and S. Xu, Work to be Published, part of an S.E.R.C. Research Project, 1981/82.

[75] Richards, D.L., and W.B. Rowe, and F. Koenigsberger, "Geometrical Configurations for Stability in the Centreless Grinding Process", 12th M.T.D.R. Conf., Sept., 1971.

[76] Spraggett, S., and W.B. Rowe, "The Design and Development of a New Centreless Grinding Machine", 3rd Joint Polytechnic Symposium on Manufacturing Engineering, May, 1982.

[77] Spraggett, S., "The Development and Application of a Rig for the Investigation of the Centreless Grinding Process", Ph.D. Thesis, 1979.

[78] Bell, W.F., "Internal Research Visit Report", Liverpool Polytechnic, 1978.

[79] Brough, D., and J. Schofield, "Gamma-nitriding of Porous Iron P.M. Components", Powder Metallurgy, No. 2, 1978.

[80] Lancaster, J.K., "Composite Self-Lubricating Bearing Materials", Proc. I. Mech. E., Vol. 182, Part 1, No. 2, 1967.

[81] Guest, J.J., "The Theory of Grinding, with Reference to the Selection of Speeds in Plain and Internal Work", Proc. I. Mech. E., Oct., 1915.

[82] Thompson, D.L., and S. Malkin, "Grinding Wheel Topography and Undeformed Chip Shape", Proc. Int. Conf. on Prod. Eng., Tokyo, 1974.

[83] Hahn, R.S., and R.P. Lindsay, "Principles of Grinding", Machinery, 1971.

APPENDICES

APPENDIX 1

Material Specifications

i) Specification for the Cast Iron Components

Material Type:- Grey cast iron conforming to B.S.1452, Grade 14 for cylinder castings. The bar was sand cast.

Material Designation:- C.I. 14, as cast.

Chemical Composition

Element	Per Cent
Total carbon	3.0 - 3.5
Silicon	1.8 - 2.3
Manganese	0.7 - 1.1
Sulphur	- - 0.08
Phosphorous	- - 0.25
Chromium	0.3 - 0.5
Molybdenum	0.3 - 0.5

Mechanical Properties

U.T.S. = 255 MN/m^2

Hardness as cast - 217 to 277 Brinell

Structure:- Graphite, mainly types B and A with maximum associated free ferrite 10 %, phosphide is found as small particles dispersed evenly throughout a matrix of fine pearlite.

ii) Specification for the En 9 Steel Components

Material Type:- "55" Carbon steel for gears, machine tool parts requiring wear resistance. The material was received as bright bar in a normalised condition.

Material Designation:- En 9 steel - normalised.

Chemical Composition

Element	Per Cent
Carbon	0.5 - 0.6
Silicon	0.05 - 0.35
Manganese	0.5 - 0.8
Sulphur	- - 0.06
Phosphurous	- - 0.06

Mechanical Properties

U.T.S = 700 MN/m^2

Hardness as received - 210 Brinell

Structure:- The structure contains slightly more than 50 % pearlite "grains" with the remainder as ferrite.

APPENDIX 2

The Replacement Coolant System

The coolant system was supplied by F.S.P. (Filtration and Separation Products) Limited. The tank is split into three chambers each performing a specific function. The dirty coolant is fed into the inlet strainer of the settlement chamber, which retains any large particles from the machine tool. From the settlement tank coolant flows through a system of weirs and traps to the hydrocyclone chamber. The large particles are removed from the settlement tank by a drag link conveyor mechanism which deposits the swarf in a sludge bin.

The pump in the second chamber delivers coolant to the cyclone cells at the required pressure. Coolant is passed into the cell by means of an axial distributor. The axial distributor sends the dirty coolant spiralling downwards, this process being called the primary vortex. While the dirty coolant is spiralling downwards, the particles in it are forced onto the wall of the cell. The restricting effect of the nozzle creates a rising secondary vortex which pushes the clarified coolant up the centre of the spiral towards the distributor. The sludge taken from the coolant as well as a small amount of coolant is discharged out through the nozzle and into the settlement tank. The clarified coolant then passes into the next cyclone cell where the process is repeated. A clarification level of 10 microns is claimed by the manufacturers. Clarified coolant is fed eventually to the storage tank.

The final chamber houses the delivery pump which is a Grundfos centrifugal pump capable of delivering coolant at a rate of 2 litres per second, at a pressure of 0.85 MPa. The quantity of coolant delivered to the machine

is regulated by a by-pass valve fitted in the delivery line.

APPENDIX 3

Derivation of Calibration Equation for the Force Measuring System

An applied load to the grinding wheel in a radial direction will give rise to pressure differentials in each pair of opposed recesses in the hydrostatic bearing. These pressure differentials are equivalent to 3 forces F_1, F_2, and F_3 acting in the directions 1, 2, and 3 shown in Figure 8. For example if a force F acts along direction 2 then the reaction is $F = F_2 + F_3.\cos60^\circ + F_1.\cos60^\circ$,

i.e. $F = F_2 + \frac{1}{2}.(F_1 + F_3)$ ..... (A1)

An out-of-balance mass m at a radial distance r from the wheel axis will give rise to a centrifugal force $4.\pi^2.n^2.m.r$ (where n is the rotational speed of the grinding wheel). This is manifest across each pair of recesses twice per revolution of the grinding wheel (in opposite senses) giving rise to 3 sinusoidal traces on the u.v. recorder. For a wheel in perfect balance initially this imposed centrifugal force could be related to the amplitude of the traces directly but any inherent unbalance in the grinding wheel complicates this. The total force acting on the wheel is the vector sum of the force $\underline{W}$ (due to the mass added deliberately) and $\underline{X}$ (due to the inherent unbalance of the grinding wheel). $\underline{X}$ is unknown but by putting two different masses m_p and m_q at three different positions j (j = a, b, c) on the wheel flange, at the same radial distance r from the centre, the effect of inherent wheel unbalance can be eliminated as follows.

The reaction force across a pair of recesses is proportional to the pressure difference across that pair of recesses and it has been verified that the displacement of the trace on the u.v. recorder varies linearly with pressure using a dead weight tester. When a force is directly in

line with a given pair of recesses, i, the reaction $F_i = K_i.A_i$, where A_i is the amplitude of the trace i, and K_i is the appropriate scale factor (reciprocal of sensitivity) in Newtons/mm for trace i (i = 1, 2, 3). When the applied force is a maximum across the pair of recesses at 2, it is 60° out of phase across recesses 1 and 3; the trace displacements 1 and 3 being $(A_1/2) + (A_3/2)$ at this instant. From equation (A1) the total reaction to the applied force $F(\underline{W} + \underline{X})$ is $F_2 + \frac{1}{2}.(F_1 + F_3) =$ $K_2.A_2 + \frac{1}{2}.(K_1.(A_1/2) + K_3.(A_3/2)) = K_2.A_2 + \frac{1}{4}.(K_1.A_1 + K_3.A_3)$.

Similarly for recesses 1 and 3,

Therefore, $\underline{W} + \underline{X} = K_2.A_2 + \frac{1}{4}.(K_1.A_1 + K_3.A_3)$

$= K_1.A_1 + \frac{1}{4}.(K_2.A_2 + K_3.A_3)$

$= K_3.A_3 + \frac{1}{4}.(K_1.A_1 + K_2.A_2)$

Hence, $\underline{W} + \underline{X} = \frac{1}{2}.\sum K_i.A_i = 3/2.\overline{K}.\overline{A}$ ..... (A2)

where $\overline{K}.\overline{A} = 1/3.(\sum K_i.A_i)$

N.B. $\underline{F}$ means vector F and $\overline{A}$ means average value of A.

If the inherent unbalanced force $\underline{X}$ makes an angle θ with direction a (towards b) then by the cosine rule applied to the appropriate triangle of forces in each case, Figure 12:-

$$(3/2.\overline{K}.A_a)_p^2 = W_p^2 + X^2 + 2.W.X.\cos\theta \quad \ldots\ldots\ldots\ldots\ldots\ldots \quad (A3)$$

$$(3/2.\overline{K}.A_b)_p^2 = W_p^2 + X^2 + 2.W.X.\cos(60 + \theta) \quad \ldots\ldots\ldots\ldots \quad (A4)$$

$$(3/2.\overline{K}.A_c)_p^2 = W_p^2 + X^2 + 2.W.X.\cos(60 - \theta) \quad \ldots\ldots\ldots\ldots \quad (A5)$$

Adding equations (A3), (A4) and (A5) results in,

$$9/4.K^2.\sum(\overline{A}_j)_p^2 = 3.W_p^2 + 3.X^2 \quad \ldots\ldots\ldots\ldots\ldots\ldots\ldots\ldots \quad (A6)$$

and similarly for mass m_q,

$$9/4.K^2.\sum(\bar{A}_j)_q^2 = 3.W_q^2 + 3.X^2 \quad \ldots\ldots\ldots\ldots\ldots\ldots\ldots\ldots\ldots \text{(A7)}$$

Subtracting (A7) from (A6) gives,

$$\bar{K} = \frac{4}{3}.\left(\frac{W_p^2 - W_q^2}{\sum(\bar{A}_j)_p^2 - \sum(\bar{A}_j)_q^2}\right) \quad \ldots\ldots\ldots\ldots\ldots\ldots\ldots\ldots\ldots \text{(A8)}$$

Now $W = 4.\pi^2.n^2.r.m$

Therefore, $\bar{K} = \frac{8}{\sqrt{3}}.\pi^2.n^2.r.\sqrt{\frac{m_p^2 - m_q^2}{\sum(\bar{A}_j)_p^2 - \sum(\bar{A}_j)_q^2}}$ ..... (A9)

K is the average scale factor for all three traces i, individual scale factors K_i can be found from ,

$$K = \bar{K}.\frac{\bar{A}}{A_i} \quad \ldots\ldots\ldots\ldots\ldots\ldots\ldots\ldots\ldots\ldots\ldots\ldots\ldots\ldots\ldots\ldots \text{(A10)}$$

APPENDIX 4

Expressions for θ_o and ϕ_o

From Figure 16,

$$\theta_o = \cos^{-1}.\left[\frac{(Rg + Rwn)^2 + (Rg)^2 - (Rw)^2}{2.(Rg + Rwn).Rg}\right] \quad \ldots\ldots\ldots\ldots\ldots\ldots \quad (B1)$$

and,

$$\phi_o = \cos^{-1}.\left[\frac{(Rg + Rwn)^2 + (Rw)^2 - (Rg + hg)^2}{2.(Rg + Rwn).Rw}\right] \quad \ldots\ldots\ldots\ldots\ldots \quad (B2)$$

Derivation of the Undeformed Chip Thickness

From equation (3.6) with hg assumed zero, the undeformed chip thickness $\bar{t}c$, is given by:-

$$\bar{t}c = Rg - Rd \quad \ldots\ldots\ldots\ldots\ldots\ldots\ldots\ldots\ldots\ldots\ldots\ldots\ldots\ldots \quad (B3)$$

Now,

$$(Rd)^2 = (Rg + Rwn)^2 + (Rw)^2 - 2.(Rg + Rwn).Rw.\cos\phi_d \quad \ldots\ldots \quad (B4)$$

$$Rd = Rg.\left[1 + \frac{2.Rwn}{Rg} + \frac{Rwn^2}{Rg^2} + \frac{Rw^2}{Rg^2} - 2.\left(1 + \frac{Rwn}{Rg}\right).\frac{Rw}{Rg}.\cos\phi_d\right]^{\frac{1}{2}} \ldots \quad (B5)$$

Therefore,

$$\bar{t}c = Rg - Rd = Rg.\left\{1 - \left[1 + \frac{2.Rwn}{Rg} + \frac{Rwn^2}{Rg^2} + \frac{Rw^2}{Rg^2} - 2.\left(1 + \frac{Rwn}{Rg}\right).\frac{Rw}{Rg}.\cos\phi_d\right]^{\frac{1}{2}}\right\}$$

$$\ldots\ldots\ldots\ldots\ldots\ldots\ldots\ldots\ldots\ldots \quad (B6)$$

From the Binomial expansion $(1 + x)^n \approx 1 + n.x$ if $x \ll 1$

Hence,

$$\bar{t}c = -\frac{Rg}{2}.\left[\frac{2.Rwn}{Rg} + \frac{Rwn^2}{Rg^2} + \frac{Rw^2}{Rg^2} - 2.\left(1 + \frac{Rwn}{Rg}\right).\frac{Rw}{Rg}.\cos\phi_d\right] \quad \ldots\ldots \quad (B7)$$

$$\bar{t}c = -\left[Rwn + \frac{Rwn^2}{2.Rg} + \frac{Rw^2}{2.Rg} - \left(1 + \frac{Rwn}{Rg}\right).Rw.\cos\phi_d\right] \quad \ldots\ldots\ldots\ldots \text{(B8)}$$

Substitute Rw - d for Rwn,

Hence,

$$-\bar{t}c = Rw - d + \left(\frac{Rw^2}{2.Rg} - \frac{2.d.Rw}{2.Rg} + \frac{d^2}{2.Rg}\right) + \frac{Rw^2}{2.Rg} - Rw.\left(1 + \frac{Rw}{Rg} - \frac{d}{Rg}\right)\cos\phi_d$$

$$\ldots\ldots\ldots\ldots\ldots\ldots\ldots\ldots\ldots\ldots\ldots\ldots\ldots\ldots\ldots\ldots \text{(B9)}$$

$$-\bar{t}c = Rw.(1 - \cos\phi_d) + \frac{Rw^2}{Rg}.\left(1 - \cos\phi_d\right) - \frac{d.Rw}{Rg}.\left(1 - \cos\phi_d\right) - d.\left(1 - \frac{d}{2.Rg}\right)$$

$$\ldots\ldots\ldots\ldots\ldots\ldots\ldots\ldots\ldots\ldots\ldots\ldots\ldots\ldots\ldots\ldots \text{(B10)}$$

Now $(1 - \cos\phi_d) << 1$ so that $1 - \cos\phi_d = \phi_d^2/2$, for $\phi_d = 10^\circ$ the error is less than $\frac{1}{4}$ %.

Thus,

$$-\bar{t}c = \frac{Rw.\phi_d^2}{2}.\left[1 + \frac{Rw}{Rg} - \frac{d}{Rg}\right] - d.\left(1 - \frac{d}{2.Rg}\right)$$

$$-\bar{t}c = \frac{Dw.\phi_d^2}{4}.\left[1 + \frac{Dw}{Dg} - \frac{2.d}{Dg}\right] - d.\left(1 - \frac{d}{Dg}\right) \quad \ldots\ldots\ldots\ldots\ldots \text{(B11)}$$

But from equation (3.8),

$\phi_d = \phi_o - B$, where $B = 2.ld.vw/(Dw.vg)$

and from equation (3.11),

$d = Dw.vi.\pi/vw$

therefore, $\phi_d = \sqrt{\frac{4.\pi.De.vi}{vw.Dw}} - \frac{2.ld.vw}{Dw.vg}$ $\ldots\ldots\ldots\ldots\ldots\ldots$ (B12)

and,

$$\phi_d^2 = \frac{4.\pi.vi.De}{vw.Dw} - \frac{4.ld.vw}{Dw.vg}.\sqrt{\frac{4.\pi.vi.De}{Dw.vw}} + 4.\left(\frac{ld.vw}{Dw.vg}\right)^2 \quad \ldots\ldots\ldots \text{(B13)}$$

Substituting (B13) in (B11) yields,

$$\bar{t}c = \left(1 - \frac{2.\pi.vi.De}{vw.Dg}\right) \cdot \left[\frac{ld.vw}{vg} \cdot \sqrt{\frac{4.\pi.De.vi}{vw.Dw}} - \frac{\pi.vi.De}{vw} \right. \quad \ldots\ldots$$

$$\left. - \left(\frac{ld.vw}{vg}\right)^2 . \frac{1}{Dw} \right] + \frac{\pi.Dw.vi}{vw} \cdot \left(1 + \frac{\pi.Dw.vi}{vw.Dg}\right) \quad \ldots\ldots \text{(B14)}$$

APPENDIX 5

Computer Print-out of Grinding Results

PERFORMANCE DATA

EXPERIMENT # 82/ENG-33L

	COMPONENT NO:-	41	42	43	44	45	46	47	48	UNITS.
INPUT DATA	WHEEL SPEED	60	60	60	60	60	60	60	60	M/S
	WORK SPEED	.43	.43	.43	.43	.43	.6	.6	.6	M/S
	Q-RATIO	140	140	140	140	140	100	100	100	---
	INFEED RATE	.159	.159	.223	.223	.223	.057	.057	.057	MM/S
	HEQ (X1000)	368	368	516	516	516	132	132	132	MICRONS
OUTPUT DATA	NORMAL FORCE	10.3	10.4	13.7	13.2	13.4	4.06	4.06	4.06	N/MM
	TANG.L FORCE	4.33	4.49	5.36	5.17	5.32	2.12	2.12	2.12	N/MM
	FN'/FT'	2.39	2.32	2.56	2.57	2.52	1.91	1.91	1.91	---
	RESULT.T FORCE	11.2	11.3	14.7	14.2	14.4	4.58	4.58	4.58	N/MM
	VOL/UNIT LENGTH	33.8	33.4	33.4	33.5	33.1	31.4	31.7	32.6	MMT3/MM
	Z' AVERAGE	7.52	7.44	8.37	8.37	8.29	3.49	3.53	3.63	MMT2/S
	Z' MAXIMUM	22.0	22.0	30.9	30.9	30.9	7.92	7.92	7.92	MMT2/S
	ELEC.POWER SUP.D	457	452	569	569	574	223	218	218	WATTS/MM
	POWER TO GRIND	260	270	322	310	319	127	127	127	WATTS/MM
	PROCESS EFFIC.Y	57	60	57	54	56	57	58	58	PERCENT
	SPECIFIC ENERGY	11.7	12.2	10.3	10.0	10.3	16.0	16.0	16.0	J/MMT3
	WHEEL C ABILITY	2.13	2.11	2.25	2.33	2.31	1.95	1.95	1.95	MMT3/N.S
	U. CHIP LENGTH	1441	1441	1707	1707	1707	730	730	730	MICRONS
	U. CHIP THICK.S	1.02	1.02	1.21	1.21	1.21	.71	.71	.71	MICRONS
	CHIP FORM.N TIME	24	24	28	28	28	12	12	12	MUSEC.
	SURFACE ROUGHNESS	0	0	0	0	0	0	0	0	MICRONS

GRINDING INFORMATION

A).GRINDING WHEEL GRADE	RA60K5VT0H			DIAMETER	.456 (M)
B).CONTROL WHEEL GRADE	A60 0R			DIAMETER	.236 (M)
C).WORKPIECE MATERIAL	EN9		CONDITION	NORMALISED	
D).DRESSING LEAD	0.5 (MM/S)		DIAMOND TYPE	SINGLE POINT	
E).COOLANT TYPE	PURFISOL	DILUTION	30/1	APPLICATION	C
COMMENTS					

APPENDIX 6

List of Expressions used for Analysis of Data and Sample Calculations

1) Dressing Lead (sd)

The dressing lead sd, is given by,

$$sd = \frac{100}{t.n} \qquad \ldots\ldots\ldots\ldots\ldots\ldots\ldots\ldots\ldots\ldots\ldots\ldots\ldots\ldots \text{(C1)}$$

where n is rotational speed of the grinding wheel in revs/sec, and t is the time for the dressing diamond to traverse 100 mm of the grinding wheel surface.

Sample Calculation

$$sd = \frac{100}{6 \times 19.6} = 0.86 \text{ mm/rev}$$

2) Maximum Specific Metal Removal Rate (Z')

The maximum specific removal rate, $Z' = \pi.Dw.vi$ .... (C2)

where vi represents the infeed-rate and Dw is the workpiece diameter.

Sample Calculation

$$Z' = \pi \times 44.8 \times 0.049 = 6.89 \text{ mm}^3/\text{mm/s}$$

3) Specific Normal Force (F_n')

From the bearing configuration illustrated in Figure 8, F_n' can be expressed as follows,

$$F_n' = \frac{F_1 + \frac{1}{2}.(F_2 + F_3)}{L} \qquad \ldots\ldots\ldots\ldots\ldots\ldots\ldots\ldots \text{(C3)}$$

where L is the component length.

And,

$$F_1 = R_1.\bar{K}_1 \quad \ldots\ldots (C4)$$

$$F_2 = R_2.\bar{K}_2 \quad \ldots\ldots (C5)$$

$$F_3 = R_3.\bar{K}_3 \quad \ldots\ldots (C6)$$

where $\bar{K}_1$, $\bar{K}_2$ and $\bar{K}_3$ are calibration values for transducers 1, 2 and 3 and R_1, R_2 and R_3 are the corresponding u.v. recorder trace maximum deflections.

Sample Calculation

$$F_1 = R_1.\bar{K}_1 = 15.5 \times 28.5 = 441.8 \text{ N/mm}$$

$$F_2 = R_2.\bar{K}_2 = 21 \times 19.3 = 405.3 \text{ N/mm}$$

$$F_3 = R_3.\bar{K}_3 = 1 \times 21.75 = 21.75 \text{ N/mm}$$

assume a value of 70 mm for the component length,

hence,

$$F'_n = \frac{441.8 + \frac{1}{2}.(405.3 - 21.75)}{70} = 9.05 \text{ N/mm}$$

4) Specific Tangential Force (F'_t)

Again, from the bearing configuration, Figure 8, an expression for F'_t can be given as follows,

$$F'_t = \frac{3}{2.L} \cdot (F_2 + F_3) \quad \ldots\ldots (C7)$$

Substituting values for F_2, F_3 and L yields,

$$F'_t = \frac{3}{2.70} \cdot (405.3 + 21.75) = 5.28 \text{ N/mm}$$

5) Specific Power Consumption (P')

The rate of energy consumption during grinding P', is the product of the

cutting speed and the cutting force,

thus,

$$P' = F'_t \cdot vg \quad \ldots\ldots\ldots\ldots\ldots\ldots\ldots\ldots\ldots\ldots\ldots\ldots\ldots\ldots\ldots\ldots \text{(C8)}$$

Sample Calculation

$$P' = 5.28 \times 30 = 158.4 \text{ W}$$

6) Maximum Specific Energy of Grinding (U)

The energy consumed per unit volume of metal removed is given by,

$$U = \frac{P'}{Z'} \quad \ldots\ldots\ldots\ldots\ldots\ldots\ldots\ldots\ldots\ldots\ldots\ldots\ldots\ldots\ldots\ldots \text{(C9)}$$

Sample Calculation

$$U = \frac{158.4}{6.89} = 22.98 \text{ J/mm}^3$$

7) Wheel Cutting Ability (λ)

The wheel cutting ability $\lambda = \frac{Z'}{F'_n}$ ..... (C10)

Substituting values for Z' and F'_n yields,

$$\lambda = \frac{6.89}{9.05} = 0.76 \text{ mm}^3/\text{N/s}$$

8) Equivalent Chip Thickness (heq)

The parameter heq, has been defined by C.I.R.P. as,

$$heq = \frac{Z'}{vg} \quad \ldots\ldots\ldots\ldots\ldots\ldots\ldots\ldots\ldots\ldots\ldots\ldots\ldots\ldots\ldots\ldots \text{(C11)}$$

Sample Calculation

$$heq = \frac{6.89}{30} = 0.229 \text{ µm}$$

9) Equivalent Diameter (De)

For external cylindrical grinding, the equivalent diameter is given by the expression,

$$De = \left(\frac{Dw.Dg}{Dw+Dg}\right) \quad \ldots\ldots\ldots\ldots\ldots\ldots\ldots\ldots\ldots\ldots\ldots\ldots\ldots\ldots \quad (C12)$$

For values of Dg = 0.48 m and Dw = 0.0448 m,

$$De = \left(\frac{0.48 \times 0.0448}{0.48 + 0.0448}\right) = 0.04098 \text{ m}$$

10) Theoretical Chip Length ($\bar{l}c$)

The expression for $\bar{l}c$ was developed in section 3.4,

thus,

$$\bar{l}c = \sqrt{\frac{\pi.Dw.vi.De}{vw}} \quad \ldots\ldots\ldots\ldots\ldots\ldots\ldots\ldots\ldots\ldots\ldots\ldots\ldots\ldots \quad (C13)$$

substituting typical values in the expression yields,

$$\bar{l}c = \sqrt{\frac{\pi \times 0.0448 \times 0.049 \times 10^{-3} \times 0.04098}{0.184}} = 1239 \ \mu m$$

11) Theoretical Chip Formation Time ($\bar{t}f$)

Again an expression for this parameter was developed in section 3.4,

$$\bar{t}f = \bar{l}c/vg = 1239 \times 10^{-6}/30 = 41.3 \ \mu sec$$

12) Undeformed Chip Thickness ($\bar{t}c$)

The expression for $\bar{t}c$ was also developed in section 3.4, thus

$$\bar{t}c = \left(1 - \frac{2.\pi.vi.De}{vw.Dg}\right).\left[\frac{ld.vw}{vg}.\sqrt{\frac{4.\pi.De.vi}{vw.Dw}} - \frac{\pi.vi.De}{vw} - \left(\frac{ld.vw}{vg}\right)^2.\frac{1}{Dw}\right]$$

$$\ldots\ldots\ldots\ldots + \frac{\pi.Dw.vi}{vw}.\left(1 + \frac{\pi.Dw.vi}{vw.Dg}\right) \quad \ldots\ldots\ldots\ldots \quad (C14)$$

Sample Calculation

Substituting values in the expression yields,

$$\bar{t}c = \left(1 - \frac{2x\ x0.049x10^{-3}x0.04098}{0.184x30}\right)x\left[\frac{0.002x0.184}{30}\sqrt{\frac{4x\ x0.04098x0.049x10^{-3}}{0.184x0.0448}}\right.$$

$$\left. \ldots\ldots - \frac{x0.049x10^{-3}x0.04098}{0.184} - \left(\frac{0.002x0.184}{30}\right)^2 . \frac{1}{0.0448}\right]$$

$$\ldots\ldots + \frac{x0.0448x0.049x10^{-3}}{0.184} . \left(1 + \frac{x\ 0.0448x0.049x10^{-3}}{0.184x30}\right)$$

$\bar{t}c = 3.86\ \mu m$

APPENDIX 7

Grinding Wheel Replication Technique

Representative areas of the grinding wheel surface can be sampled at any stage during grinding through the aid of a "replicator" device. The replicator is inserted in to the grinding wheel guard adjacent to the wheel. Plate 14 shows the replicator in position, ready to take a sample. The replicator is a device which enables a flat portion of lead mounted on a steel block to be pushed into the surface of the grinding wheel under a known controlled pressure. Thus, the surface topography of the wheel is impressed into the lead blank to a pre-determined depth and elastic distortion. The force measuring system enable this to be achieved to the required accuracy. The lead blanks are annealed and then pressed between ground and polished surfaces to give no appreciable departure from a straight line stylus trace at 5000 x magnification.

The replicator consists of a cylindrical outer body and sliding core, square in section, at the end of which is a dove-tailed face normal to the axis of sliding. A lead blank can be mounted in the dove-tail and clamped. The centre section can be moved along its axis relative to the outer body by turning a lead screw. A portion of the outer body is threaded and fitted with a clamping nut. The replicator is mounted on the grinding machine at the aperture in the machine guard used for the dressing device.

Impressions in the lead blanks obtained from the grinding wheel each covered an area of 50 mm x 10 mm approximately. The stylus trace was taken in a direction perpendicular to the wheel axis. Usually samples were taken from at least three different parts of the wheel surface.

Analysis of Replicas

The replica traces represent an inverted profile of the replica surface. The fact, that the cutting-edge peaks become valleys in the lead impression is quite useful for a number of reasons:- the work-hardened valleys are not sensitive to ploughing by the diamond stylus , only cutting peaks to a predetermined depth will be observed and by suitable choice of stylus (extremely thin and sharp) peaks and other artefacts which play no useful part in the grinding process can be filtered out. A Talysurf model 5 was employed for obtaining the traces using a diamond conical stylus of thickness 2 um. This stylus had a profile of similar size and shape to the uncut chip size range being investigated. A minimum length of trace of about 5 mm was usually analysed.

Analysis of the replica traces in terms of adjacent cutting-edges was carried out with the aid of a Commodore PET computer interfaced with a Hewlett-Packard digital plotter (model 9872A). Instead of a pen, an eye-piece with cross-wires was fitted to the plotting arm. The eye-piece was positioned over each peak in the trace in turn, programming soft-ware allowed the co-ordinates of that particular peak selected to be entered into the computer automatically. The computer is programmed to compensate for the effect of grinding wheel curvature upon peak co-ordinates. The program also calculates the frequency distribution of pairs of adjacent cutting-edges as a function of lateral separation, lg, and height differences, hg. Another program can read in data representing any required grinding conditions and calculate, from the trace peak co-ordinates, the frequency distribution of pairs of adjacent cutting-edges which would be active under the proposed grinding conditions. Taking the first surface peak to be active, the locus of the point on the workpiece surface, coincident with this peak, past the other cutting-edges is represented

by an appropriate equation in the computer program. The co-ordinates of the adjacent peak are considered. If these co-ordinates lie within the workpiece surface, as defined by the locus equation, then that cutting-edge is considered to be active. The process is then repeated from this point. Otherwise that peak is ignored and the co-ordinates of the next peak are considered.

APPENDIX 8

Specification of the Wickman Scrivener 2K Centreless Grinding Machine

The grinding machine was supplied with oil hydrostatic bearings for the main spindle and the control wheel spindle. A hydraulic power unit, 200 litres in capacity, capable of delivering oil at the rate of 45 litres per minute, at a supply pressure of 5.2 MPa provides the oil requirements of the spindles and the wheel dressing units. The wheel dressing units are hydraulically operated and have profile truing capability.

The maximum possible grinding wheel speed with the drive arrangement fitted is 120 m/s, the main drive motor is a 75 kW d.c. unit with a KTK Thyristor control system. The machine guarding is sufficient for this speed. Maximum dimensions for the grinding wheel diameter and width are 500 mm and 200 mm respectively, the bore is a nominal 304.8 mm. The control wheel supplied with the machine had a 304.8 mm diameter x 200 mm width x 127 mm bore. Variable speed drives are fitted to both wheel heads, the power supplied to the main drive motor can be monitored.

The control wheel can be adjusted in the vertical and horizontal planes. Adjustment in the vertical plane is 4° - 0 - 4°, and the adjustment in the horizontal plane is $\pm$0.35 mm per 200 mm. Infeed adjustment of the control wheel head is graduated in units of 0.001 mm. The control wheel head infeed for plunge feed grinding is hydraulically actuated, it is fitted with a rapid retract emergency facility.

The coolant tank fitted has a 750 litre capacity, coolant can be supplied at the rate of 2 litres per second, at a supply pressure of 0.85 MPa. Coolant can be supplied to the grinding zone from either a manifold or a flood nozzle, it can be supplied from both if required.

All electrical equipment operates from 415 volts, 3 phase, 50 Hz supply, with control circuits operating at 110 volts, single phase, at 50 Hz.

Plate 3 illustrates the model 2K centreless grinding machine. The control wheel fitted is a resinoid bonded wheel, grade A60 OR. Two grades of grinding wheel were used for the experimental programme. The cast iron components were ground with a resinoid bonded wheel - grade C46 BBT. A vitrified bonded wheel was used to grind the steel components, the grade of that wheel was WA6OMVRC.

FIGURES

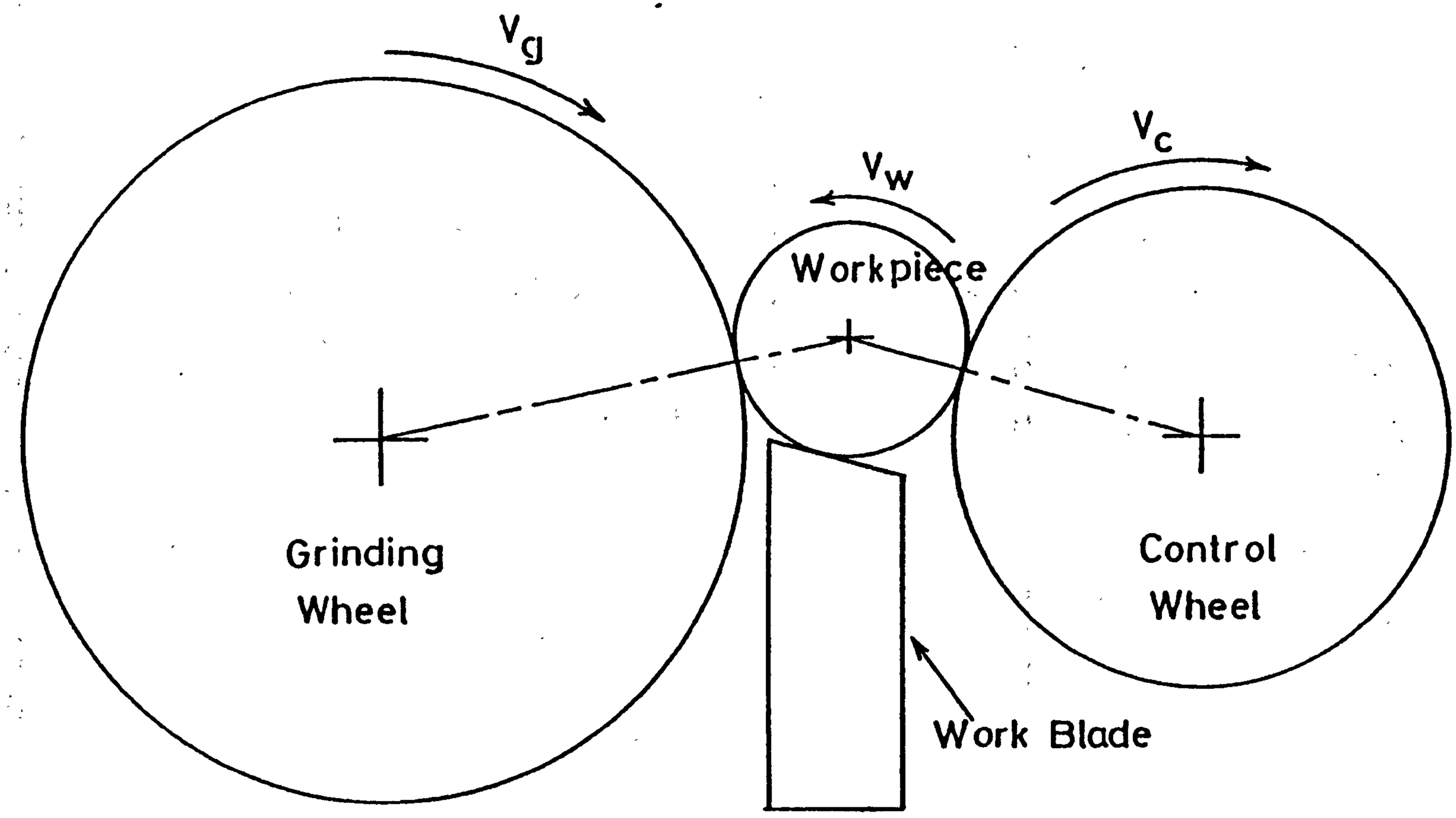

CENTRELESS GRINDING - BASIC SCHEME FIG.1

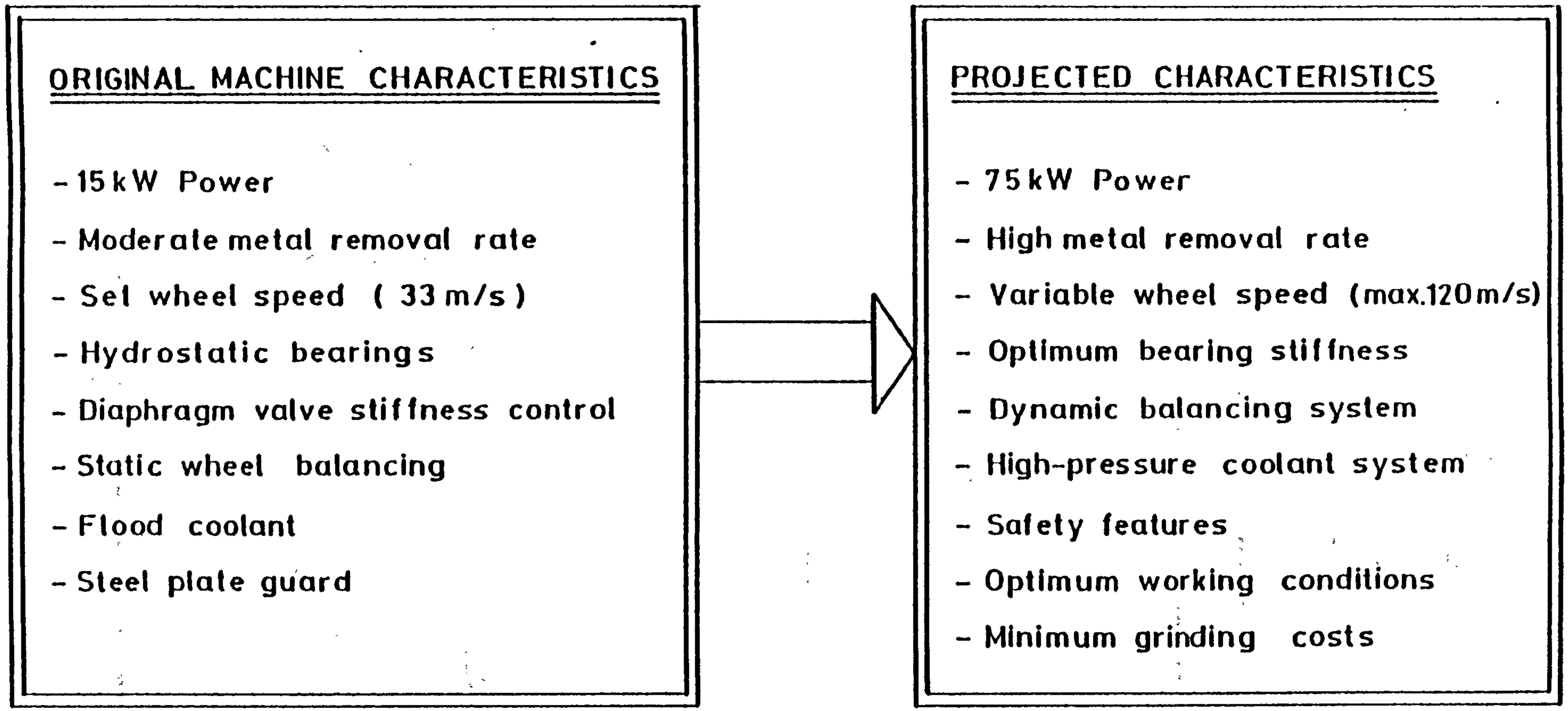

PROPOSED MACHINE MODIFICATIONS

FIG.2

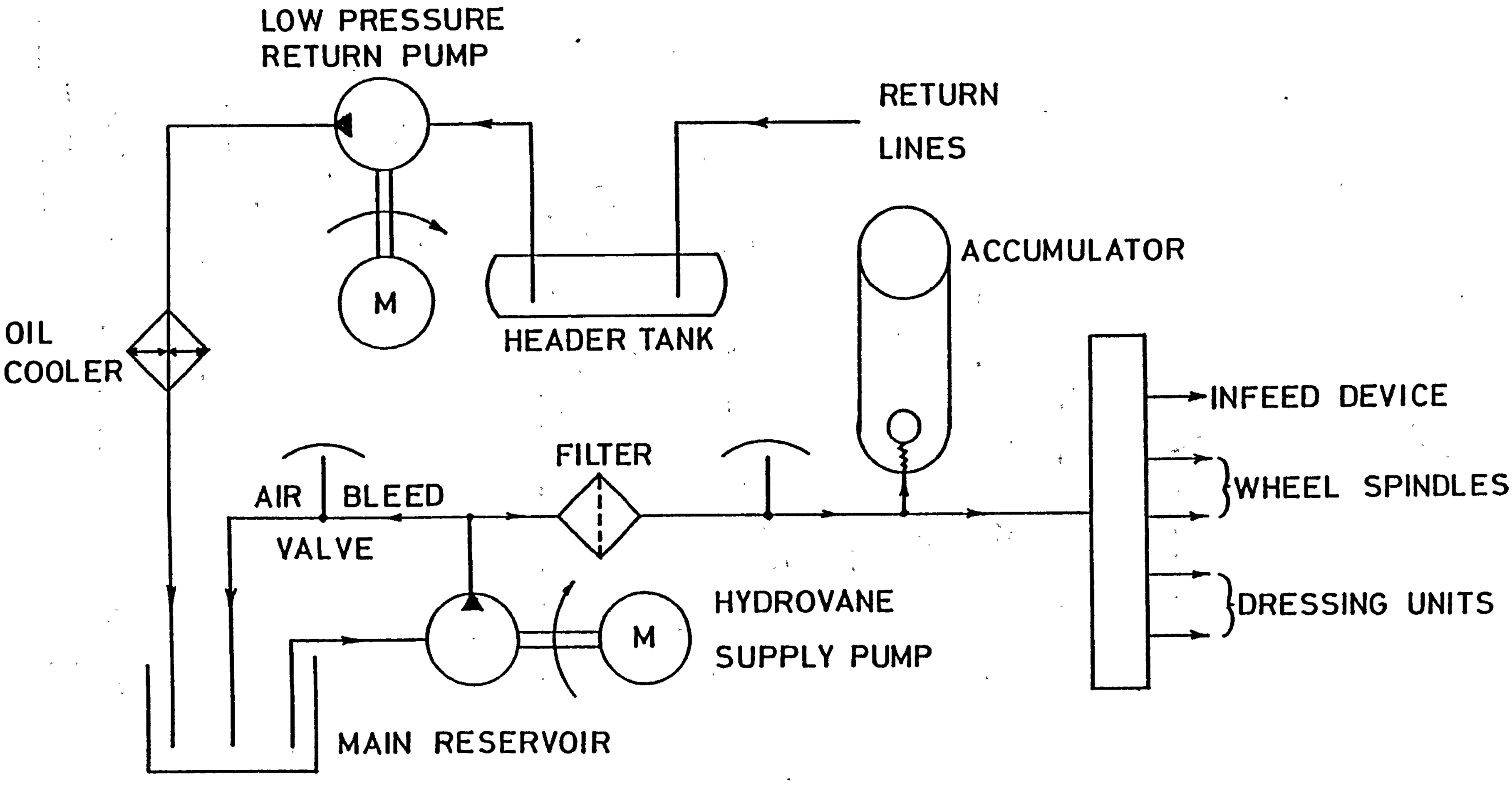

SCHEMATIC ARRANGEMENT OF HYDRAULIC CIRCUIT

FIG.3

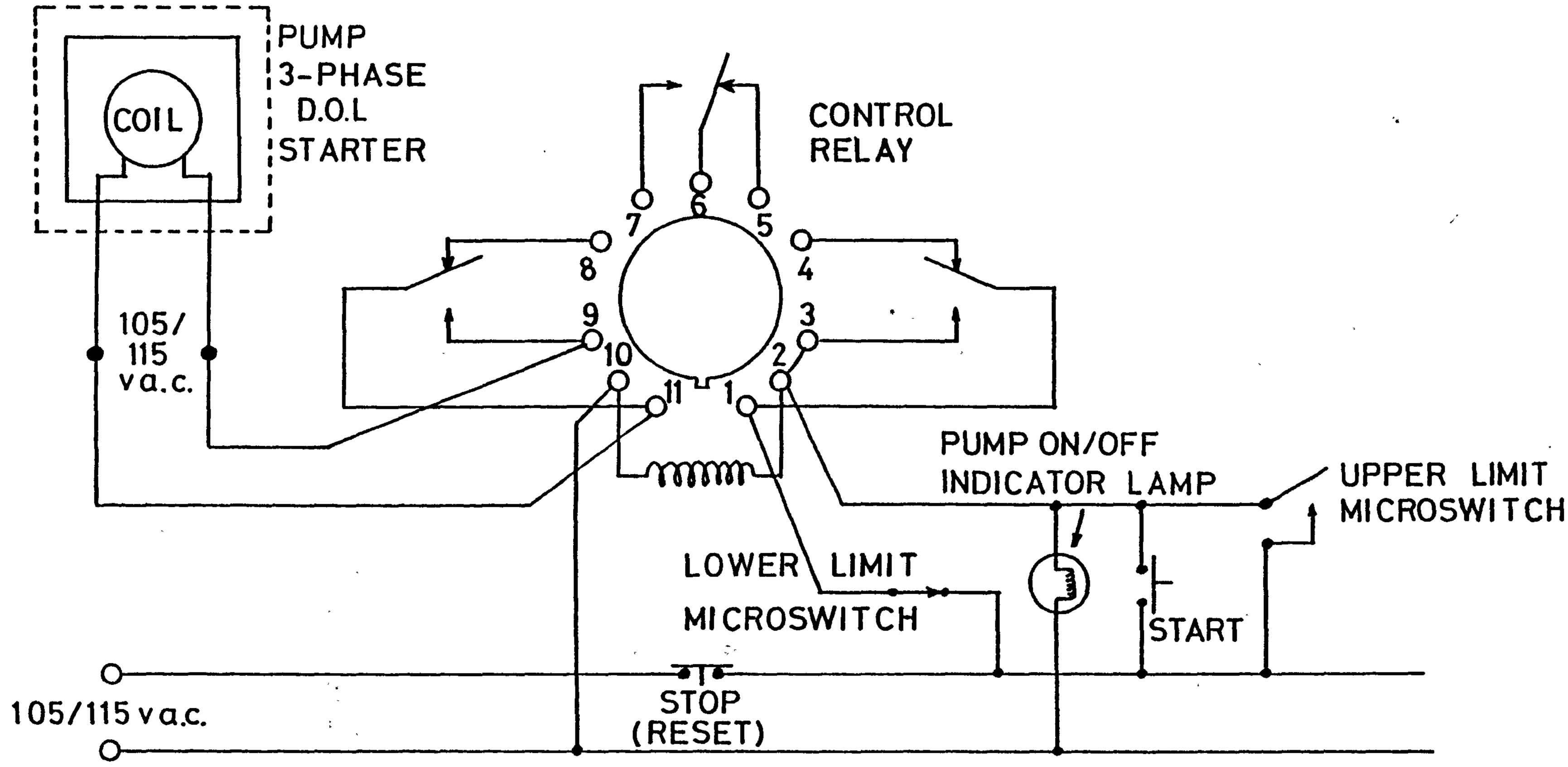

HYDRAULIC OIL HEADER TANK LEVEL CONTROL CIRCUIT FIG. 4

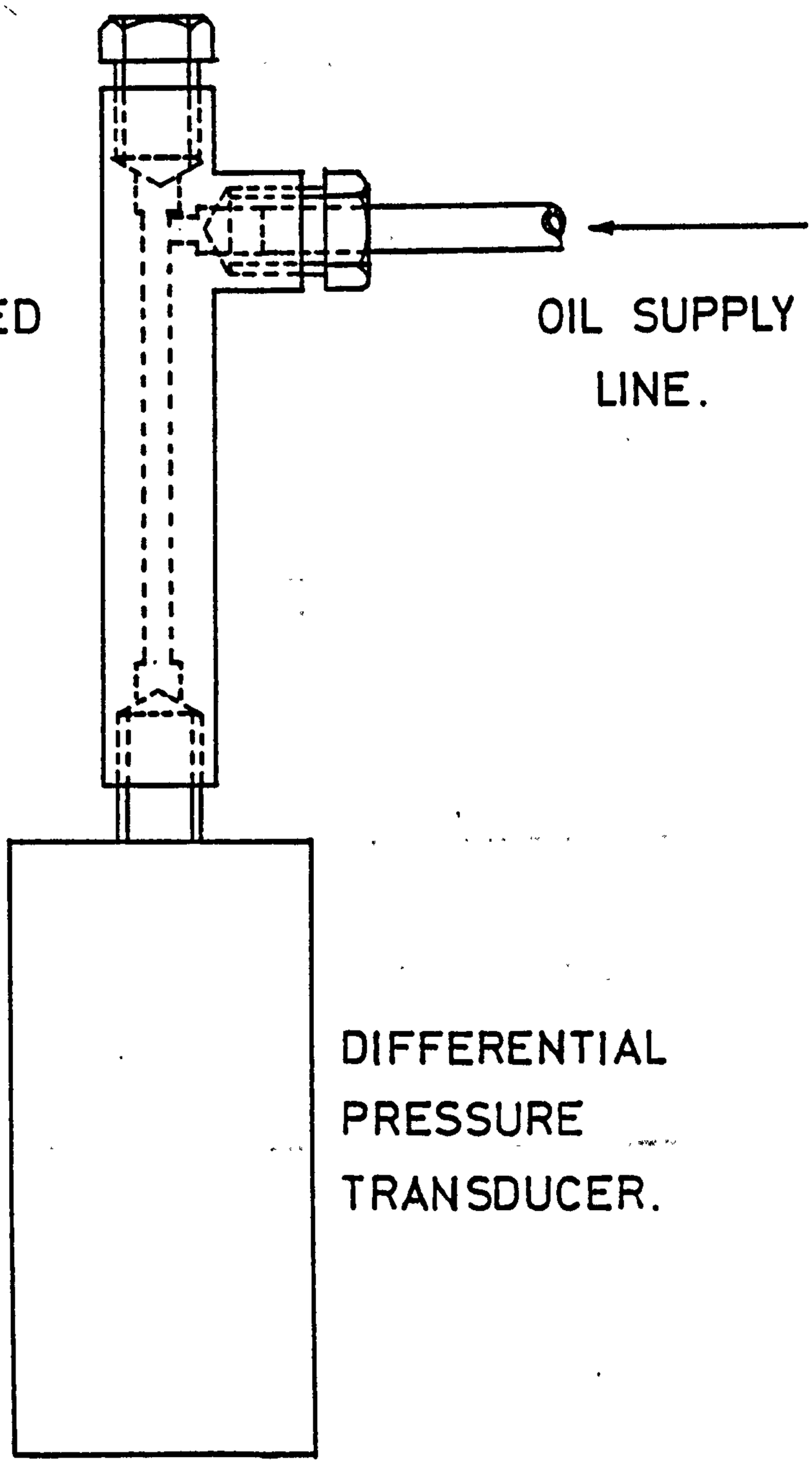

FIG.5

SCALE : FULL SIZE

TRANSDUCER AIR BLEED VALVE

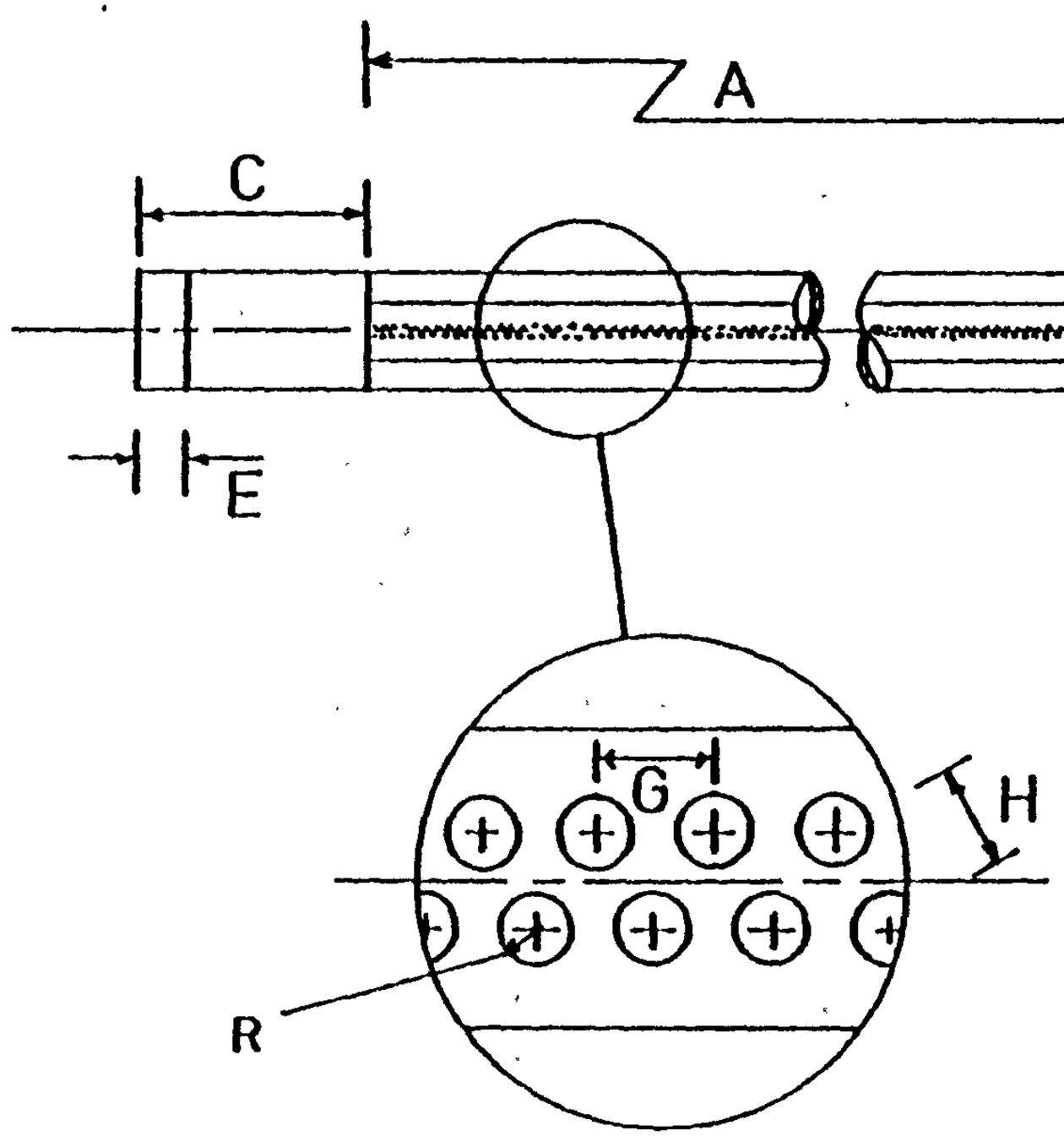

DIMENSIONS	SHORT MANIFOLD	LONG MANIFOLD
A	110 mm	210mm
B	145mm	145mm
C	27mm	27mm
D	25mm	65mm
E	5mm	5mm
F	12mm	12mm
G	0.75mm	0.75mm
H	0.75mm	0.75mm
R	0.25mm	0.25mm
PIPE BORE	8mm	8mm

COOLANT MANIFOLD SPECIFICATION

FIG.6

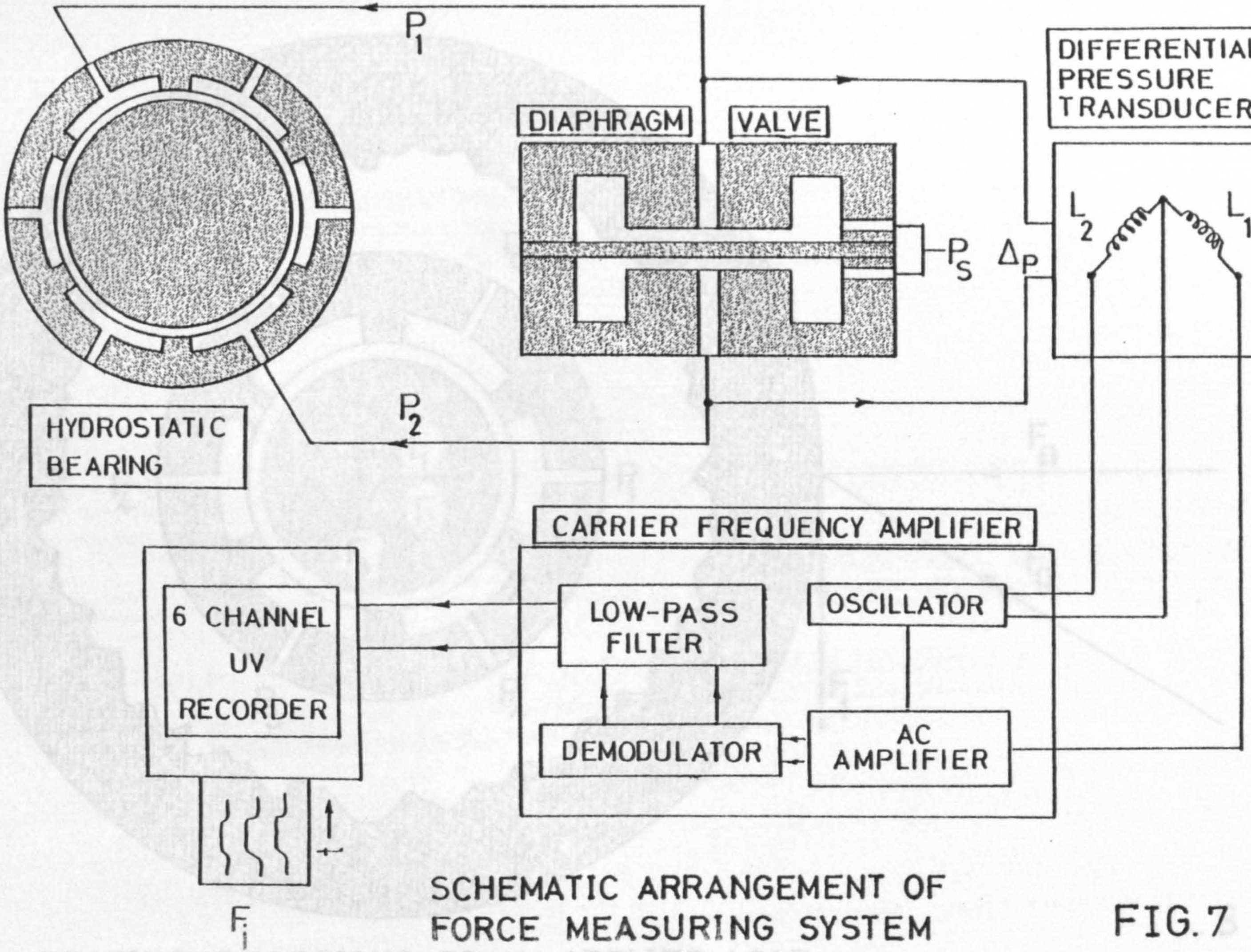

SCHEMATIC ARRANGEMENT OF FORCE MEASURING SYSTEM

FIG.7

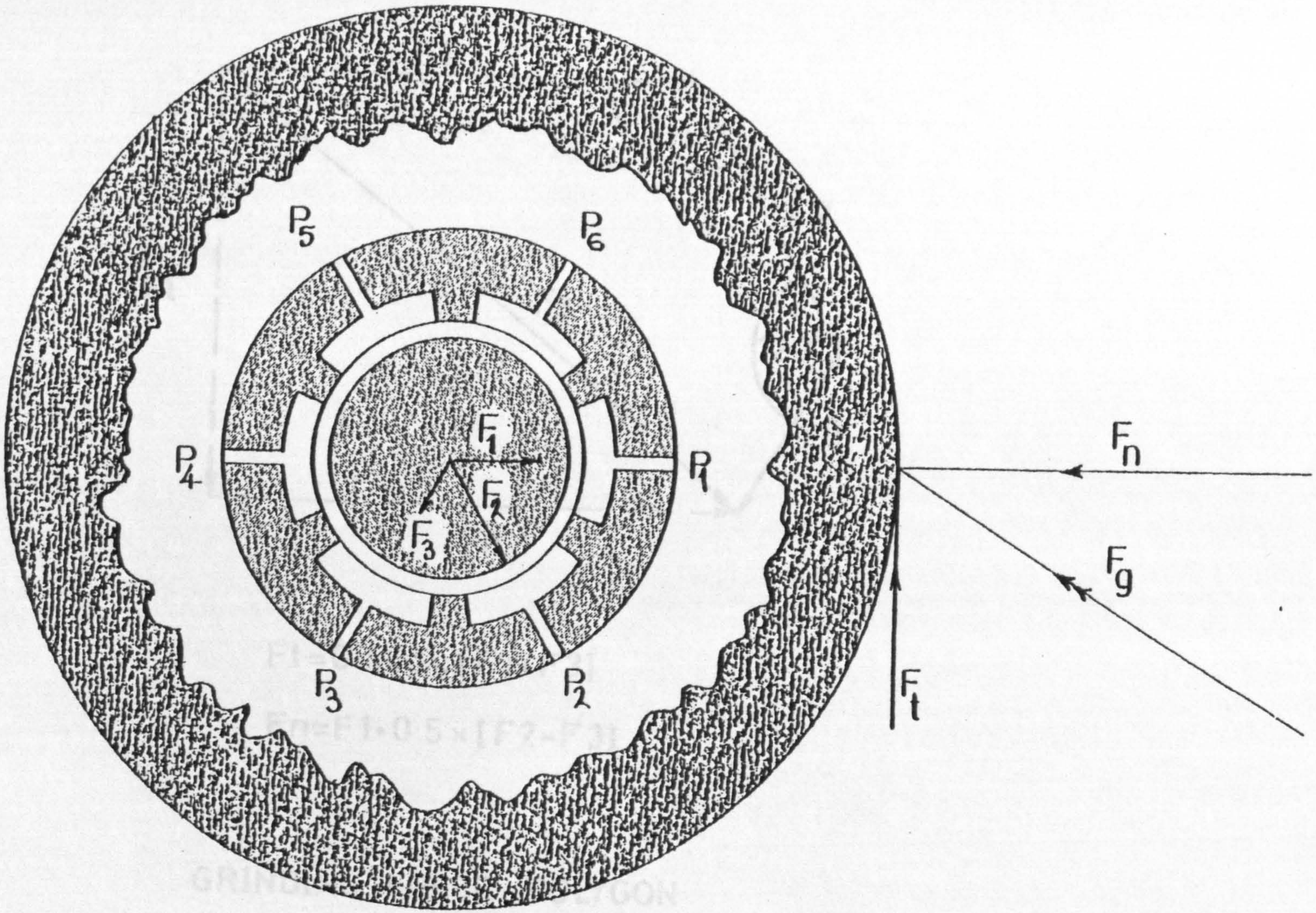

BEARING REACTIONS TO AN APPLIED LOAD

FIG. 8

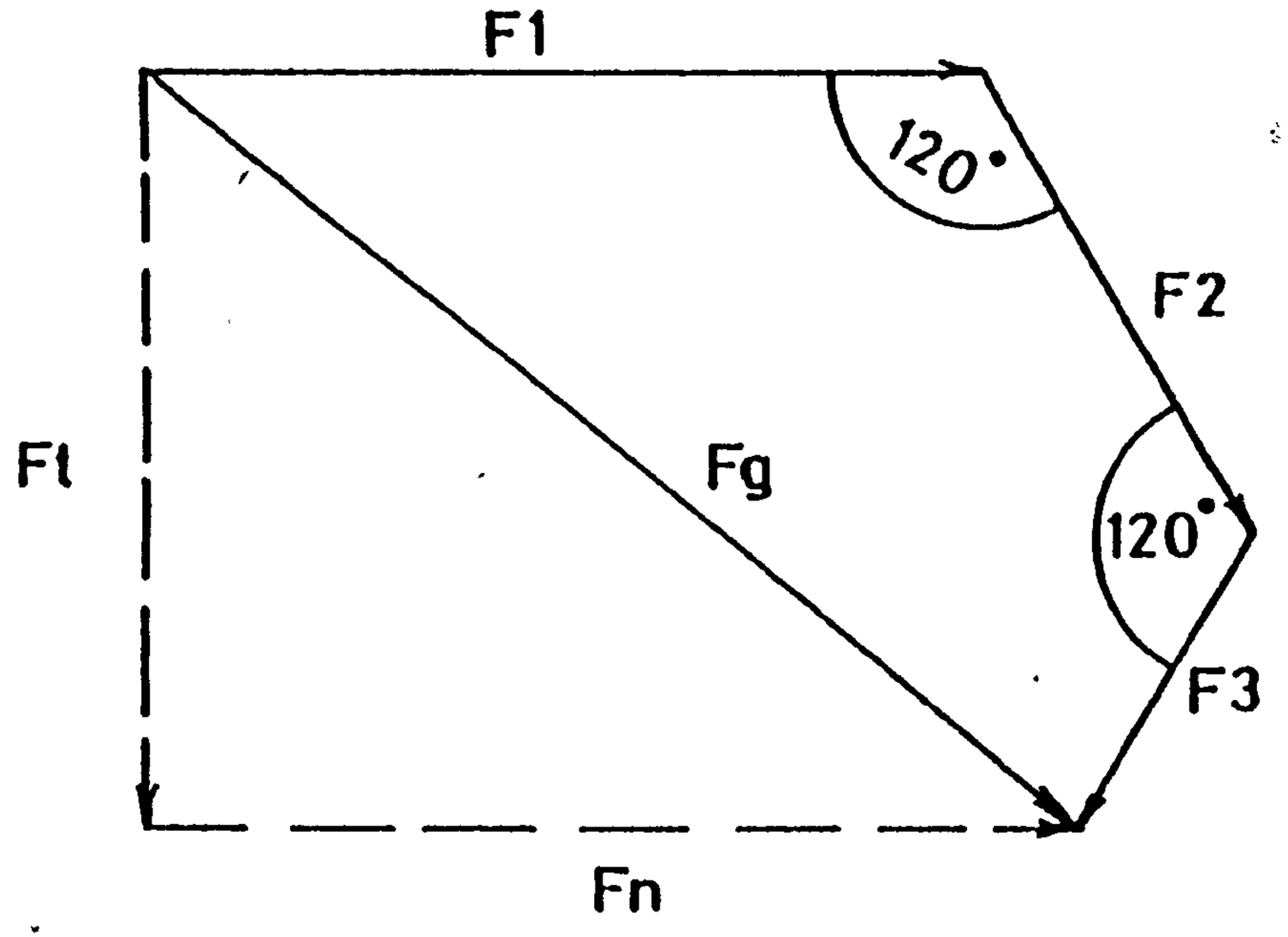

$$Ft = 0{\cdot}866 \times [F2 + F3]$$

$$Fn = F1 + 0{\cdot}5 \times [F2 - F3]$$

GRINDING FORCE POLYGON

FIG.9

FIG.10

TRANSDUCER CALIBRATION TRACES

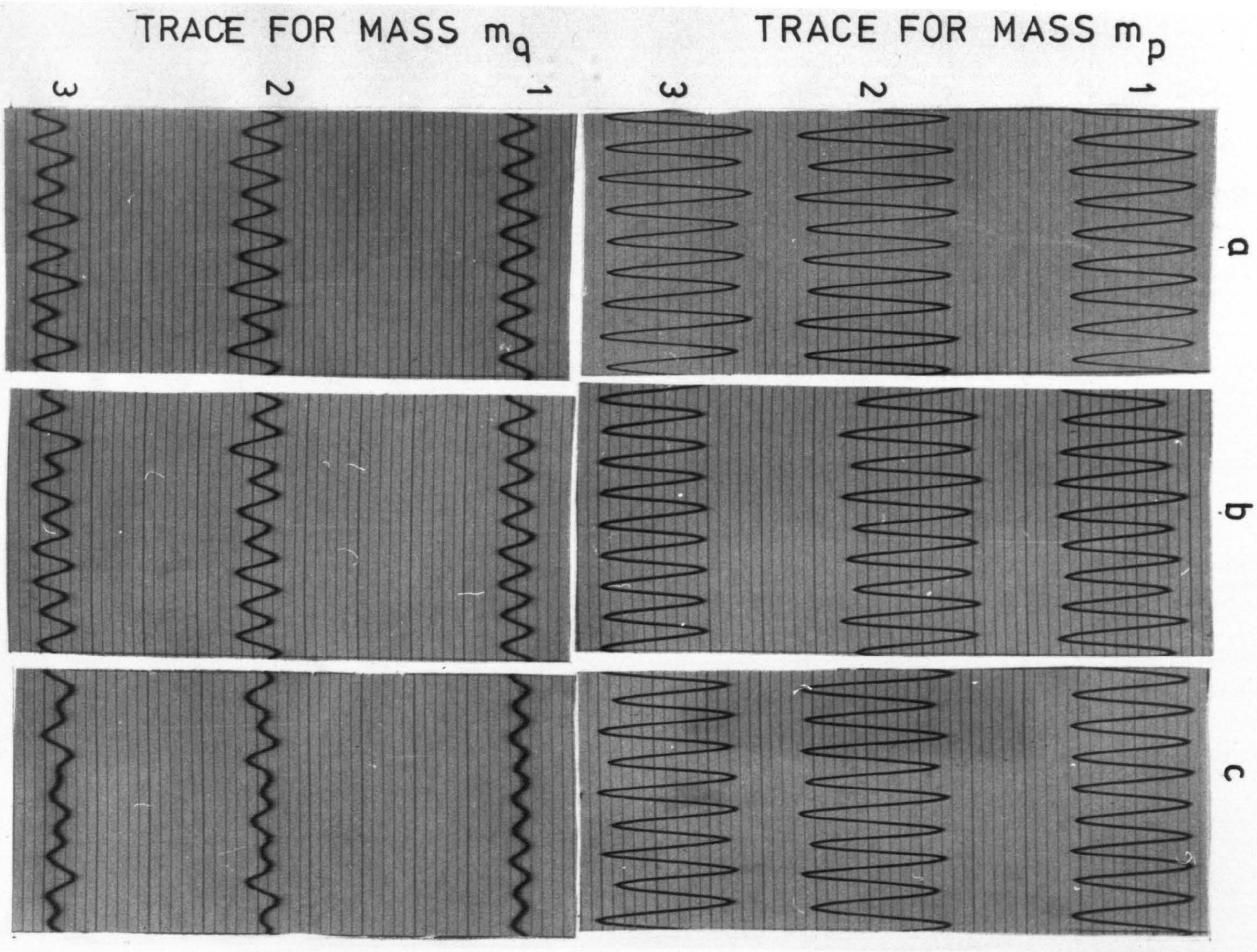
TRACE FOR MASS m_q
TRACE FOR MASS m_p
3
2
1
3
2
1
a
b
c

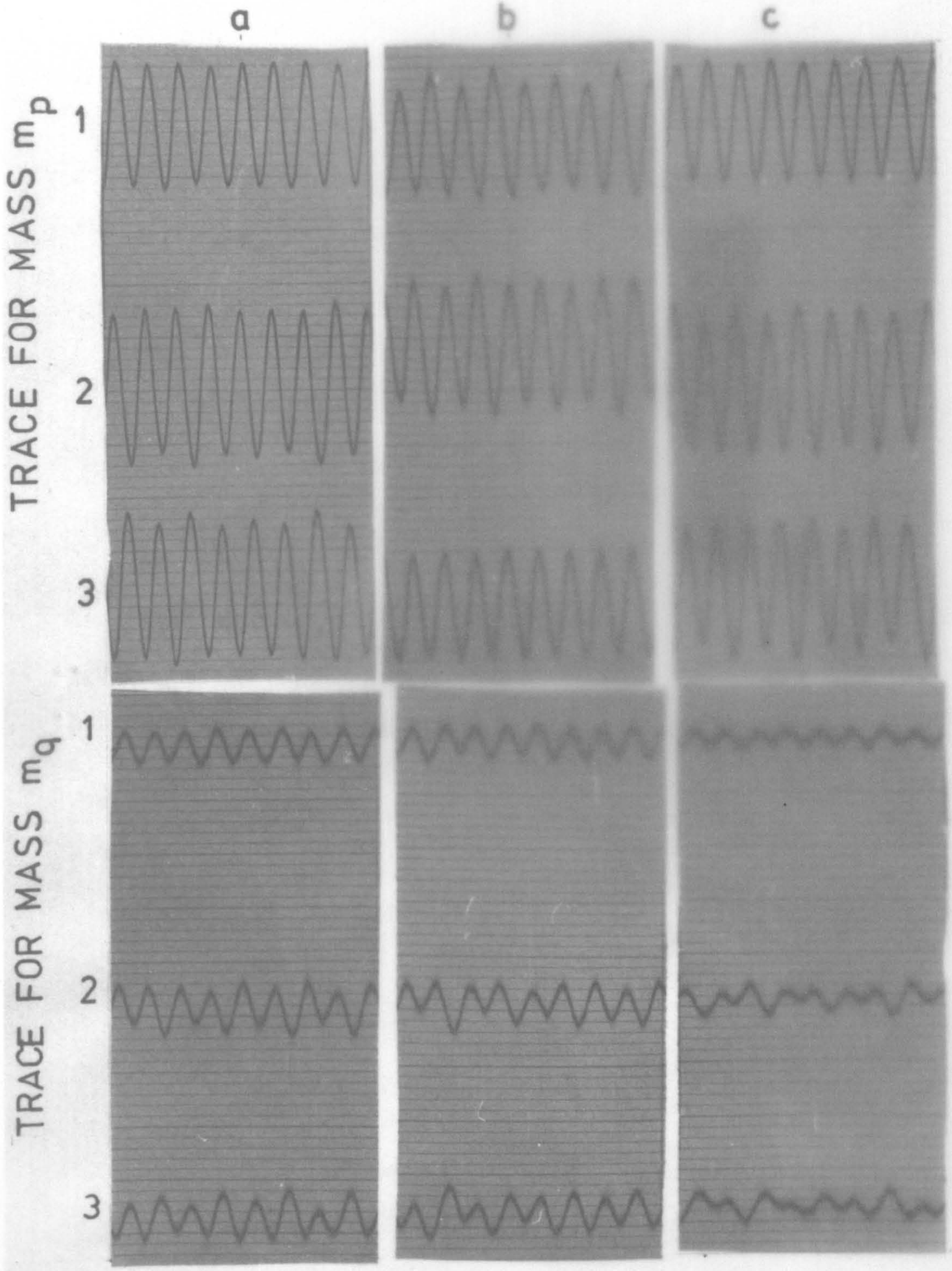

FIG.10

TRANSDUCER CALIBRATION TRACES

TRANSDUCER CALIBRATION VALUES VS GRINDING WHEEL SPEED

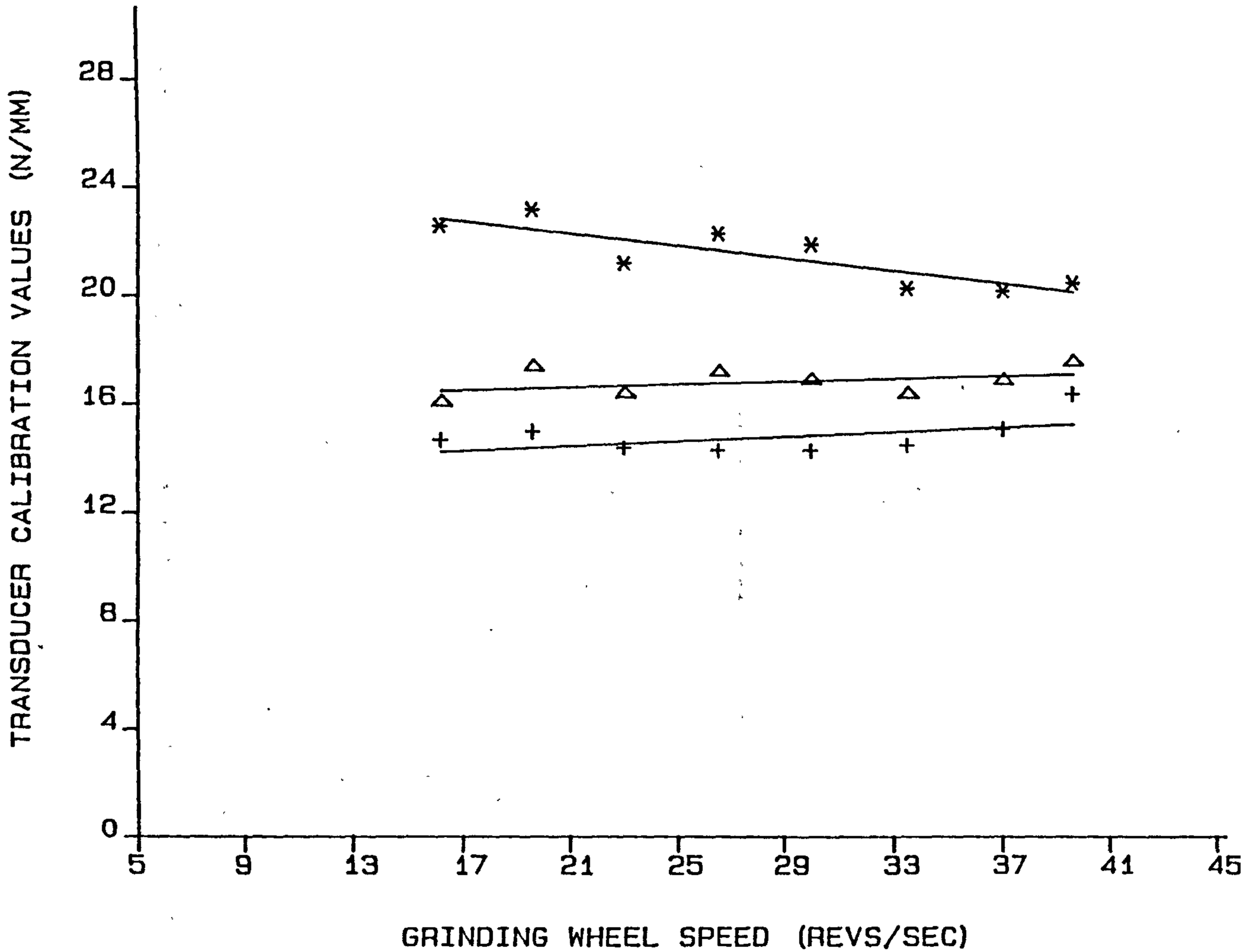

**REFER TO TABLE(S) 1
FOR EXP.L CONDITIONS.

LEGEND

*: - TRANSDUCER - F1
+: - TRANSDUCER - F2
△: - TRANSDUCER - F3

ADDITIONAL DATA

WHEEL - C46 BBT
OIL TEMPERATURE - 27 C

FIG. 11

FIG.12

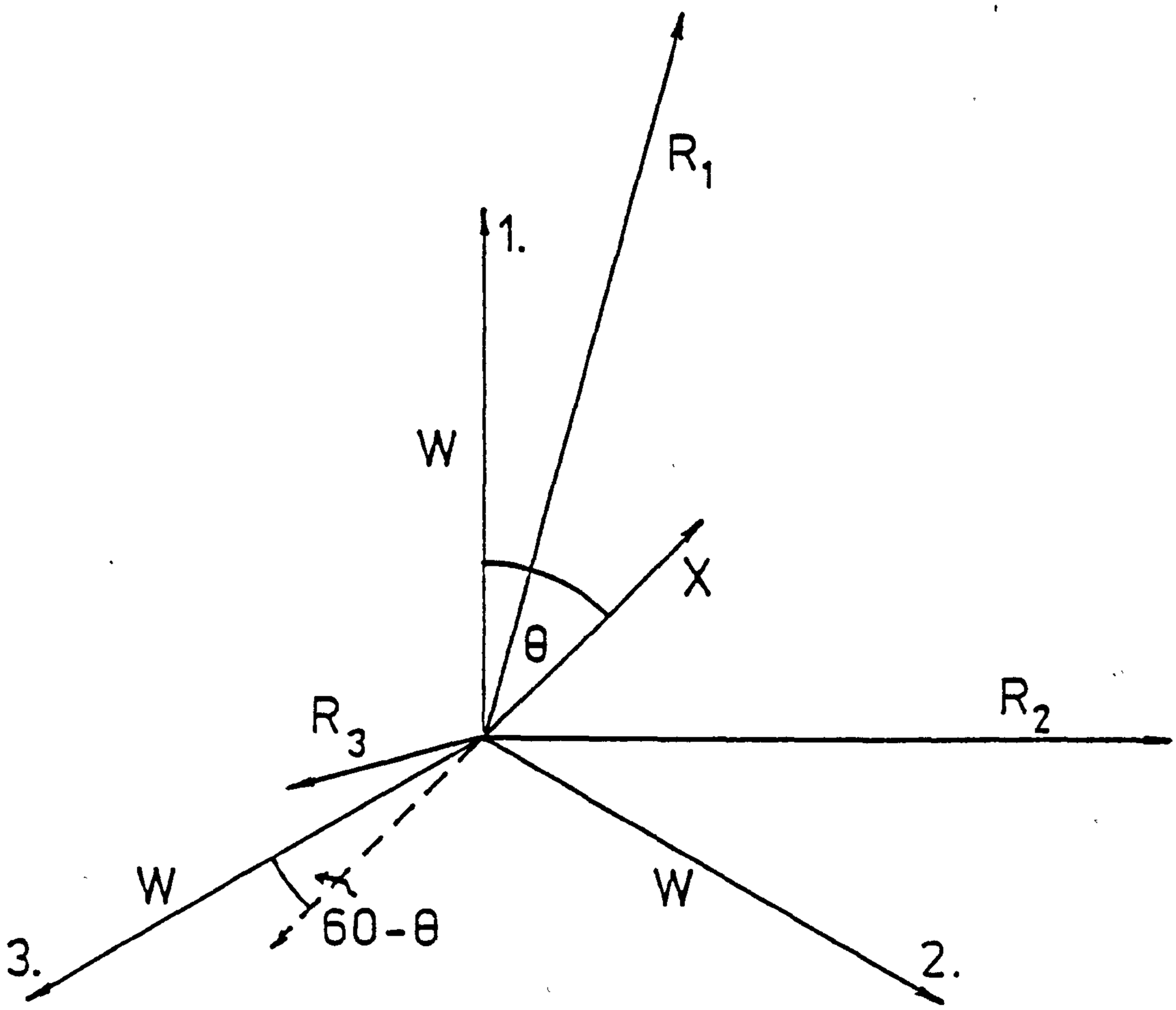

VECTOR DIAGRAM FOR DYNAMIC WHEEL BALANCING

GRINDING FORCES VS GRINDING WHEEL SPEED

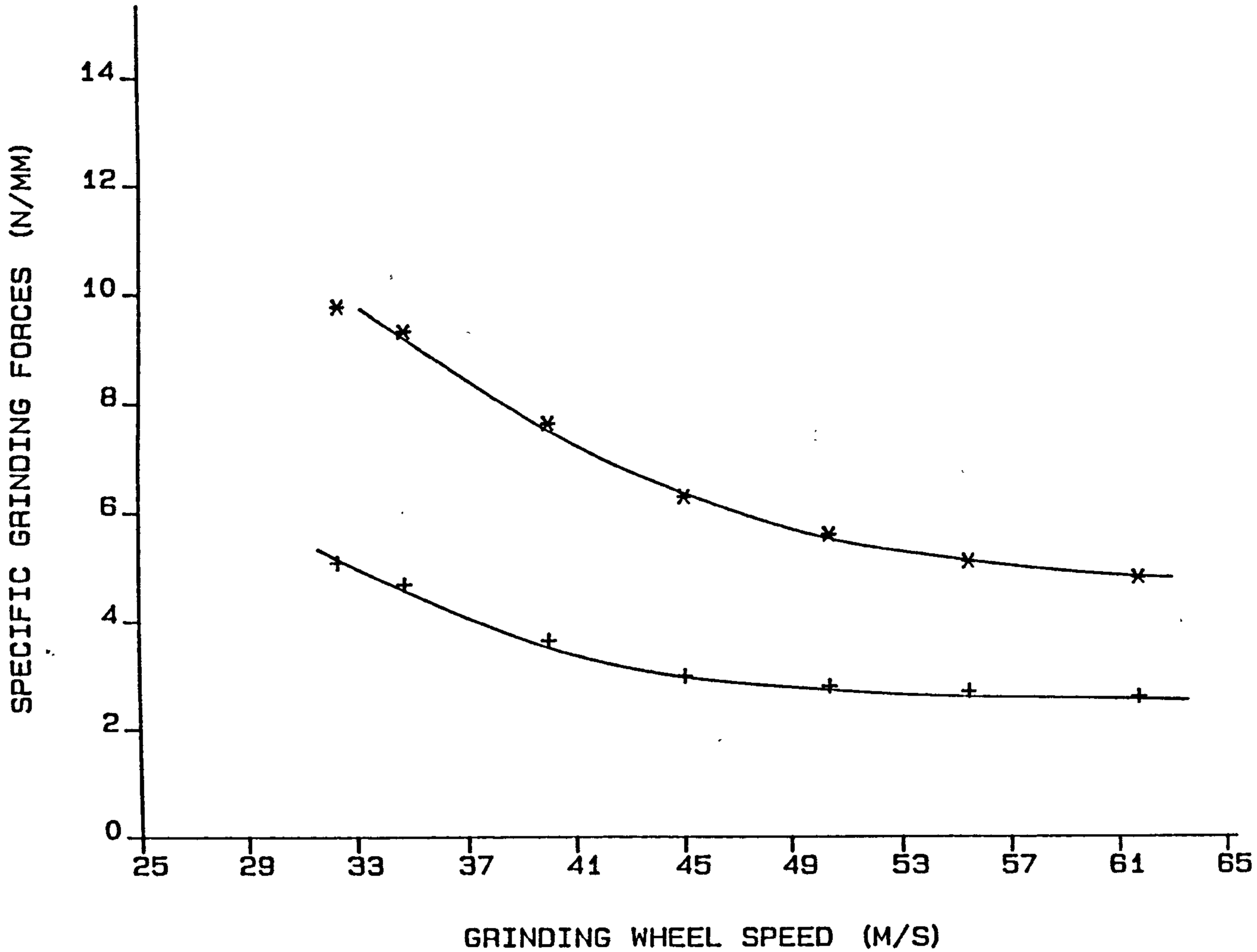

**REFER TO TABLE(S) 5
FOR EXP.L CONDITIONS.

LEGEND

*:- FN'
+:- FT'

ADDITIONAL DATA

WHEEL - WA60MVRC
MATERIAL - EN 8
Q-RATIO = 120
Z' = 7 CU.MM/MM/S

FIG. 13

SURFACE ROUGHNESS VS GRINDING WHEEL SPEED

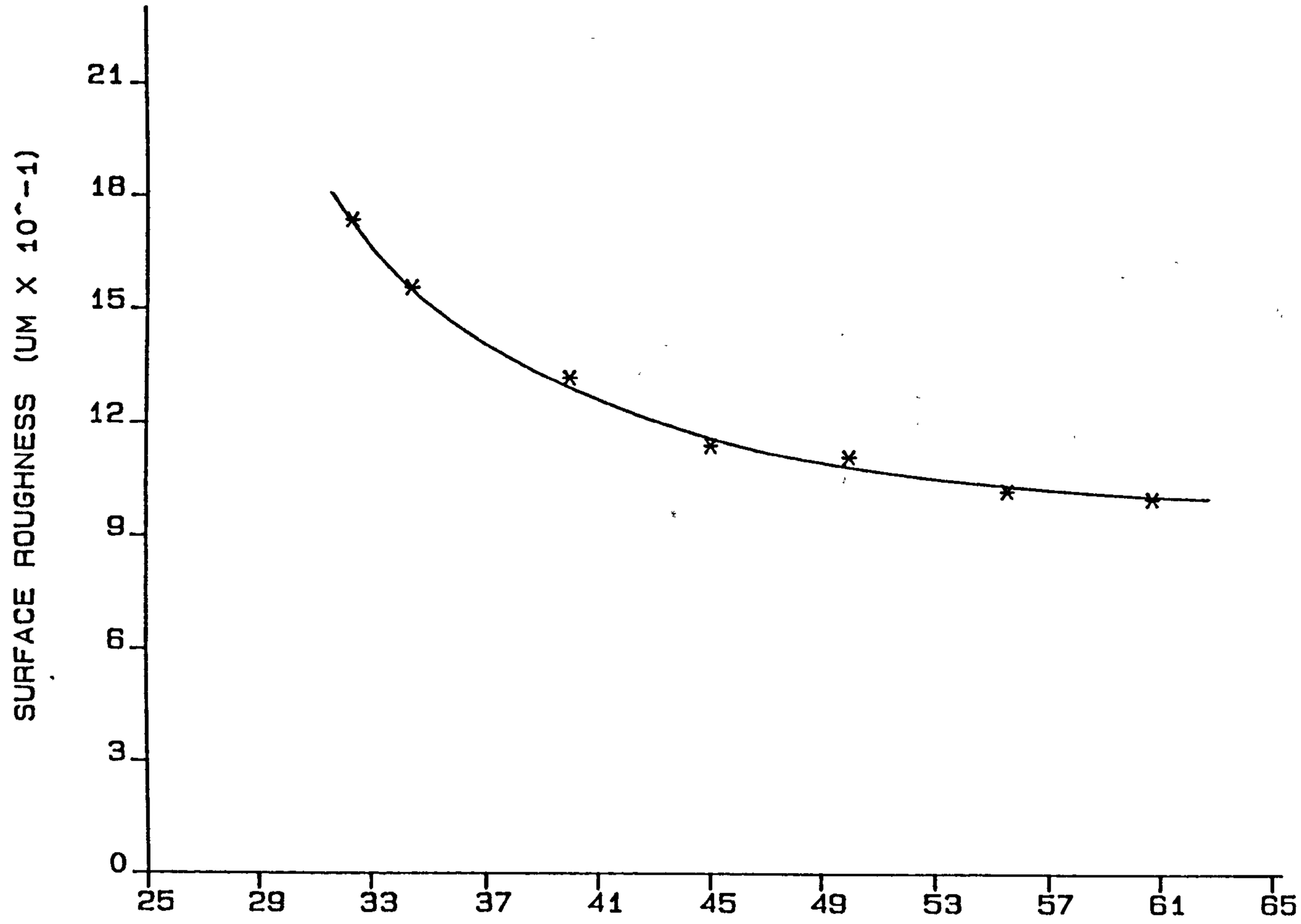

**REFER TO TABLE(S) 5
FOR EXP.L CONDITIONS.

LEGEND

*: - RA

ADDITIONAL DATA

WHEEL - WA60MVRC
MATERIAL - EN 9
G-RATIO = 120
Z' = 7 CU.MM/MM/S

FIG. 14

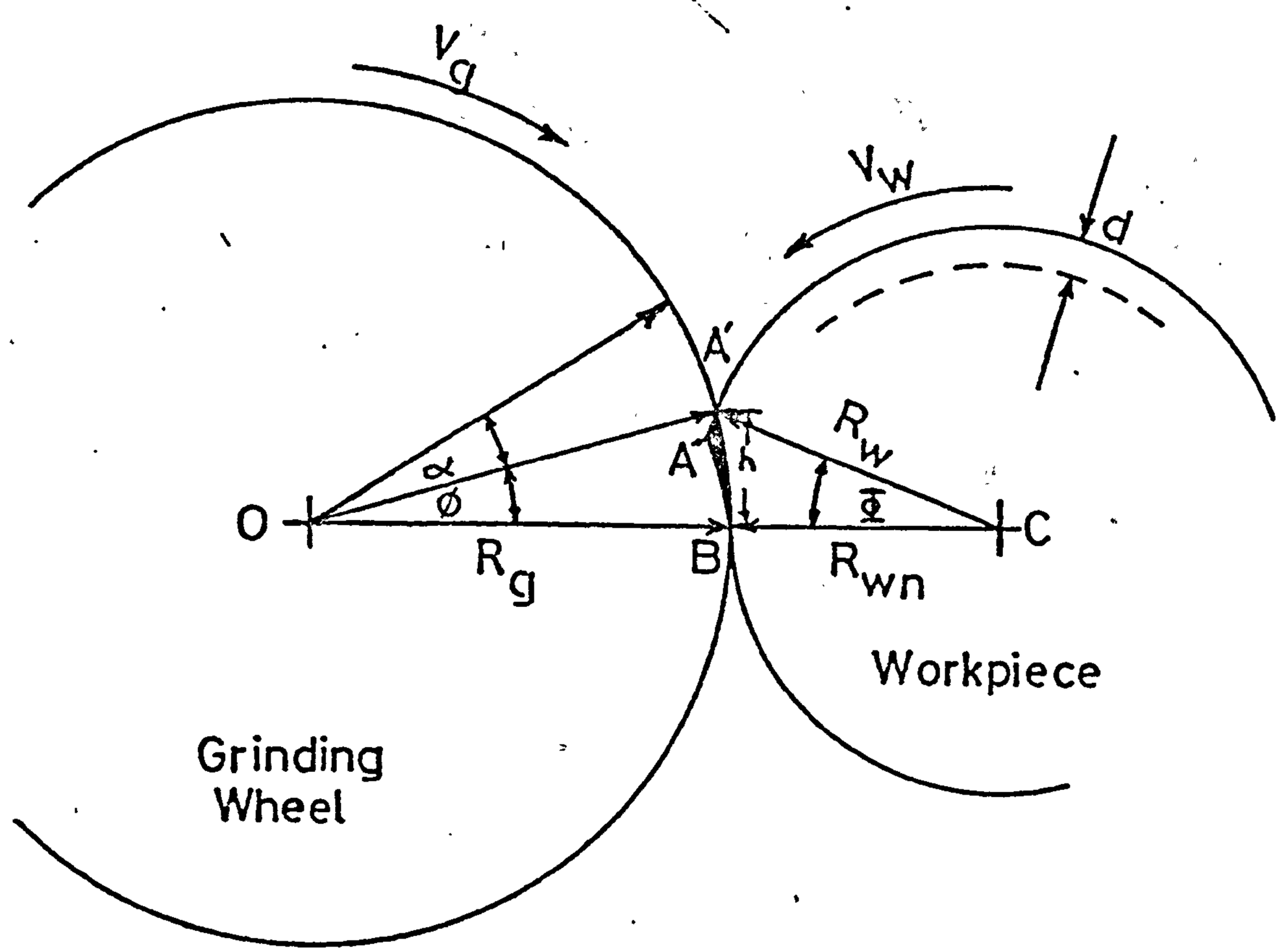

KINEMATIC MODEL OF CHIP FORMATION FOR PLUNGE FEED CYLINDRICAL GRINDING

FIG.15A

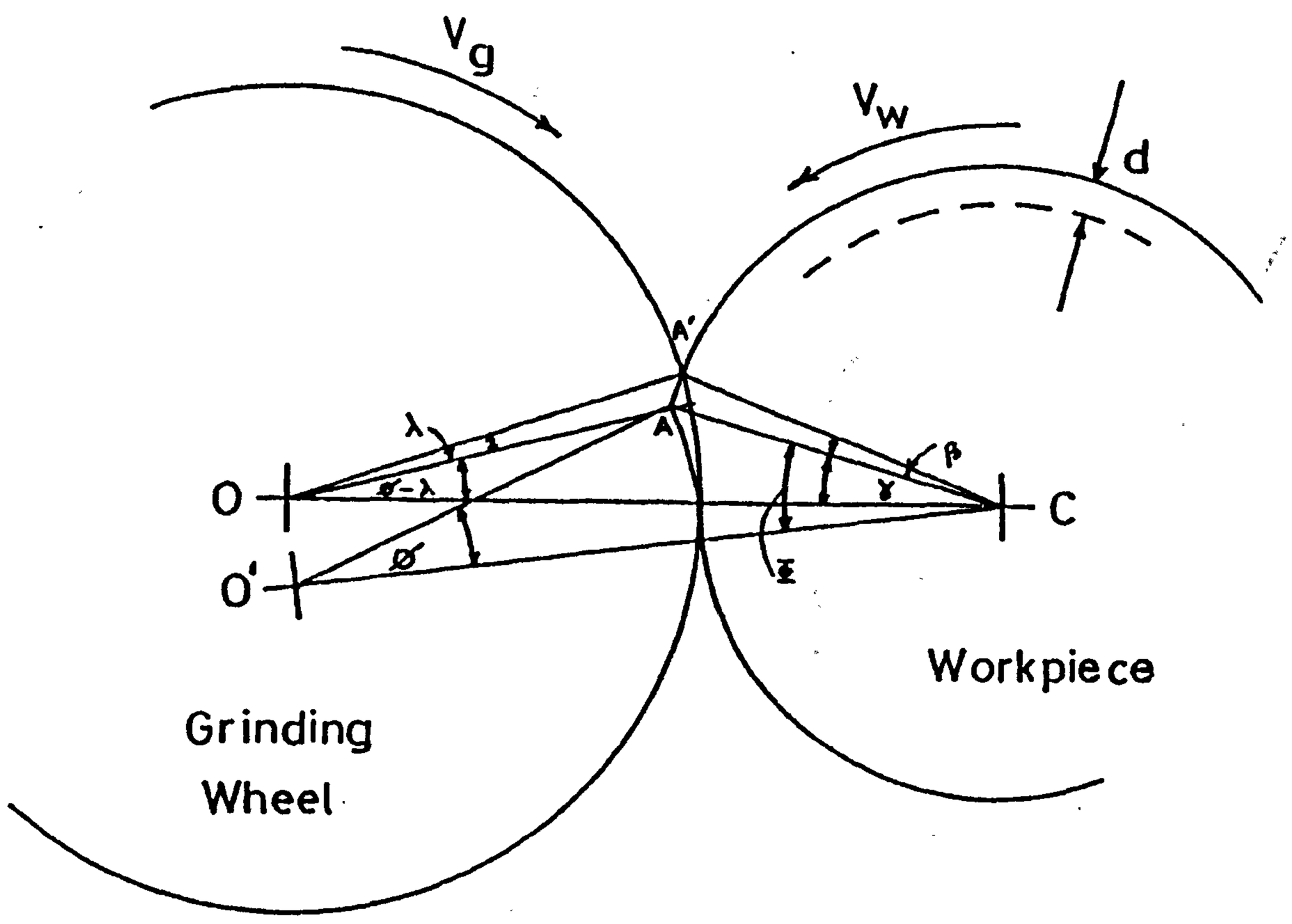

GEOMETRY APPERTAINING TO INSTANT OF CONTACT
OF SECOND ACTIVE GRIT

FIG.15 B

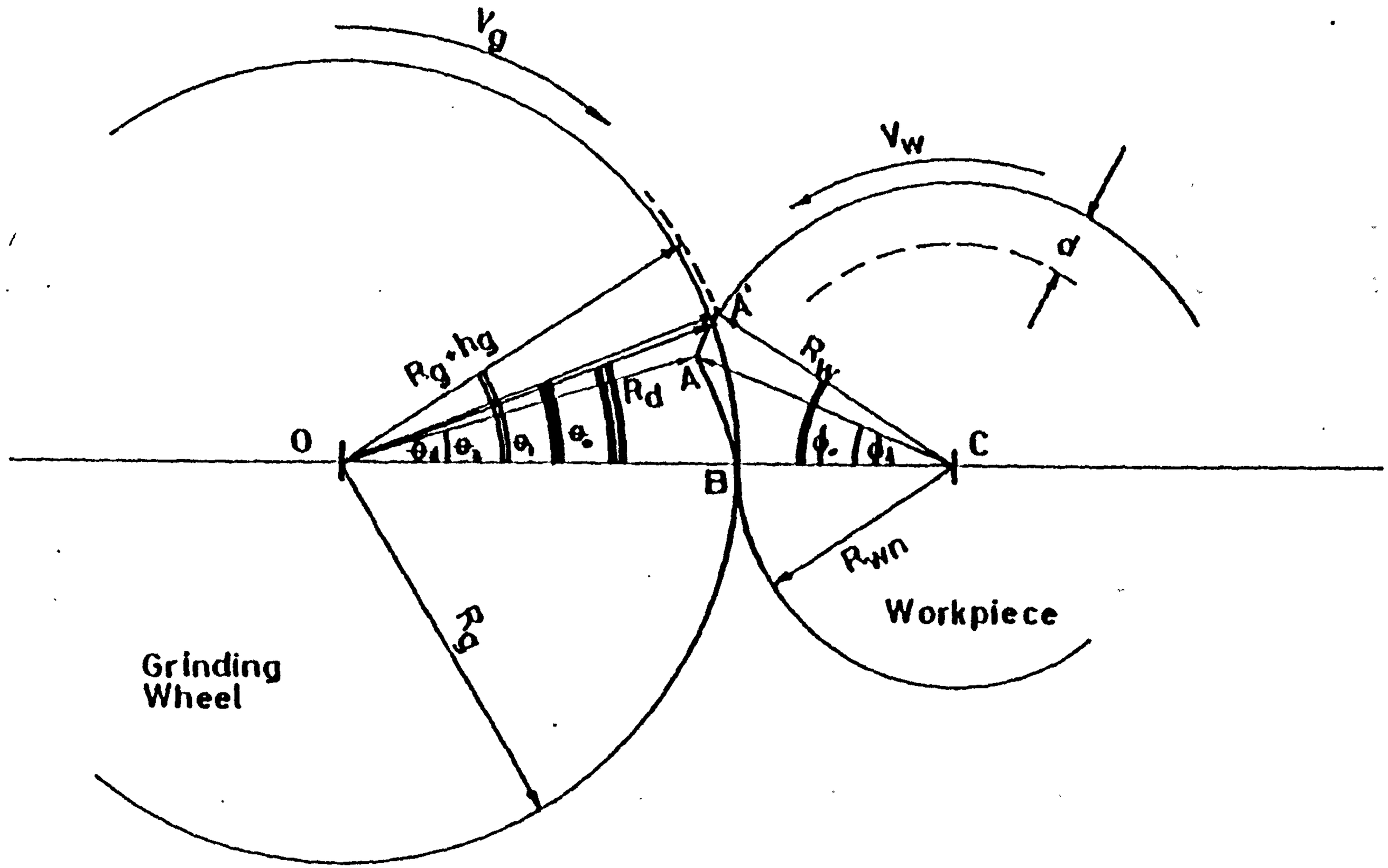

GEOMETRIC BASIS FOR CALCULATION OF IDEALISED UNCUT CHIP DIMENSIONS

FIG.16

UNDEFORMED CHIP THICKNESS VS GRINDING WHEEL SPEED

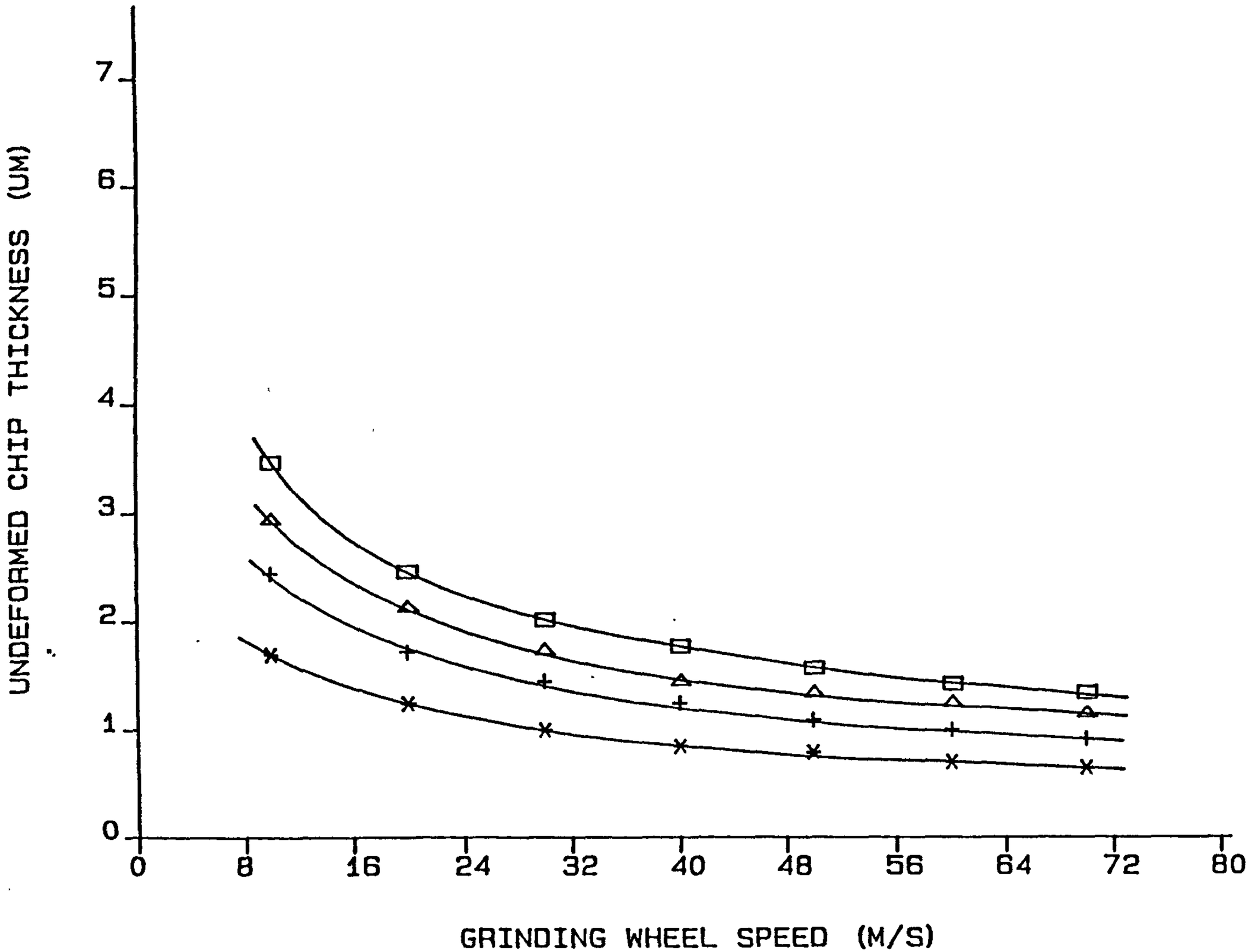

**REFER TO TABLE(S) 8
FOR THEO.L CONDITIONS.

LEGEND

*: - VI = 0.1 MM/S
+: - VI = 0.2 MM/S
△: - VI = 0.3 MM/S
□: - VI = 0.4 MM/S

ADDITIONAL DATA

G-RATIO = 180

FIG. 17

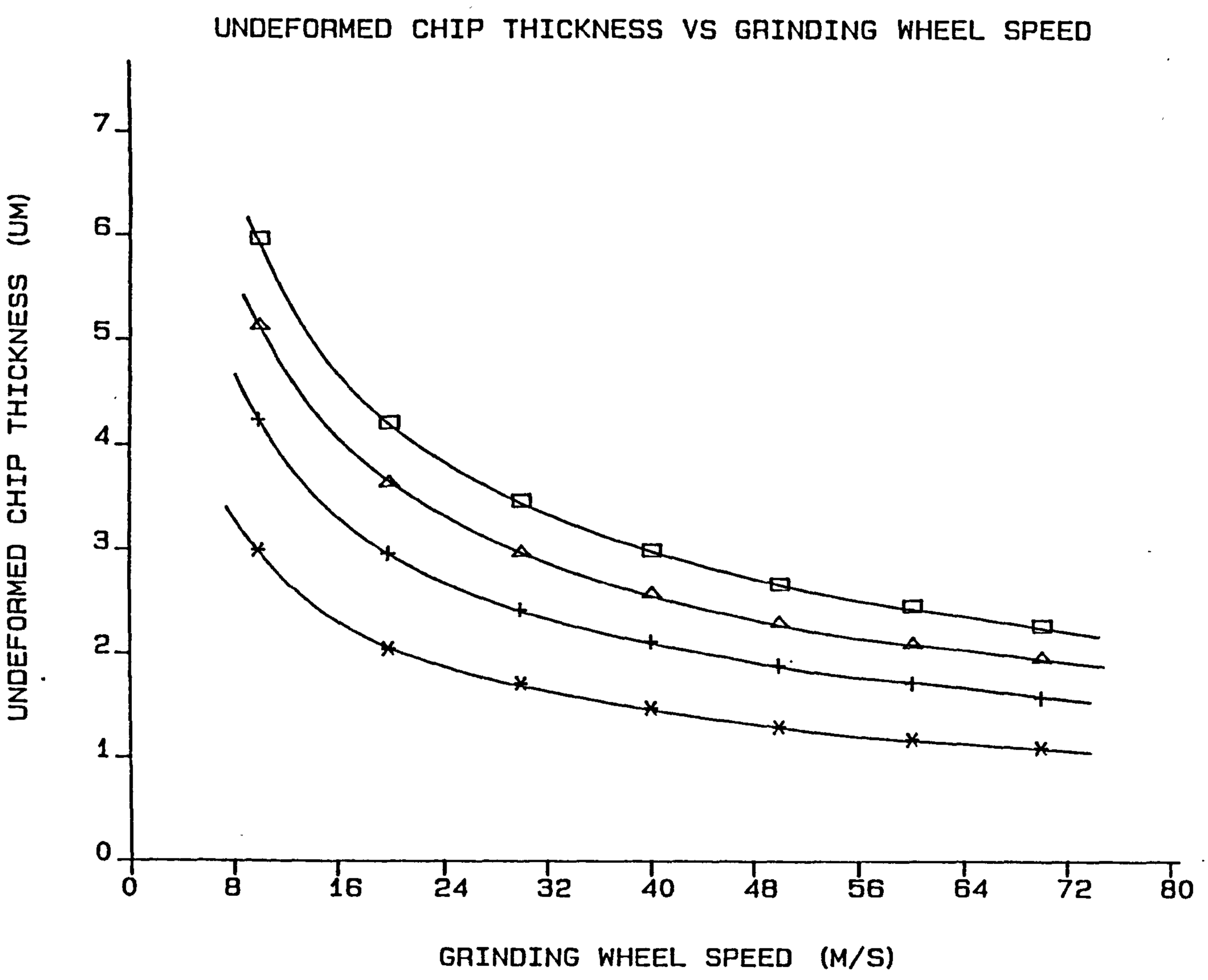
UNDEFORMED CHIP THICKNESS VS GRINDING WHEEL SPEED
UNDEFORMED CHIP THICKNESS (UM)
0
1
2
3
4
5
6
7
0
8
16
24
32
40
48
56
64
72
80
GRINDING WHEEL SPEED (M/S)
**REFER TO TABLE(S) 8
FOR THEO.L CONDITIONS.
LEGEND
*: - VI = 0.1 MM/S
+: - VI = 0.2 MM/S
△: - VI = 0.3 MM/S
□: - VI = 0.4 MM/S
ADDITIONAL DATA
G-RATIO = 60

FIG. 18

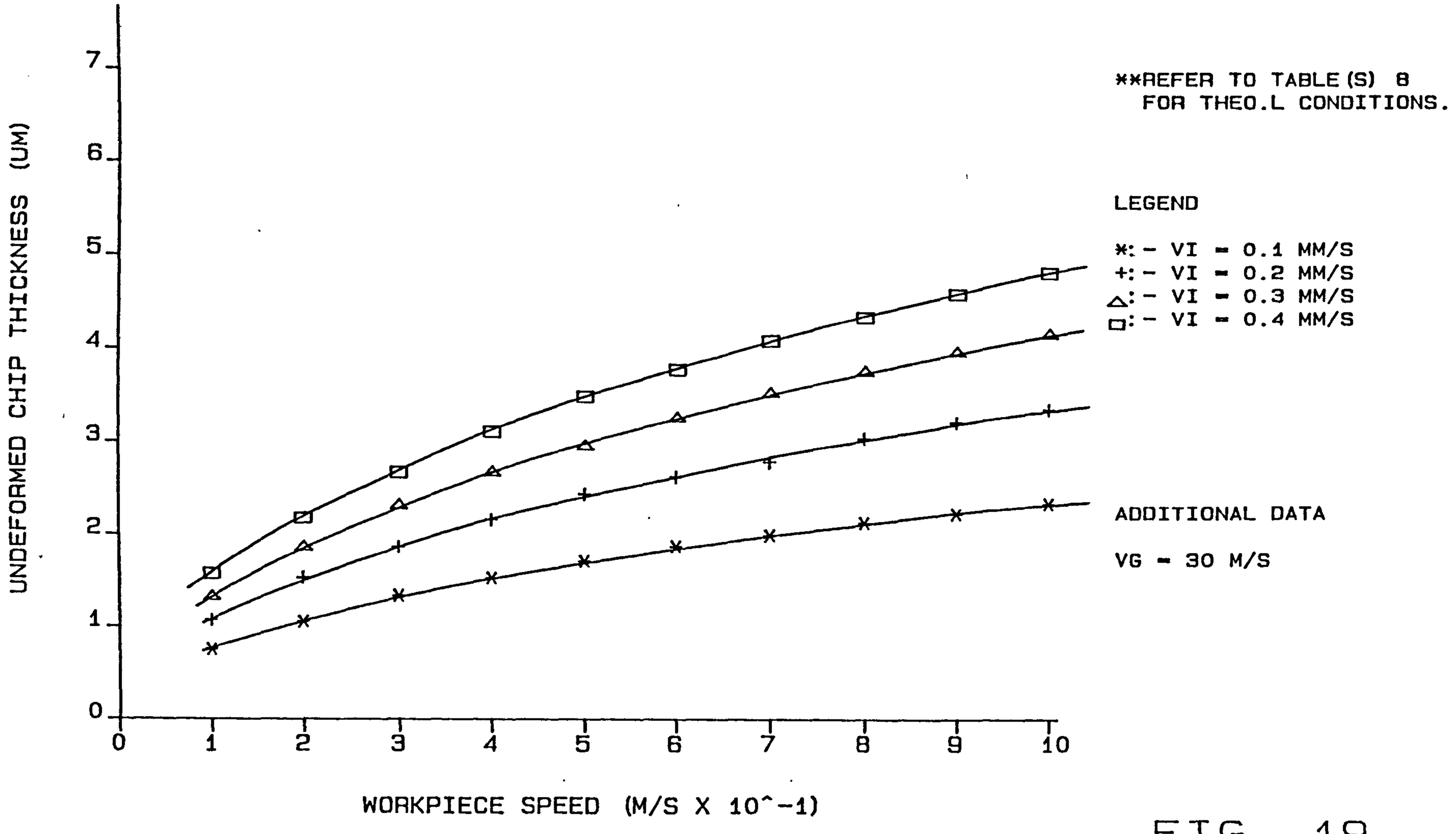
UNDEFORMED CHIP THICKNESS VS WORKPIECE SPEED
UNDEFORMED CHIP THICKNESS (UM)
0
1
2
3
4
5
6
7
0
1
2
3
4
5
6
7
8
9
10
WORKPIECE SPEED (M/S X 10^-1)
**REFER TO TABLE(S) 8
FOR THEO.L CONDITIONS.
LEGEND
*:- VI = 0.1 MM/S
+:- VI = 0.2 MM/S
△:- VI = 0.3 MM/S
□:- VI = 0.4 MM/S
ADDITIONAL DATA
VG = 30 M/S

FIG. 19

UNDEFORMED CHIP THICKNESS VS WORKPIECE SPEED

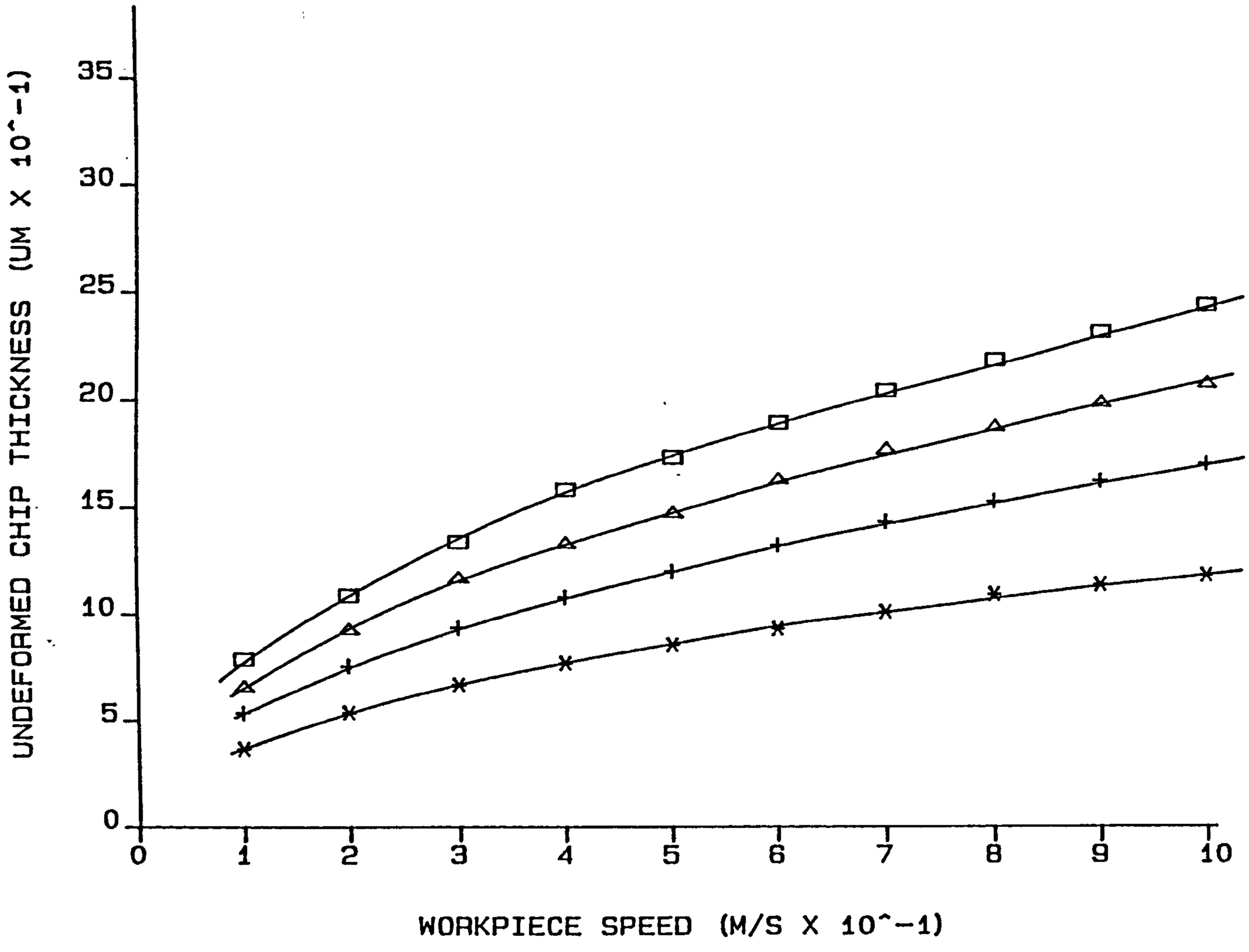

**REFER TO TABLE(S) 8
FOR THEO.L CONDITIONS.

LEGEND

*:- VI = 0.1 MM/S
+:- VI = 0.2 MM/S
△:- VI = 0.3 MM/S
□:- VI = 0.4 MM/S

ADDITIONAL DATA

VG = 60 M/S

FIG.20A

UNDEFORMED CHIP THICKNESS VS GRINDING WHEEL SPEED

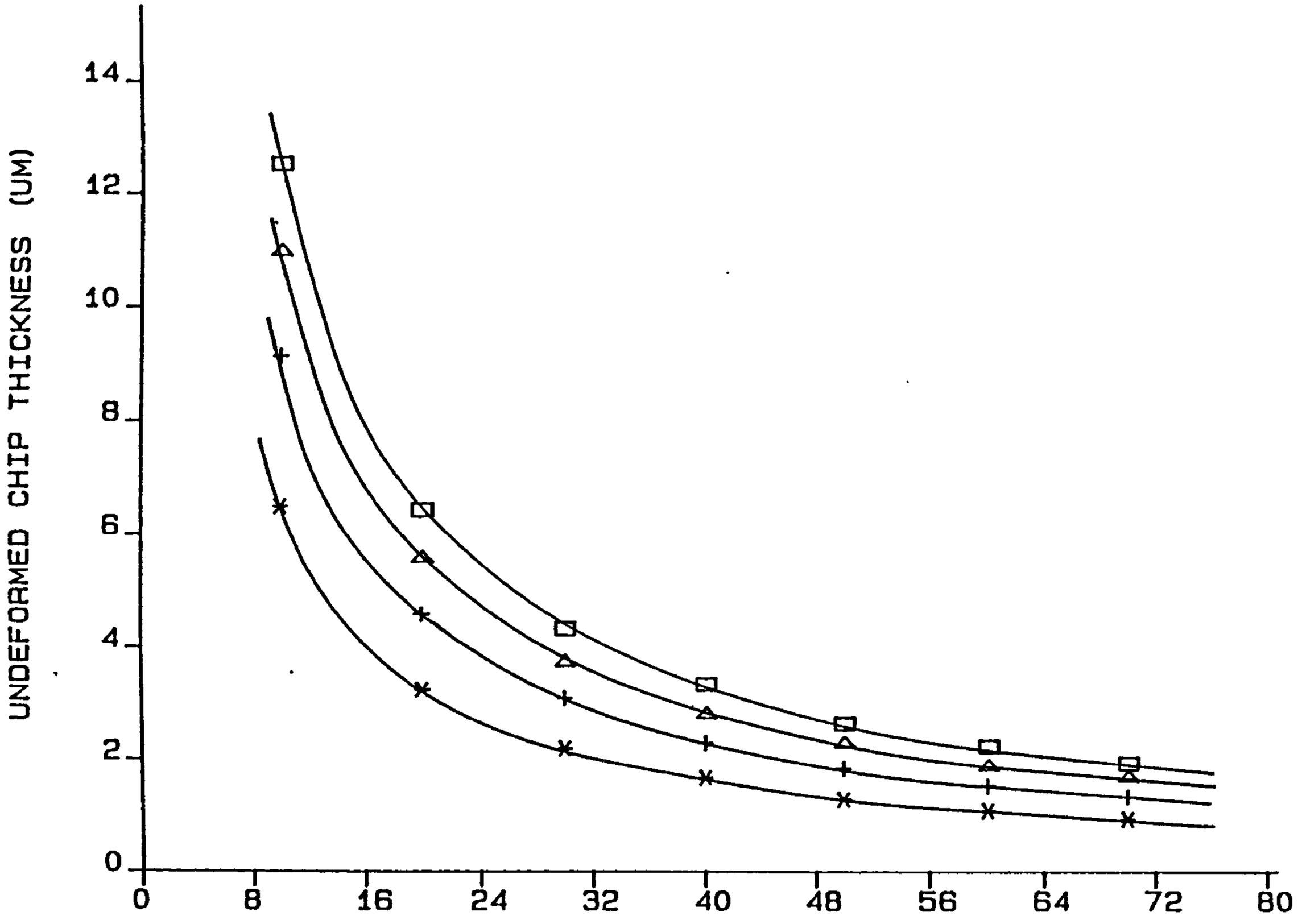

**REFER TO TABLE(S) 8
FOR THEO.L CONDITIONS.

LEGEND

*:- VW = 0.2 M/S
+:- VW = 0.4 M/S
△:- VW = 0.6 M/S
□:- VW = 0.8 M/S

ADDITIONAL DATA

VI = 0.4 MM/S

FIG.20B

UNDEFORMED CHIP THICKNESS VS GRINDING WHEEL SPEED

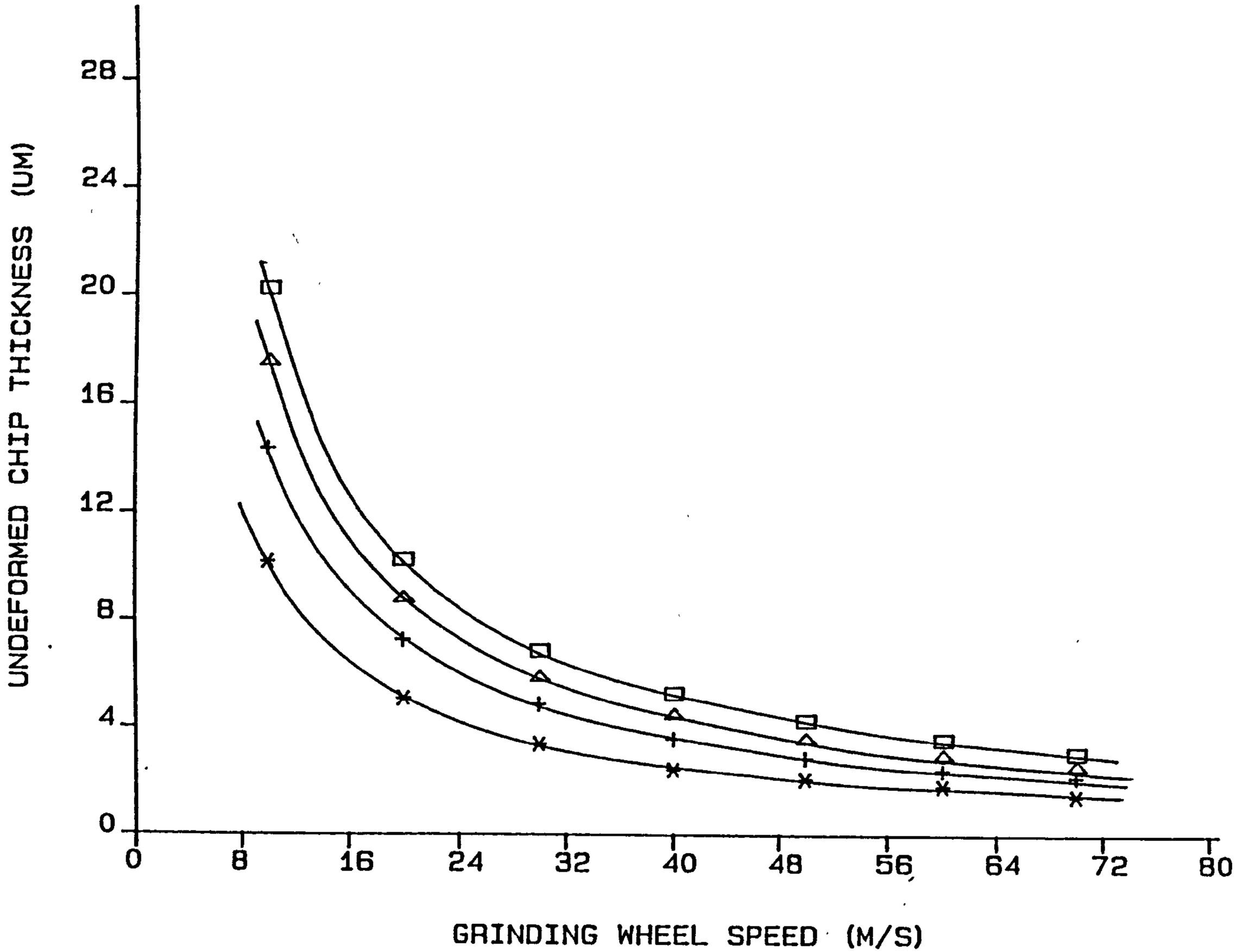

**REFER TO TABLE(S) 8
FOR THEO.L CONDITIONS.

LEGEND

*: - VW = 0.2 M/S
+: - VW = 0.4 M/S
△: - VW = 0.6 M/S
□: - VW = 0.8 M/S

ADDITIONAL DATA

VI = 1 MM/S

FIG.20C

UNDEFORMED CHIP THICKNESS VS GRINDING WHEEL SPEED

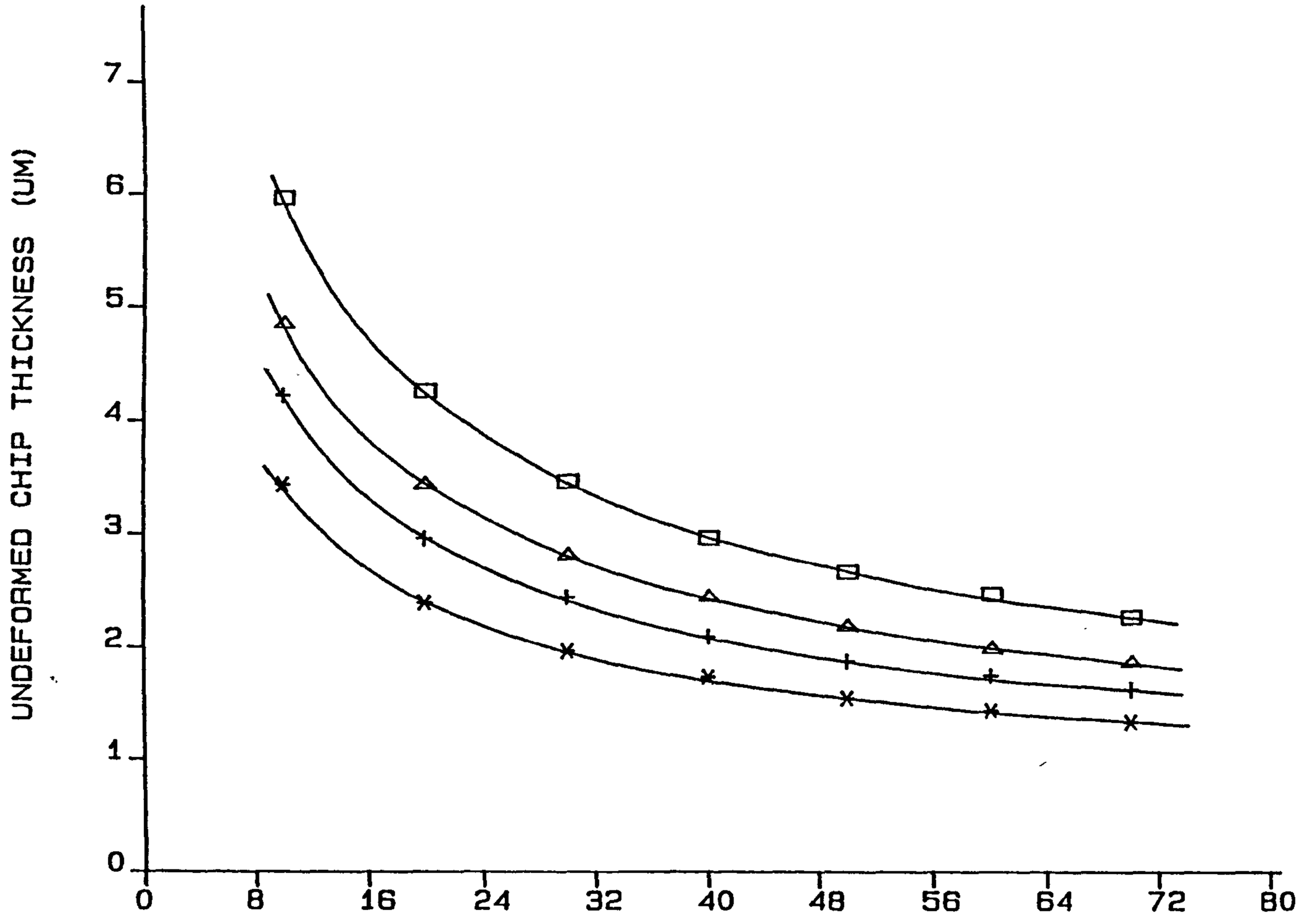

**REFER TO TABLE(S) 8
FOR THEO.L CONDITIONS.

LEGEND

*: - Q-RATIO = 180
+: - Q-RATIO = 120
△: - Q-RATIO = 90
□: - Q-RATIO = 60

ADDITIONAL DATA

VI = 0.4 MM/S

FIG. 21

UNDEFORMED CHIP THICKNESS VS GRINDING WHEEL SPEED

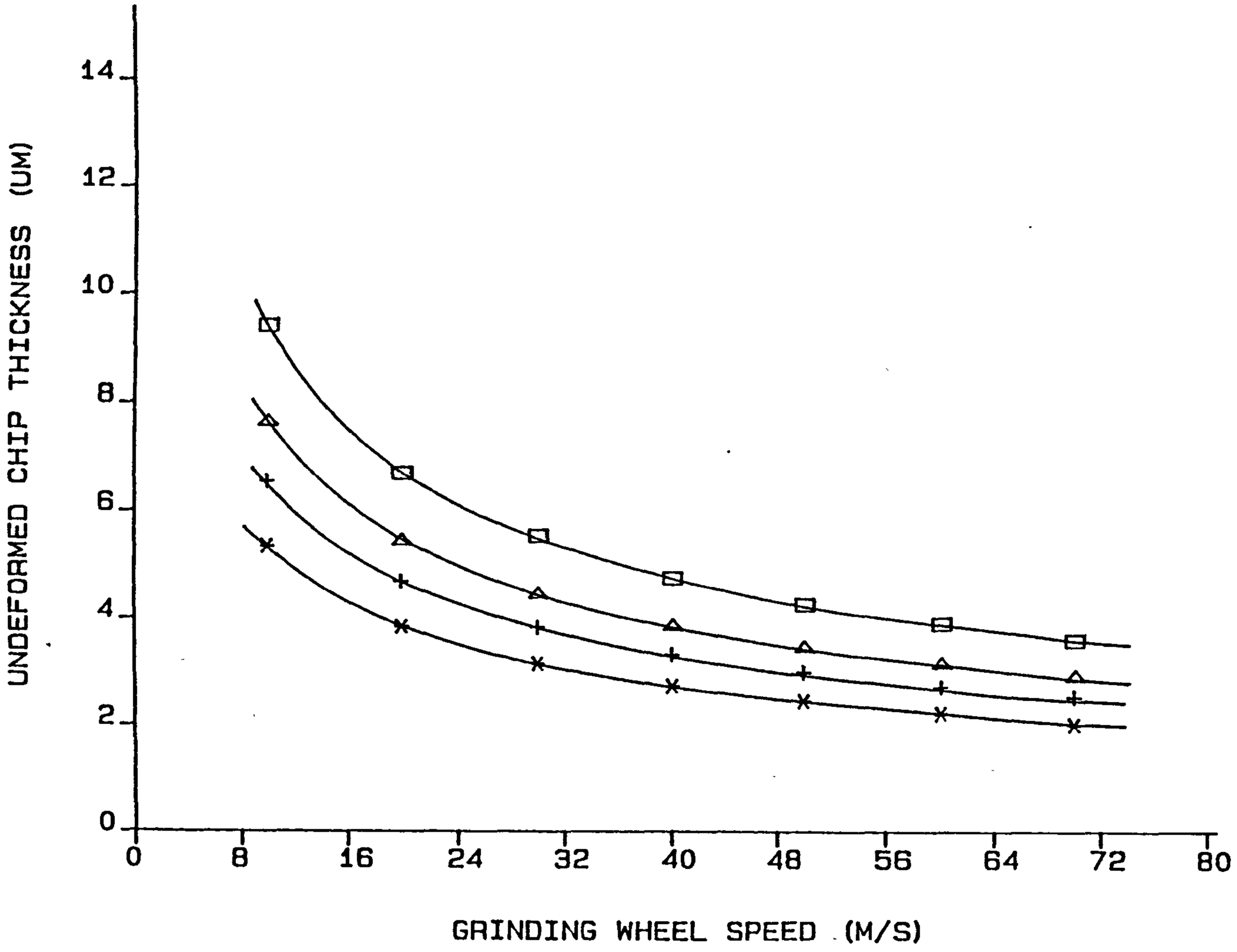

**REFER TO TABLE(S) 8
FOR THEO.L CONDITIONS.

LEGEND

*: - Q-RATIO = 180
+: - Q-RATIO = 120
△: - Q-RATIO = 90
□: - Q-RATIO = 60

ADDITIONAL DATA

VI = 1 MM/S

FIG. 22

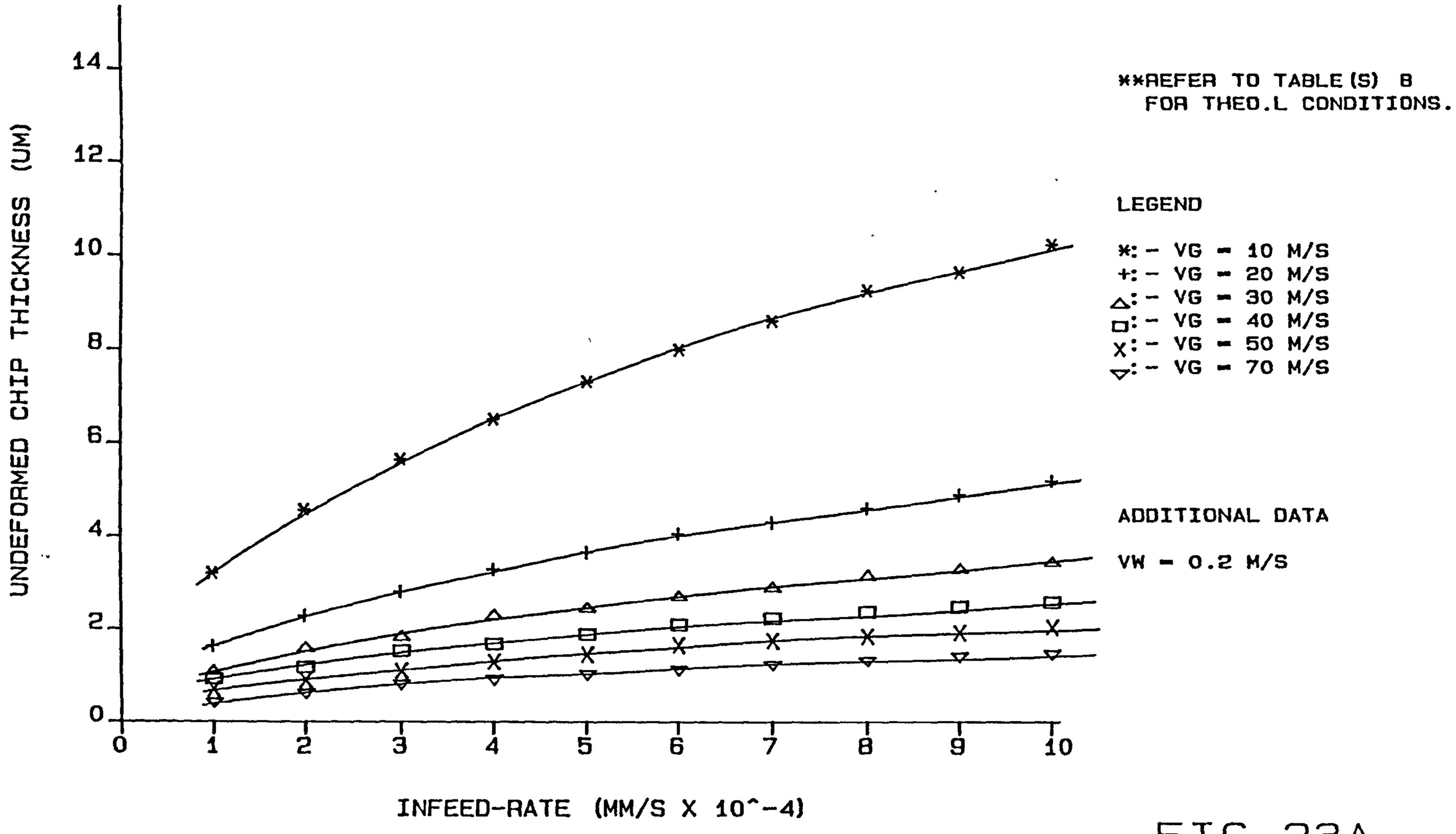
UNDEFORMED CHIP THICKNESS VS INFEED-RATE
UNDEFORMED CHIP THICKNESS (UM)
INFEED-RATE (MM/S X 10^-4)
0
2
4
6
8
10
12
14
0
1
2
3
4
5
6
7
8
9
10
**REFER TO TABLE(S) 8
FOR THEO.L CONDITIONS.
LEGEND
*: - VG = 10 M/S
+: - VG = 20 M/S
△: - VG = 30 M/S
□: - VG = 40 M/S
X: - VG = 50 M/S
▽: - VG = 70 M/S
ADDITIONAL DATA
VW = 0.2 M/S

FIG.23A

UNDEFORMED CHIP THICKNESS VS INFEED-RATE

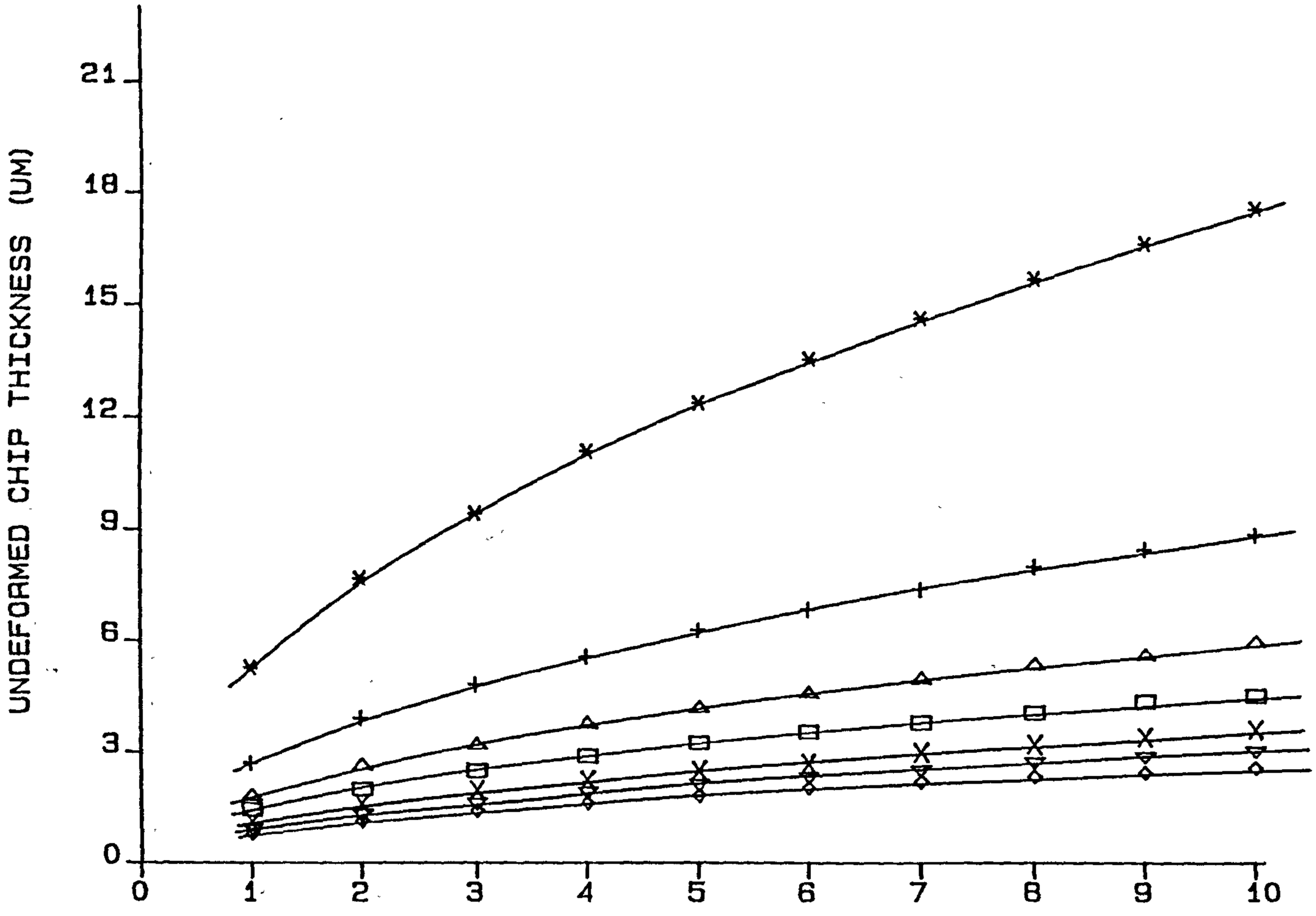

**REFER TO TABLE(S) 8
FOR THEO.L CONDITIONS.

LEGEND

*: - VG = 10 M/S
+: - VG = 20 M/S
△: - VG = 30 M/S
□: - VG = 40 M/S
X: - VG = 50 M/S
▽: - VG = 60 M/S
◇: - VG = 70 M/S

ADDITIONAL DATA

VW = 0.6 M/S

FIG.23B

UNDEFORMED CHIP THICKNESS VS INFEED-RATE

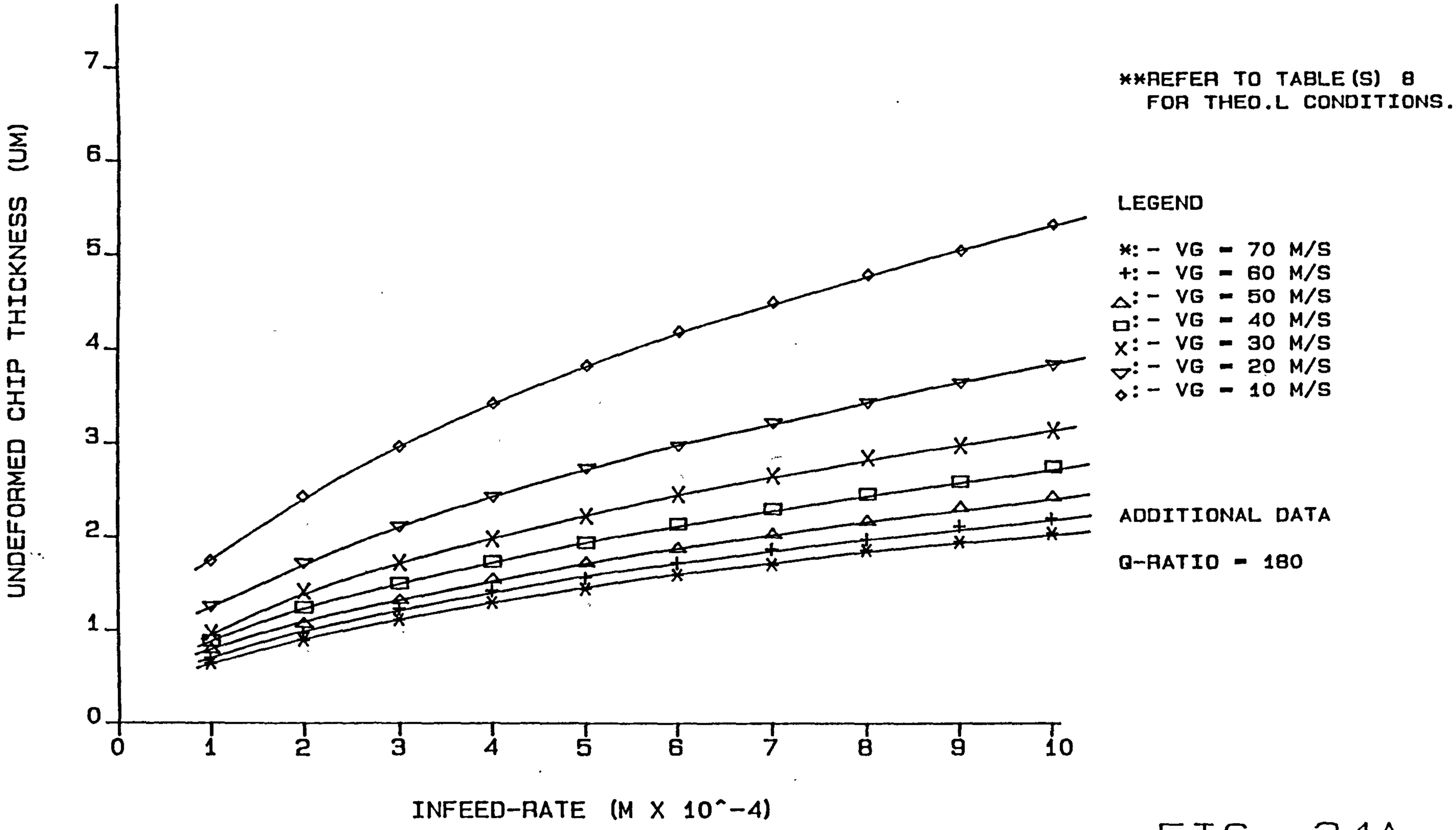

**REFER TO TABLE(S) 8
FOR THEO.L CONDITIONS.

LEGEND

*:- VG = 70 M/S
+:- VG = 60 M/S
△:- VG = 50 M/S
□:- VG = 40 M/S
X:- VG = 30 M/S
▽:- VG = 20 M/S
◇:- VG = 10 M/S

ADDITIONAL DATA

Q-RATIO = 180

FIG. 24A

UNDEFORMED CHIP THICKNESS VS INFEED-RATE

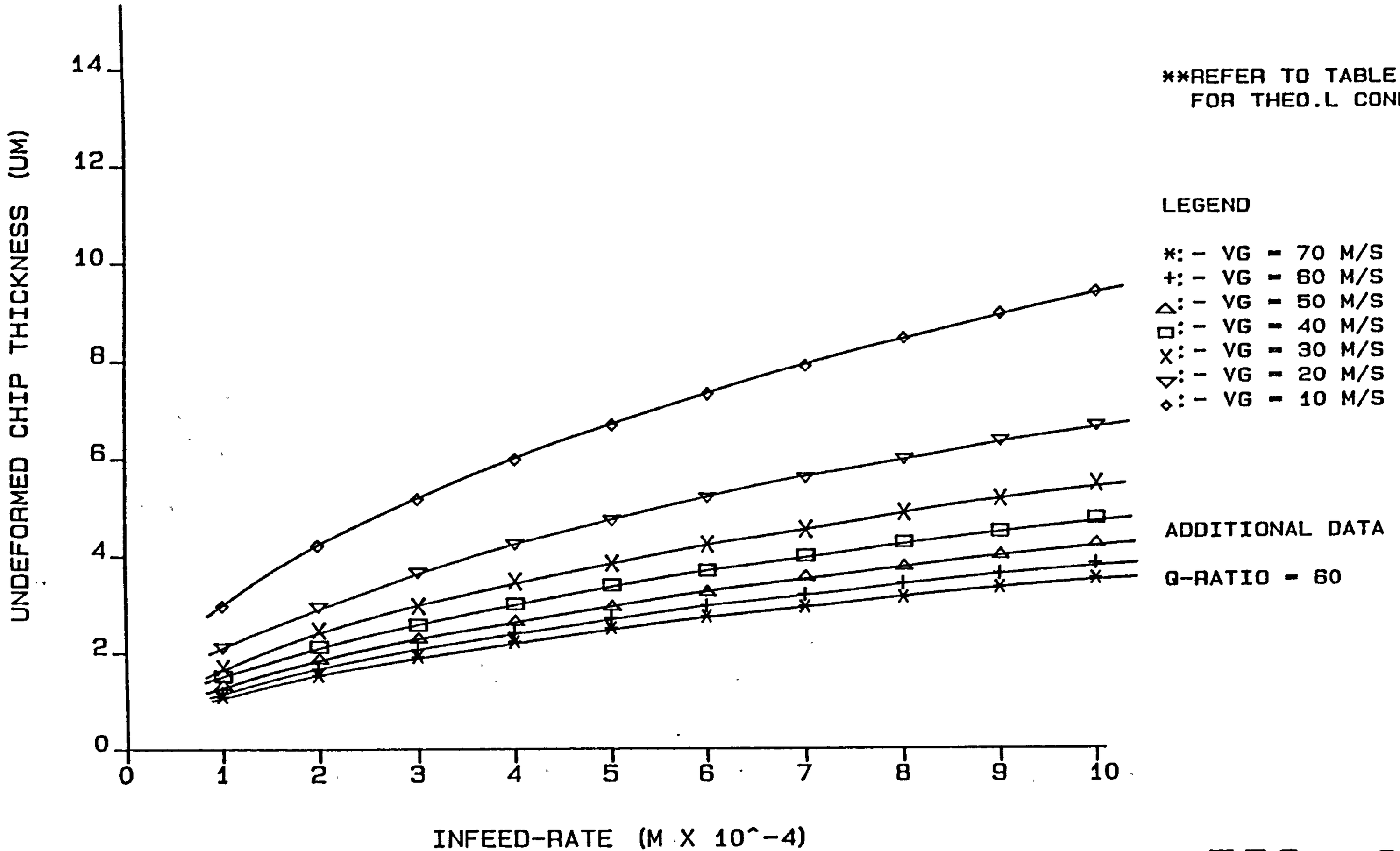

**REFER TO TABLE(S) 8
FOR THEO.L CONDITIONS.

LEGEND

*: - VG = 70 M/S
+: - VG = 60 M/S
△: - VG = 50 M/S
□: - VG = 40 M/S
X: - VG = 30 M/S
▽: - VG = 20 M/S
◇: - VG = 10 M/S

ADDITIONAL DATA

G-RATIO = 60

FIG. 24B

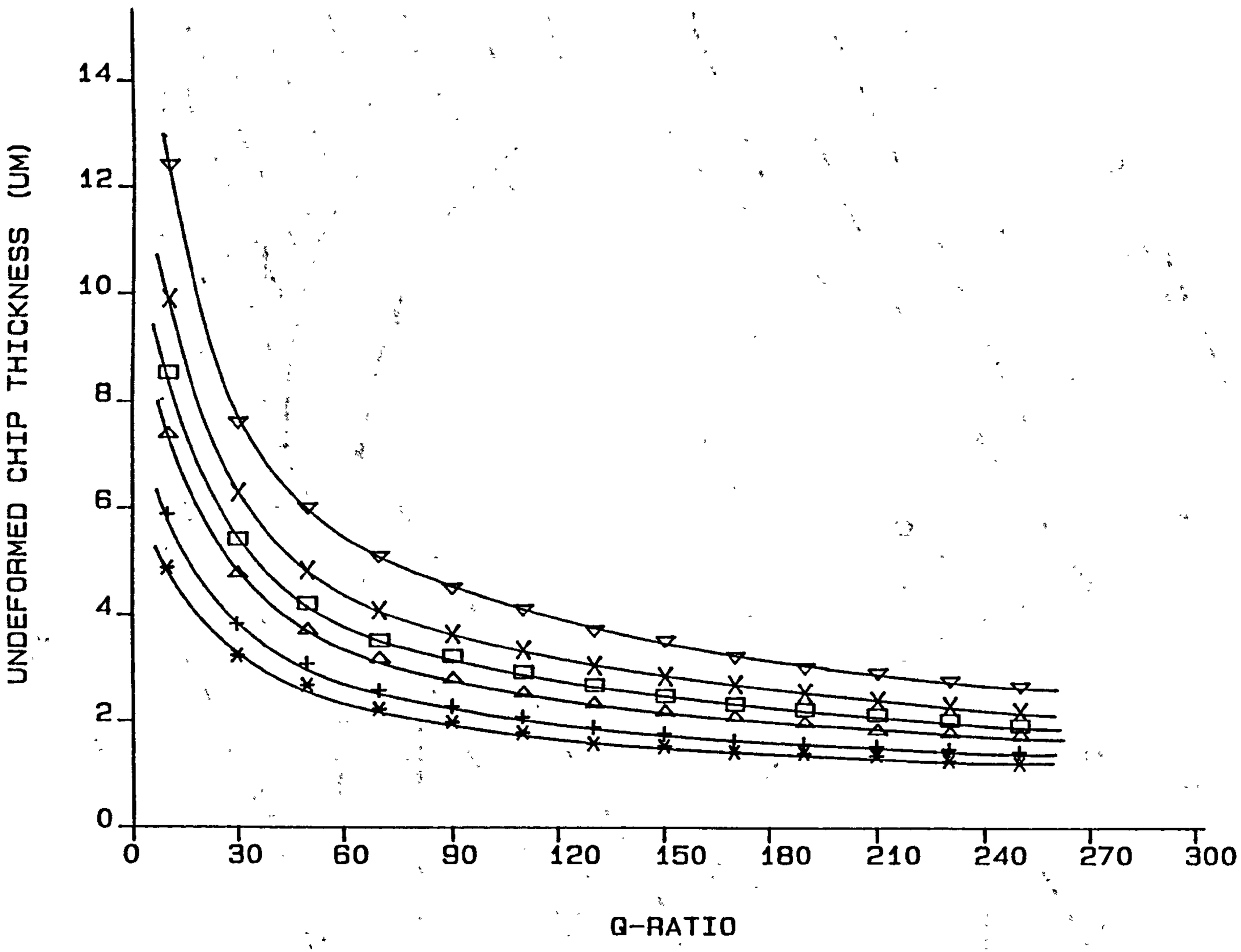

**REFER TO TABLE(S) 8
FOR THEO.L CONDITIONS.

LEGEND

*: - VG=60 M/S (VI=0.4 MM/S)
+: - VG=45 M/S (VI=0.4 MM/S)
△: - VG=30 M/S (VI=0.4 MM/S)
□: - VG=60 M/S (VI=1 MM/S)
×: - VG=45 M/S (VI=1 MM/S)
▽: - VG=30 M/S (VI=1 MM/S)

ADDITIONAL DATA

NONE

FIG. 25

Text cut off in original

RELATIONSHIP BETEEN UNDEFORMED CHIP THICKNESS, GRINDING WHEEL SPEED AND INFEED-RATE

FIG.26A

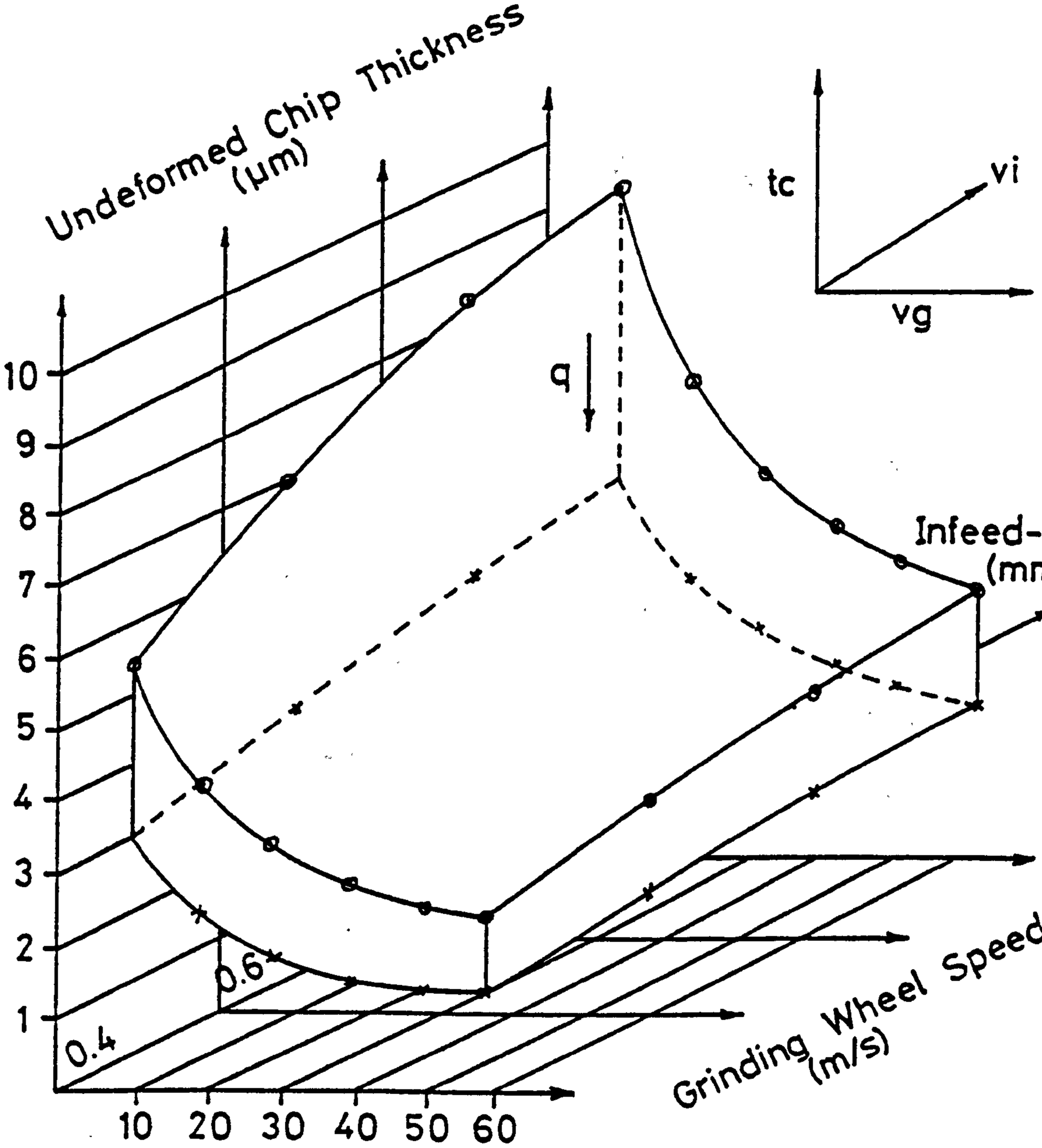

LEGEND

x~q-ratio=180

o~q-ratio=60

TRENDS OF VARIOUS SOLUTIONS FOR CHIP THICKNESS VS Q-RATIO

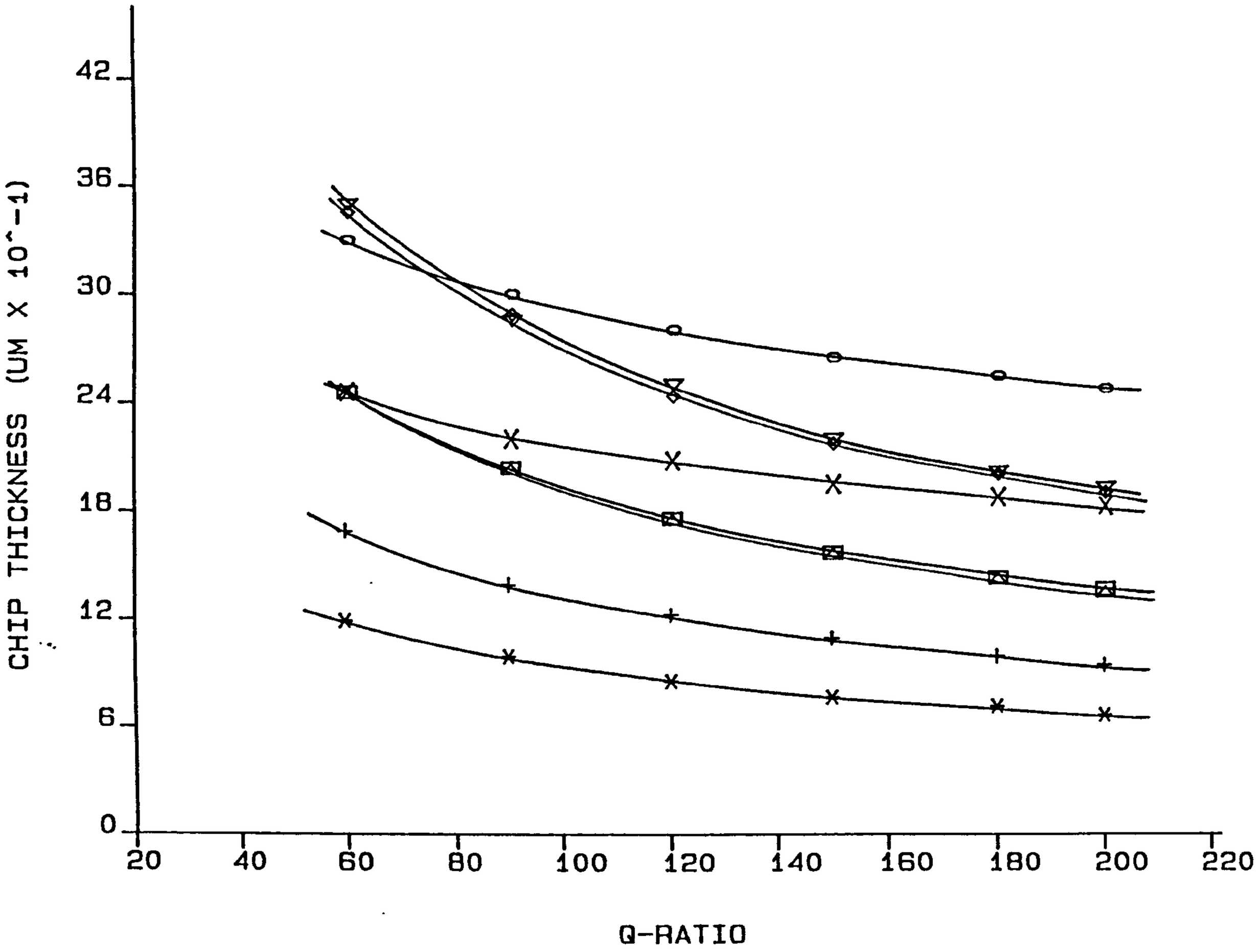

**REFER TO TABLE(S) N/A
FOR THEO.L CONDITIONS.

LEGEND

*: - VG=60M/S-OPITZ & PEKLENIK
+: - VG=30M/S-OPITZ & PEKLENIK
△: - VG=60M/S-ROWE & PAHLITSCH
□: - VG=60M/S BELL ET AL
×: - VG=60M/S SHAW ET AL
▽: - VG=30M/S-ROWE & PAHLITSCH
◇: - VG=30M/S BELL ET AL
○: - VG=30M/S SHAW ET AL

ADDITIONAL DATA

DG=0.484 M
DW=0.04 M
VI=0.4 MM/S

FIG. 27A

UNDEFORMED CHIP THICKNESS VS Q-RATIO

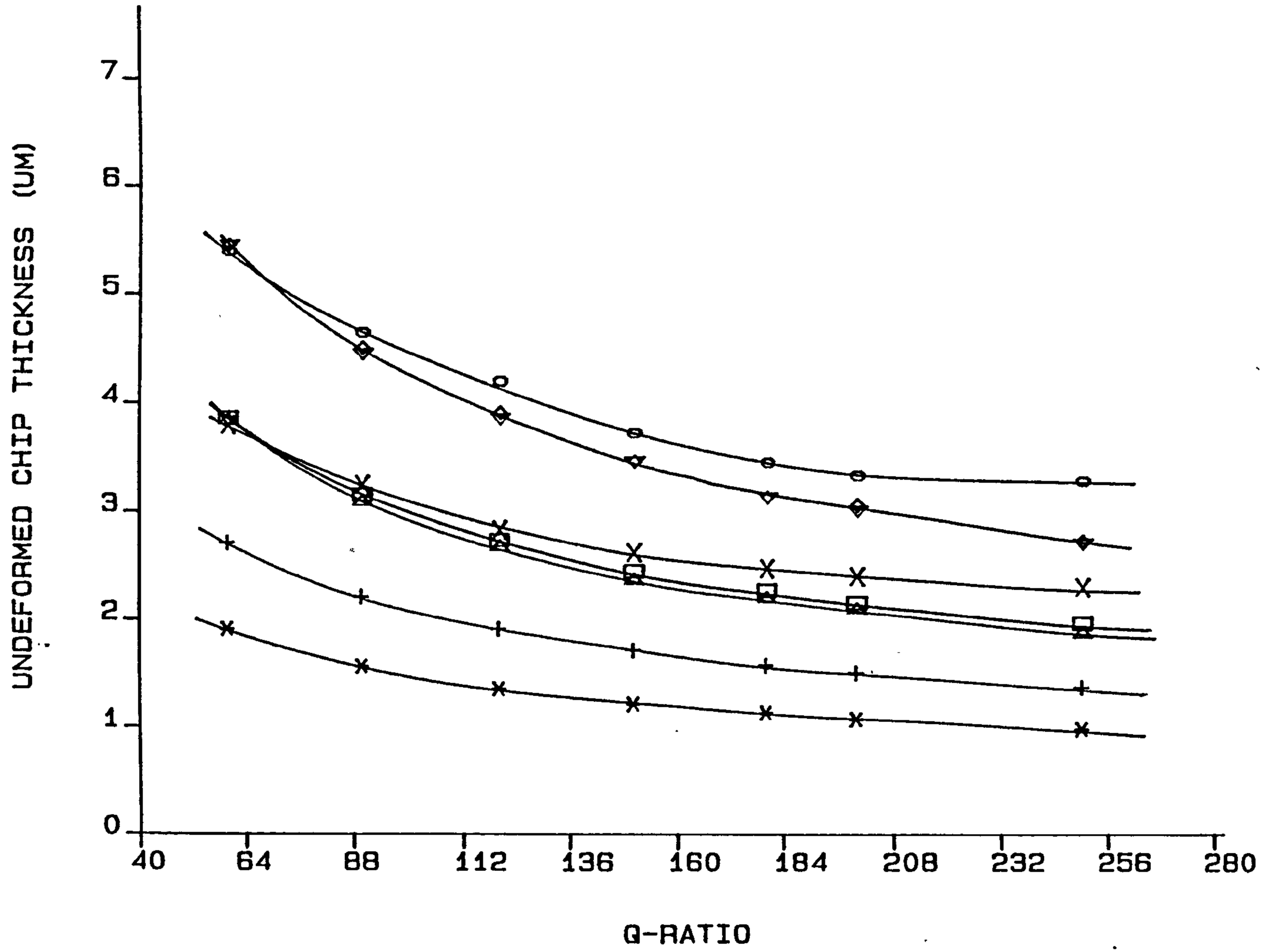

**REFER TO TABLE(S) N/A
FOR THEO.L CONDITIONS.

LEGEND

*: - VG=60M/S-OPITZ & PEKLENIK
+: - VG=30M/S-OPITZ & PEKLENIK
△: - VG=60M/S-BELL ET AL
□: - VG=60M/S-ROWE & PAHLITSCH
X: - VG=60M/S-SHAW ET AL
▽: - VG=30M/S-BELL ET AL
◇: - VG=30M/S-ROWE & PAHLITSCH
○: - VG=30M/S-SHAW ET AL

ADDITIONAL DATA

DG = 0.484 M
DW = 0.04 M
VI = 1 MM/S

FIG.27B

UNDEFORMED CHIP LENGTH VS WORKPIECE SPEED

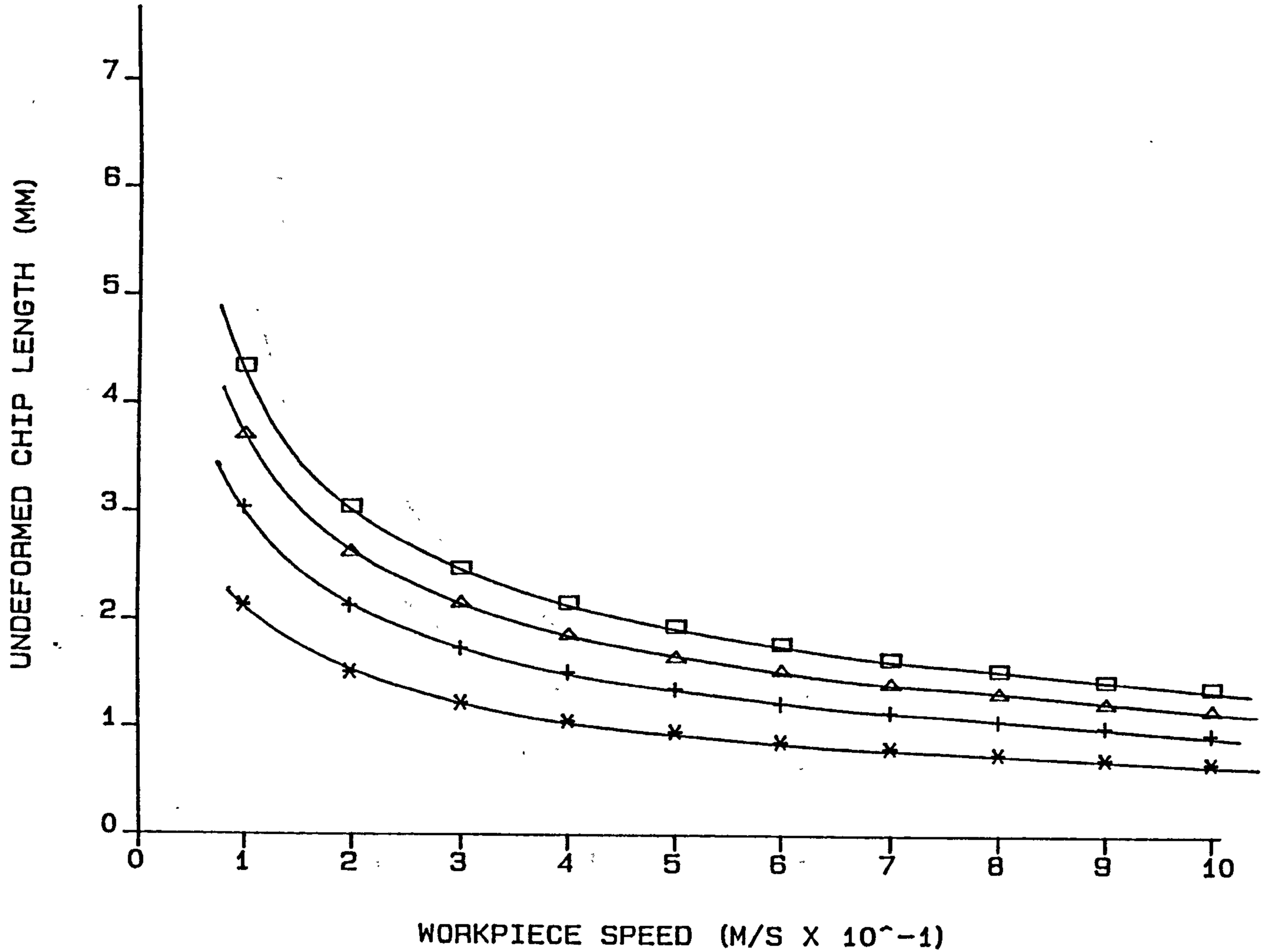

**REFER TO TABLE(S) 8
FOR THEO.L CONDITIONS.

LEGEND

*: - VI = 0.1 MM/S
+: - VI = 0.2 MM/S
△: - VI = 0.3 MM/S
□: - VI = 0.4 MM/S

ADDITIONAL DATA

VG - VARIOUS

FIG.28

UNDEFORMED CHIP FORMATION TIME VS GRINDING WHEEL SPEED

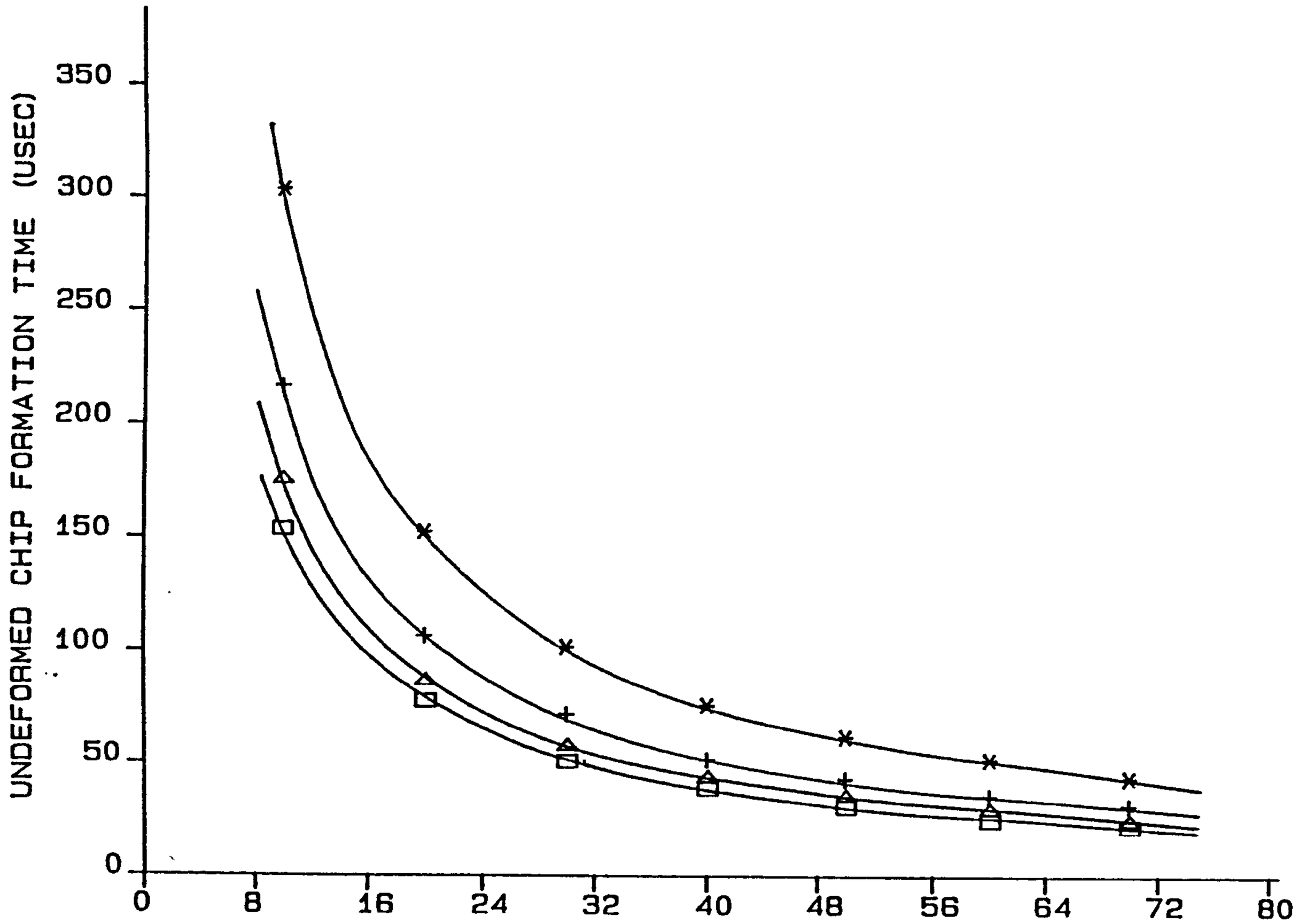

**REFER TO TABLE(S) B
FOR THEO.L CONDITIONS.

LEGEND

*: - VW = 0.2 M/S
+: - VW = 0.4 M/S
△: - VW = 0.6 M/S
□: - VW = 0.8 M/S

ADDITIONAL DATA

VI = 0.4 MM/S

FIG.29A

UNDEFORMED CHIP FORMATION TIME VS GRINDING WHEEL SPEED

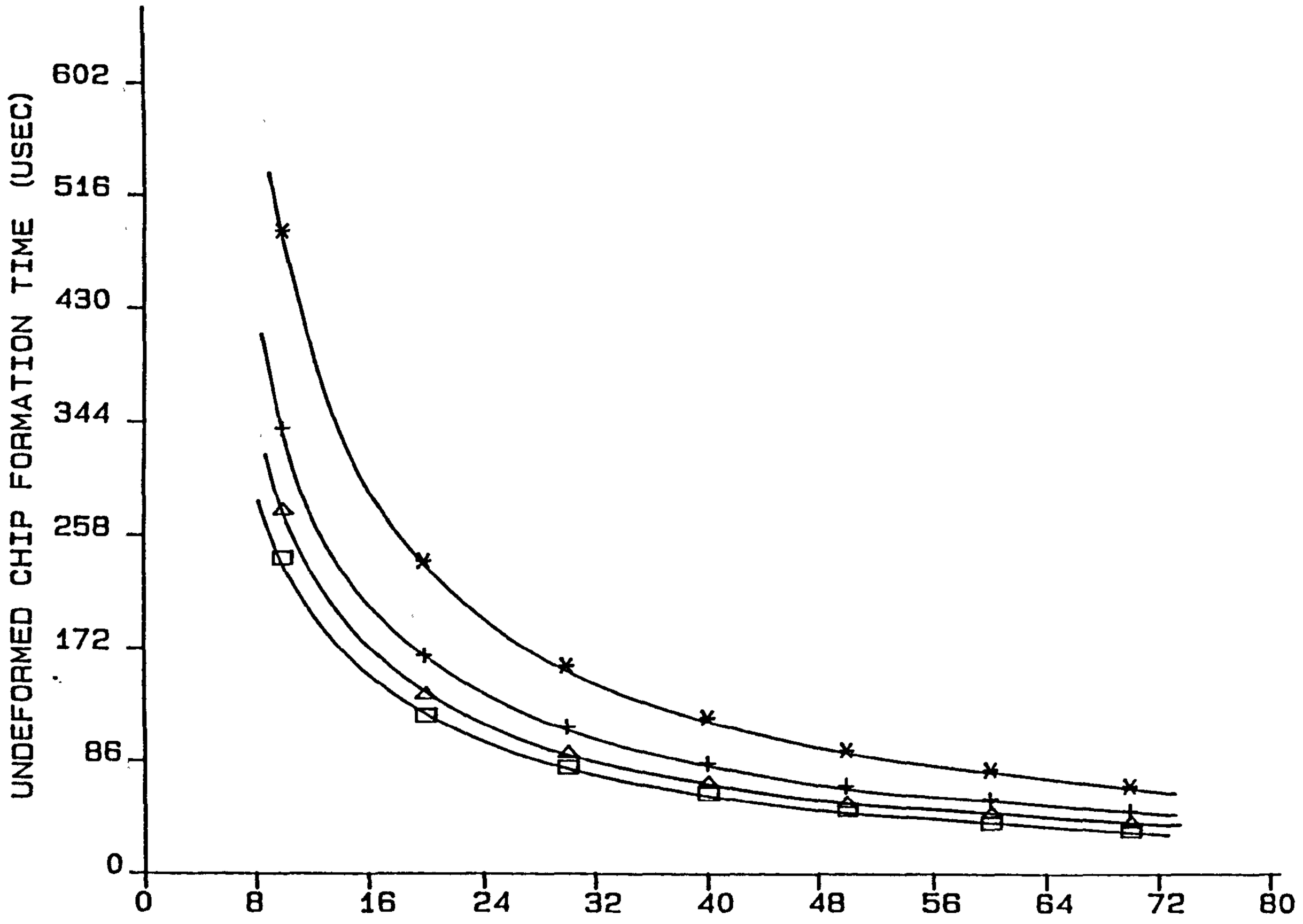

**REFER TO TABLE(S) 8
FOR THEO.L CONDITIONS.

LEGEND

*: - VW = 0.2 M/S
+: - VW = 0.4 M/S
△: - VW = 0.6 M/S
□: - VW = 0.8 M/S

ADDITIONAL DATA

VI = 1 MM/S

FIG.29B

UNDEFORMED CHIP FORMATION TIME VS GRINDING WHEEL SPEED

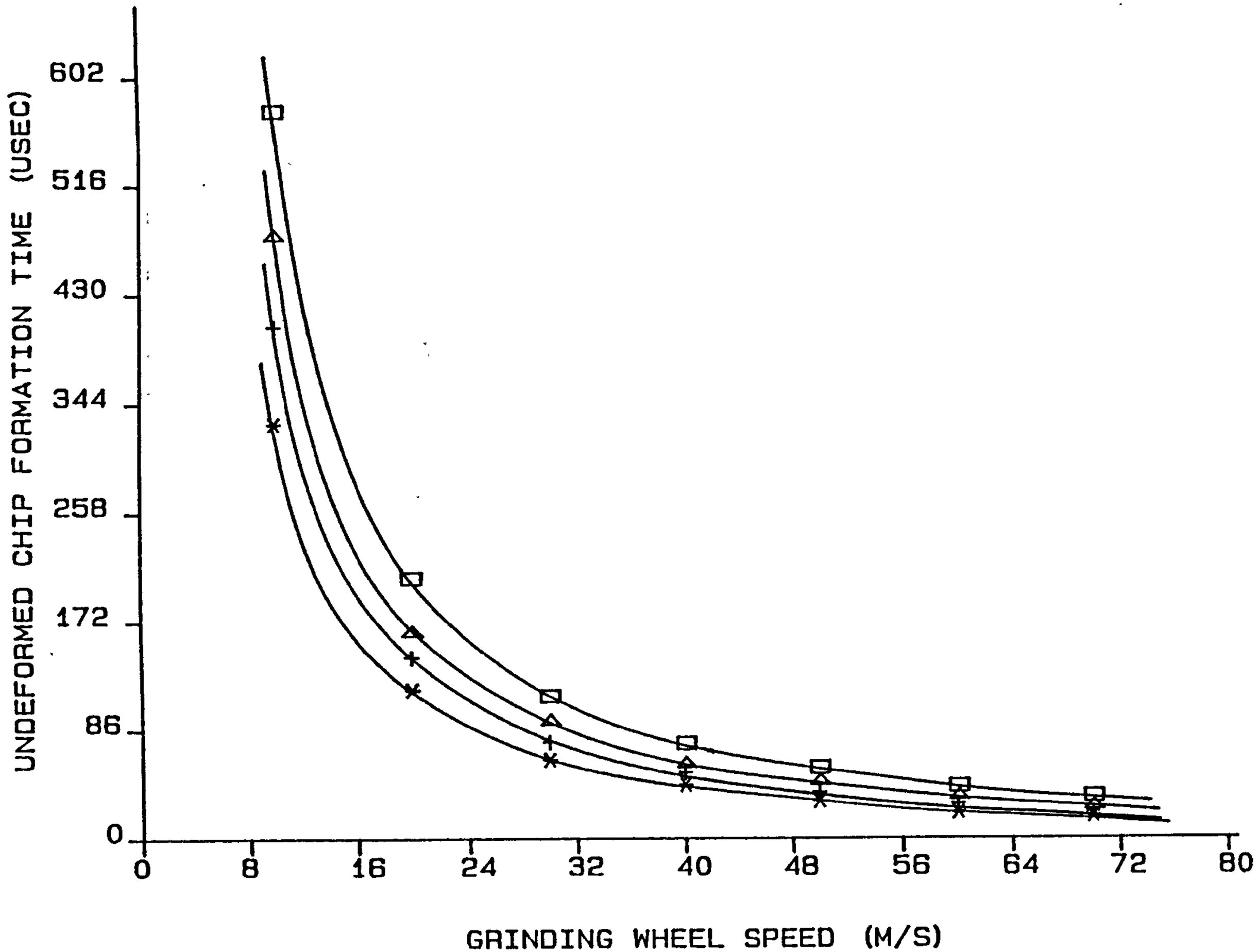

**REFER TO TABLE(S) 8
FOR THEO.L CONDITIONS.

LEGEND

*: - Q-RATIO = 60
+: - Q-RATIO = 90
△: - Q-RATIO = 120
□: - Q-RATIO = 180

ADDITIONAL DATA

VI = 0.4 MM/S

FIG. 30A

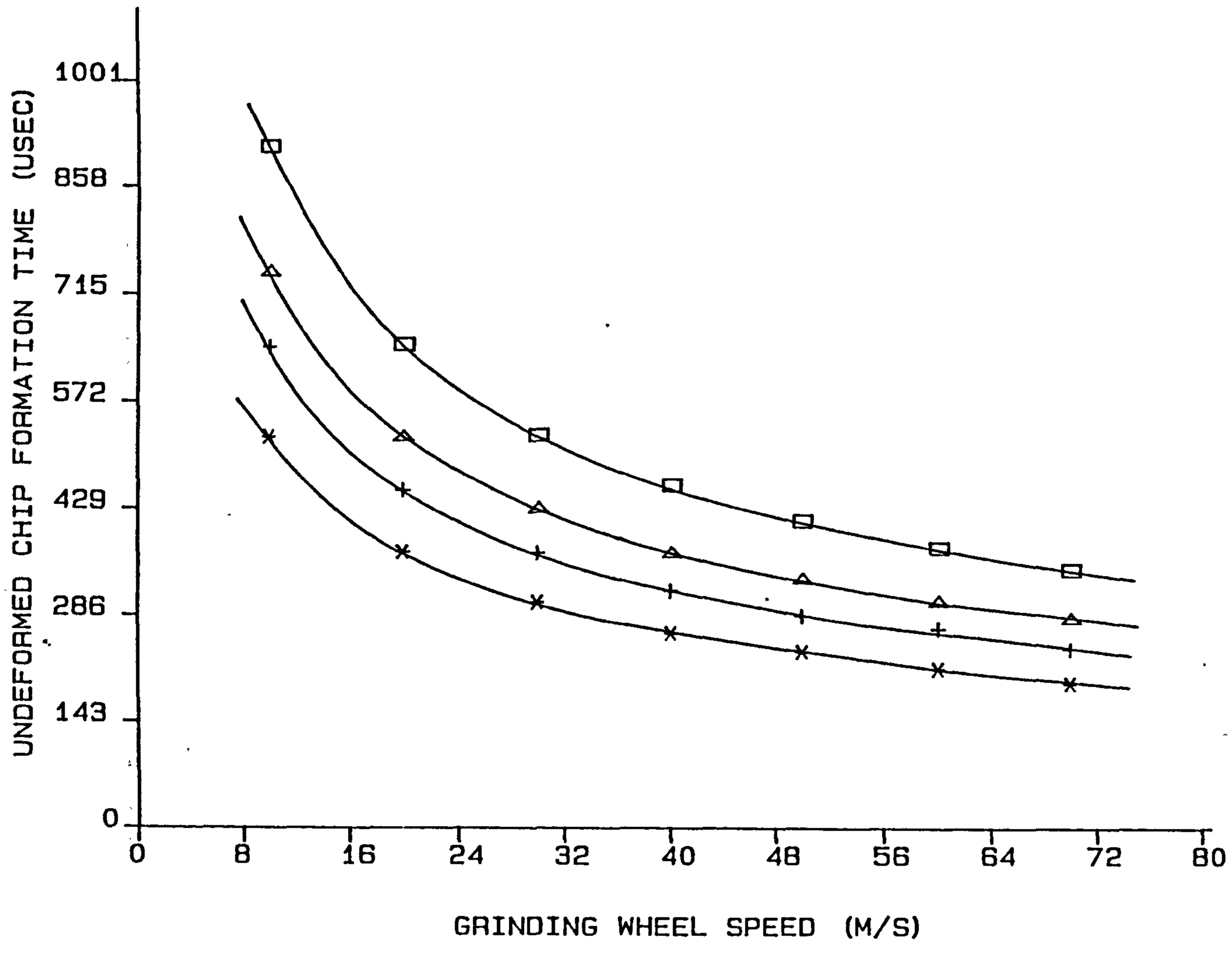
UNDEFORMED CHIP FORMATION TIME VS GRINDING WHEEL SPEED
UNDEFORMED CHIP FORMATION TIME (USEC)
1001
858
715
572
429
286
143
0
0
8
16
24
32
40
48
56
64
72
80
GRINDING WHEEL SPEED (M/S)
**REFER TO TABLE(S) 8
FOR THEO.L CONDITIONS.
LEGEND
*: - Q-RATIO = 60
+: - Q-RATIO = 90
△: - Q-RATIO = 120
□: - Q-RATIO = 180
ADDITIONAL DATA
VI = 1 MM/S

FIG. 30B

UNDEFORMED CHIP FORMATION TIME VS WORKPIECE SPEED

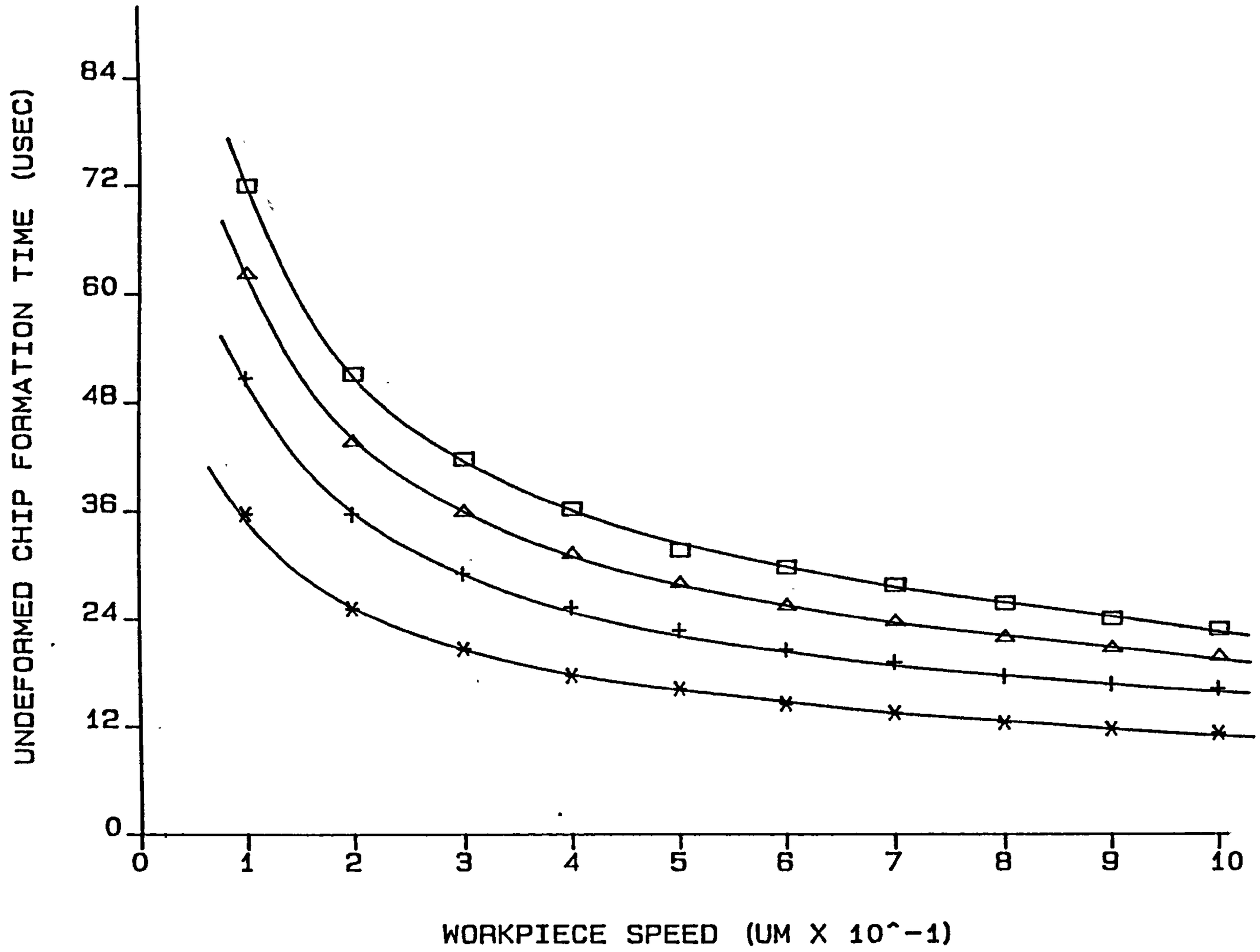

**REFER TO TABLE(S) 8
FOR THEO.L CONDITIONS.

LEGEND

*: - VI = 0.1 MM/S
+: - VI = 0.2 MM/S
△: - VI = 0.3 MM/S
□: - VI = 0.4 MM/S

ADDITIONAL DATA

VG = 80 M/S

FIG.31A

UNDEFORMED CHIP FORMATION TIME VS WORKPIECE SPEED

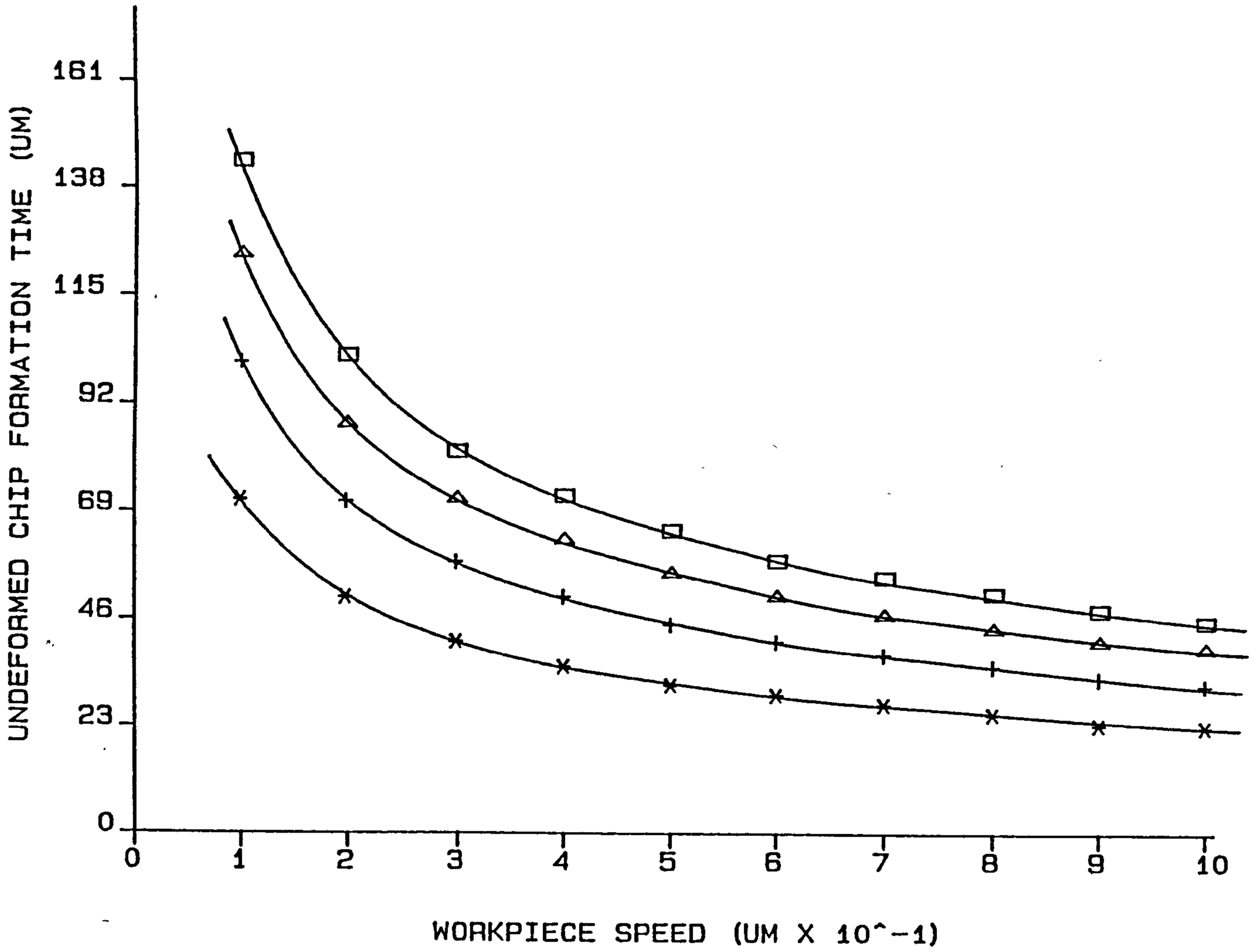

**REFER TO TABLE(S) 8
FOR THEO.L CONDITIONS.

LEGEND

*: - VI = 0.1 MM/S
+: - VI = 0.2 MM/S
△: - VI = 0.3 MM/S
□: - VI = 0.4 MM/S

ADDITIONAL DATA

VG = 30 M/S

FIG.31B

UNDEFORMED CHIP FORMATION TIME VS INFEED-RATE

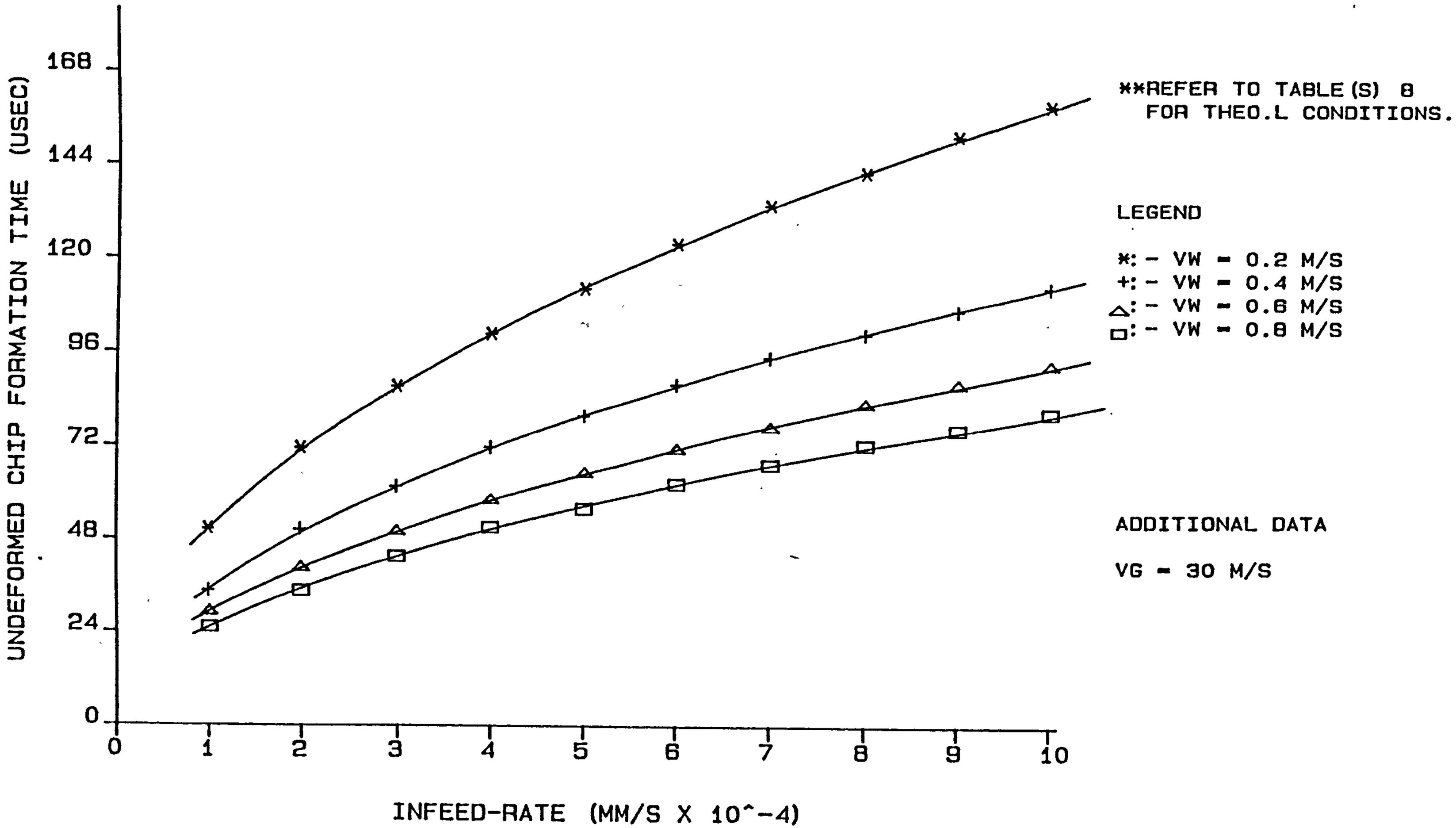

FIG.32A

UNDEFORMED CHIP FORMATION TIME VS INFEED-RATE

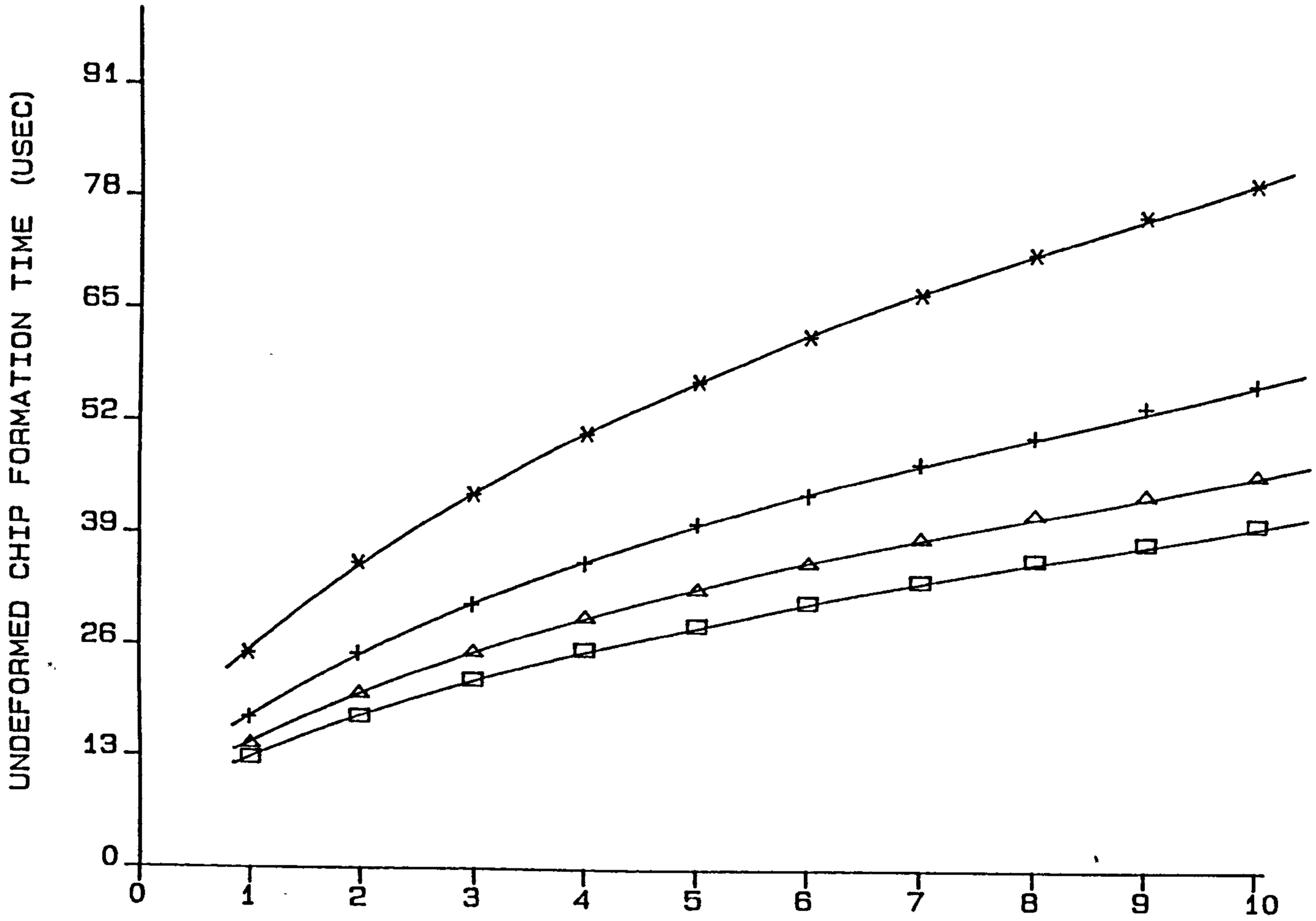

**REFER TO TABLE(S) 8
FOR THEO.L CONDITIONS.

LEGEND

*: - VW = 0.2 M/S
+: - VW = 0.4 M/S
△: - VW = 0.6 M/S
□: - VW = 0.8 M/S

ADDITIONAL DATA

VG = 60 M/S

FIG.32B

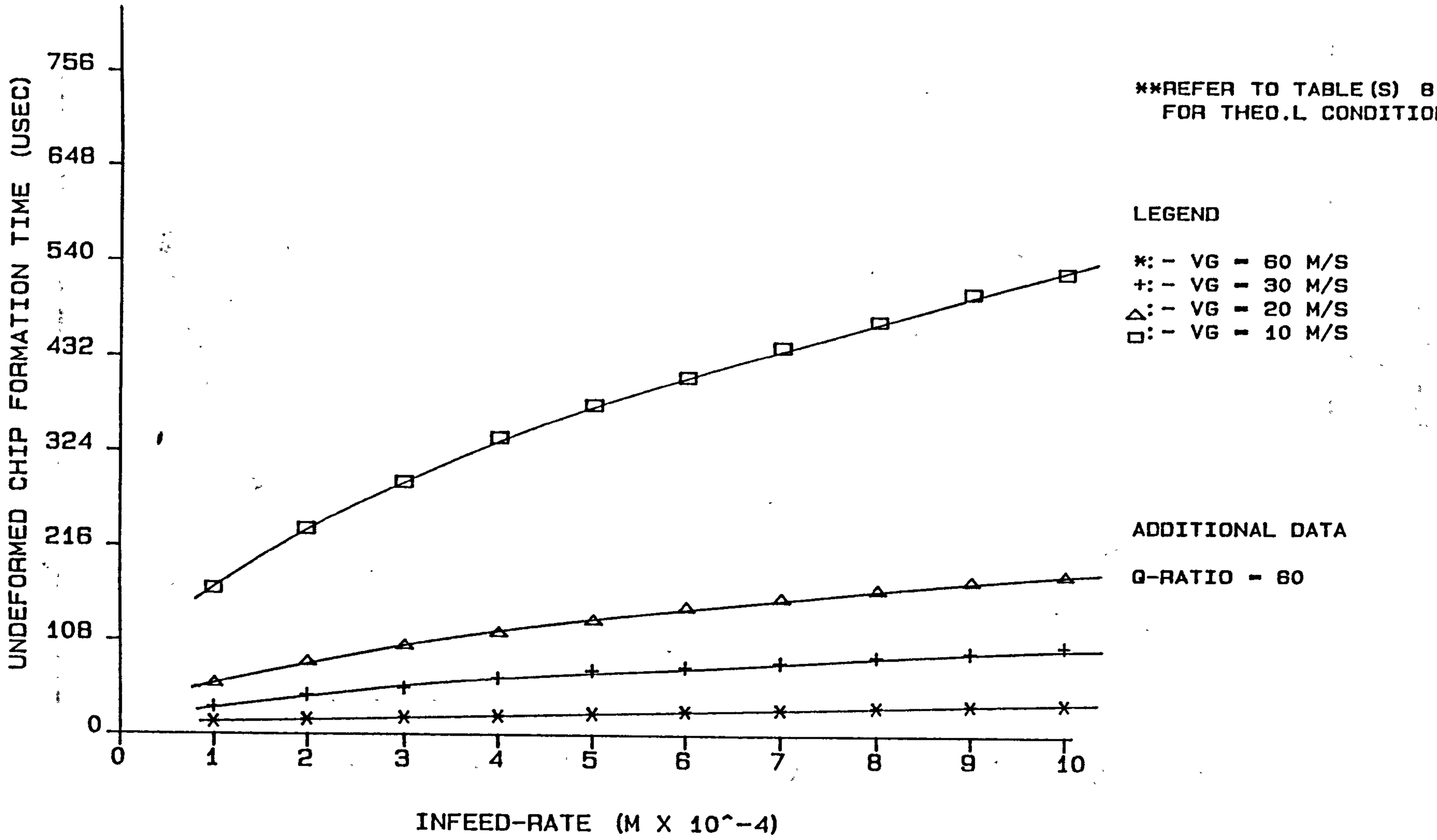
UNDEFORMED CHIP FORMATION TIME VS INFEED-RATE
UNDEFORMED CHIP FORMATION TIME (USEC)
756
648
540
432
324
216
108
0
0
1
2
3
4
5
6
7
8
9
10
INFEED-RATE (M X 10^-4)
**REFER TO TABLE(S) 8
FOR THEO.L CONDITIONS.
LEGEND
*: - VG = 60 M/S
+: - VG = 30 M/S
△: - VG = 20 M/S
□: - VG = 10 M/S
ADDITIONAL DATA
Q-RATIO = 60

FIG. 34

Relationship Between Various Average Uncut Chip Data and Q-ratio

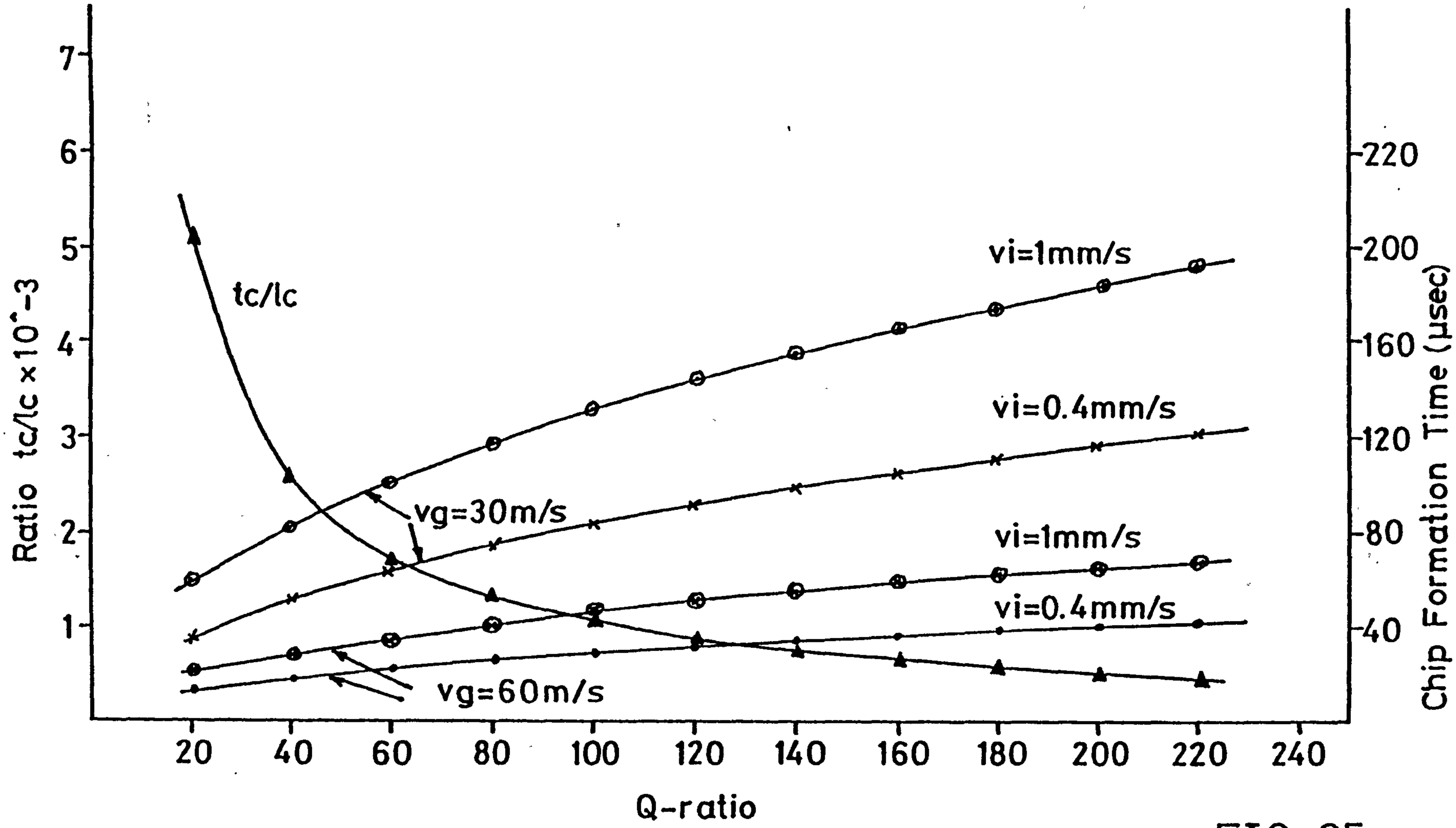

FIG. 35

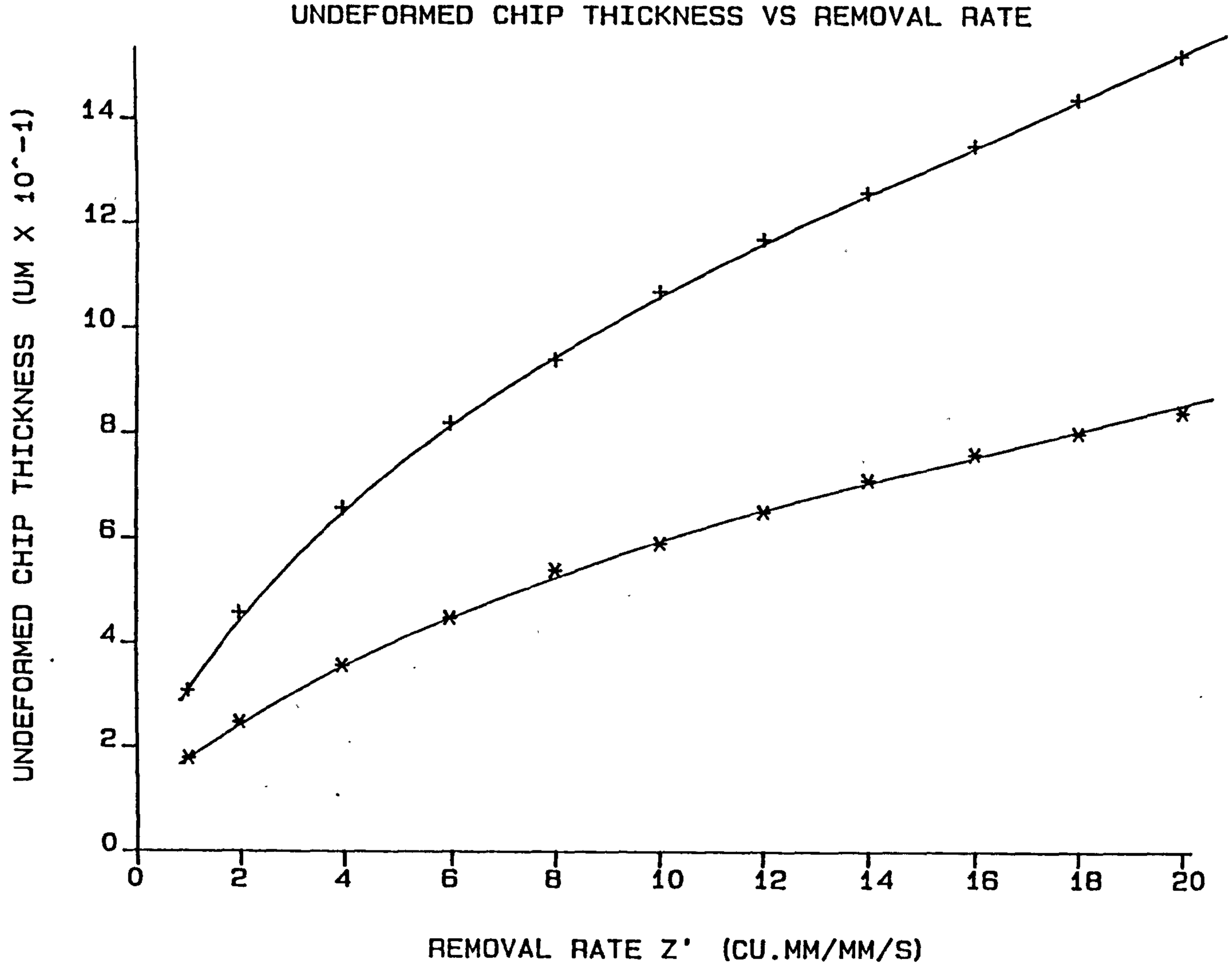

**REFER TO TABLE(S) EN 8 (5&7) FOR EXP.L CONDITIONS.

LEGEND

*:- Q-RATIO = 200
+:- Q-RATIO = 60

ADDITIONAL DATA

WHEEL - WA60MVRC
MATERIAL - EN 8
VG = 50 M/S
SIMPLIFIED SOLUTION

FIG. 36

UNDEFORMED CHIP THICKNESS VS REMOVAL RATE

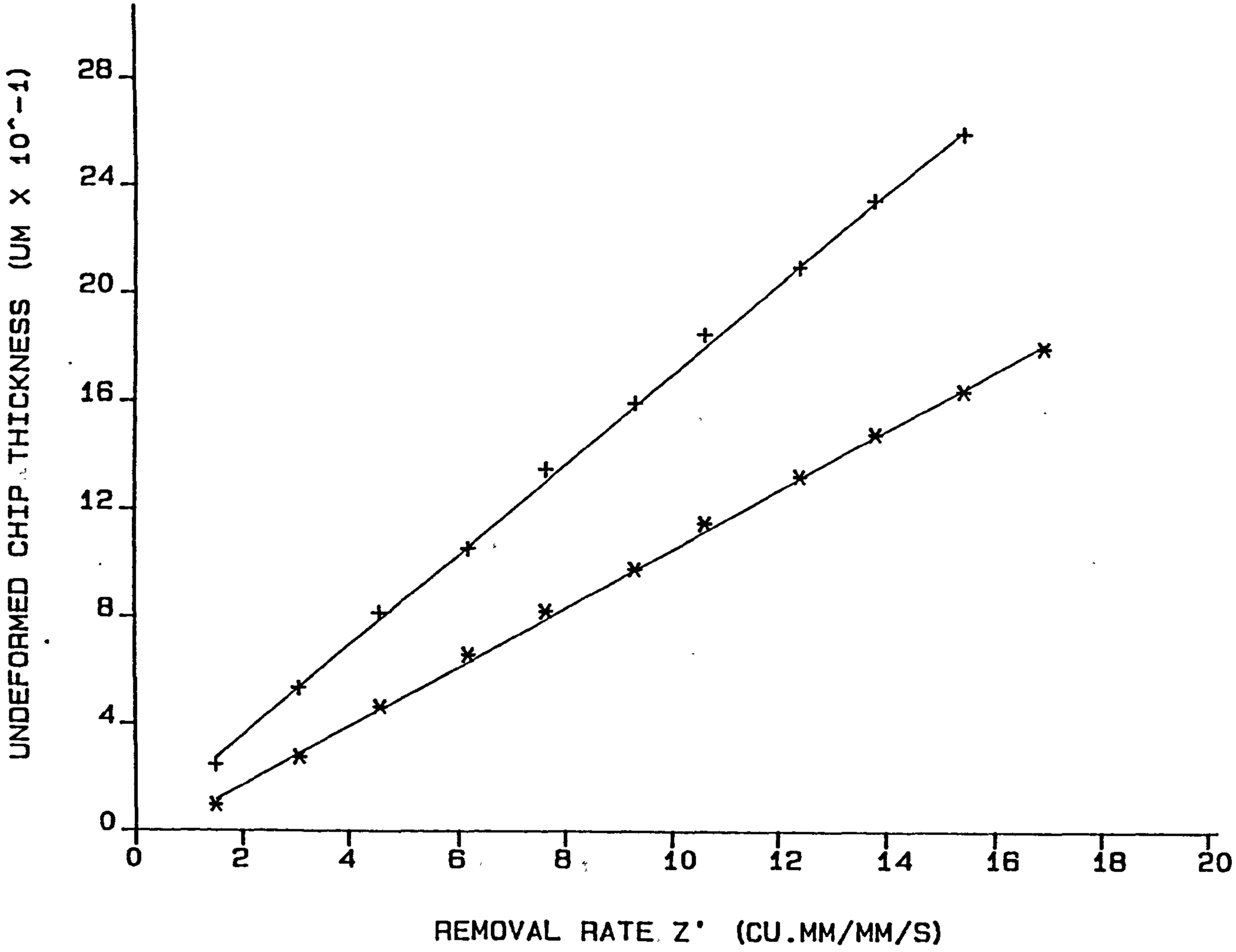

**REFER TO TABLE(S) EN 9 (5&7)
FOR EXP.L CONDITIONS.

LEGEND

*: - Q-RATIO = 200
+: - Q-RATIO = 60

ADDITIONAL DATA

WHEEL - WA60MVRC
MATERIAL - EN 9
VG = 50 M/S
ACCURATE SOLUTION

FIG. 37

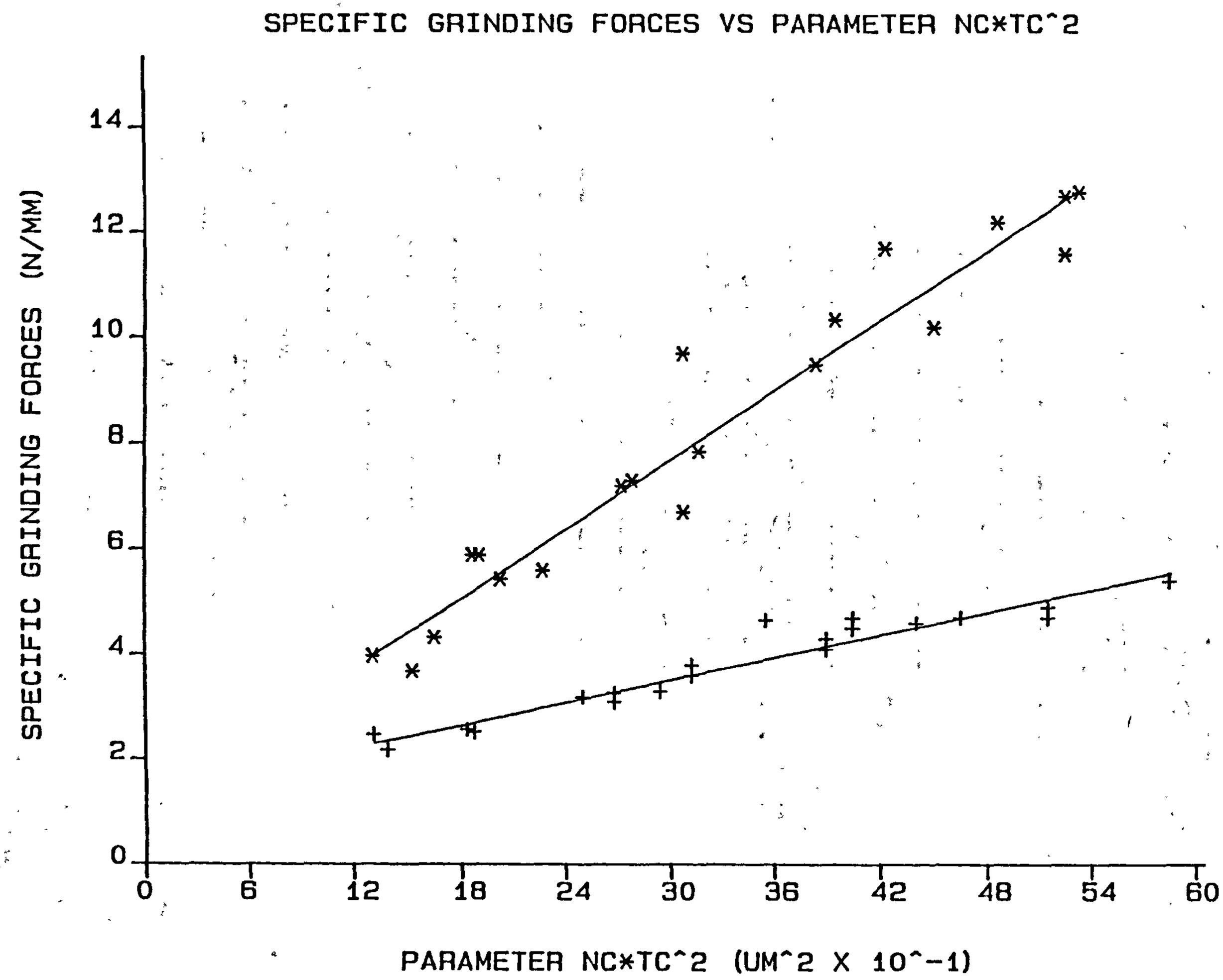

**REFER TO TABLE(S) EN 9 SERIES FOR EXP.L CONDITIONS.

LEGEND

*: - FN'
+: - FT'

ADDITIONAL DATA

WHEEL - WA60MVRC
MATERIAL - EN 9
VG - VARIOUS
Q-RATIO - VARIOUS

FIG. 38A

Variation of Theoretical Grinding Forces with Infeed-Rate, Workpiece Speed and Grinding Wheel Speed

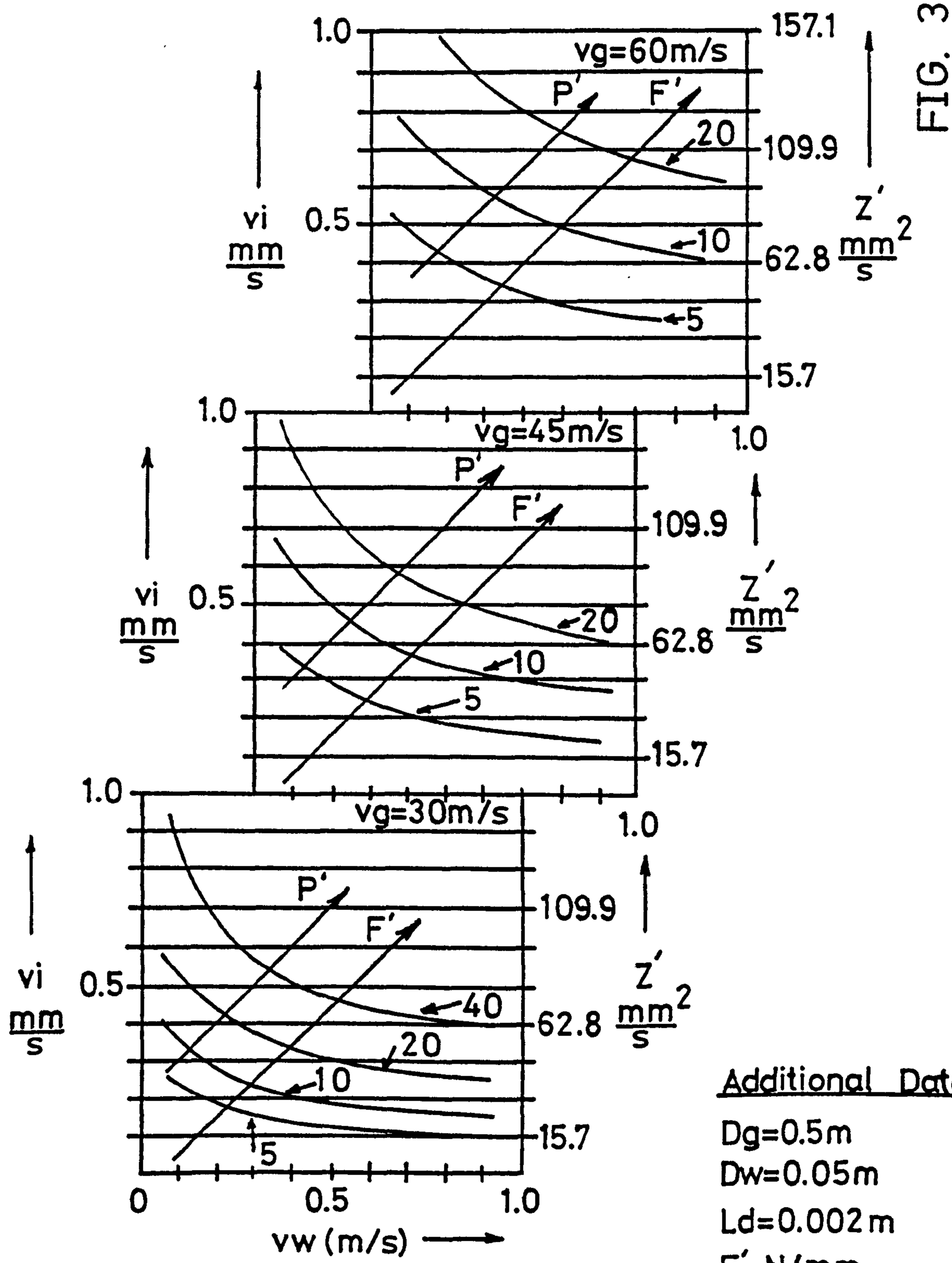

FIG. 38B

Additional Data

Dg=0.5m
Dw=0.05m
Ld=0.002m
F'-N/mm
P'-Power

SURFACE ROUGHNESS VS UNDEFORMED CHIP THICKNESS

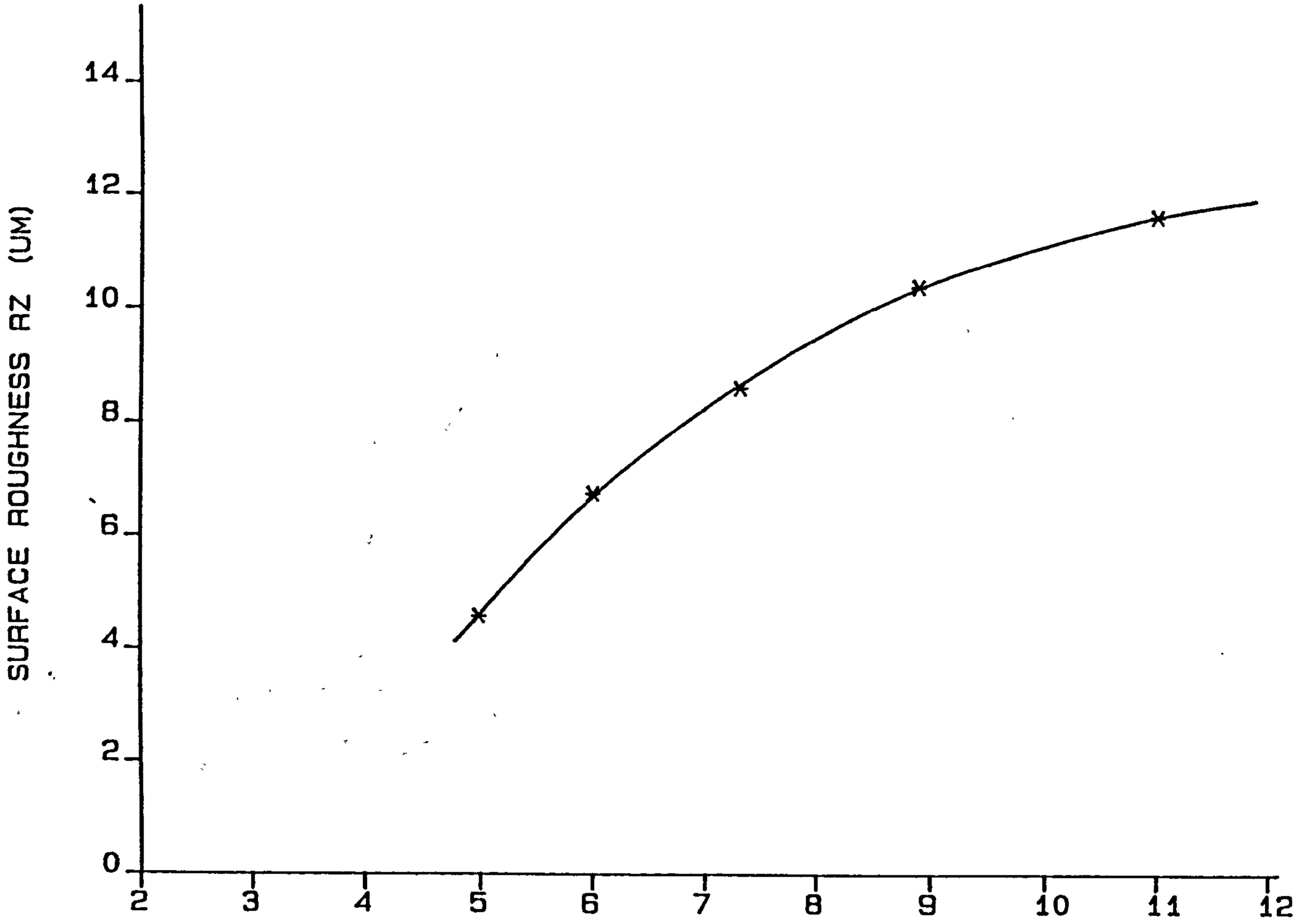

**REFER TO TABLE(S) EN 9 SERIES FOR EXP.L CONDITIONS.

LEGEND

*: - XX

ADDITIONAL DATA

WHEEL - WA60MVRC
SD - 0.6 MM/REV
VG - 60 M/S
Q-RATIO - 200

FIG.38C

SPECIFIC GRINDING FORCES VS MAXIMUM METAL REMOVAL RATE

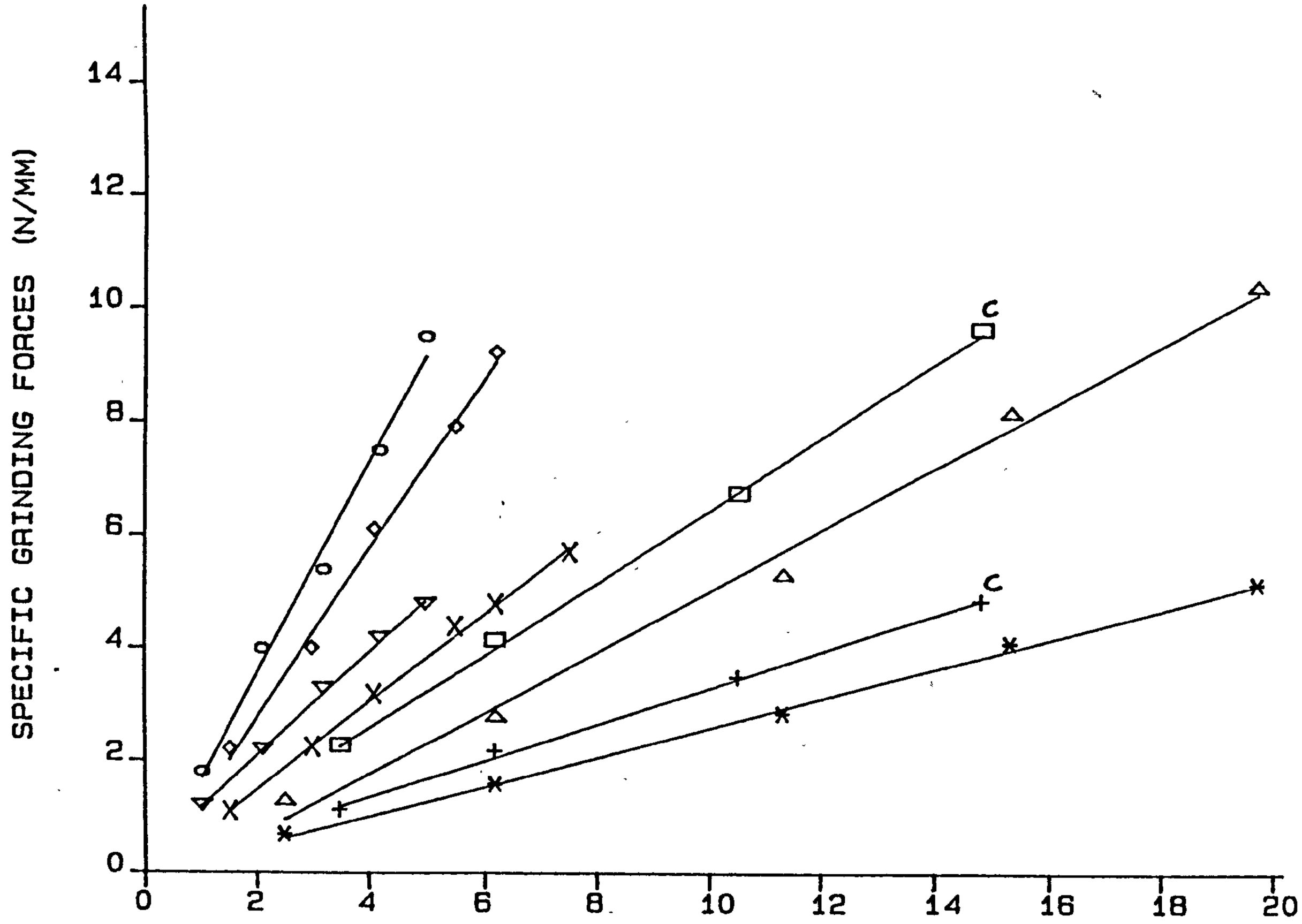

**REFER TO TABLE(S) EN 9 SERIES FOR EXP.L CONDITIONS.

LEGEND

*: - FT'- Q=200 (VG=60 M/S)
+: - FT'- Q=100 (VG=60 M/S)
△: - FN'- Q=200 (VG=60 M/S)
□: - FN'- Q=100 (VG=60 M/S)
X: - FT'- Q=200 (VG=30 M/S)
▽: - FT'- Q=60 (VG=30 M/S)
◇: - FN'- Q=200 (VG=30 M/S)
○: - FN'- Q=60 (VG=30 M/S)

ADDITIONAL DATA

WHEEL - WA60MVRC
MATERIAL - EN 9
C - GRINDING VIBRATIONS

FIG. 39

SPECIFIC GRINDING FORCES VS MAXIMUM METAL REMOVAL RATE

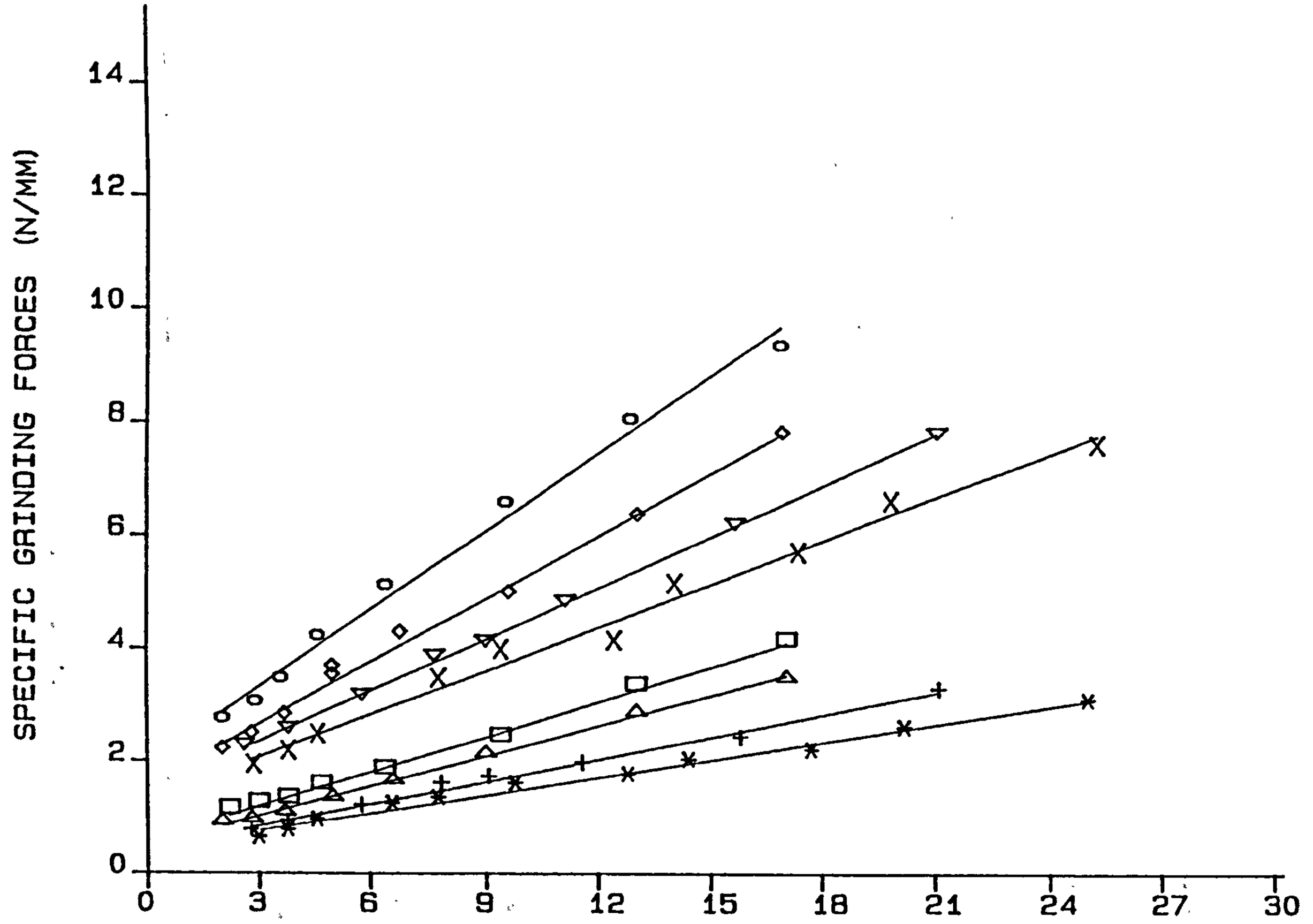

**REFER TO TABLE(S) CI SERIES
FOR EXP.L CONDITIONS.

LEGEND

*:- FT'- Q=200 (VG=60 M/S)
+:- FT'- Q=100 (VG=60 M/S)
△:- FT'- Q=200 (VG=30 M/S)
□:- FT'- Q=100 (VG=30 M/S)
X:- FN'- Q=200 (VG=60 M/S)
▽:- FN'- Q=100 (VG=60 M/S)
◇:- FN'- Q=200 (VG=30 M/S)
o:- FN'- Q=100 (VG=30 M/S)

ADDITIONAL DATA

WHEEL - C46 BBT
MATERIAL - CAST IRON

FIG. 40

SPECIFIC GRINDING FORCES VS MAXIMUM METAL REMOVAL RATE

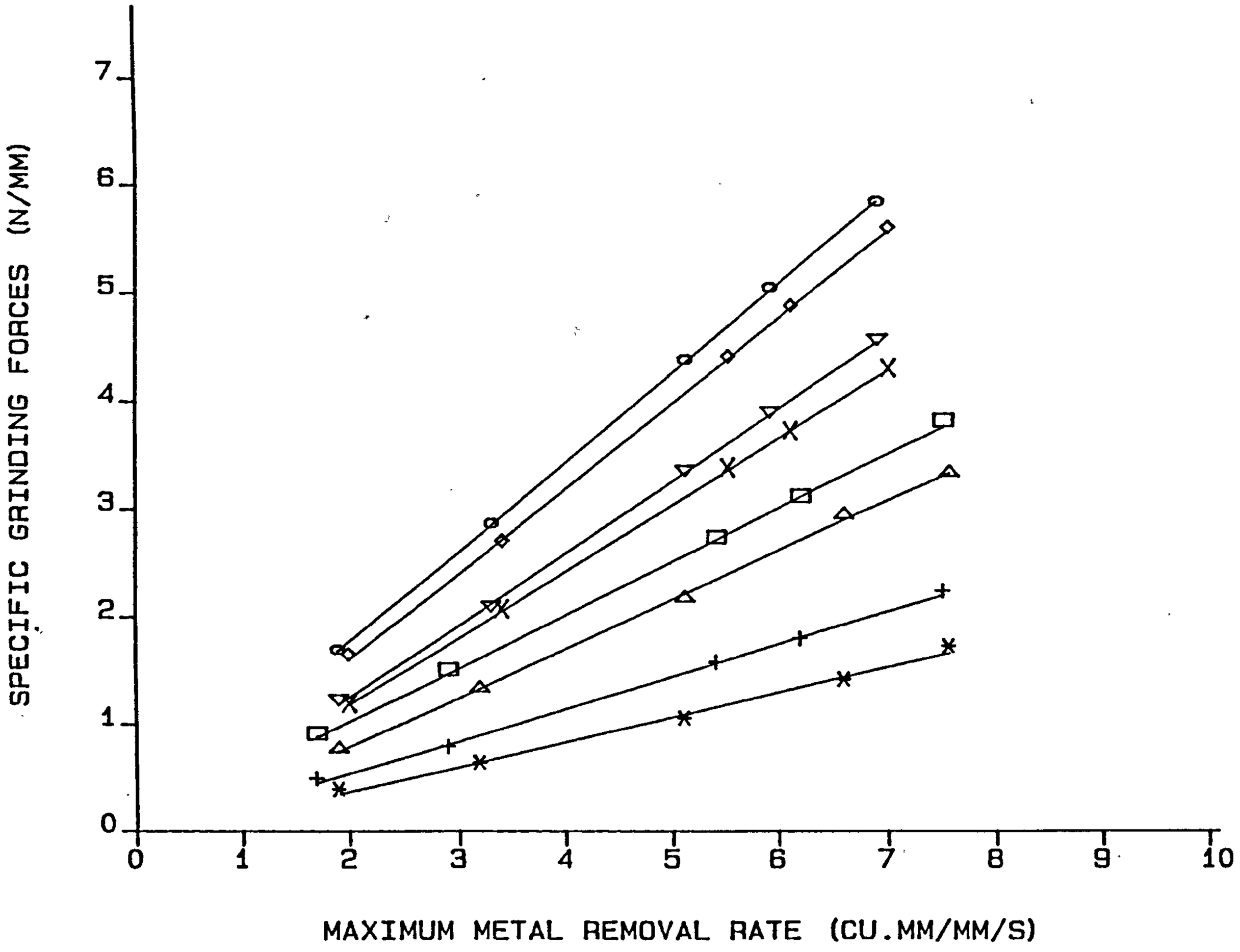

**REFER TO TABLE(S) PM SERIES
FOR EXP.L CONDITIONS.

LEGEND

*: - FT'- Q=130 (VG=60 M/S)
+: - FT'- Q=90 (VG=60 M/S)
△: - FN'- Q=130 (VG=60 M/S)
□: - FN'- Q=90 (VG=60 M/S)
x: - FT'- Q=130 (VG=30 M/S)
▽: - FT'- Q=90 (VG=30 M/S)
◇: - FN'- Q=130 (VG=30 M/S)
○: - FN'- Q=90 (VG=30 M/S)

ADDITIONAL DATA

WHEEL - WA60MVRC
MATERIAL - PM (IRON)

FIG. 41

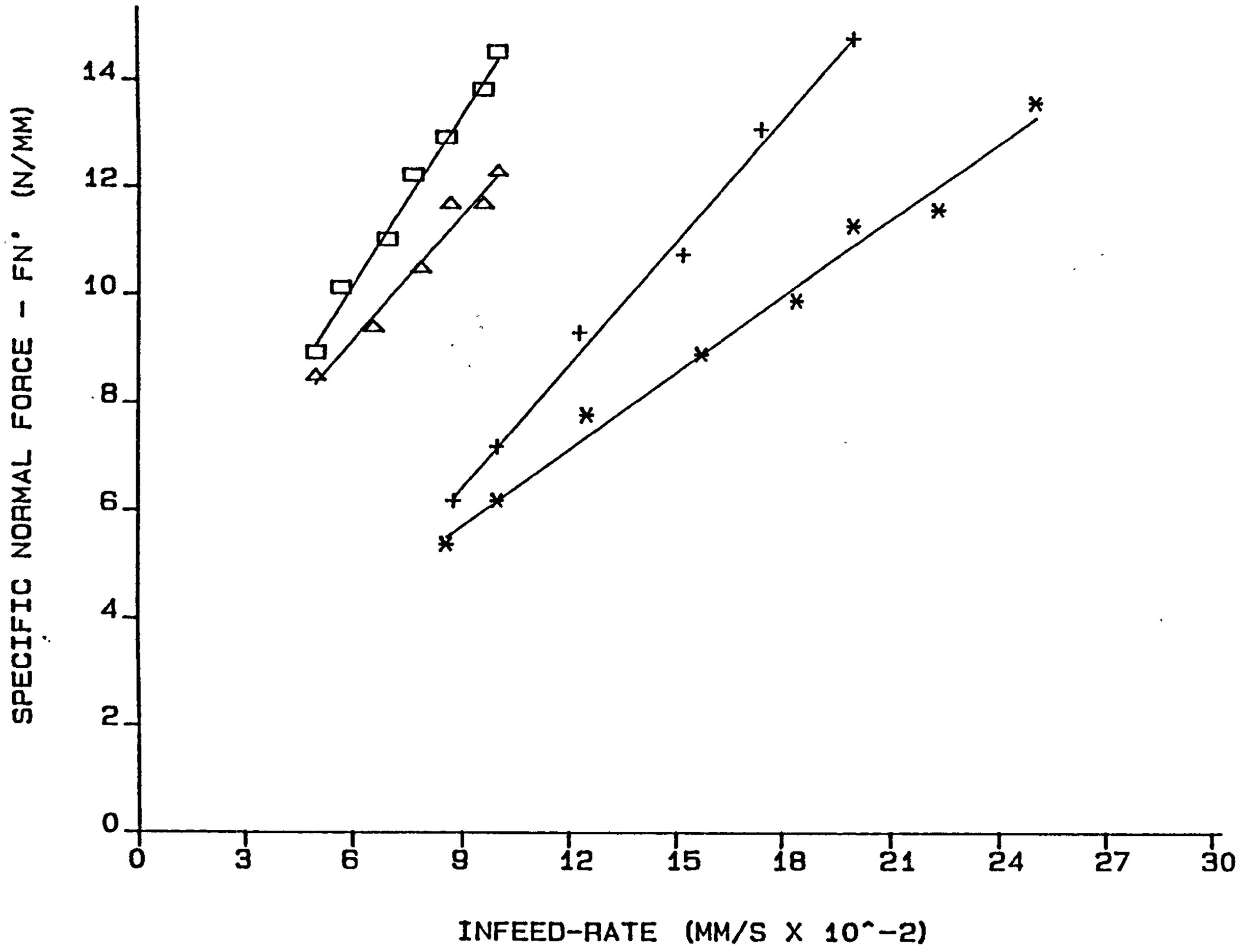

**REFER TO TABLE(S) EN 8 SERIES FOR EXP.L CONDITIONS.

LEGEND

*: - Q-RATIO-200 (VG-60 M/S)
+: - Q-RATIO-100 (VG-60 M/S)
△: - Q-RATIO-200 (VG-30 M/S)
□: - Q-RATIO-100 (VG-30 M/S)

ADDITIONAL DATA

WHEEL - WA60MVRC
MATERIAL - EN 8

FIG. 42

SPECIFIC NORMAL FORCE VS INFEED-RATE

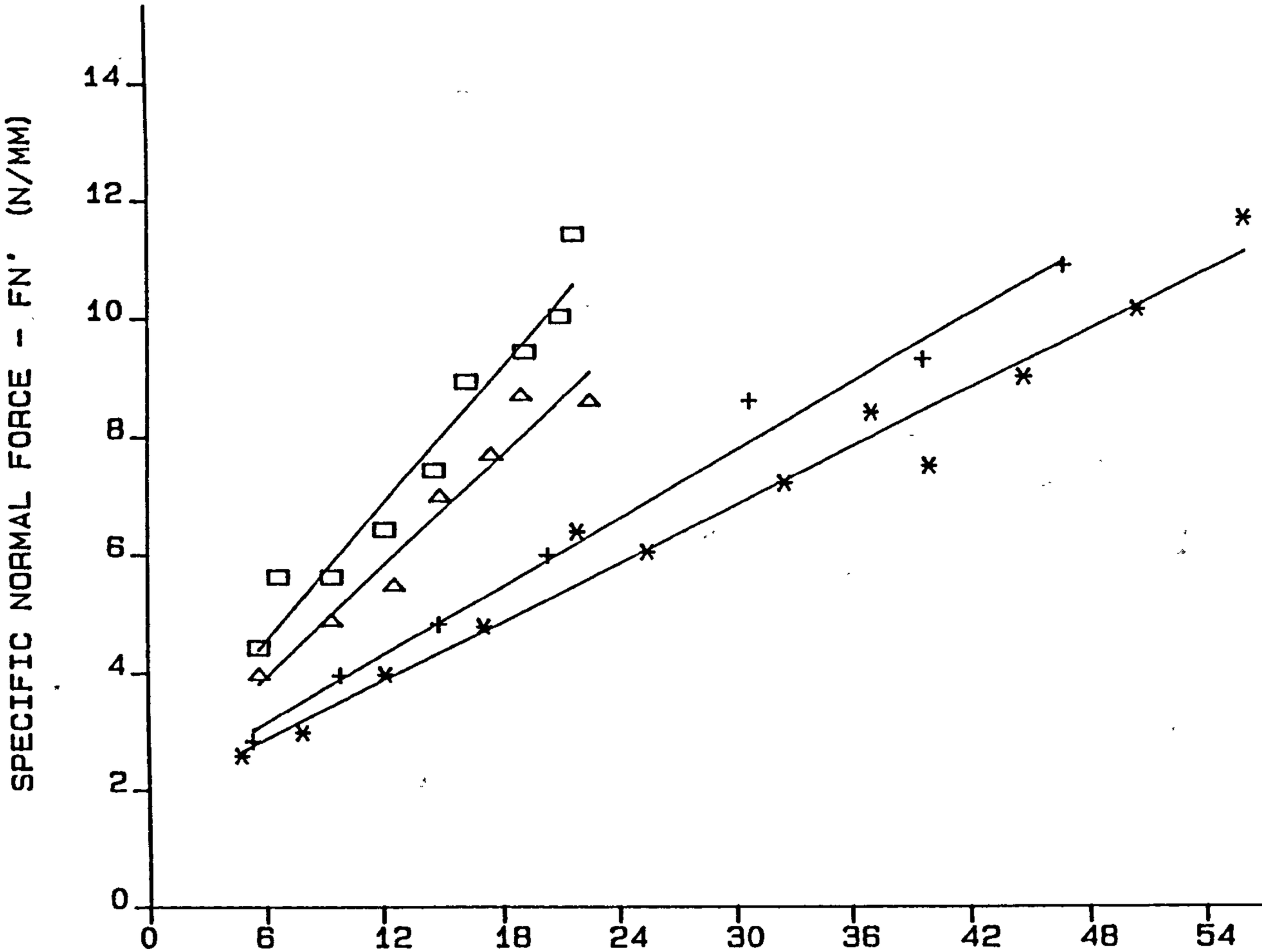

**REFER TO TABLE(S) CI SERIES
FOR EXP.L CONDITIONS.

LEGEND

*: - Q-RATIO=200 (VG=60 M/S)
+: - Q-RATIO=100 (VG=60 M/S)
△: - Q-RATIO=200 (VG=30 M/S)
□: - Q-RATIO=100 (VG=30 M/S)

ADDITIONAL DATA

WHEEL -C46 BBT
MATERIAL - CAST IRON

FIG. 43

SPECIFIC GRINDING FORCES VS INFEED-RATE

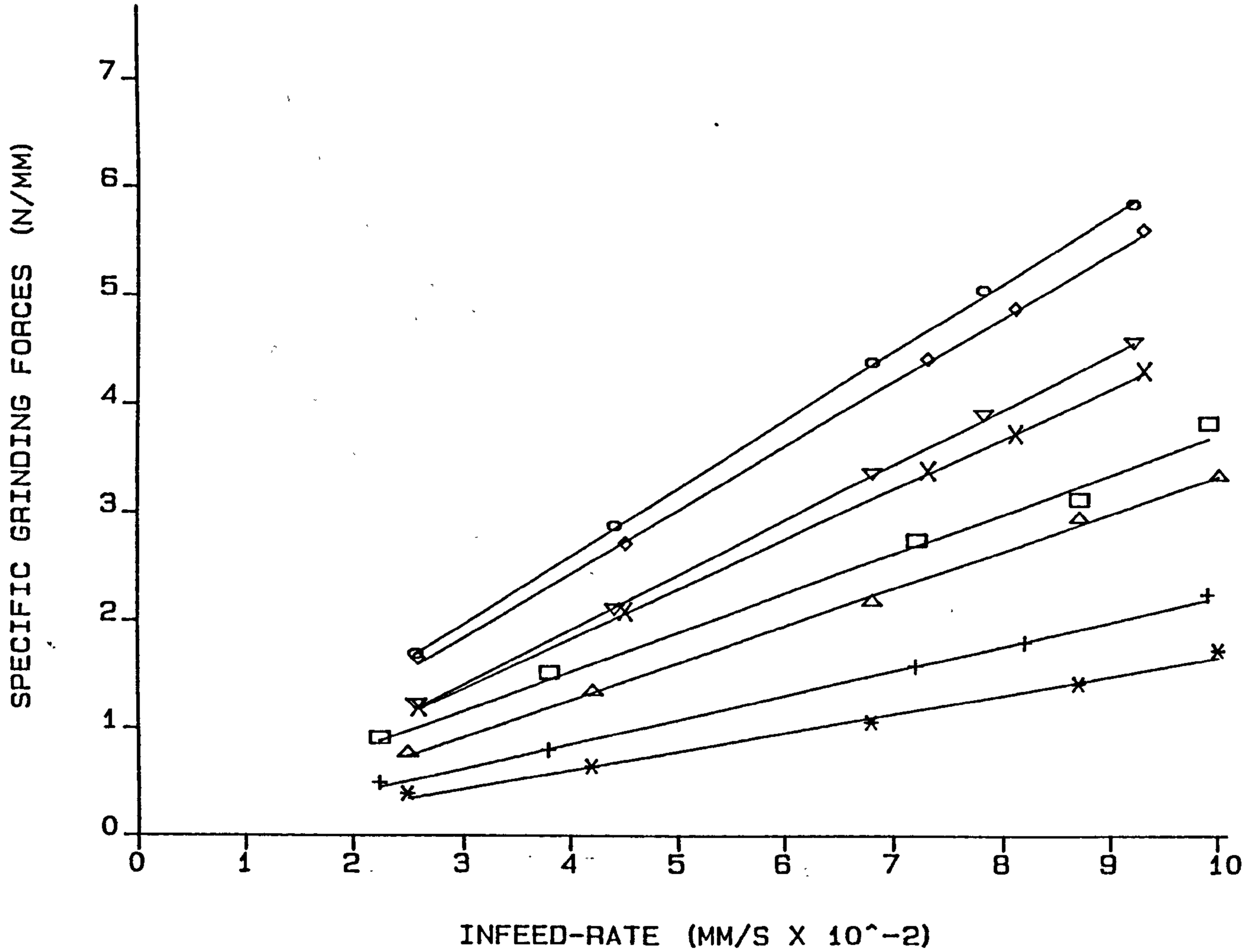

**REFER TO TABLE(S) PM SERIES FOR EXP.L CONDITIONS.

LEGEND

*: - FT'- Q=130 (VG=60 M/S)
+: - FT'- Q=90 (VG=60 M/S)
△: - FN'- Q=130 (VG=60 M/S)
□: - FN'- Q=90 (VG=60 M/S)
X: - FT'- Q=130 (VG=30 M/S)
▽: - FT'- Q=90 (VG=30 M/S)
◇: - FN'- Q=130 (VG=30 M/S)
○: - FN'- Q=90 (VG=30 M/S)

ADDITIONAL DATA

WHEEL - WA60MVRC
MATERIAL - PM (IRON)

FIG. 44

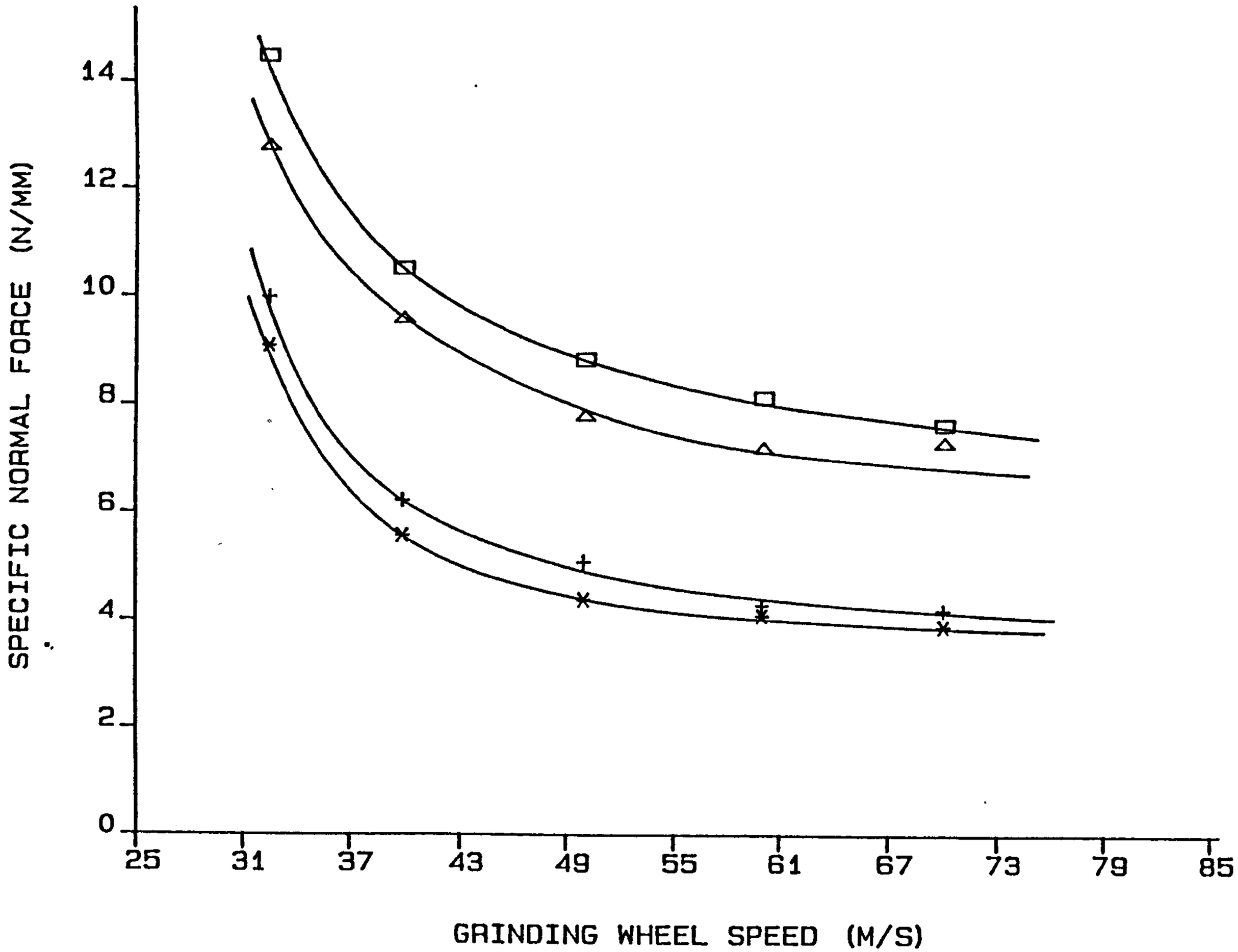

**REFER TO TABLE(S) EN 8 SERIES
FOR EXP.L CONDITIONS.

LEGEND

*: - Q-RATIO=200 (VI=0.056MM/S)
+: - Q-RATIO=100 (VI=0.056MM/S)
△: - Q-RATIO=200 (VI=0.116MM/S)
□: - Q-RATIO=100 (VI=0.116MM/S)

ADDITIONAL DATA

WHEEL - WA60MVRC
MATERIAL - EN 9

FIG. 45

SPECIFIC NORMAL FORCE VS GRINDING WHEEL SPEED

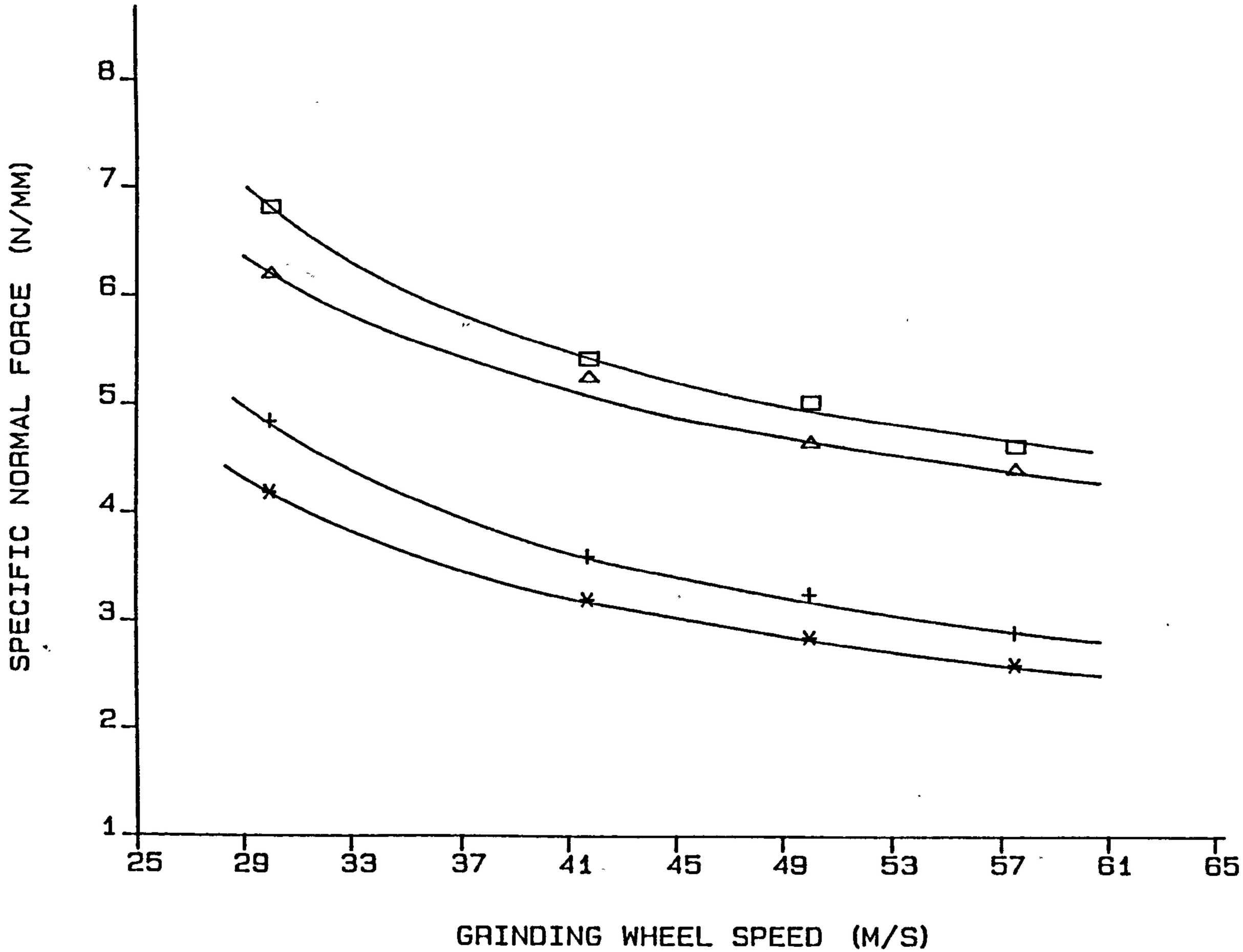

**REFER TO TABLE(S) CI SERIES
FOR EXP.L CONDITIONS.

LEGEND

*: - Q-RATIO=200 (VI=.056MM/S)
+: - Q-RATIO=100 (VI=0.056MM/S)
△: - Q-RATIO=200 (VI=0.151MM/S)
□: - Q-RATIO=100 (VI=0.151MM/S)

ADDITIONAL DATA

WHEEL - C46 BBT
MATERIAL - CAST IRON

FIG. 46

SPECIFIC NORMAL FORCE VS Q-RATIO

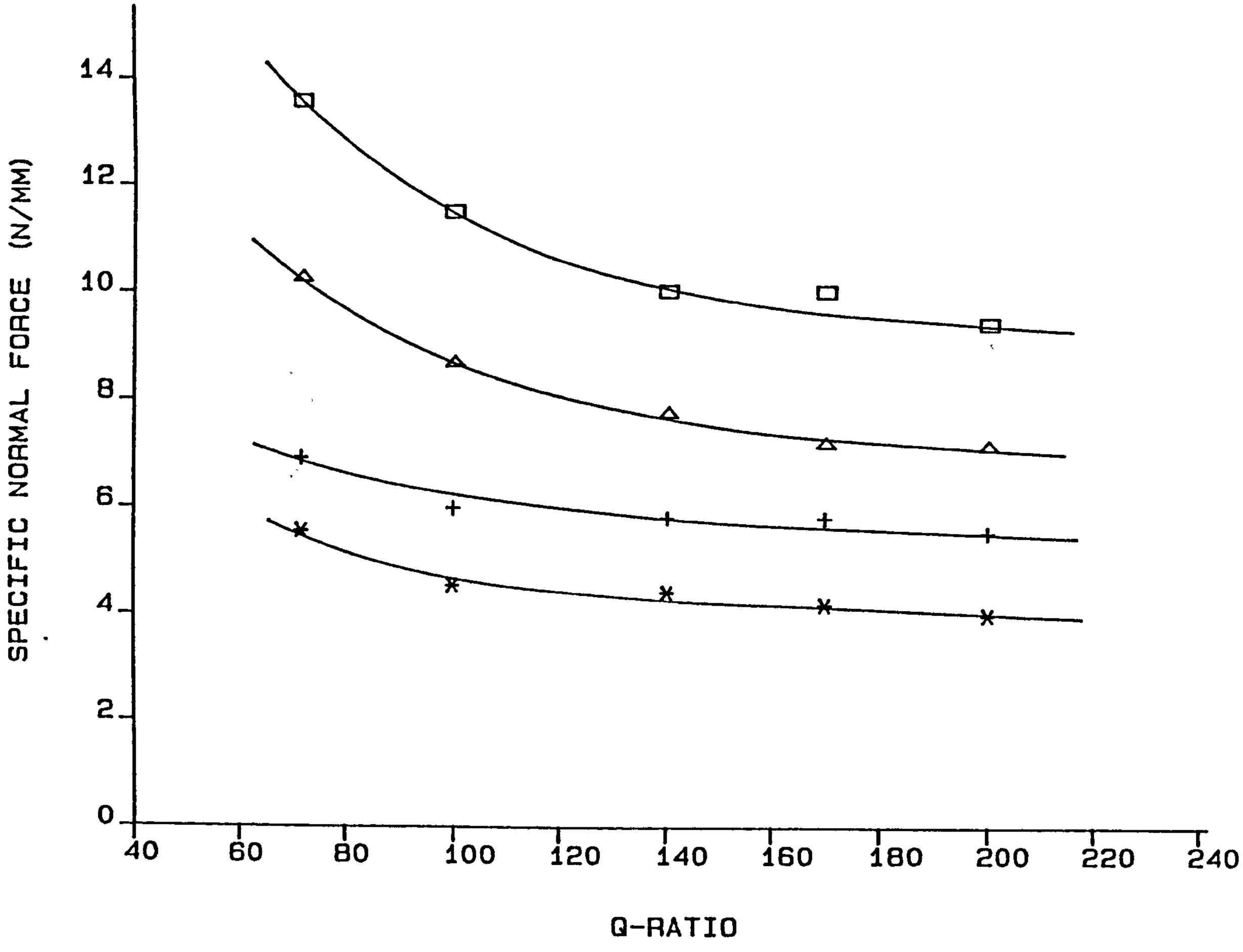

**REFER TO TABLE(S) EN 9 SERIES
FOR EXP.L CONDITIONS.

LEGEND

*: - VI=0.056MM/S (VG=60M/S)
+: - VI=0.056MM/S (VG=40M/S)
△: - VI=0.116MM/S (VG=60M/S)
□: - VI=0.116MM/S (VG=40M/S)

ADDITIONAL DATA

WHEEL - WA60MVRC
MATERIAL - EN 9

FIG. 47

SPECIFIC NORMAL FORCE VS Q-RATIO

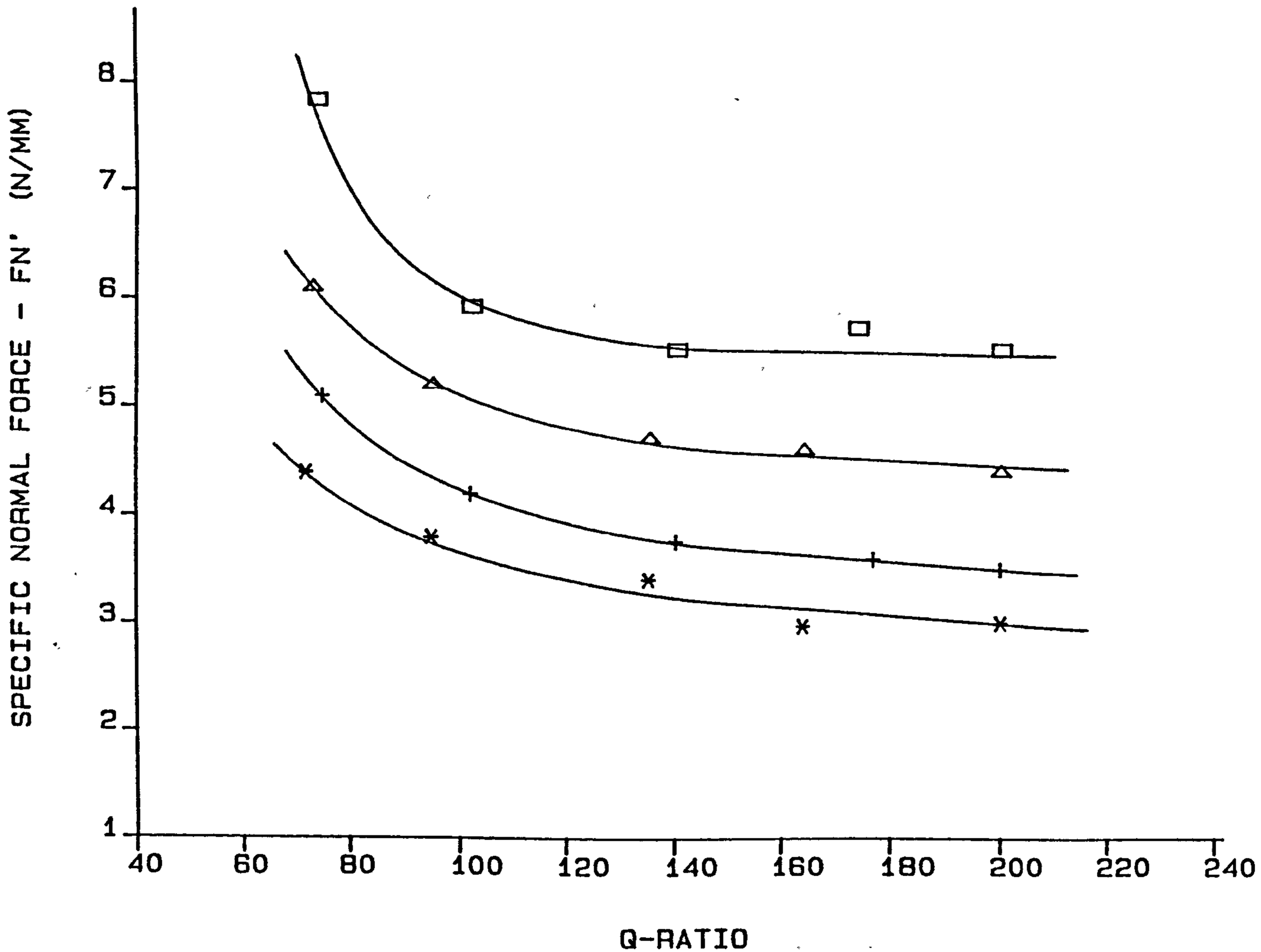

**REFER TO TABLE(S) CI SERIES FOR EXP.L CONDITIONS.

LEGEND

*: - VG=60 M/S (VI=0.062 MM/S)
+: - VG=40 M/S (VI=0.062 MM/S)
△: - VG=60 M/S (VI=0.124 MM/S)
□: - VG=40 M/S (VI=0.124 MM/S)

ADDITIONAL DATA

WHEEL - C46 BBT
MATERIAL - CAST IRON

FIG. 48

SURFACE ROUGHNESS VS MAXIMUM METAL REMOVAL RATE

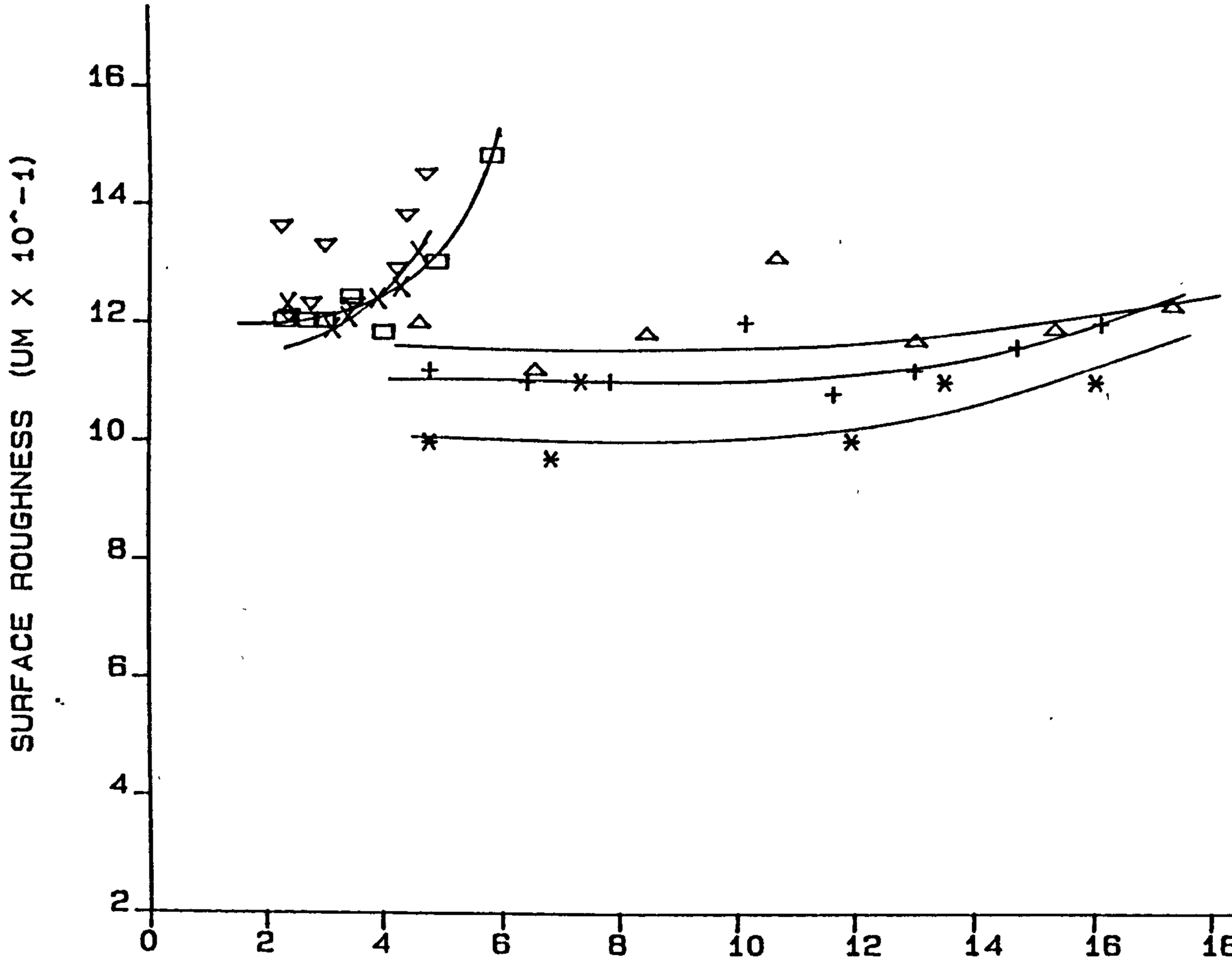

**REFER TO TABLE(S) EN 8 SERIES
FOR EXP.L CONDITIONS.

LEGEND

*: - Q-RATIO-200 (VG-60 M/S)
+: - Q-RATIO-160 (VG-60 M/S)
△: - Q-RATIO-100 (VG-60 M/S)
□: - Q-RATIO-180 (VG-30 M/S)
X: - Q-RATIO-120 (VG-30 M/S)
▽: - Q-RATIO-60 (VG-30 M/S)

ADDITIONAL DATA

WHEEL - WA60MVRC
MATERIAL - EN 8
0.25 MM CUT-OFF

FIG. 49

SURFACE ROUGHNESS VS MAXIMUM METAL REMOVAL RATE

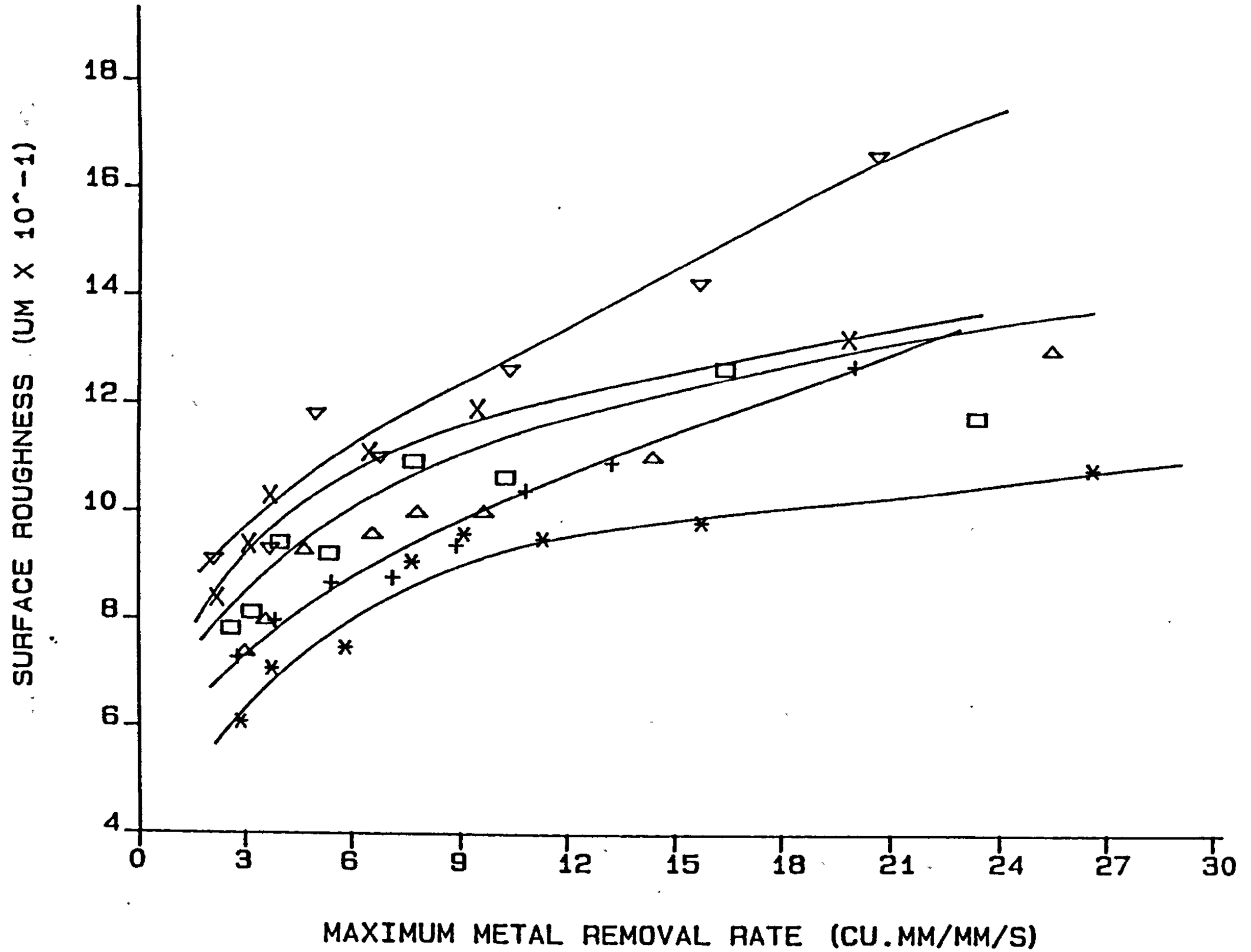

**REFER TO TABLE(S) CI SERIES FOR EXP.L CONDITIONS.

LEGEND

*: - Q-RATIO=200 (VG=61 M/S)
+: - Q-RATIO=150 (VG=61 M/S)
△: - Q-RATIO=100 (VG=61 M/S)
□: - Q-RATIO=200 (VG=43 M/S)
X: - Q-RATIO=120 (VG=43 M/S)
▽: - Q-RATIO=60 (VG=43 M/S)

ADDITIONAL DATA

WHEEL - C46 BBT
MATERIAL - CAST IRON
0.25 MM CUT-OFF

FIG. 50

GRINDING FORCES VS WORKPIECE VOLUME REMOVED

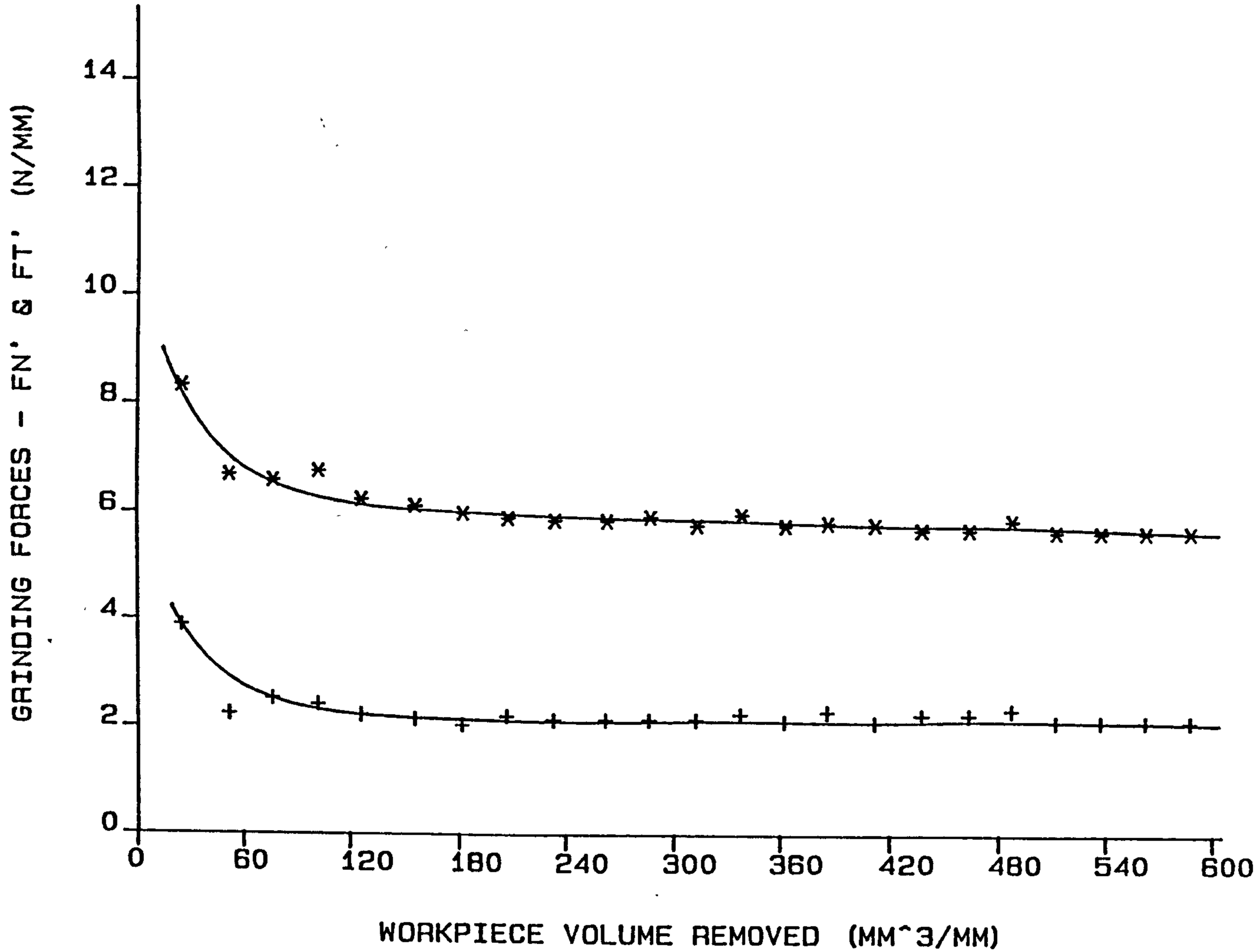

**REFER TO TABLE(S) CI SERIES
FOR EXP.L CONDITIONS.

LEGEND

*: - FN'
+: - FT'

ADDITIONAL DATA

WHEEL - C46 BBT
VG = 50 M/S
MATERIAL - CAST IRON
Z'= 9 CU.MM/MM/S

FIG. 51

SURFACE ROUGHNESS VS Q-RATIO

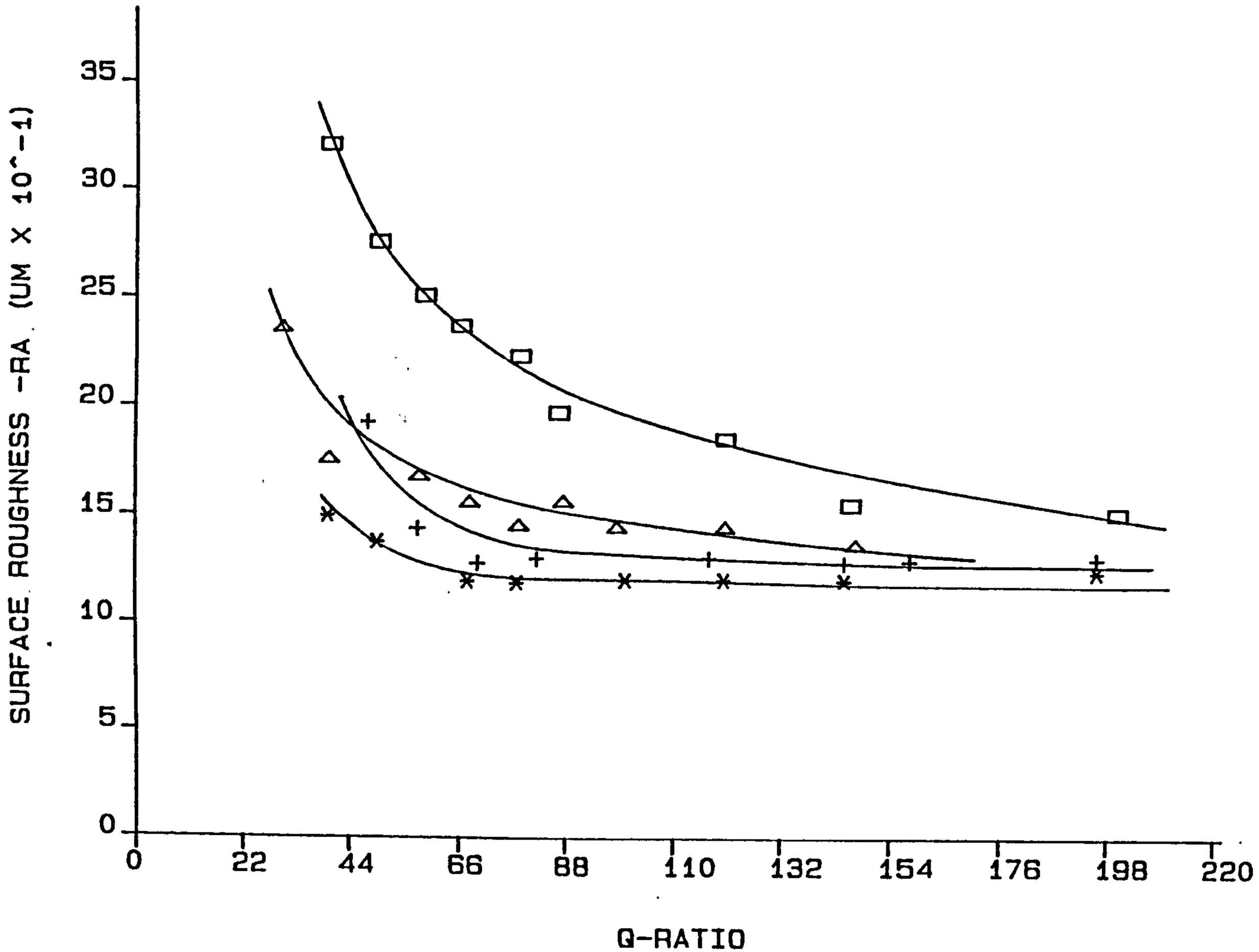

**REFER TO TABLE(S) EN 9 SERIES FOR EXP.L CONDITIONS.

LEGEND

*: - VG=60 M/S (VI=0.033 MM/S)
+: - VG=60 M/S (VI=0.086 MM/S)
△: - VG=30 M/S (VI=0.033 MM/S)
□: - VG=30 M/S (VI=0.086 MM/S)

ADDITIONAL DATA

WHEEL - WA60MVRC
MATERIAL - EN 9

FIG. 52

SURFACE ROUGHNESS VS GRINDING WHEEL SPEED

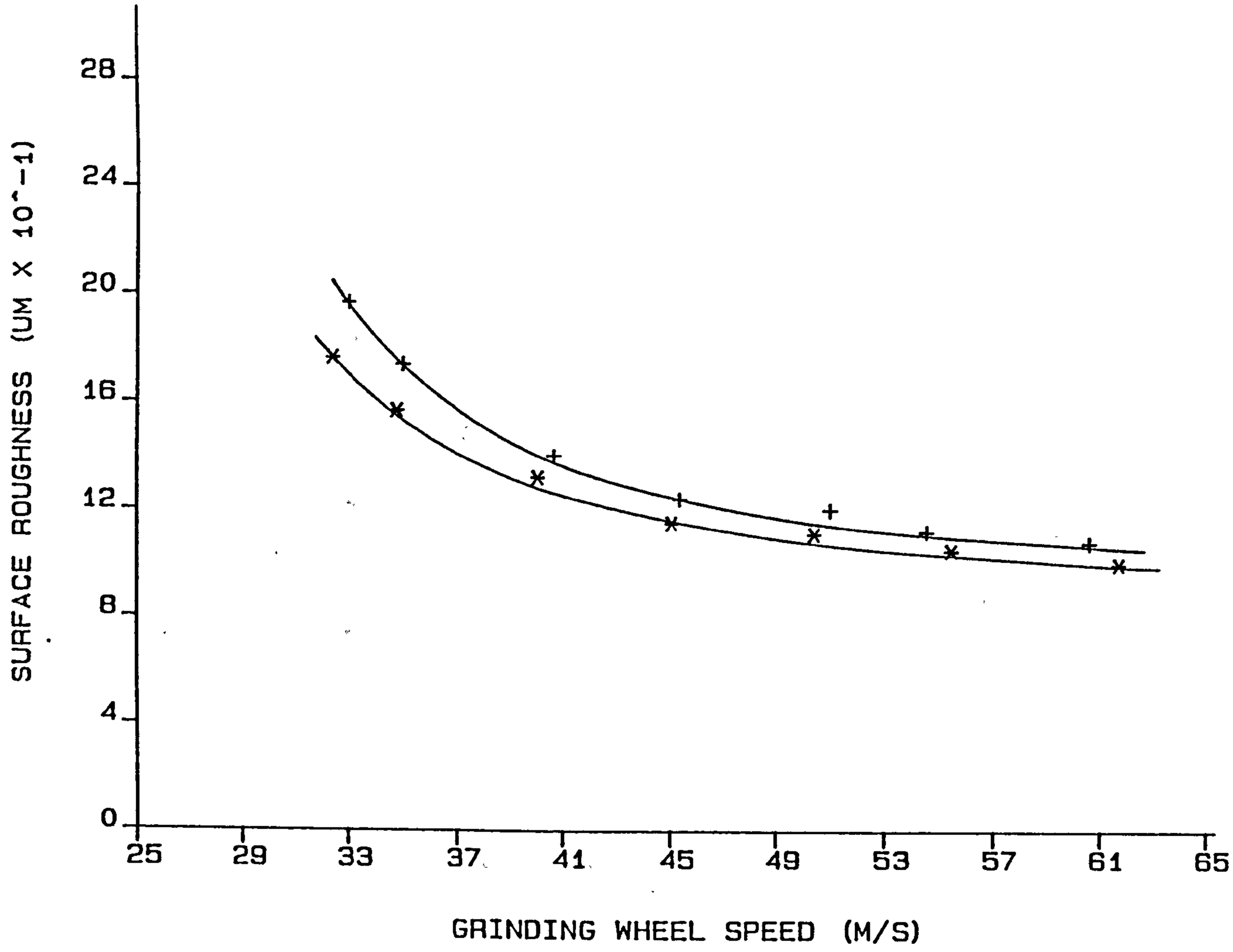

**REFER TO TABLE(S) EN 9 SERIES
FOR EXP.L CONDITIONS.

LEGEND

*:- Z' = 7 CU.MM/MM/S
+:- Z' = 15 CU/MM/MM/S

ADDITIONAL DATA

WHEEL - WA60MVRC
MATERIAL -EN 9
G-RATIO = 120
0.25 MM CUT-OFF

FIG. 53

SURFACE ROUGHNESS VS Q-RATIO

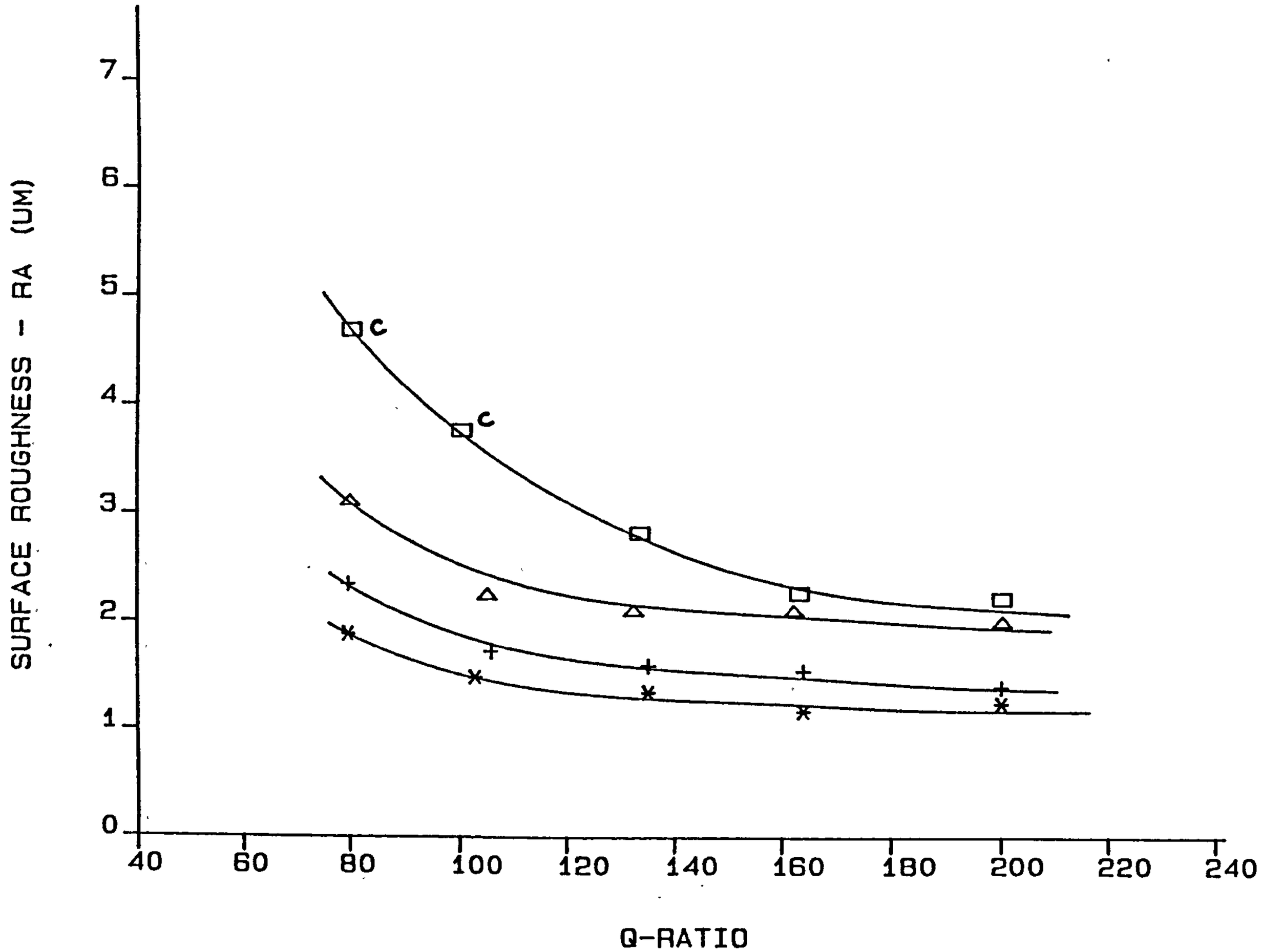

**REFER TO TABLE(S) CI SERIES
FOR EXP.L CONDITIONS.

LEGEND

*: - VG=60 M/S (VI=0.056 MM/S)
+: - VG=30 M/S (VI=0.056 MM/S)
△: - VG=60 M/S (VI=0.186 MM/S)
□: - VG=30 M/S (VI=0.186 MM/S)

ADDITIONAL DATA

WHEEL - C46 BBT
MATERIAL - CAST IRON
C - GRINDING VIBRATIONS

FIG. 54

SURFACE ROUGHNESS VS GRINDING WHEEL SPEED

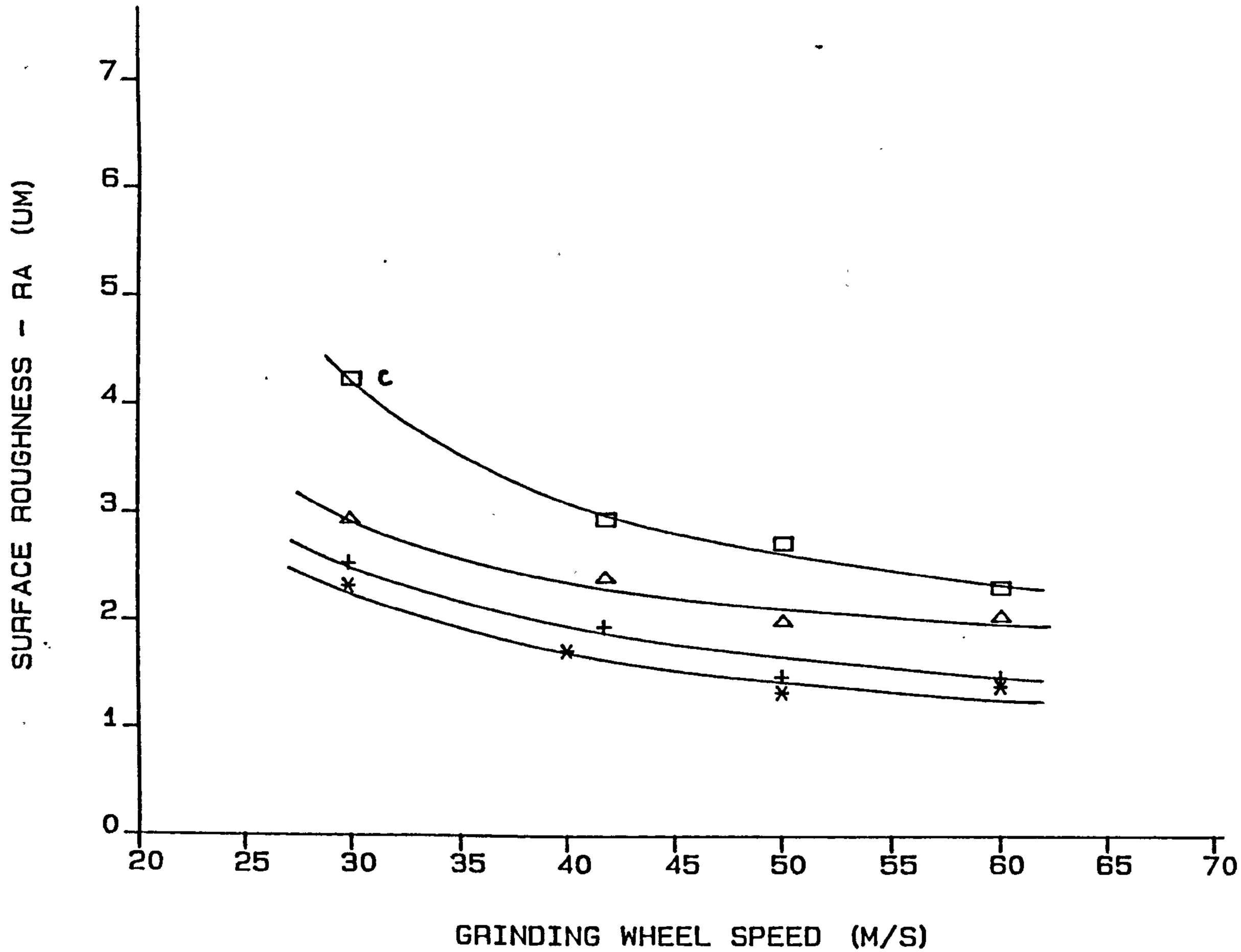

**REFER TO TABLE(S) CI SERIES
FOR EXP.L CONDITIONS.

LEGEND

*: - Q-RATIO=200 (Z'=10 MM^2/S)
+: - Q-RATIO=100 (Z'=10 MM^2/S)
△: - Q-RATIO=200 (Z'=40 MM^2/S)
□: - Q-RATIO=100 (Z'=40 MM^2/S)

ADDITIONAL DATA

WHEEL - C46 BBT
MATERIAL - CAST IRON
C - GRINDING VIBRATIONS

FIG. 55

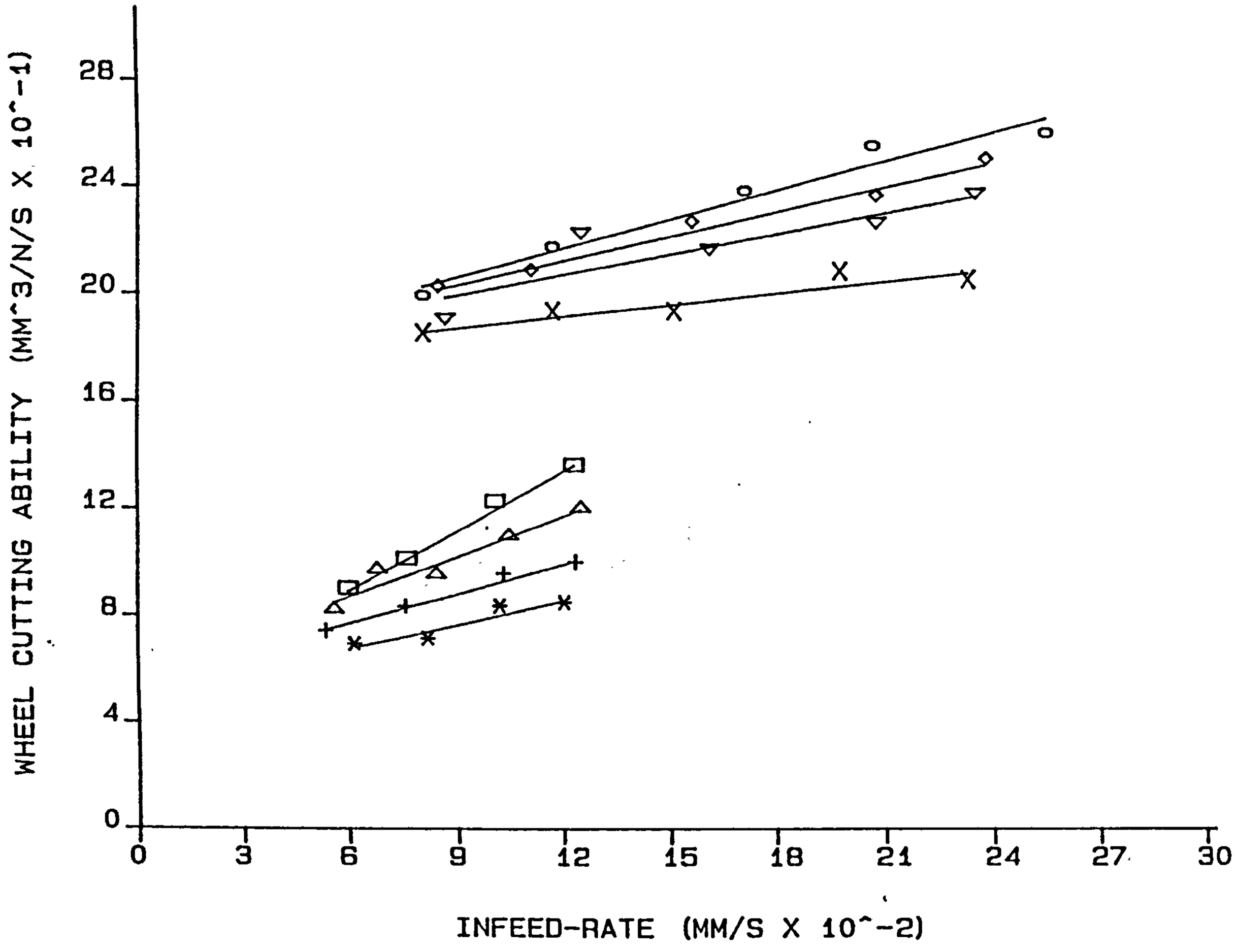

**REFER TO TABLE(S) EN 8 SERIES
FOR EXP.L CONDITIONS.

LEGEND

*: - Q-RATIO=100 (VG=30 M/S)
+: - Q-RATIO=140 (VG=30 M/S)
△: - Q-RATIO=170 (VG=30 M/S)
□: - Q-RATIO=200 (VG=30 M/S)
X: - Q-RATIO=100 (VG=60 M/S)
▽: - Q-RATIO=140 (VG=60 M/S)
◇: - Q-RATIO=170 (VG=60 M/S)
○: - Q-RATIO=200 (VG=60 M/S)

ADDITIONAL DATA

WHEEL - WA60MVRC
MATERIAL - EN 9

FIG. 56

WHEEL CUTTING ABILITY VS INFEED-RATE

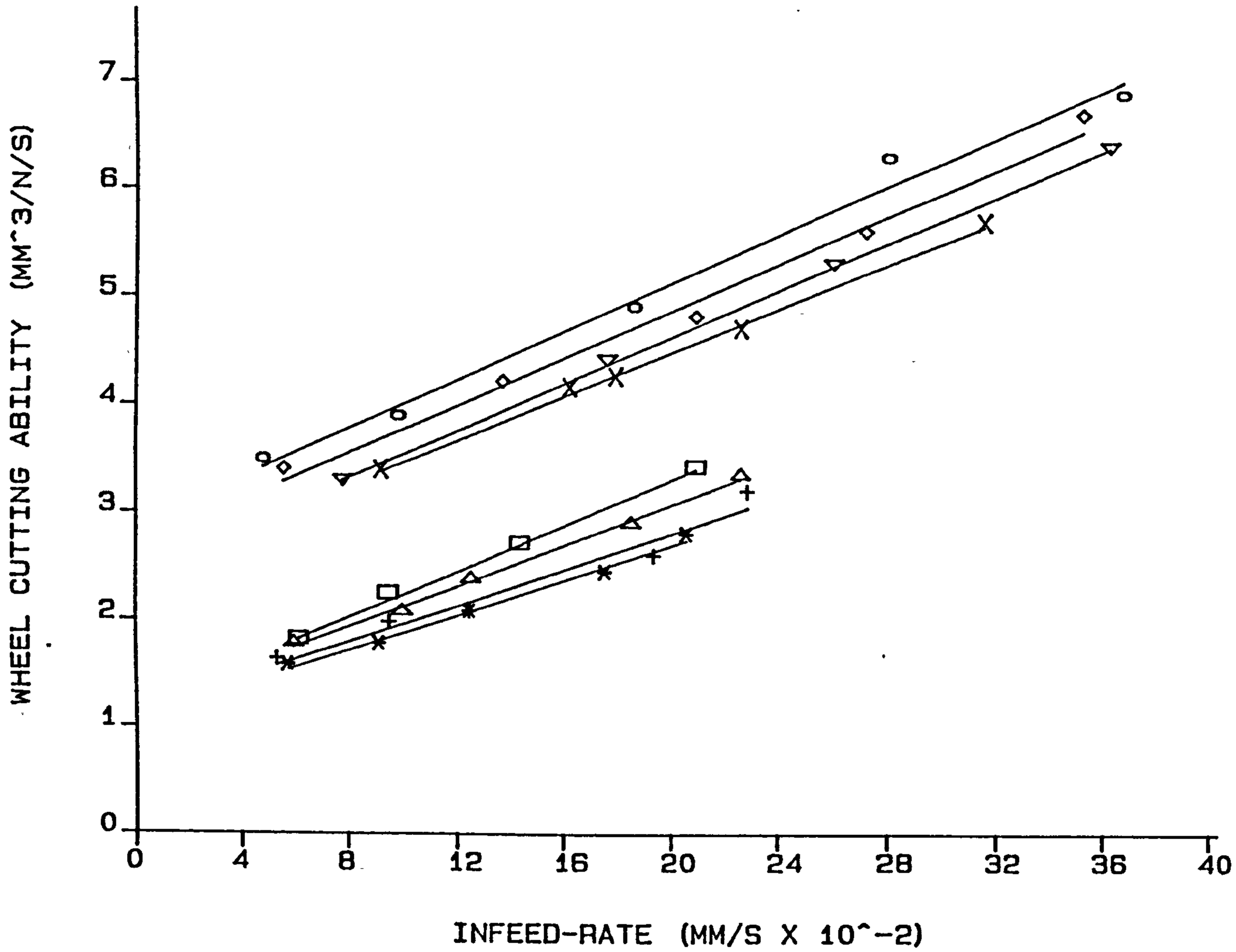

**REFER TO TABLE(S) CI SERIES FOR EXP.L CONDITIONS.

LEGEND

*: - Q-RATIO-86 (VG-30 M/S)
+: - Q-RATIO-135 (VG-30 M/S)
△: - Q-RATIO-164 (VG-30 M/S)
□: - Q-RATIO-200 (VG-30 M/S)
X: - Q-RATIO-86 (VG-60 M/S)
▽: - Q-RATIO-135 (VG-60 M/S)
◇: - Q-RATIO-164 (VG-60 M/S)
○: - Q-RATIO-200 (VG-60 M/S)

ADDITIONAL DATA

WHEEL - C46 BBT
MATERIAL - EN 8

FIG. 57

WHEEL CUTTING ABILITY VS GRINDING WHEEL SPEED

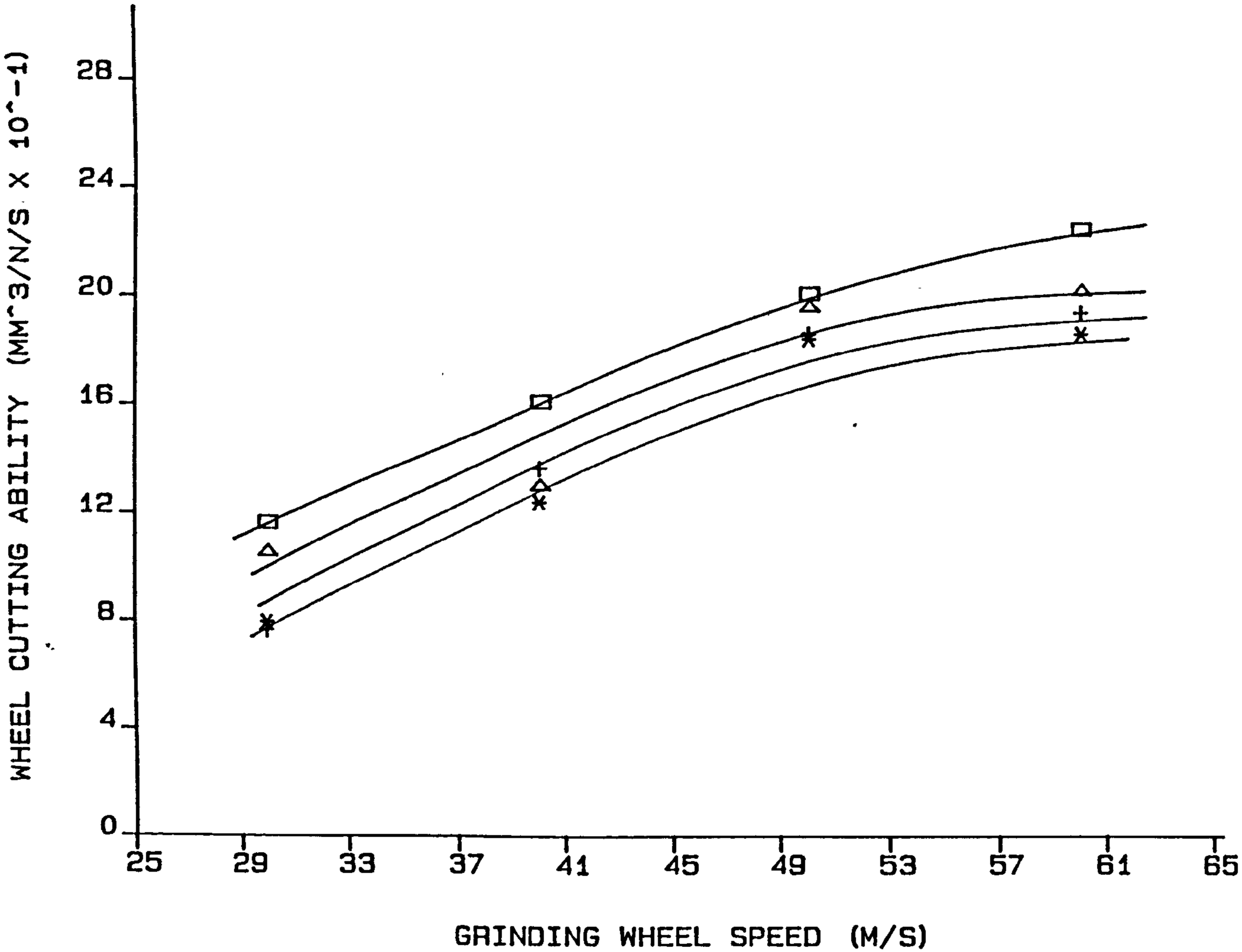

**REFER TO TABLE(S) EN 8 SERIES FOR EXP.L CONDITIONS.

LEGEND

*: - Q-RATIO=100 (VI=0.056MM/S)
+: - Q-RATIO=200 (VI=0.056MM/S)
△: - Q-RATIO=100 (VI=0.116MM/S)
□: - Q-RATIO=200 (VI=0.116MM/S)

ADDITIONAL DATA

WHEEL - RA60K5V70H
MATERIAL - EN 8

FIG. 58

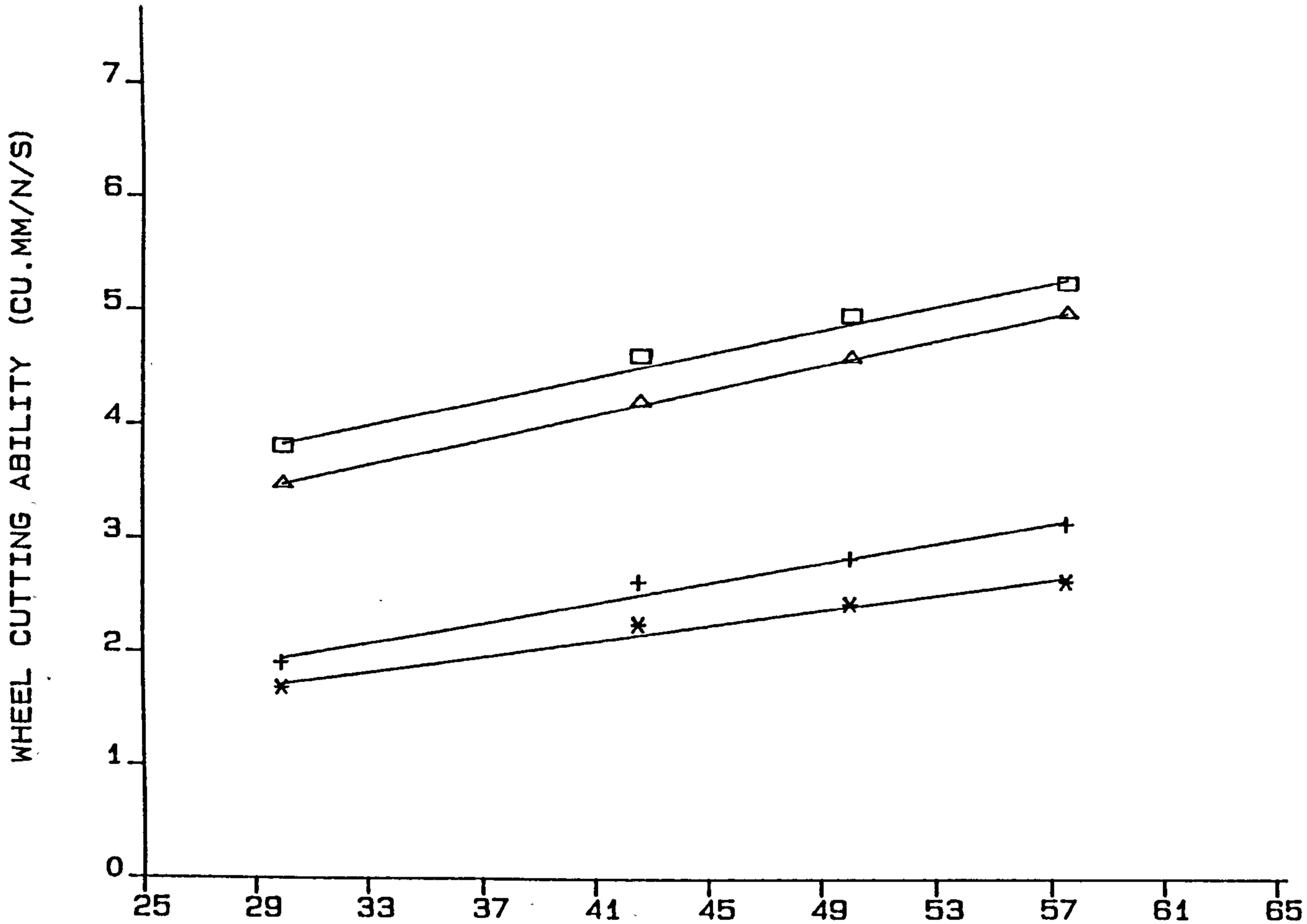

**REFER TO TABLE(S) CI SERIES
FOR EXP.L CONDITIONS.

LEGEND

*: - VI=0.062MM/S (Q-RATIO=100)
+: - VI=0.062MM/S (Q-RATIO=200)
△: - VI=0.154MM/S (Q-RATIO=100)
□: - VI=0.154MM/S (Q-RATIO=200)

ADDITIONAL DATA

WHEEL - C46 BBT
MATERIAL - CAST IRON

FIG. 59

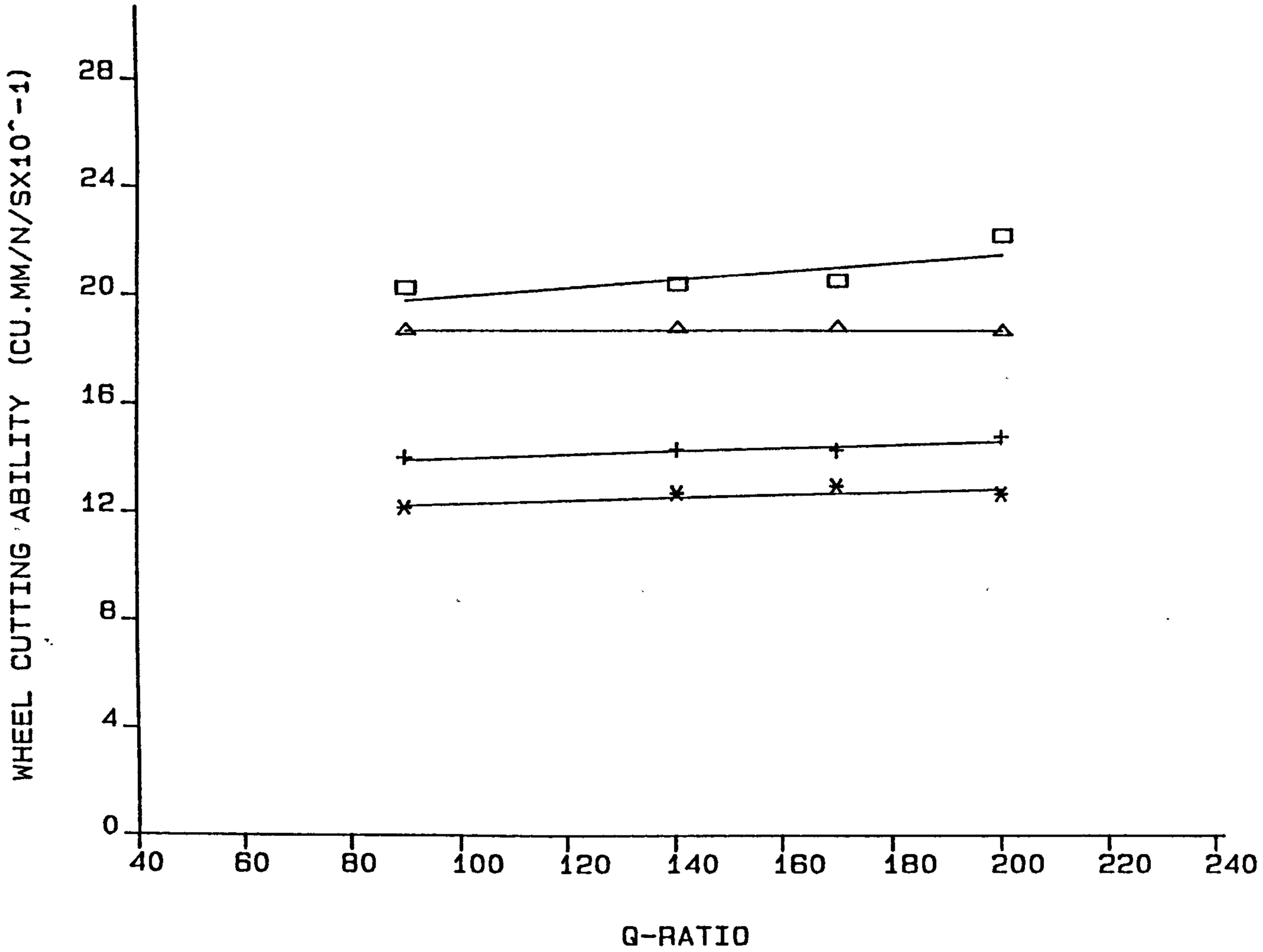

**REFER TO TABLE(S) EN 9 SERIES
FOR EXP.L CONDITIONS.

LEGEND

*:- VI=0.056MM/S (VG=40M/S)
+:- VI=0.116MM/S (VG=40M/S)
△:- VI=0.056MM/S (VG=60M/S)
□:- VI=0.116MM/S (VG=60M/S)

ADDITIONAL DATA

WHEEL - WA60MVRC
MATERIAL - EN 9

FIG. 60

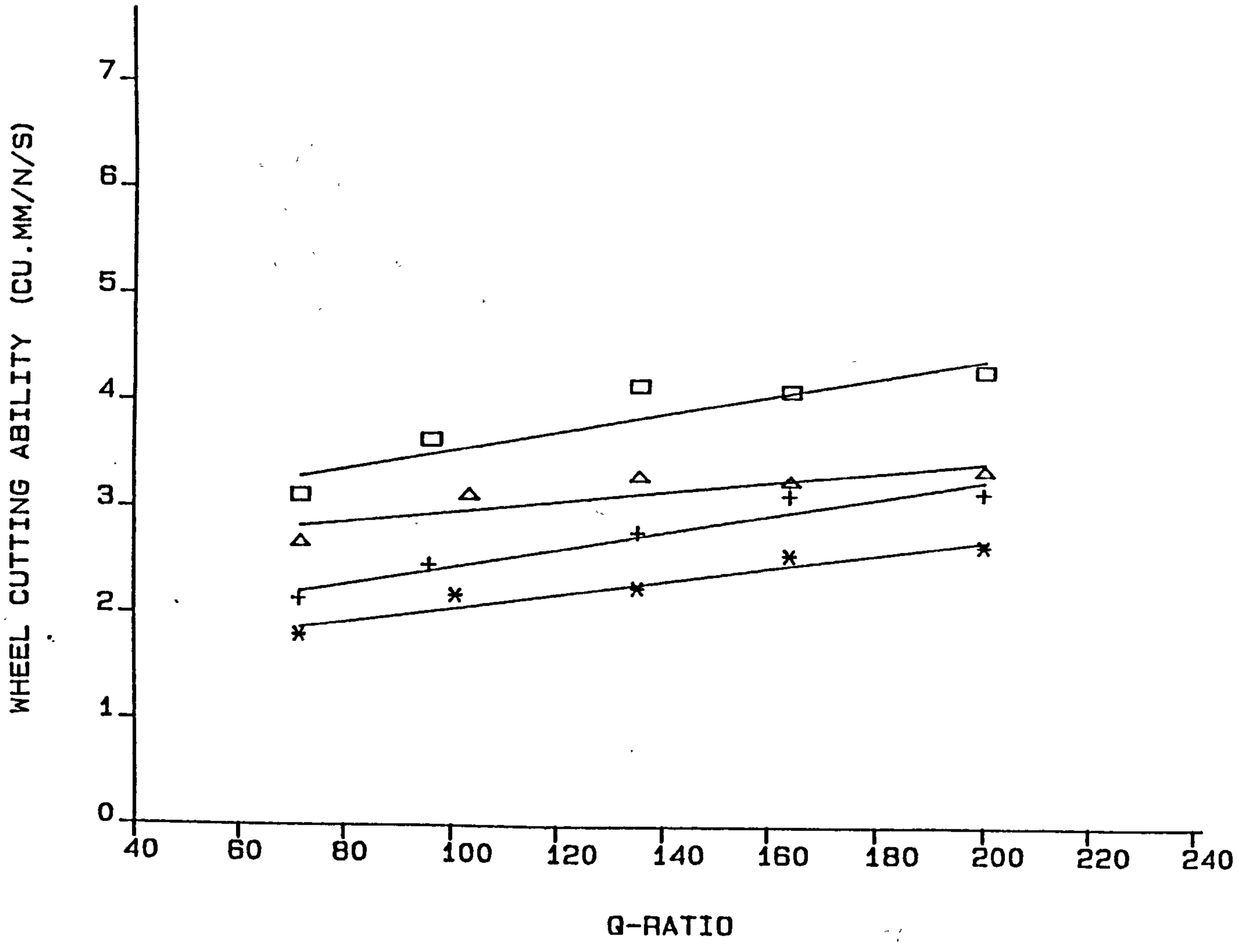

**REFER TO TABLE(S) CI SERIES
FOR EXP.L CONDITIONS.

LEGEND

*: - VI=0.062MM/S (VG=40M/S)
+: - VI=0.124MM/S (VG=40M/S)
△: - VI=0.062MM/S (VG=60M/S)
□: - VI=0.124MM/S (VG=60M/S)

ADDITIONAL DATA

WHEEL - C46 BBT
MATERIAL - CAST IRON

FIG. 61

SPECIFIC GRINDING ENERGY VS INFEED-RATE

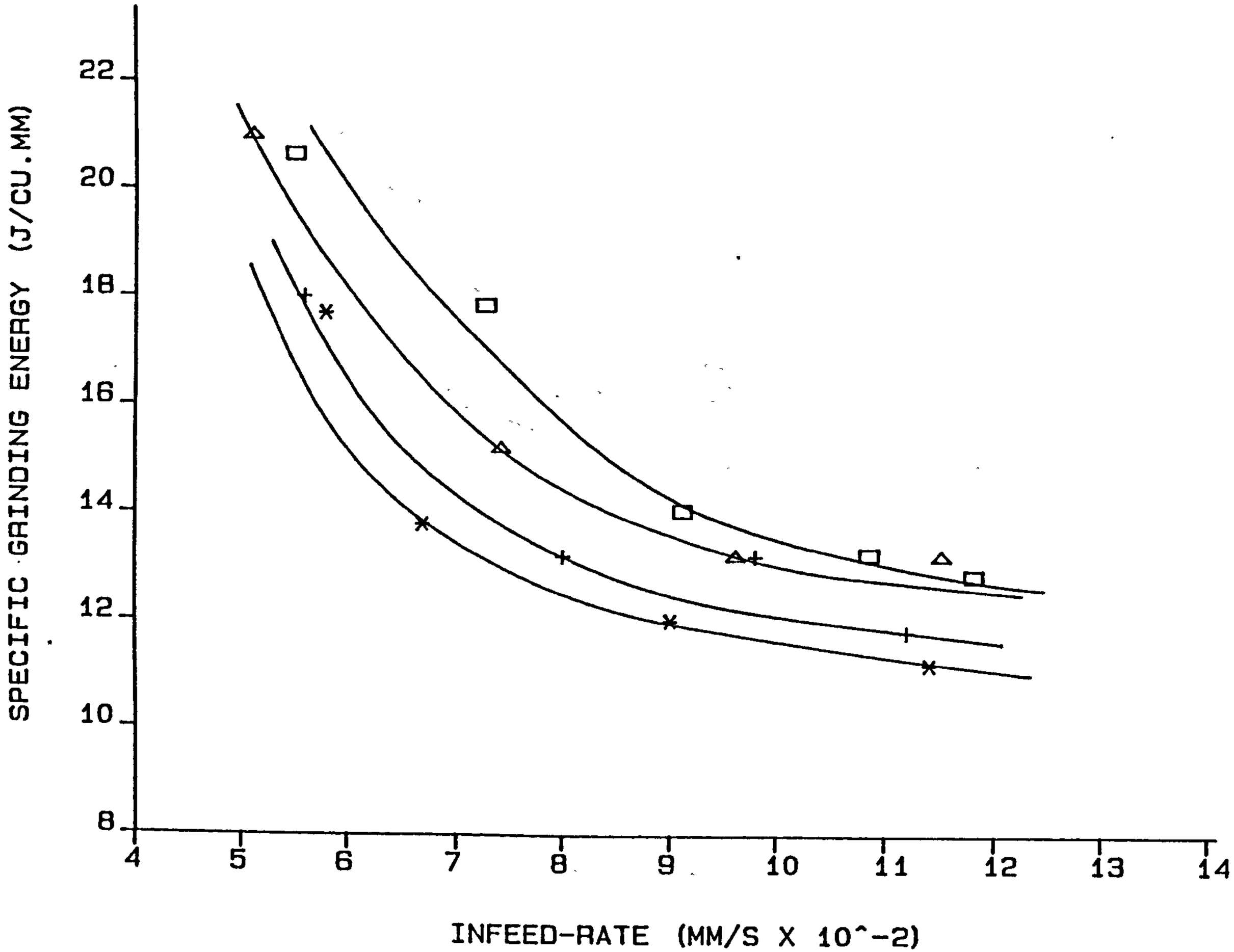

**REFER TO TABLE(S) EN 9 SERIES FOR EXP.L CONDITIONS.

LEGEND

*: - Q-RATIO = 200
+: - Q-RATIO = 170
△: - Q-RATIO = 140
□: - Q-RATIO = 100

ADDITIONAL DATA

WHEEL - WA60MVRC
MATERIAL - EN 9
VG = 30 M/S

FIG. 62

SPECIFIC GRINDING ENERGY VS INFEED-RATE

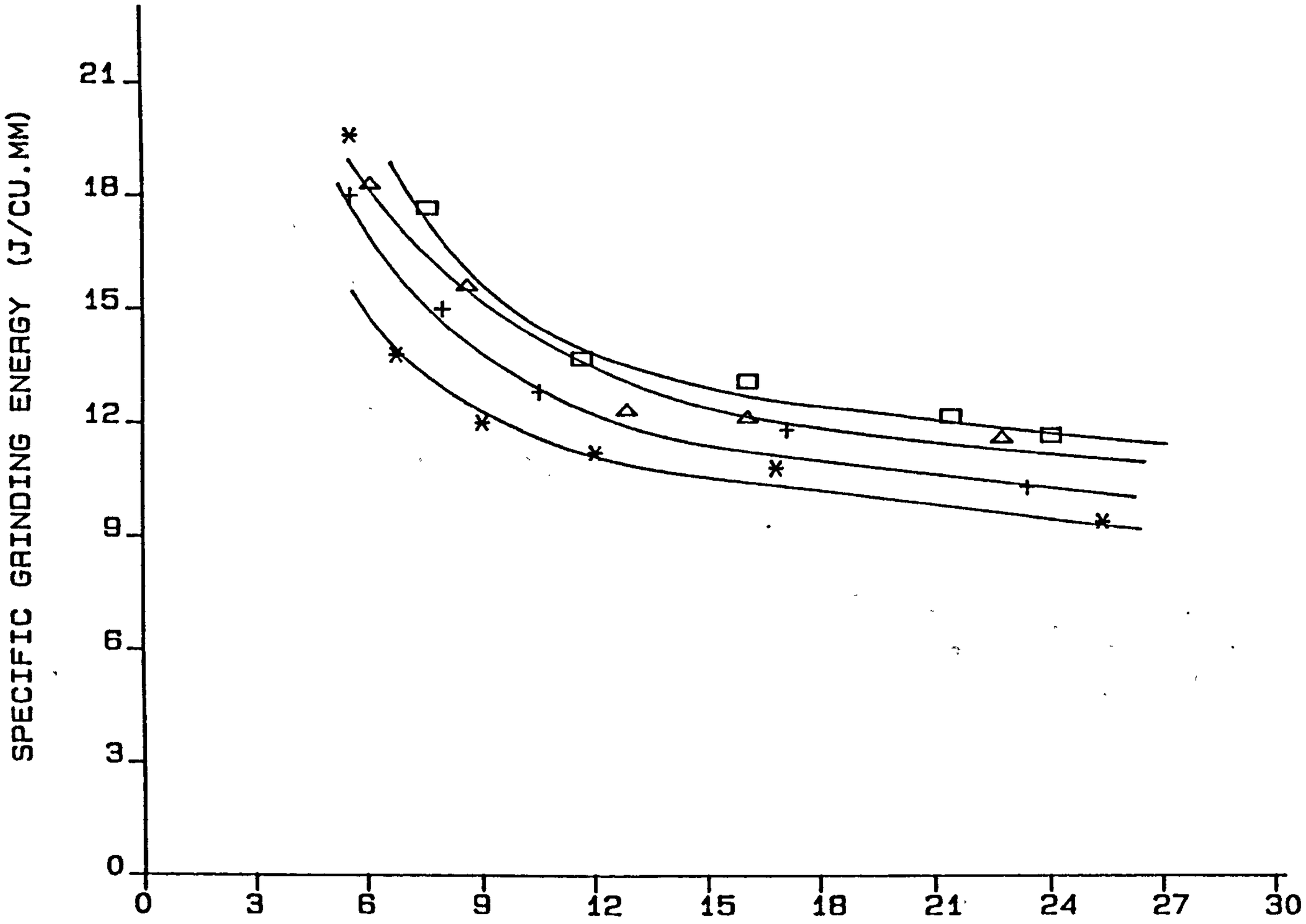

**REFER TO TABLE(S) EN 9 SERIES FOR EXP.L CONDITIONS.

LEGEND

*: - Q-RATIO = 200
+: - Q-RATIO = 170
△: - Q-RATIO = 140
□: - Q-RATIO = 100

ADDITIONAL DATA

WHEEL - WA60MVRC
MATERIAL - EN 9
VG = 60 M/S

FIG. 63

SPECIFIC GRINDING ENERGY VS INFEED-RATE

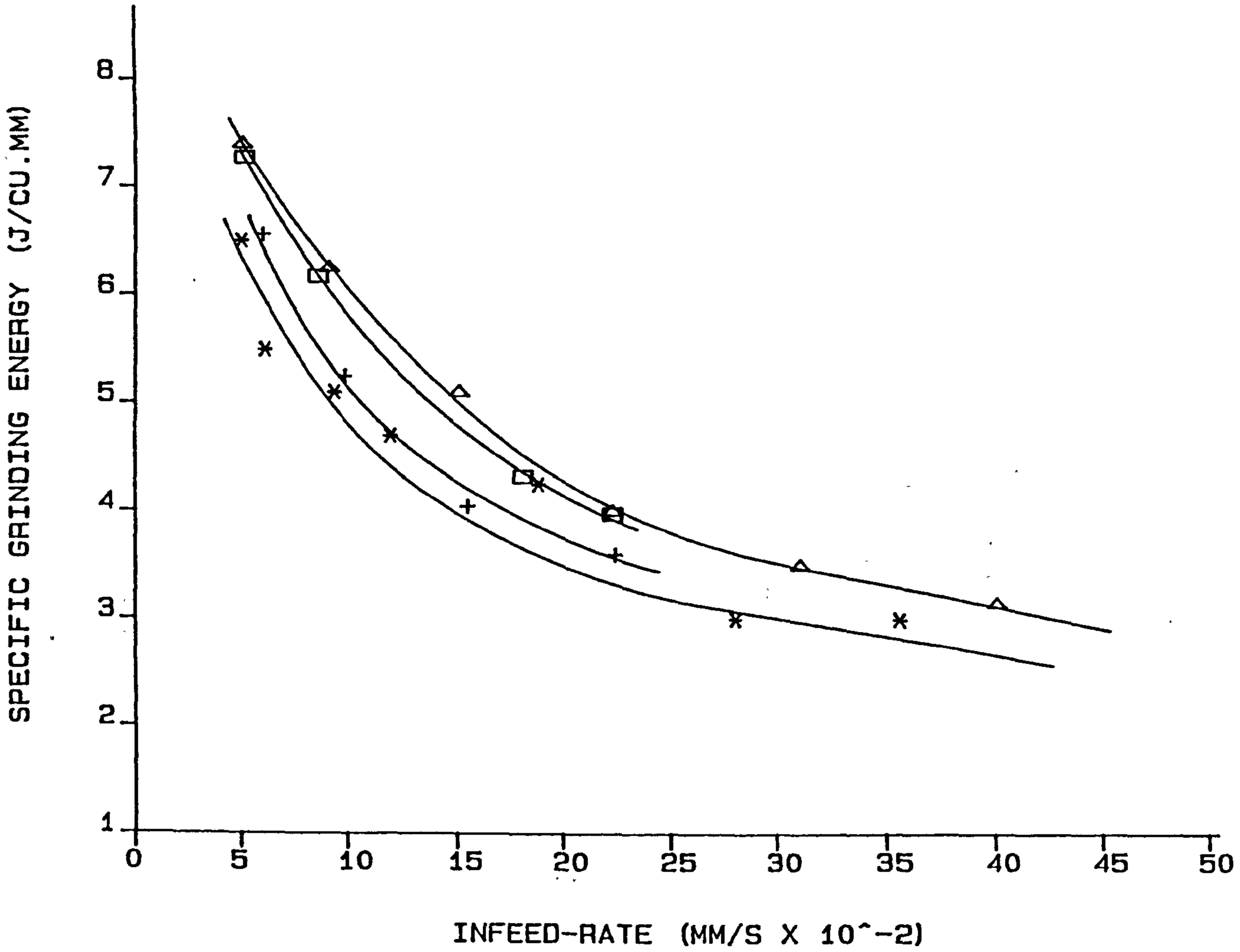

**REFER TO TABLE(S) CI SERIES
FOR EXP.L CONDITIONS.

LEGEND

*: - Q-RATIO=100 (VG=60 M/S)
+: - Q-RATIO=100 (VG=30 M/S)
△: - Q-RATIO=200 (VG=60 M/S)
□: - Q-RATIO=200 (VG=30 M/S)

ADDITIONAL DATA

WHEEL - C46 8BT
MATERIAL - CAST IRON

FIG. 64

SPECIFIC GRINDING ENERGY VS GRINDING WHEEL SPEED

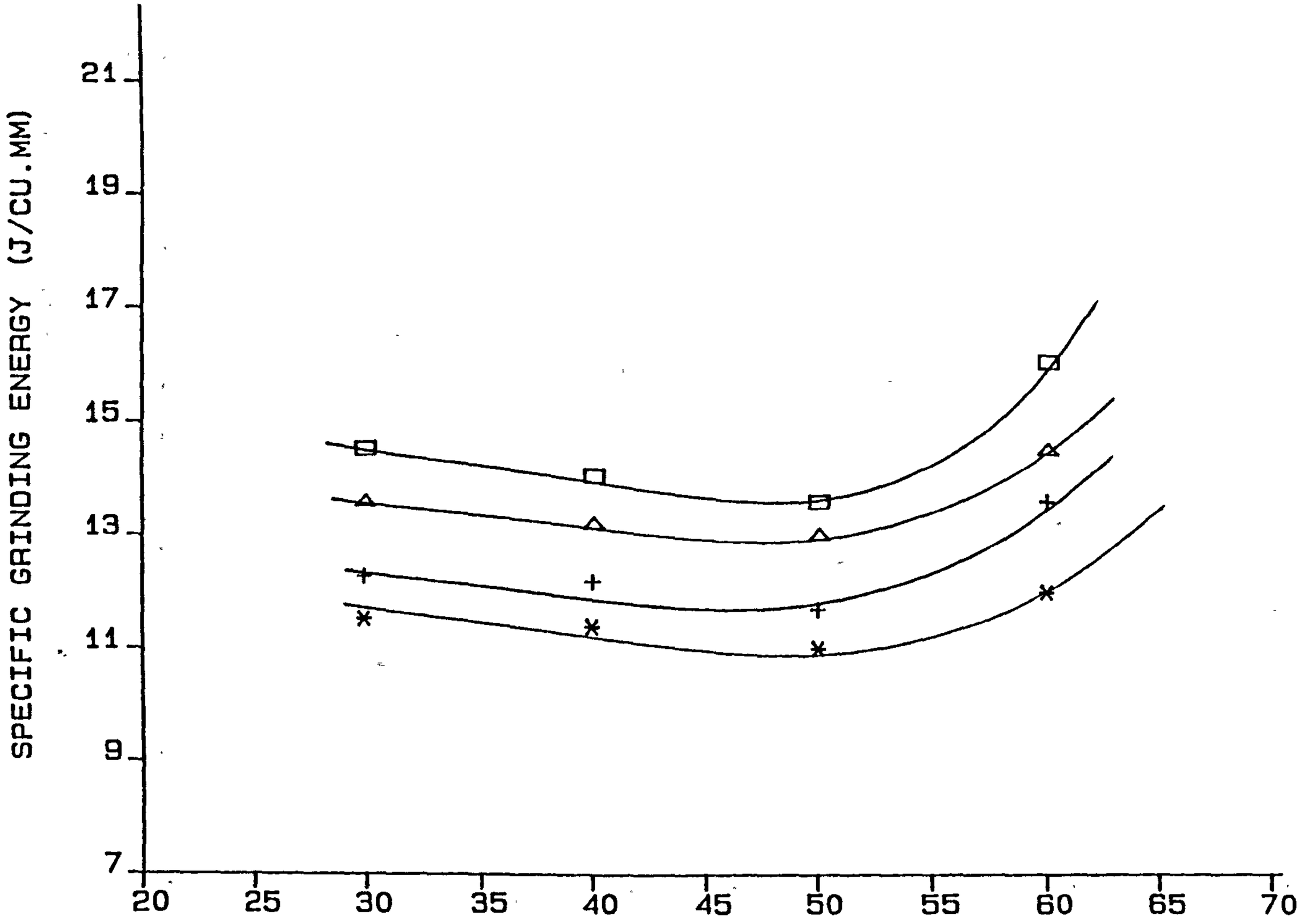

**REFER TO TABLE(S) EN 9 SERIES
FOR EXP.L CONDITIONS.

LEGEND

*: - Q-RATIO=200 (VI=.116MM/S)
+: - Q-RATIO=100 (VI=0.116MM/S)
△: - Q-RATIO=200 (VI=0.056MM/S)
□: - Q-RATIO=100 (VI=0.056MM/S)

ADDITIONAL DATA

WHEEL - WA60MVRC
MATERIAL - EN 9

FIG. 65

SPECIFIC GRINDING ENERGY VS GRINDING WHEEL SPEED

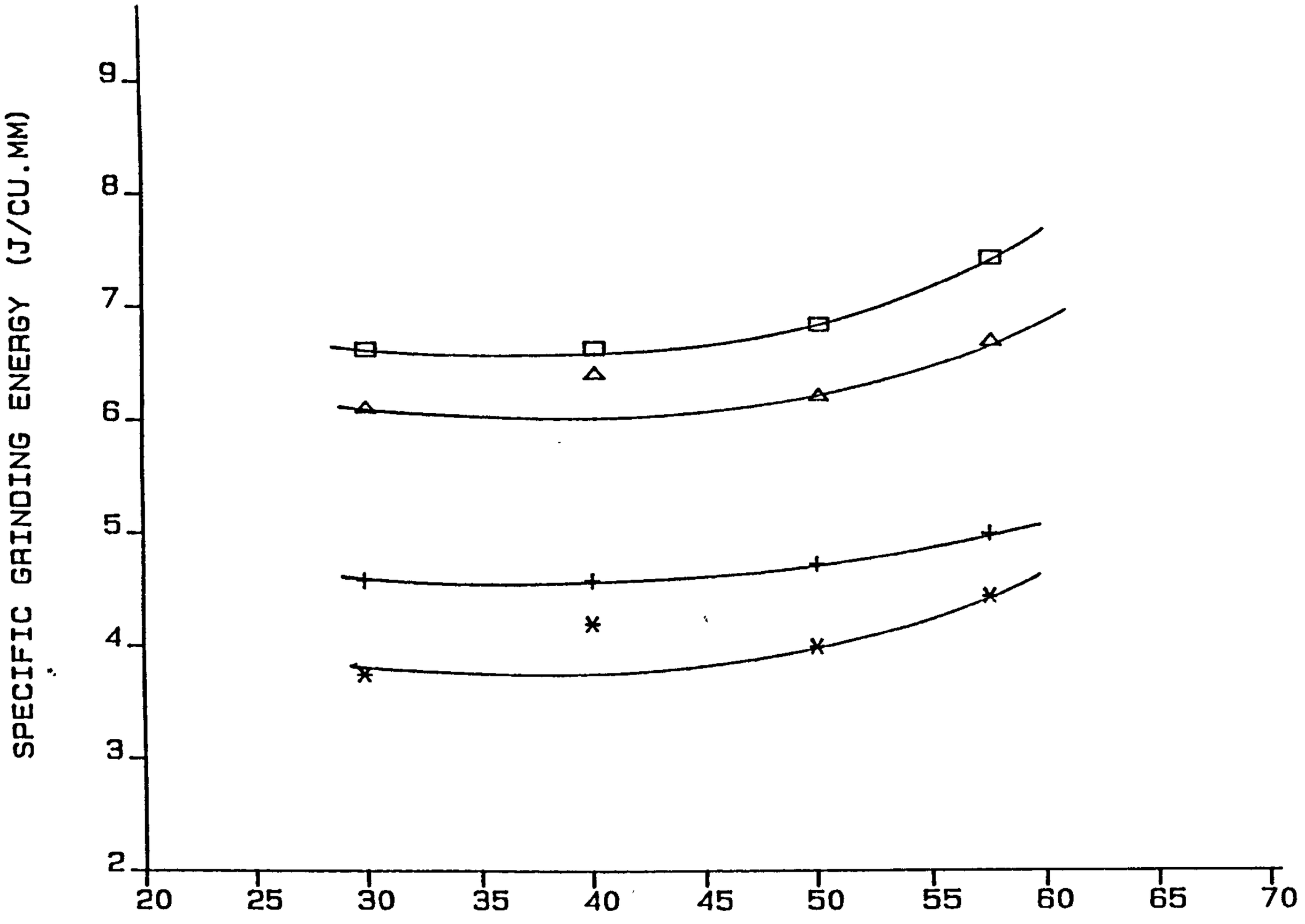

**REFER TO TABLE(S) CI SERIES FOR EXP.L CONDITIONS.

LEGEND

*: - Q-RATIO=200 (VI=0.124MM/S)
+: - Q-RATIO=100 (VI=0.124MM/S)
△: - Q-RATIO=200 (VI=0.056MM/S)
□: - Q-RATIO=100 (VI=0.056MM/S)

ADDITIONAL DATA

WHEEL - C46 BBT
MATERIAL - CAST IRON

FIG. 66

SPECIFIC GRINDING ENERGY VS Q-RATIO

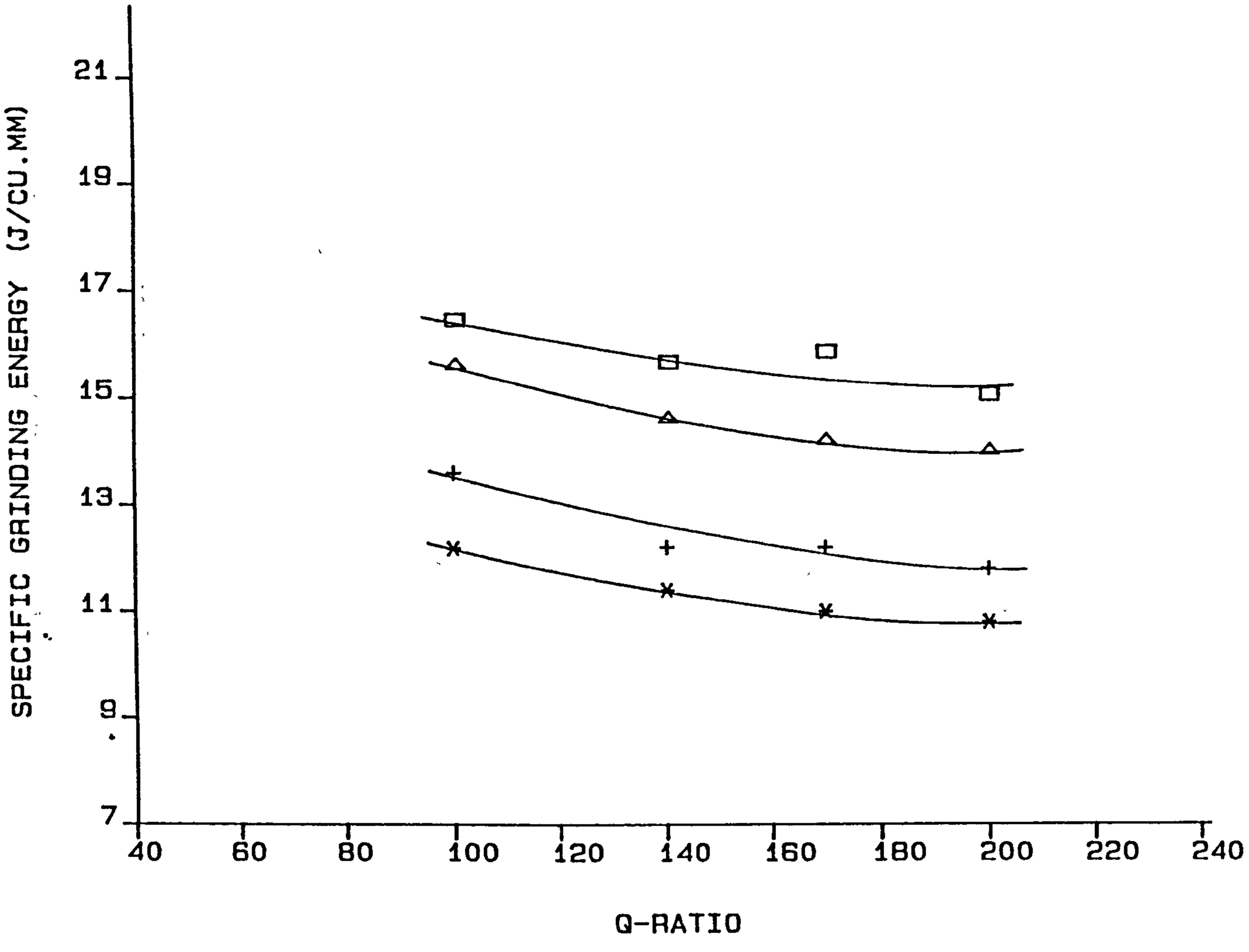

**REFER TO TABLE(S) EN 9 SERIES FOR EXP.L CONDITIONS.

LEGEND

*: - VG=40 M/S (VI=0.116 MM/S)
+: - VG=60 M/S (VI=0.116 MM/S)
△: - VG=40 M/S (VI=0.056 MM/S)
□: - VG=60 M/S (VI=0.056 MM/S)

ADDITIONAL DATA

WHEEL - WA60MVRC
MATERIAL - EN 9

FIG. 67

SPECIFIC GRINDING ENERGY VS Q-RATIO

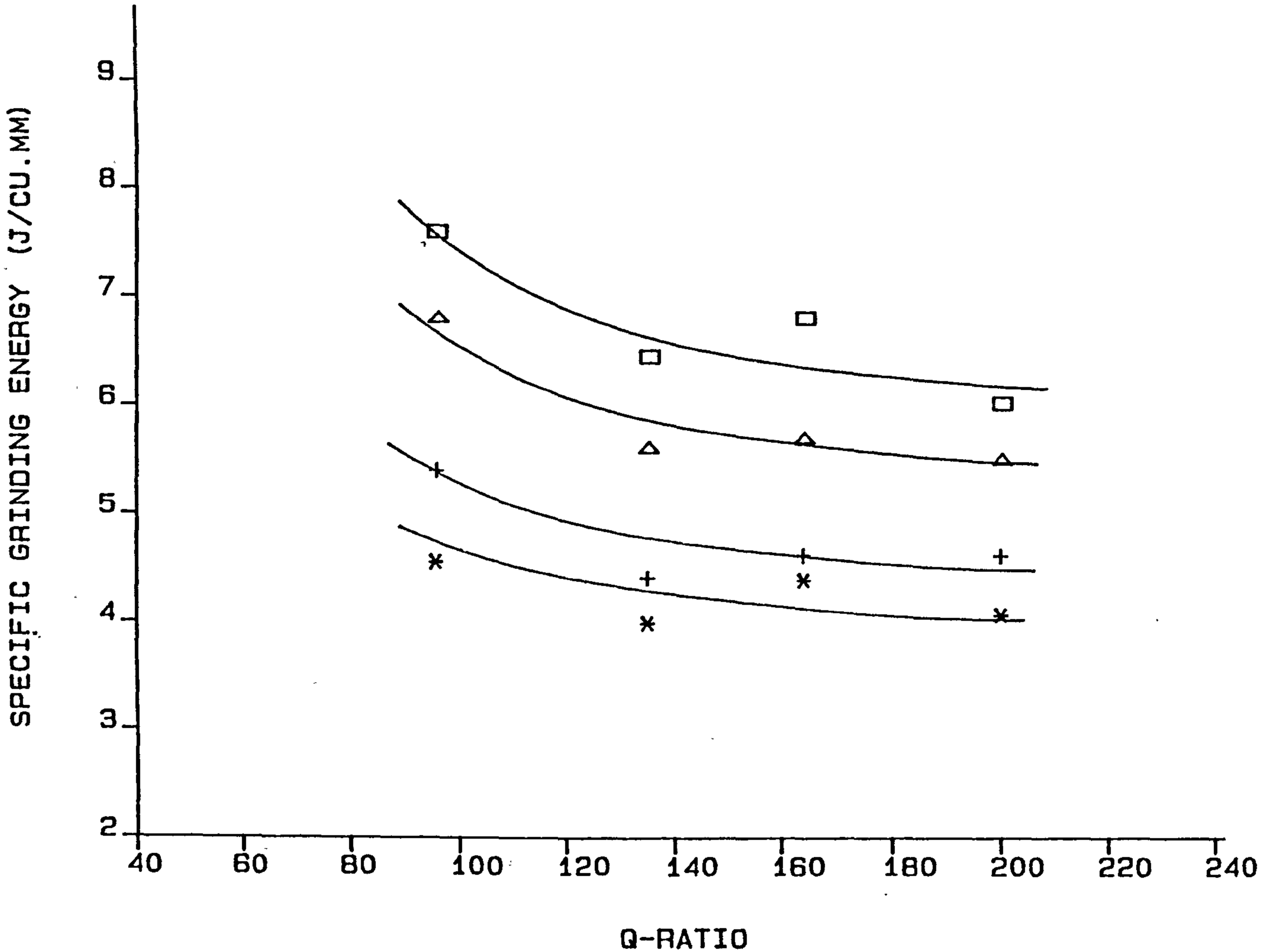

**REFER TO TABLE(S) CI SERIES
FOR EXP.L CONDITIONS.

LEGEND

*: - VI=0.124 MM/S (VG=30 M/S)
+: - VI=0.124 MM/S (VG=60 M/S)
△: - VI=0.056 MM/S (VG=30 M/S)
□: - VI=0.056 MM/S (VG=60 M/S)

ADDITIONAL DATA

WHEEL - C46 BBT
MATERIAL - CAST IRON

FIG. 68

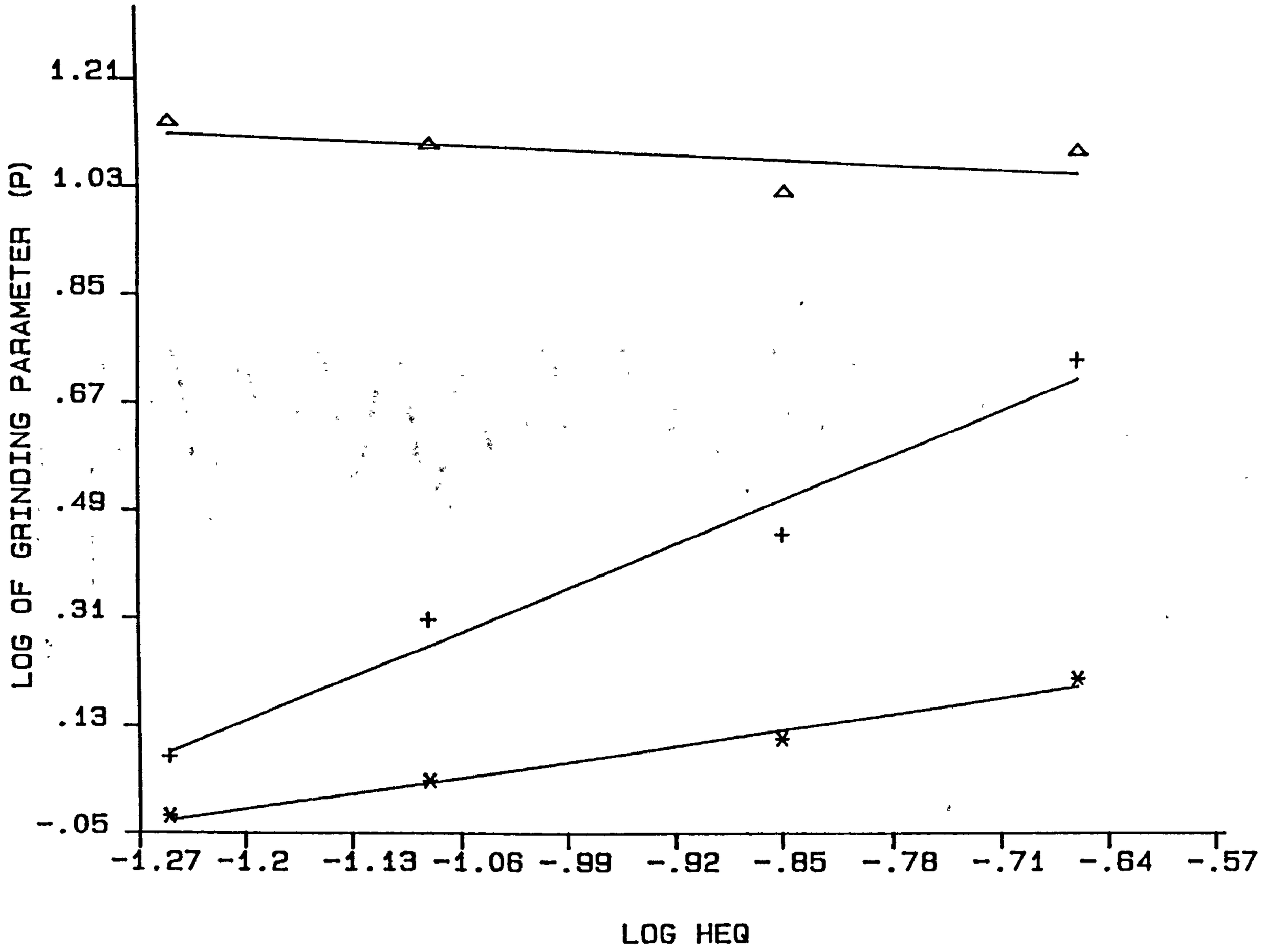

**REFER TO TABLE(S) EN 9 SERIES FOR EXP.L CONDITIONS.

LEGEND

*: - SURFACE ROUGHNESS (RA)
+: - NORMAL FORCE (FN')
△: - SPECIFIC ENERGY (U)

ADDITIONAL DATA

WHEEL - RA60K5V70H
MATERIAL - EN 9
Q-RATIO = 200

FIG. 69

GEOMETRIC STABILITY CHART FOR CENTRELESS GRINDING

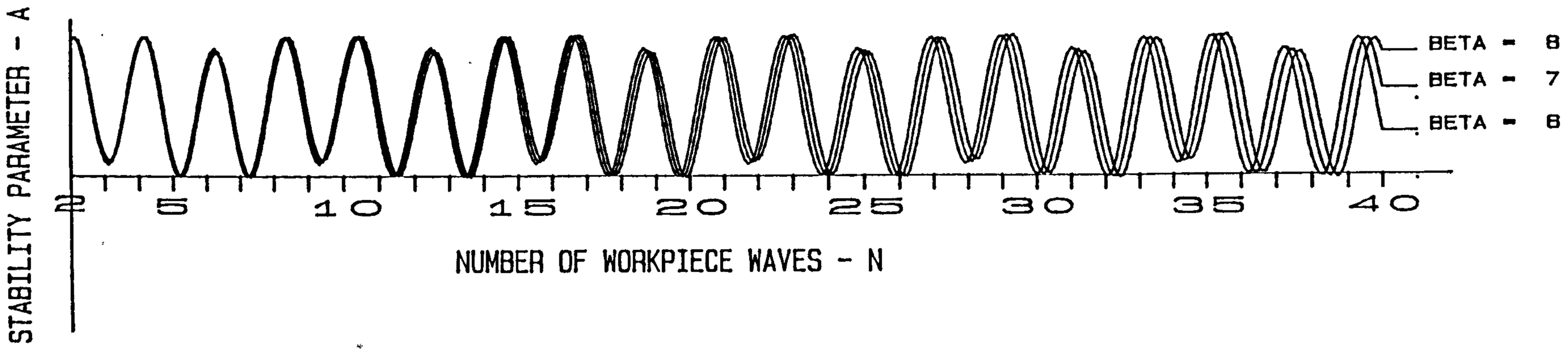

WORKBLADE ANGLE = 30 DEGREES
DC/DG = 0.6

FIG. 70

Q-RATIO VS GRINDING WHEEL SPEED

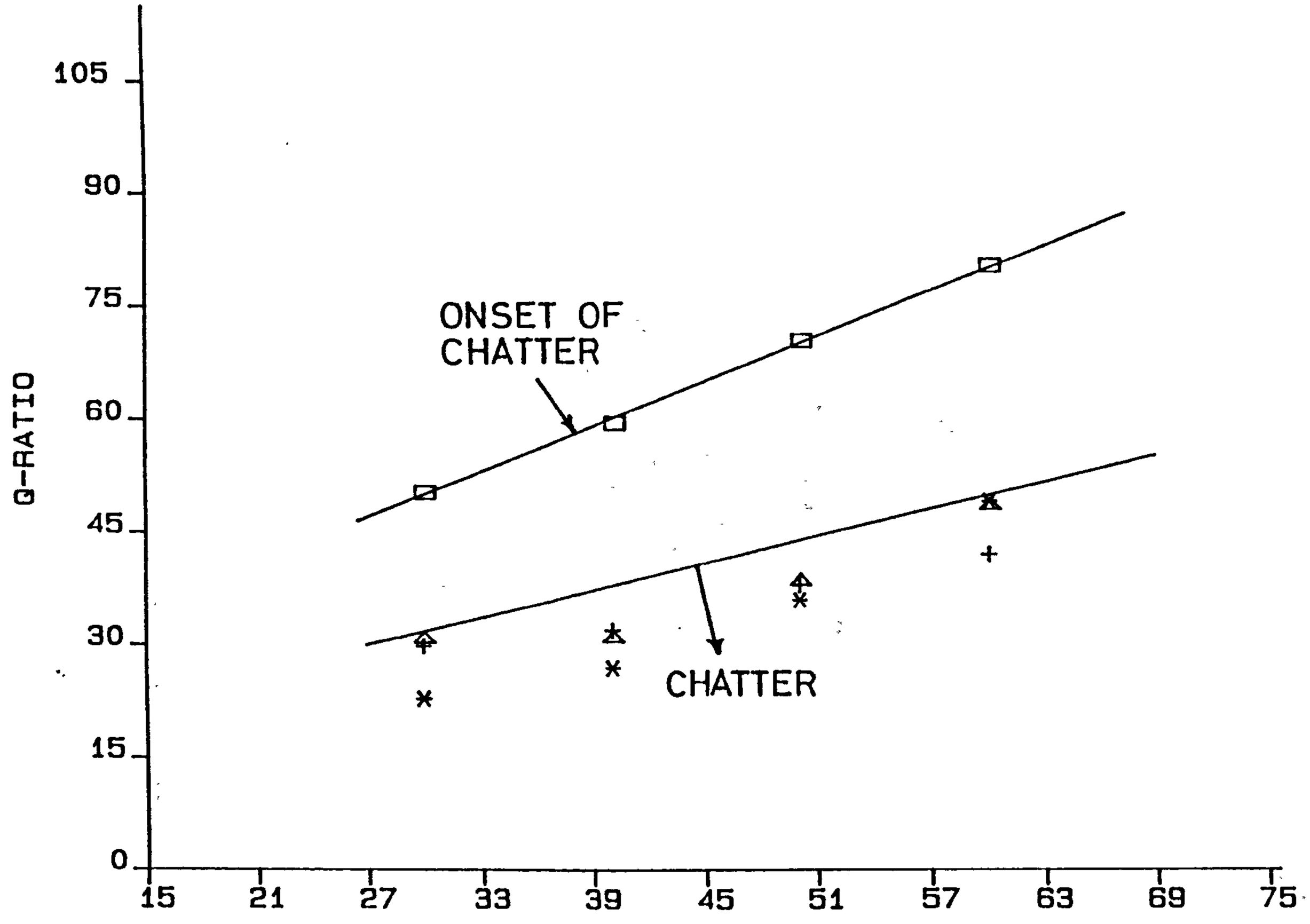

**REFER TO TABLE(S) EN 8 SERIES
FOR EXP.L CONDITIONS.

LEGEND

*: - VI = 0.033 MM/S
+: - VI = 0.053 MM/S
△: - VI = 0.086 MM/S
□: - ONSET OF CHATTER

ADDITIONAL DATA

WHEEL - WA60MVRC
MATERIAL - EN 9

FIG.71

Q-RATIO VS GRINDING WHEEL SPEED

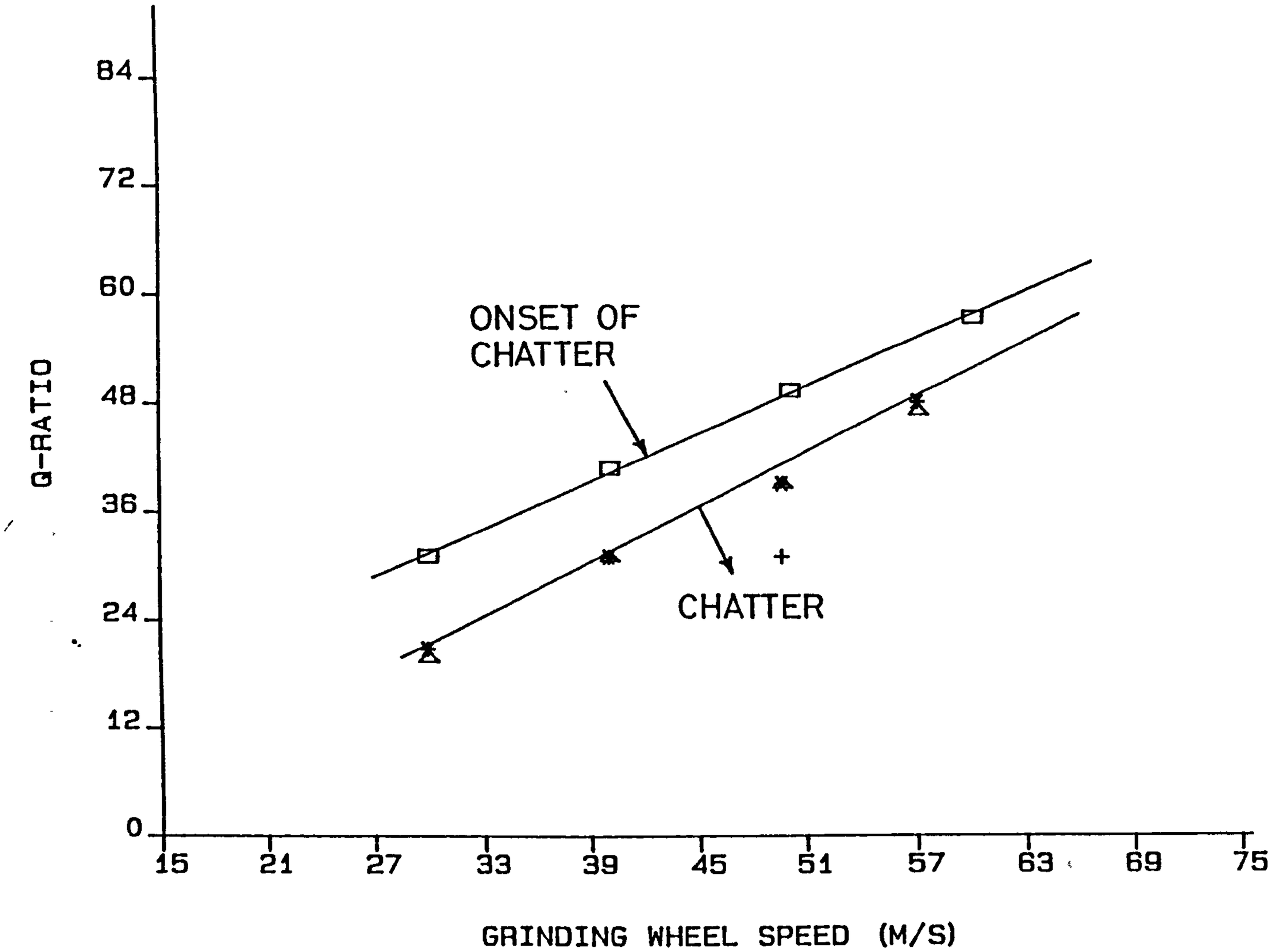

**REFER TO TABLE(S) CI SERIES FOR EXP.L CONDITIONS.

LEGEND

*:- VI = 0.034 MM/S
+:- VI = 0.056 MM/S
△:- VI = 0.088 MM/S
□:- ONSET OF CHATTER

ADDITIONAL DATA

WHEEL - C46 BBT
MATERIAL - CAST IRON

FIG.71A

SURFACE ROUGHNESS VS Q-RATIO

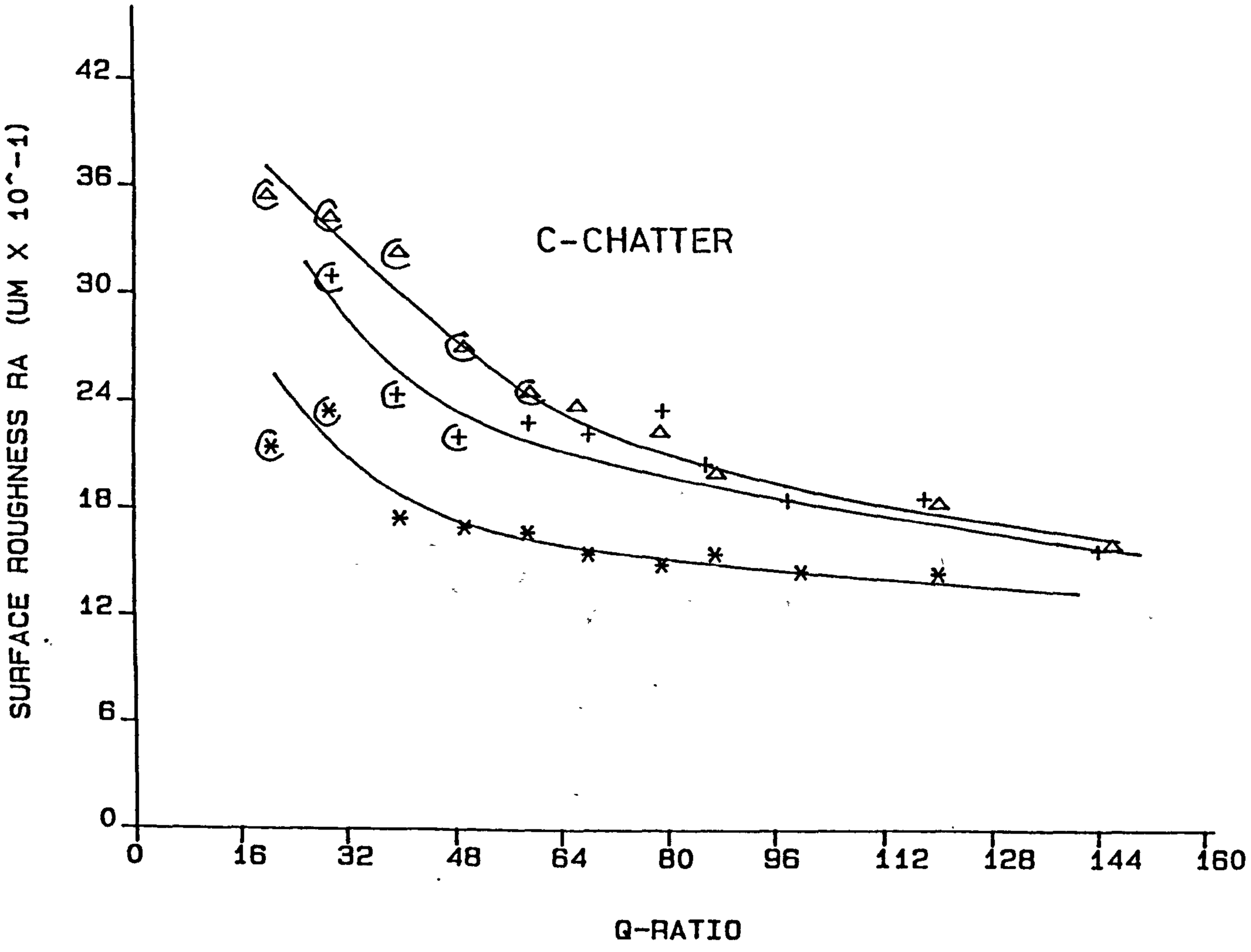

**REFER TO TABLE(S) EN 9 SERIES FOR EXP.L CONDITIONS.

LEGEND

*:- VI = 0.033 MM/S
+:- VI = 0.053 MM/S
△:- VI = 0.086 MM/S

ADDITIONAL DATA

WHEEL - WA60MVRC
VG - 30 M/S
MATERIAL - EN 9

FIG.72

SURFACE ROUGHNESS VS Q-RATIO

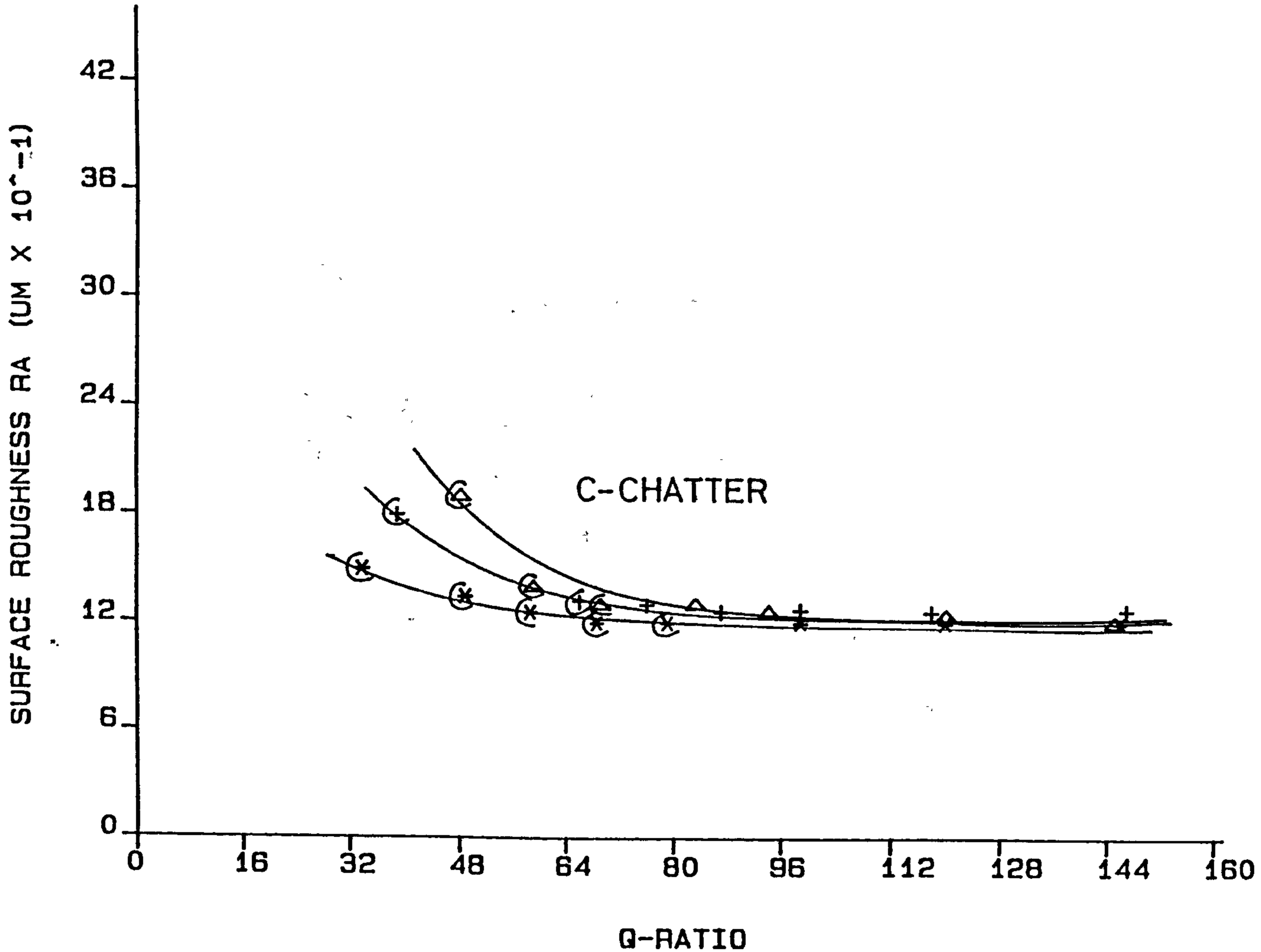

**REFER TO TABLE(S) EN 9 SERIES FOR EXP.L CONDITIONS.

LEGEND

*:- VI = 0.035 MM/S
+:- VI = 0.05 MM/S
△:- VI = 0.08 MM/S

ADDITIONAL DATA

WHEEL - WA80MVRC
VG - 80 M/S
MATERIAL - EN 9

FIG.73

SURFACE ROUGHNESS VS Q-RATIO

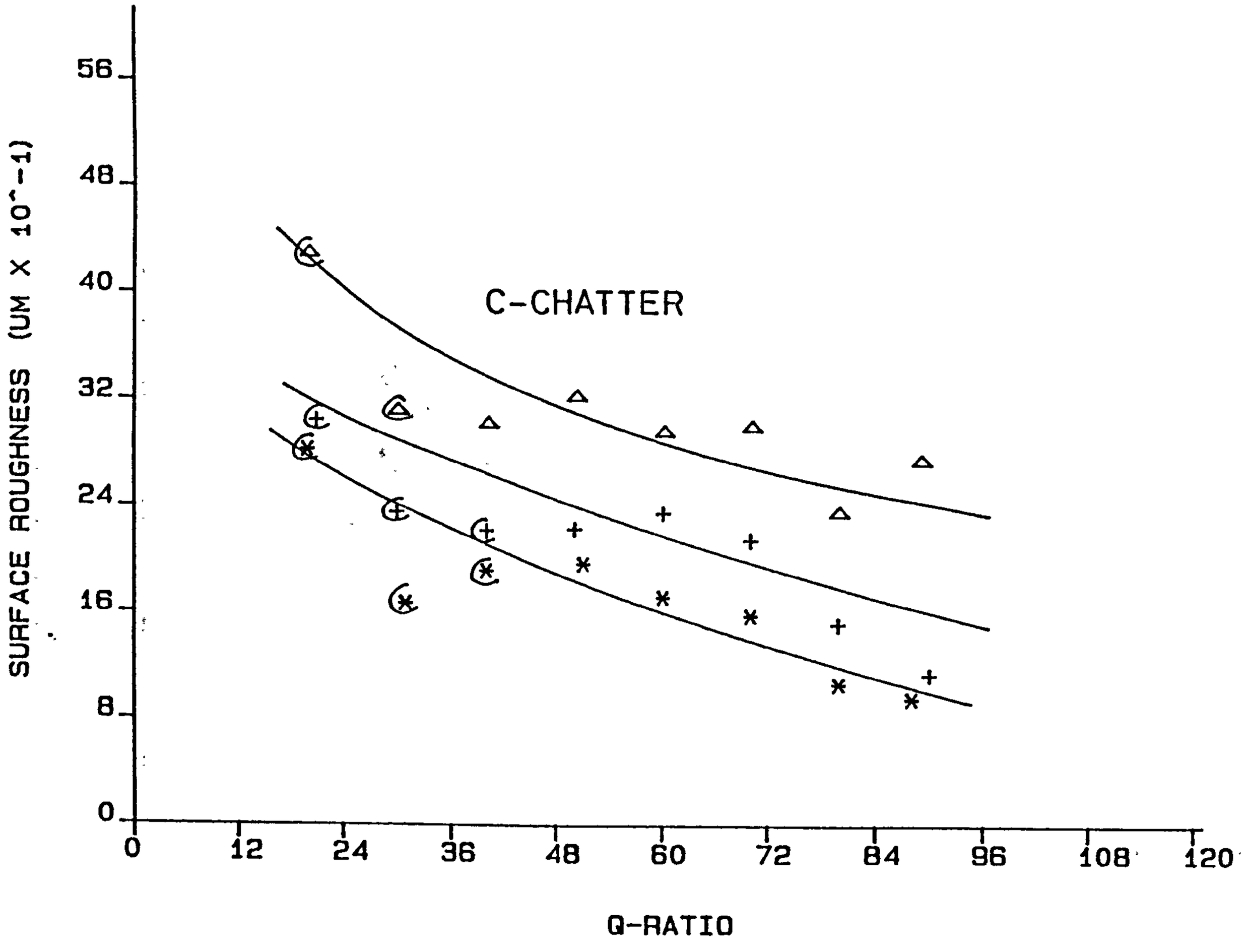

**REFER TO TABLE(S) CI SERIES
FOR EXP.L CONDITIONS.

LEGEND

*:- VI = 0.034 MM/S
+:- VI = 0.058 MM/S
△:- VI = 0.086 MM/S

ADDITIONAL DATA

WHEEL - C46 BBT
VG - 30 M/S
MATERIAL - CAST IRON

FIG.74

SURFACE ROUGHNESS VS Q-RATIO

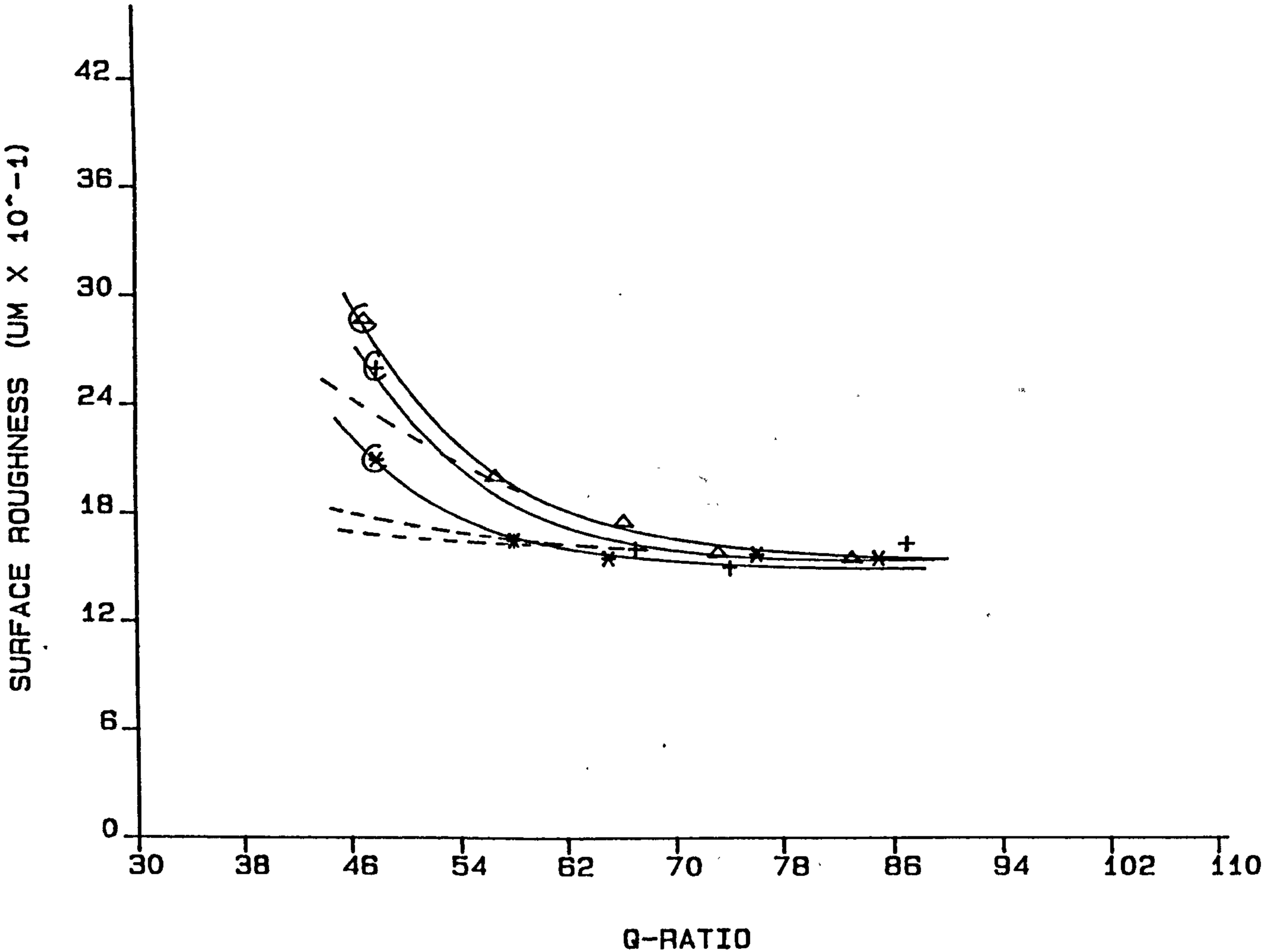

**REFER TO TABLE(S) CI SERIES
FOR EXP.L CONDITIONS.

LEGEND

*:- VI = 0.034 MM/S
+:- VI = 0.058 MM/S
△:- VI = 0.088 MM/S

ADDITIONAL DATA

WHEEL - C46 BBT
VG - 80 M/S
MATERIAL - CAST IRON

FIG.75

SURFACE ROUGHNESS VS Q-RATIO

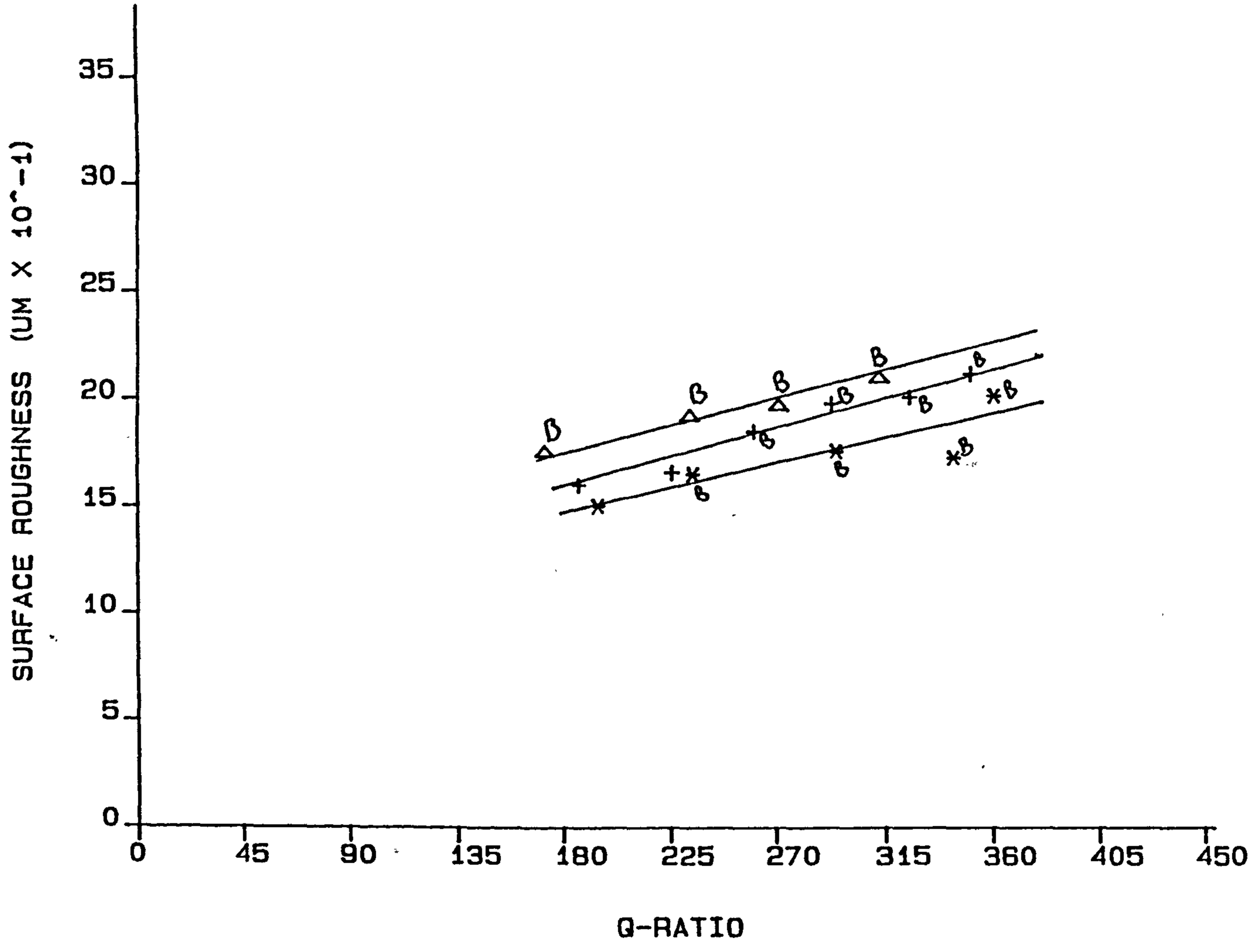

**REFER TO TABLE(S) EN 8 SERIES FOR EXP.L CONDITIONS.

LEGEND

*:- VI = 0.034 MM/S
+:- VI = 0.058 MM/S
△:- VI = 0.088 MM/S

ADDITIONAL DATA

WHEEL - WA60MVRC
VG - 41 M/S
MATERIAL - EN 8
B - BURN

FIG.76

SURFACE ROUGHNESS VS Q-RATIO

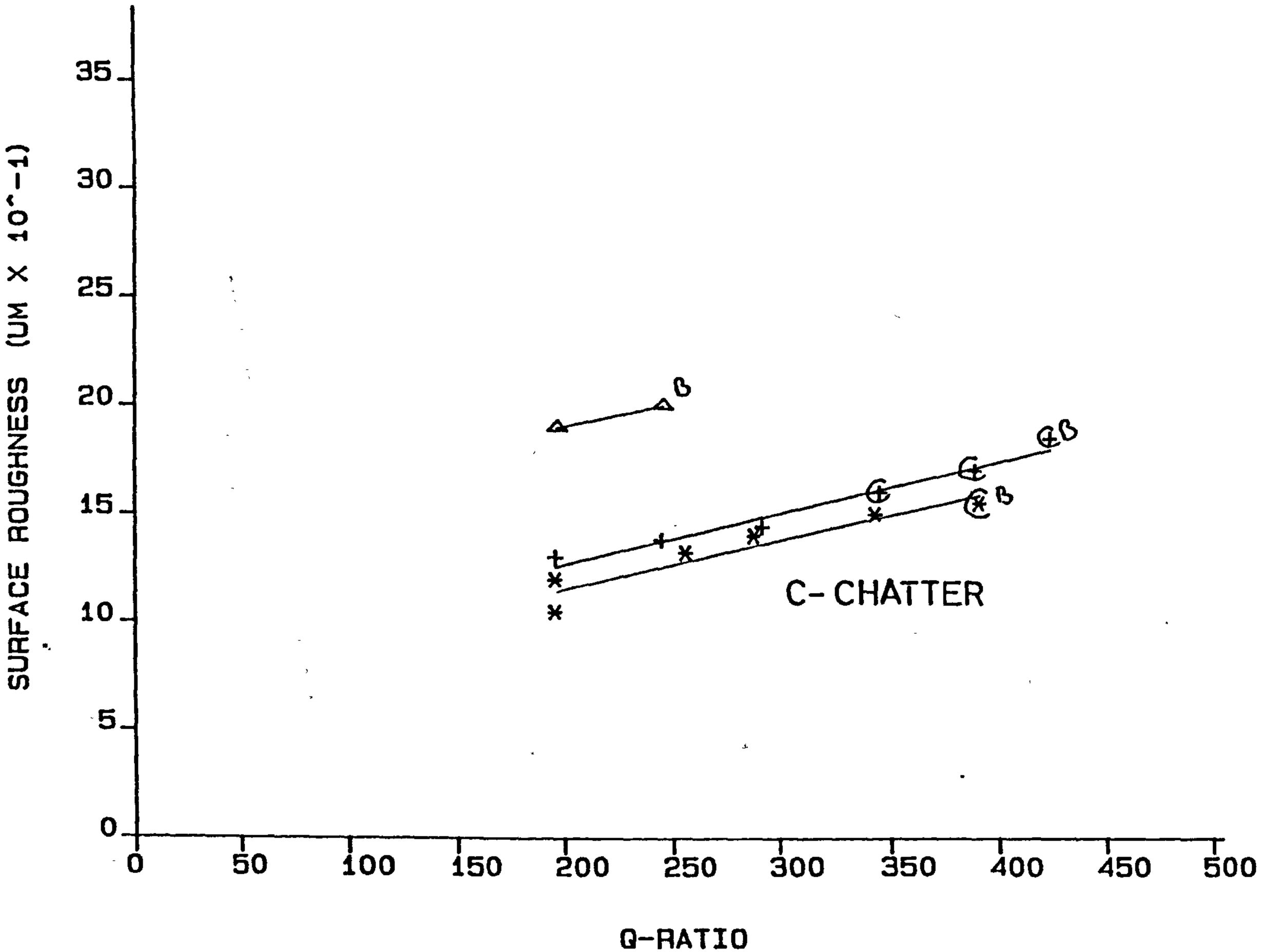

**REFER TO TABLE(S) CI SERIES FOR EXP.L CONDITIONS.

LEGEND

*:- VI = 0.034 MM/S
+:- VI = 0.055 MM/S
△:- VI = 0.086 MM/S

ADDITIONAL DATA

WHEEL - C46 BBT
VG - 39.6 M/S
MATERIAL - CAST IRON
B - BURN

FIG.77

ROUNDNESS ERROR VS Q-RATIO

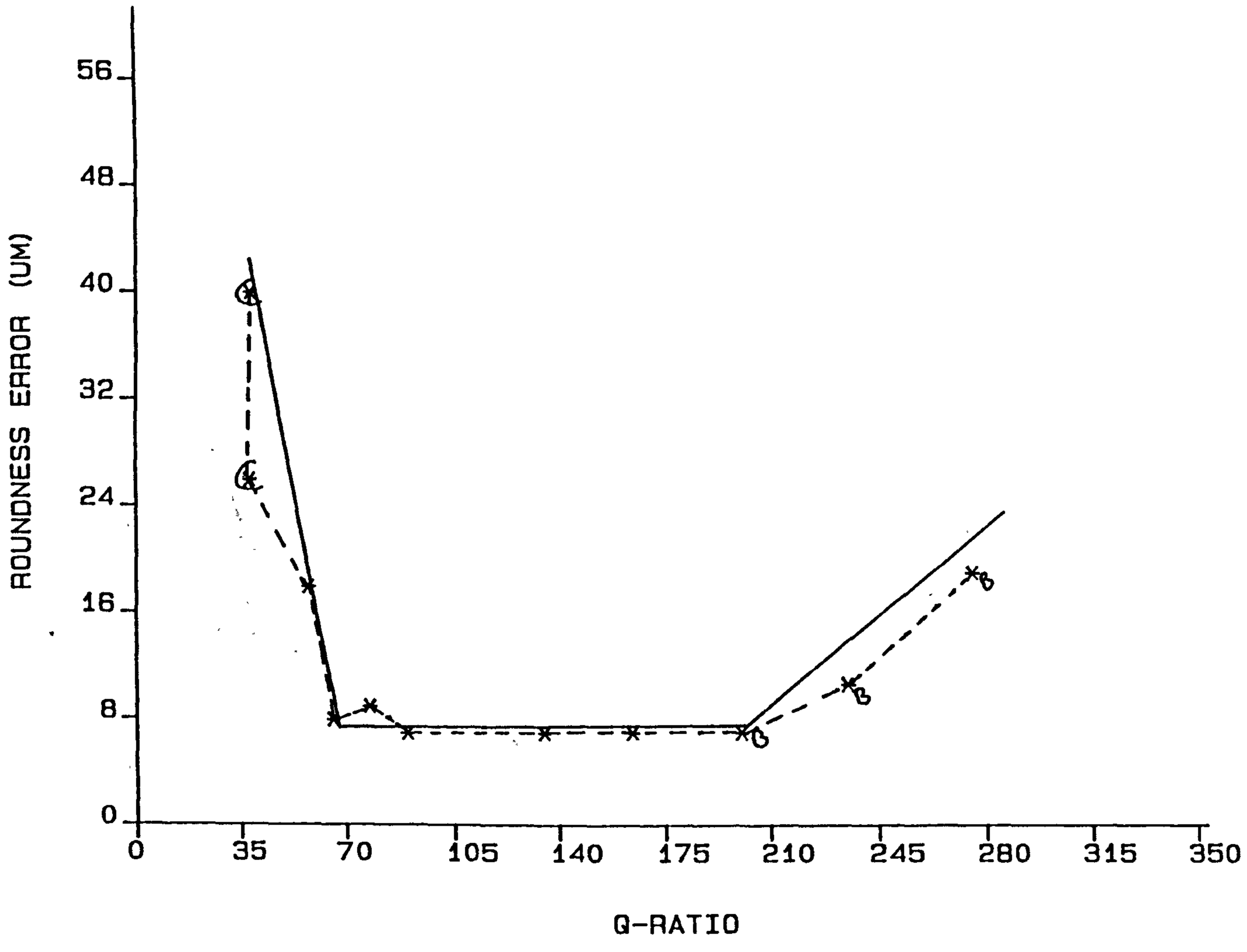

**REFER TO TABLE(S) CI SERIES
FOR EXP.L CONDITIONS.

LEGEND

*: - XX

ADDITIONAL DATA

VG = 50 M/S
VI = 0.086 MM/S
B = BURN
C = CHATTER

FIG.78

ROUNDNESS ERROR VS Q-RATIO

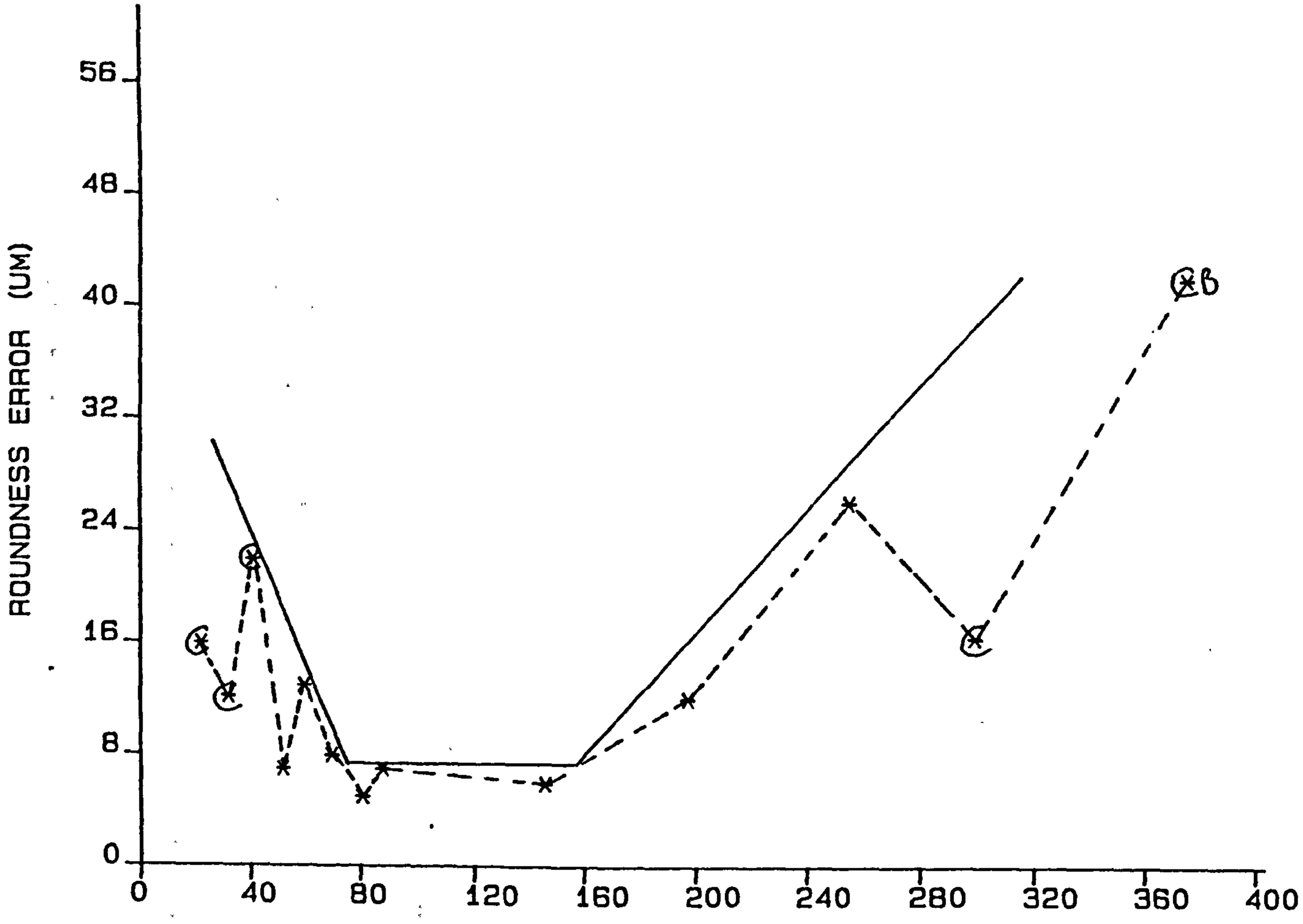

**REFER TO TABLE(S) CI SERIES FOR EXP.L CONDITIONS.

LEGEND

*: - XX

ADDITIONAL DATA

VG = 30 M/S
VI = 0.034 MM/S
B = BURN
C = CHATTER

FIG.79

ROUNDNESS ERROR VS Q-RATIO

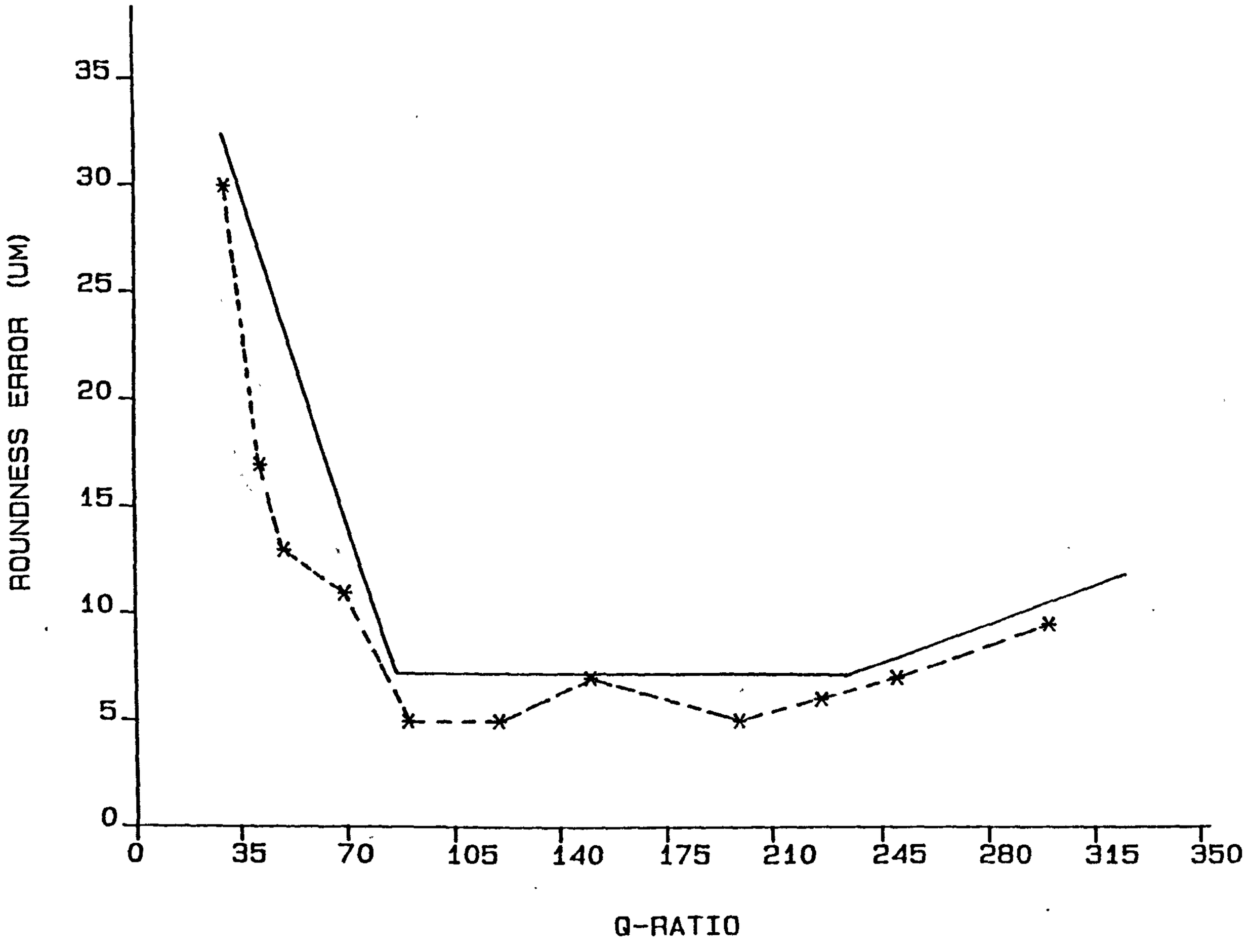

**REFER TO TABLE(S) EN 8 SERIES FOR EXP.L CONDITIONS.

LEGEND

*: - XX

ADDITIONAL DATA

VG = 50 M/S
VI = 0.088 MM/S
B = BURN
C = CHATTER

FIG.80

ROUNDNESS ERROR VS Q-RATIO

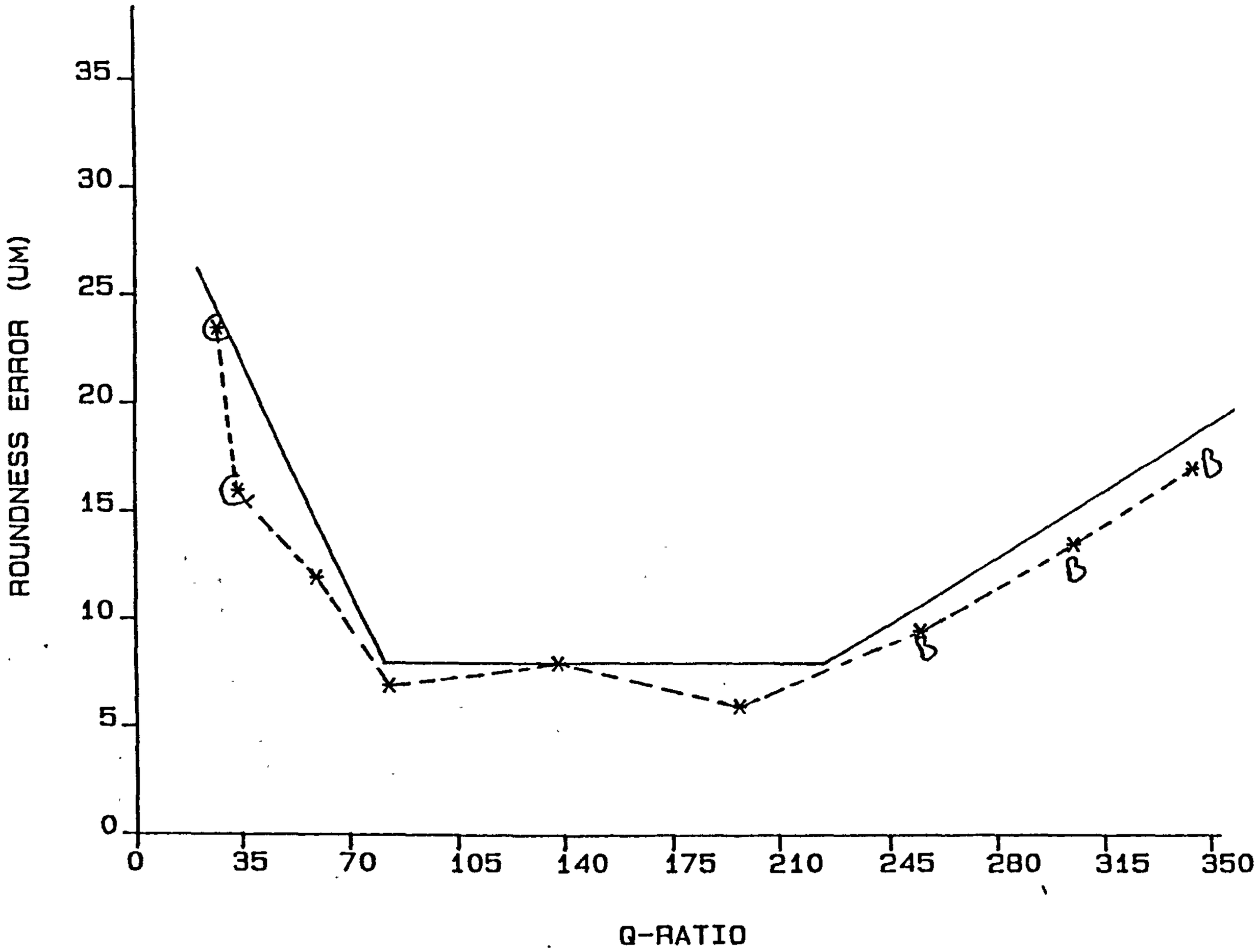

**REFER TO TABLE(S) EN 9 SERIES FOR EXP.L CONDITIONS.

LEGEND

*:- XX

ADDITIONAL DATA

VG = 30 M/S
VI = 0.053 MM/S
B = BURN
C = CHATTER

FIG.81

ROUNDNESS ERROR VS WORKPIECE SPEED

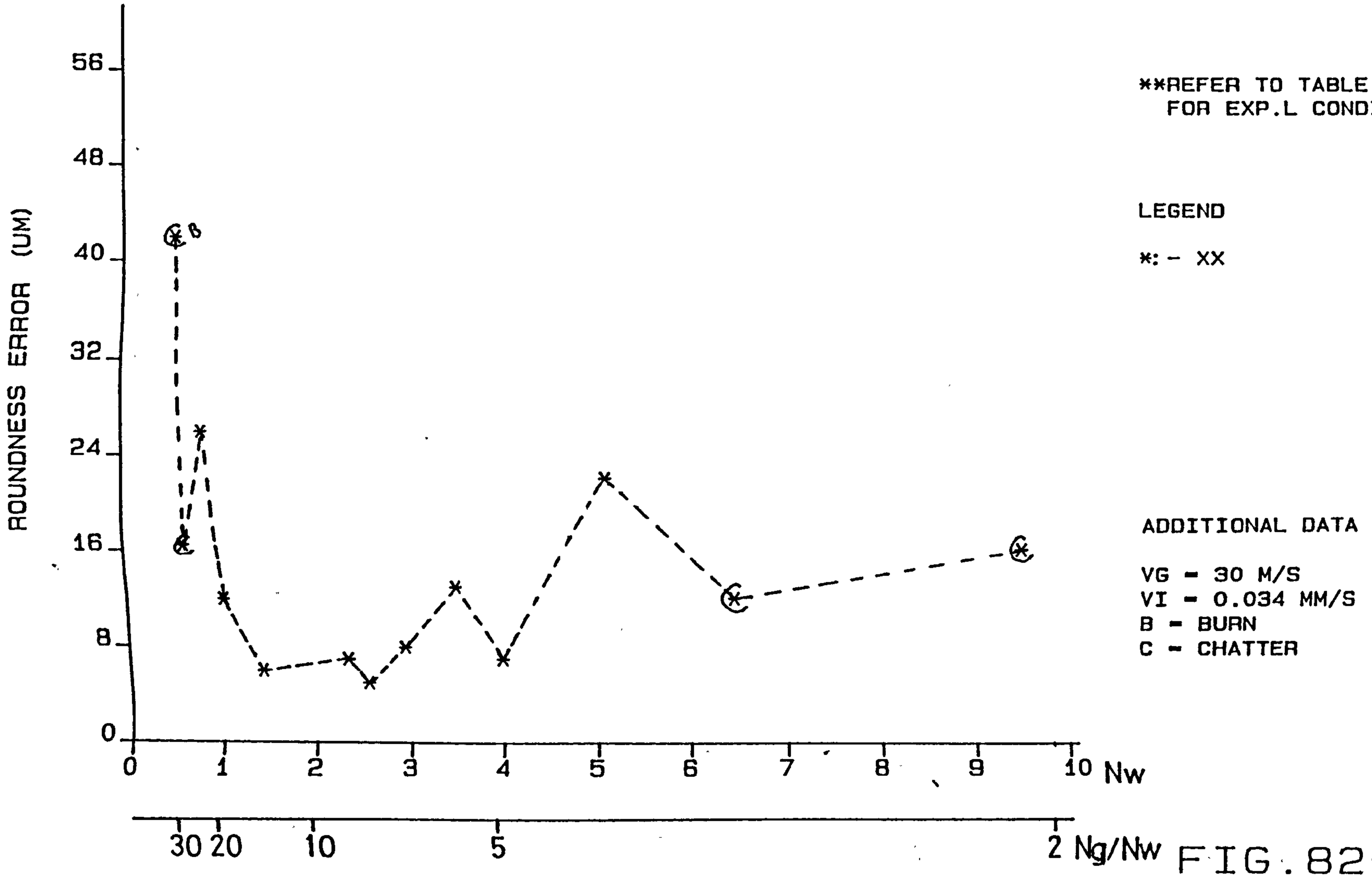

**REFER TO TABLE(S) CI SERIES
FOR EXP.L CONDITIONS.

LEGEND

*:- XX

ADDITIONAL DATA

VG = 30 M/S
VI = 0.034 MM/S
B = BURN
C = CHATTER

FIG. 82

ROUNDNESS ERROR VS WORKPIECE SPEED

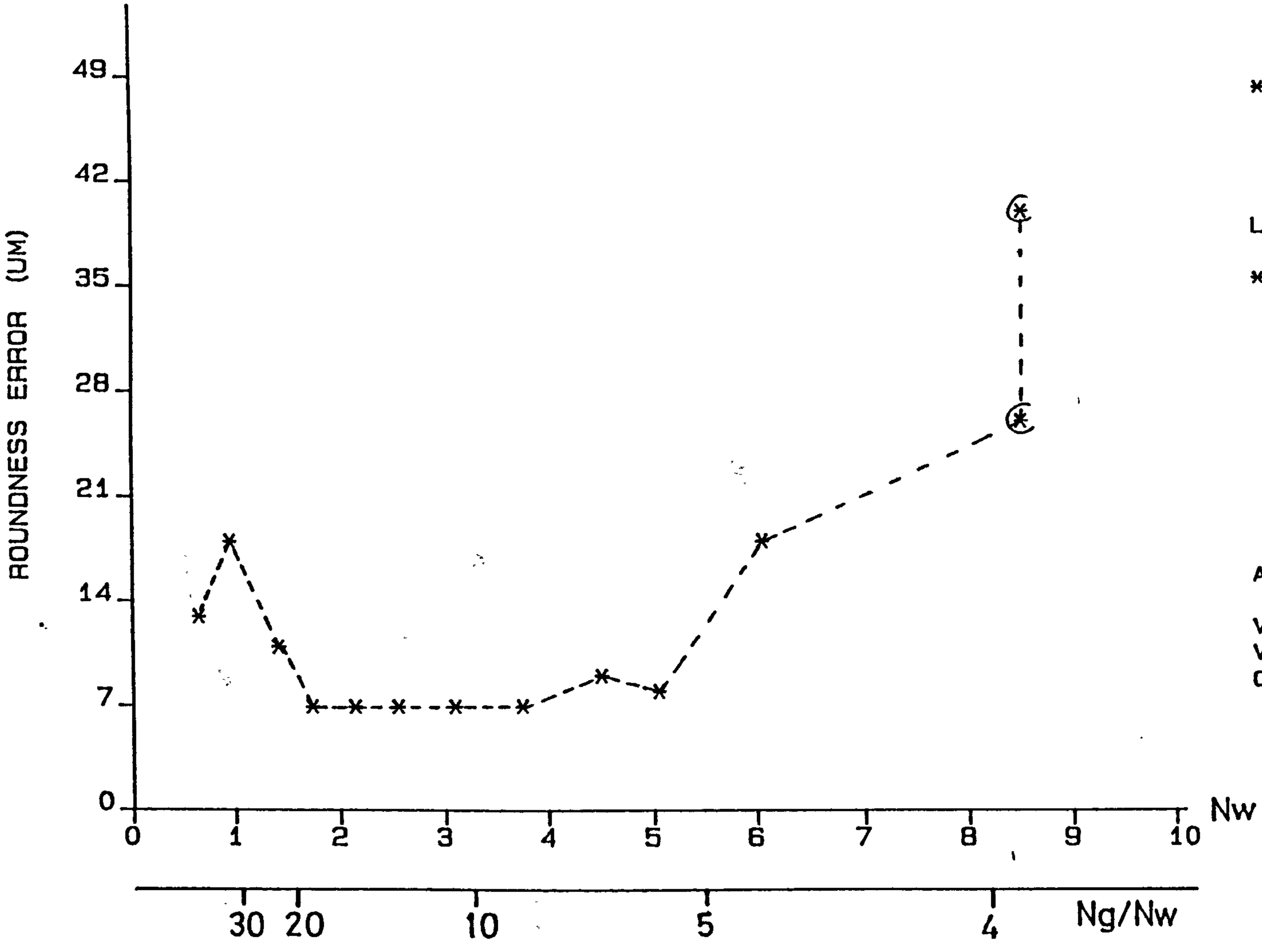

**REFER TO TABLE(S) CI SERIES FOR EXP.L CONDITIONS.

LEGEND

*: - XX

ADDITIONAL DATA

VG = 50 M/S
VI = 0.088 MM/S
C = CHATTER

FIG.83

ROUNDNESS ERROR VS WORKPIECE SPEED

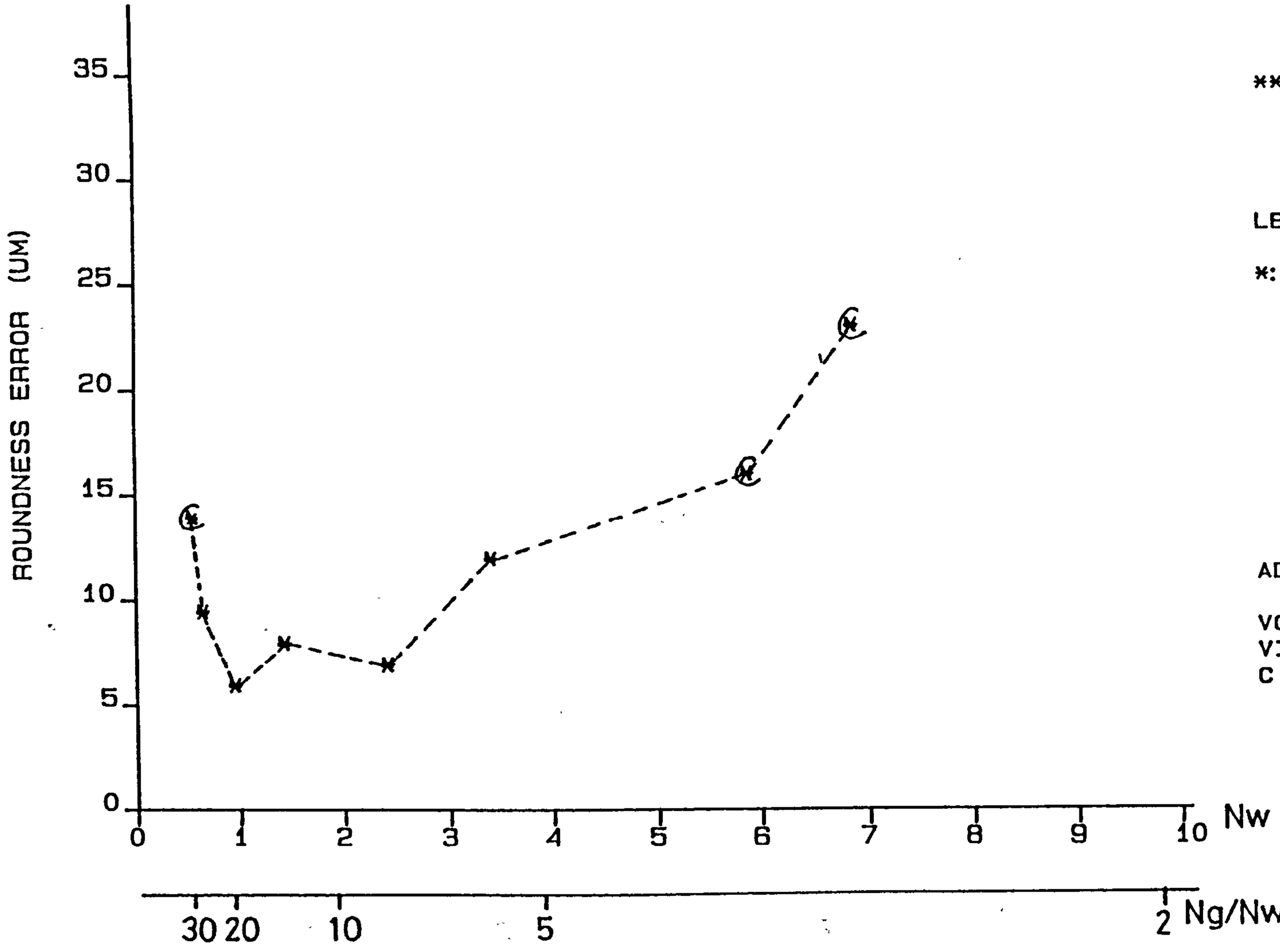

**REFER TO TABLE(S) EN 8 SERIES
FOR EXP.L CONDITIONS.

LEGEND

*:- XX

ADDITIONAL DATA

VG = 30 M/S
VI = 0.053 MM/S
C = CHATTER

FIG.84

ROUNDNESS ERROR VS WORKPIECE SPEED

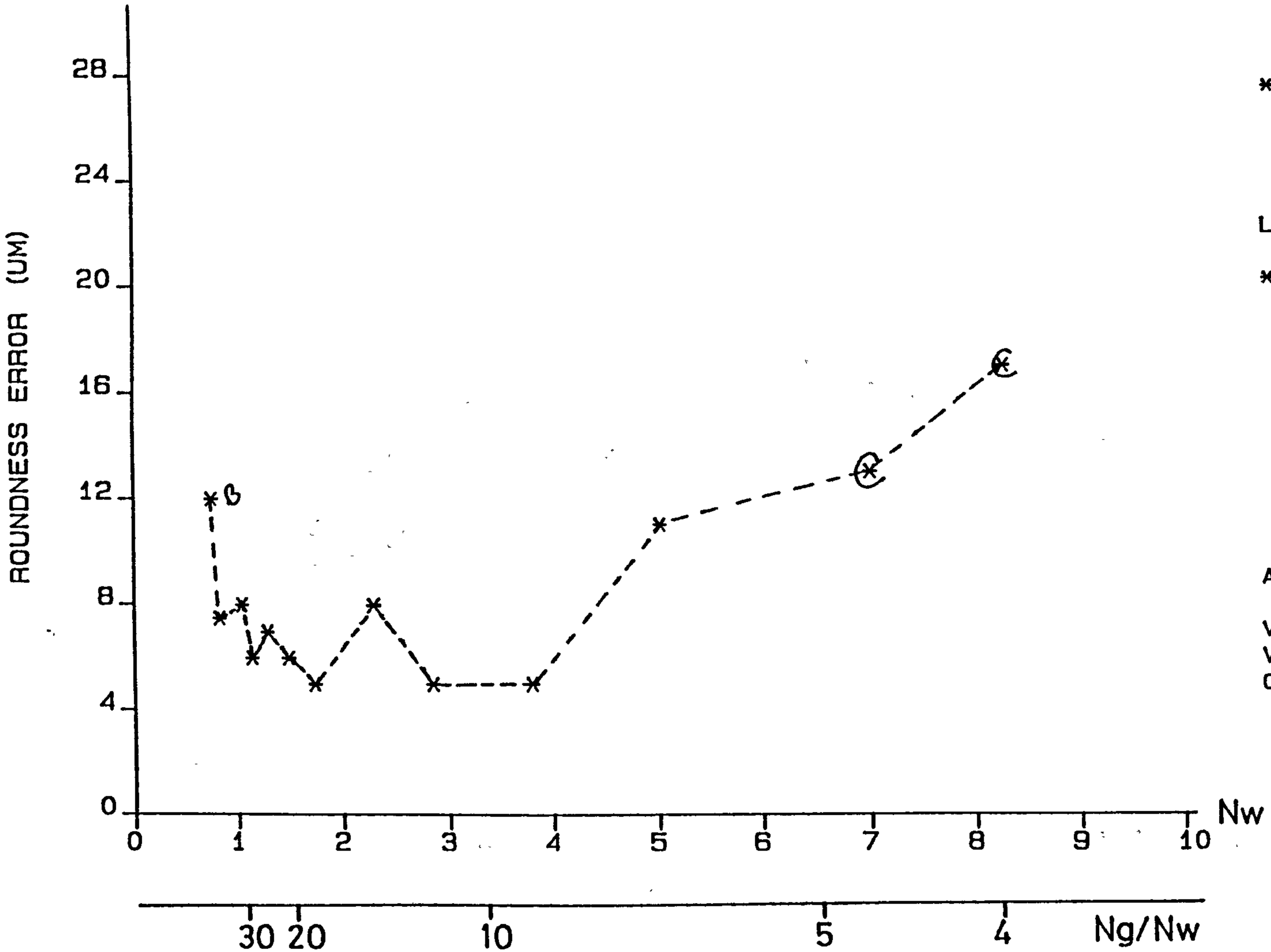

**REFER TO TABLE(S) EN 9 SERIES FOR EXP.L CONDITIONS.

LEGEND

*: - XX

ADDITIONAL DATA

VG = 51 M/S
VI = 0.086 MM/S
C = CHATTER

FIG. 85

GRINDING RATIO VS STOCK REMOVED

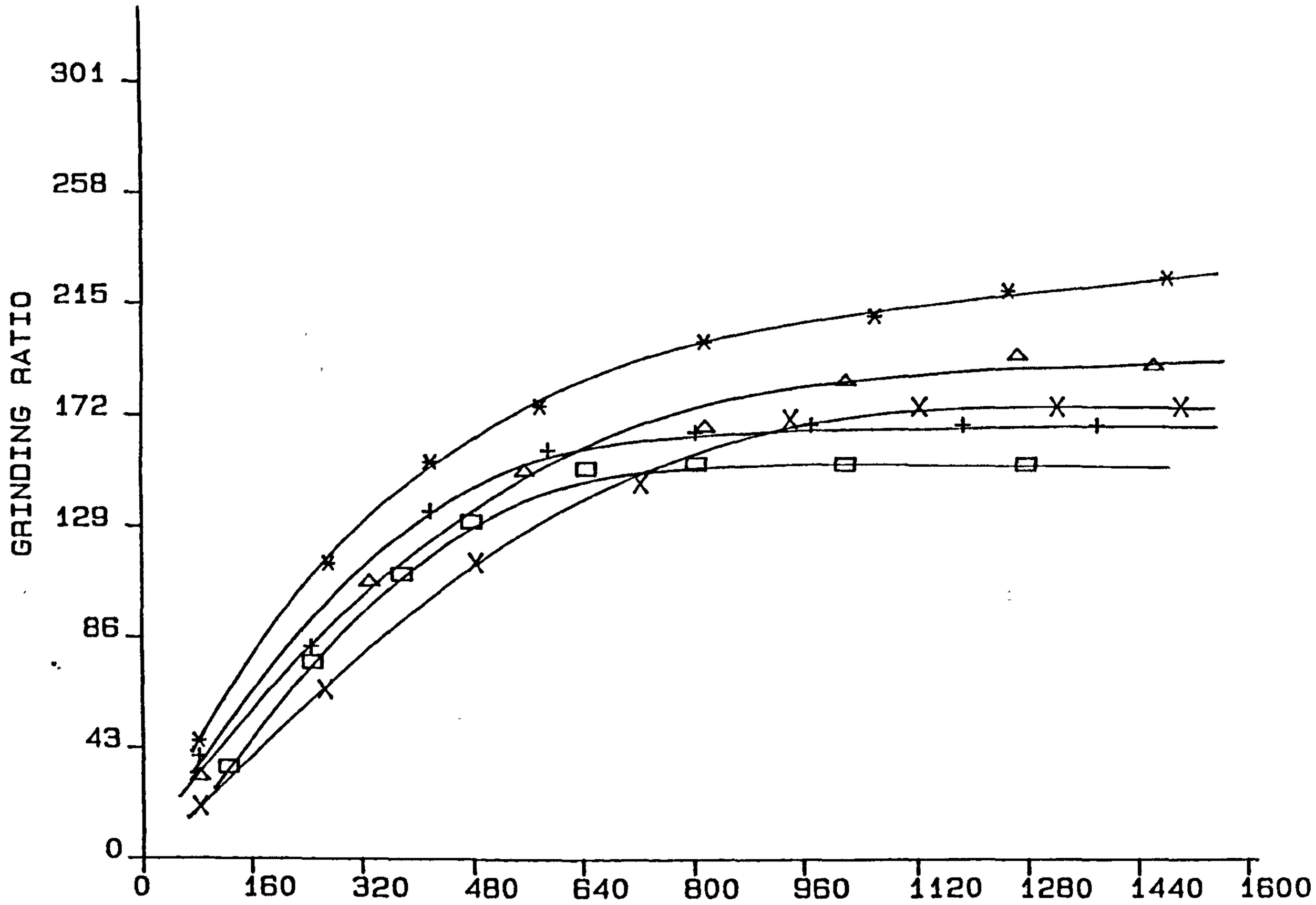

**REFER TO TABLE(S) CI AND EN 9 FOR EXP.L CONDITIONS.

EN 9 STEEL

*-VG=60 M/S, VI=0.086 MM/S
△-VG=40 M/S, VI=0.086 MM/S
×-VG=40 M/S, VI= 0.176MM/S

CAST IRON

+-VG=60M/S, VI=0086MM/S
□-VG=40M/S, VI=0.086MM/S

ADDITIONAL DATA

Q-RATIO = 100

FIG.86

INFEED-RATE VS WORKPIECE SPEED

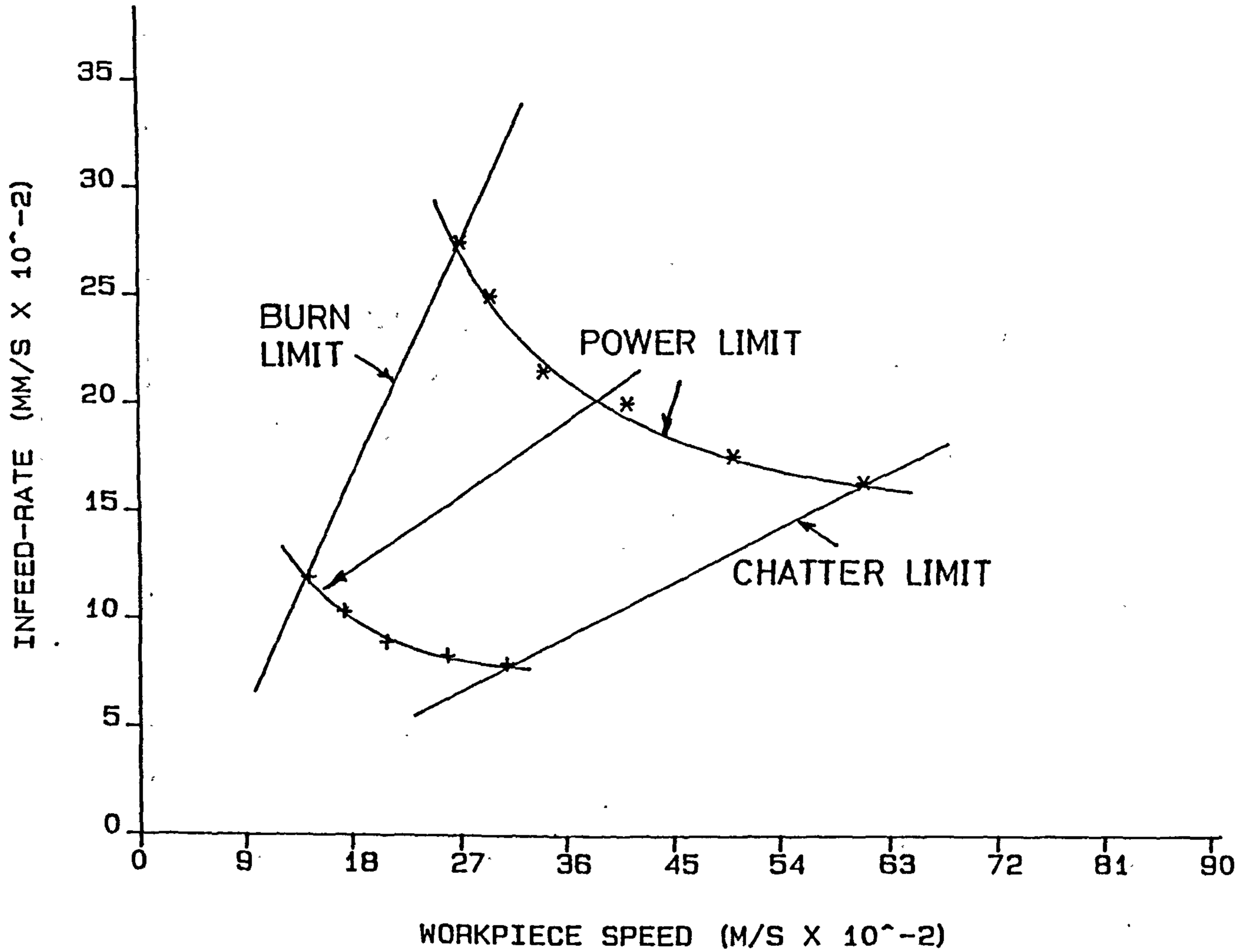

**REFER TO TABLE(S) EN 9 SERIES FOR EXP.L CONDITIONS.

LEGEND

*:- VG = 60 M/S
+:- VG = 30 M/S

ADDITIONAL DATA

WHEEL - WA60MVRC
MATERIAL - EN 9 STEEL

FIG.87

INFEED-RATE VS WORKPIECE SPEED

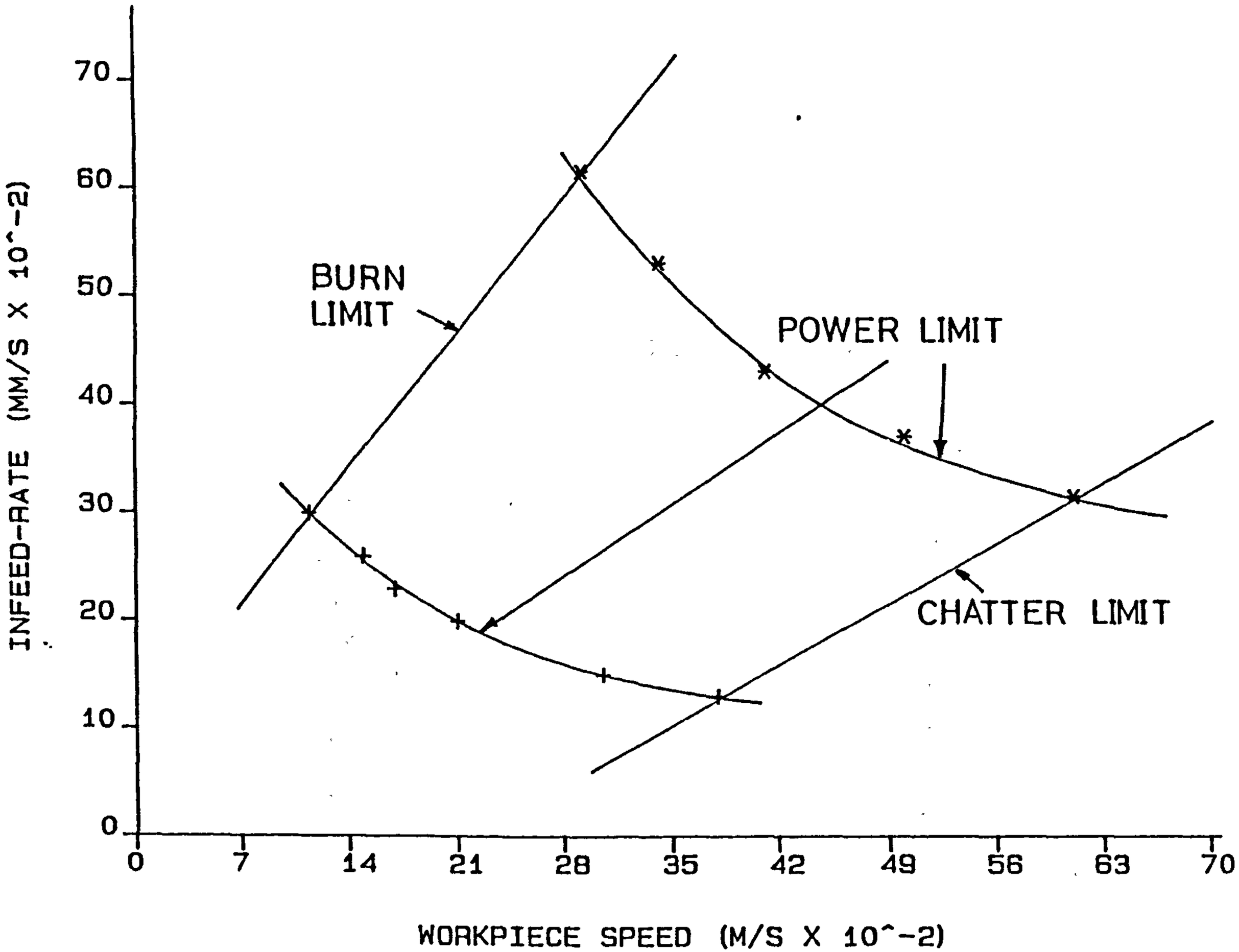

**REFER TO TABLE(S) CI SERIES FOR EXP.L CONDITIONS.

LEGEND

*: - VG = 60 M/S
+: - VG = 30 M/S

ADDITIONAL DATA

WHEEL - C46 BBT
MATERIAL - CAST IRON

FIG.88

INFEED-RATE VS Q-RATIO

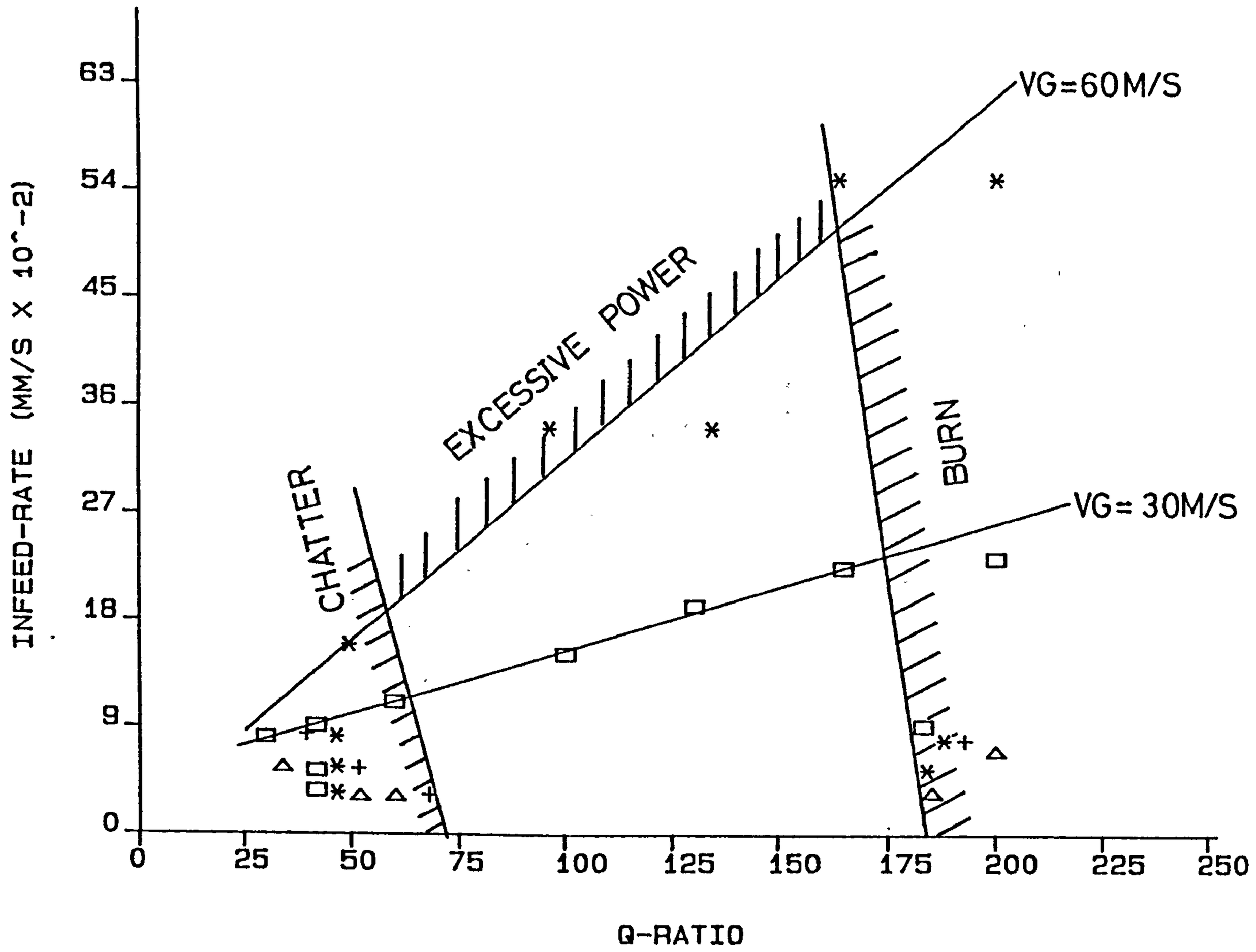

**REFER TO TABLE(S) CI SERIES FOR EXP.L CONDITIONS.

LEGEND

*:- VG = 60 M/S
+:- VG = 50 M/S
△:- VG = 40 M/S
□:- VG = 30 M/S

ADDITIONAL DATA

WHEEL - C46 BBT
MATERIAL - CAST IRON

FIG.89

INFEED-RATE VS Q-RATIO

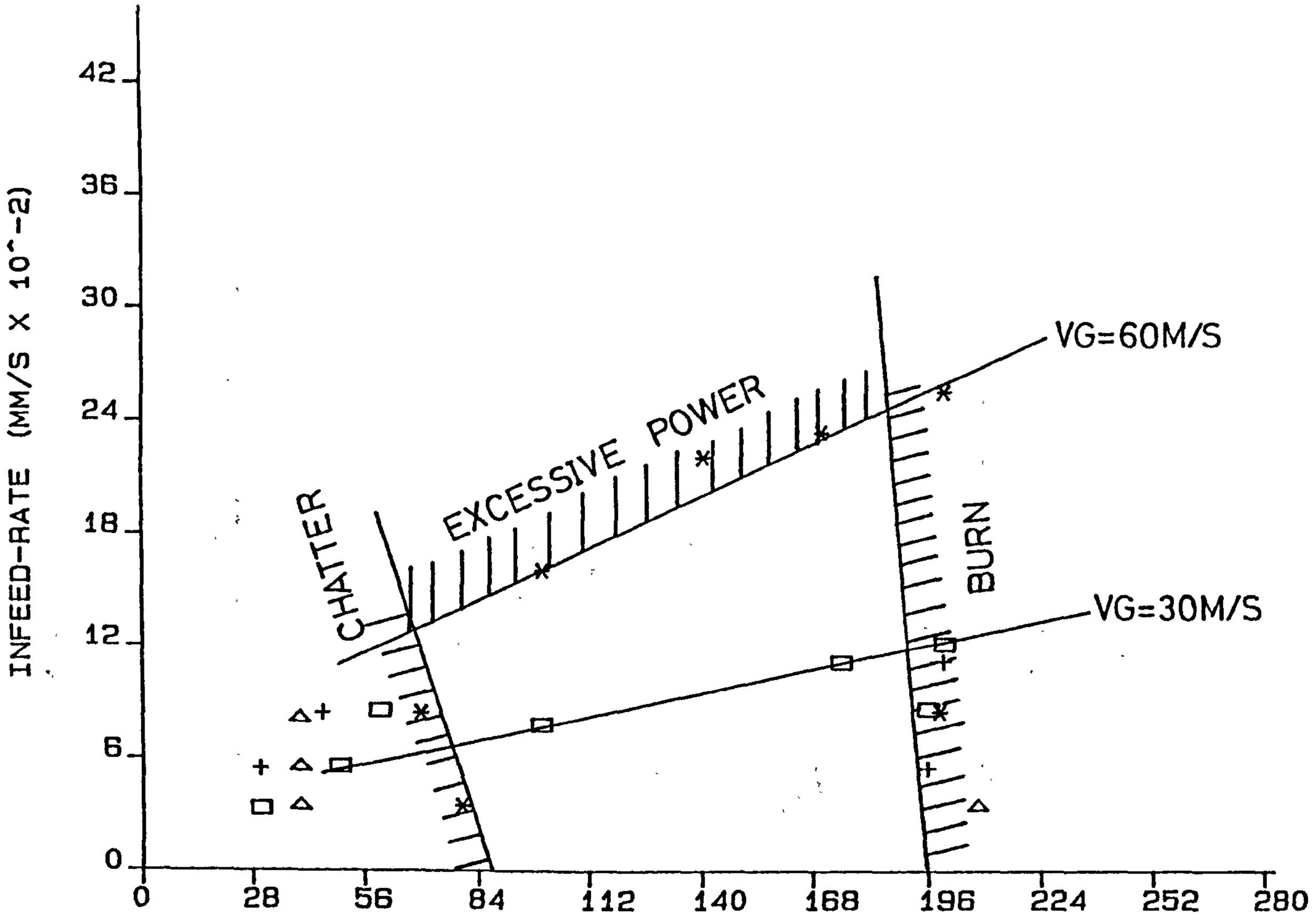

**REFER TO TABLE(S) EN 9 SERIES FOR EXP.L CONDITIONS.

LEGEND

*: - VG = 60 M/S
+: - VG = 50 M/S
△: - VG = 40 M/S
□: - VG = 30 M/S

ADDITIONAL DATA

WHEEL - WA60MVRC
MATERIAL - EN 9 STEEL

FIG.90

Q-RATIO VS GRINDING WHEEL SPEED

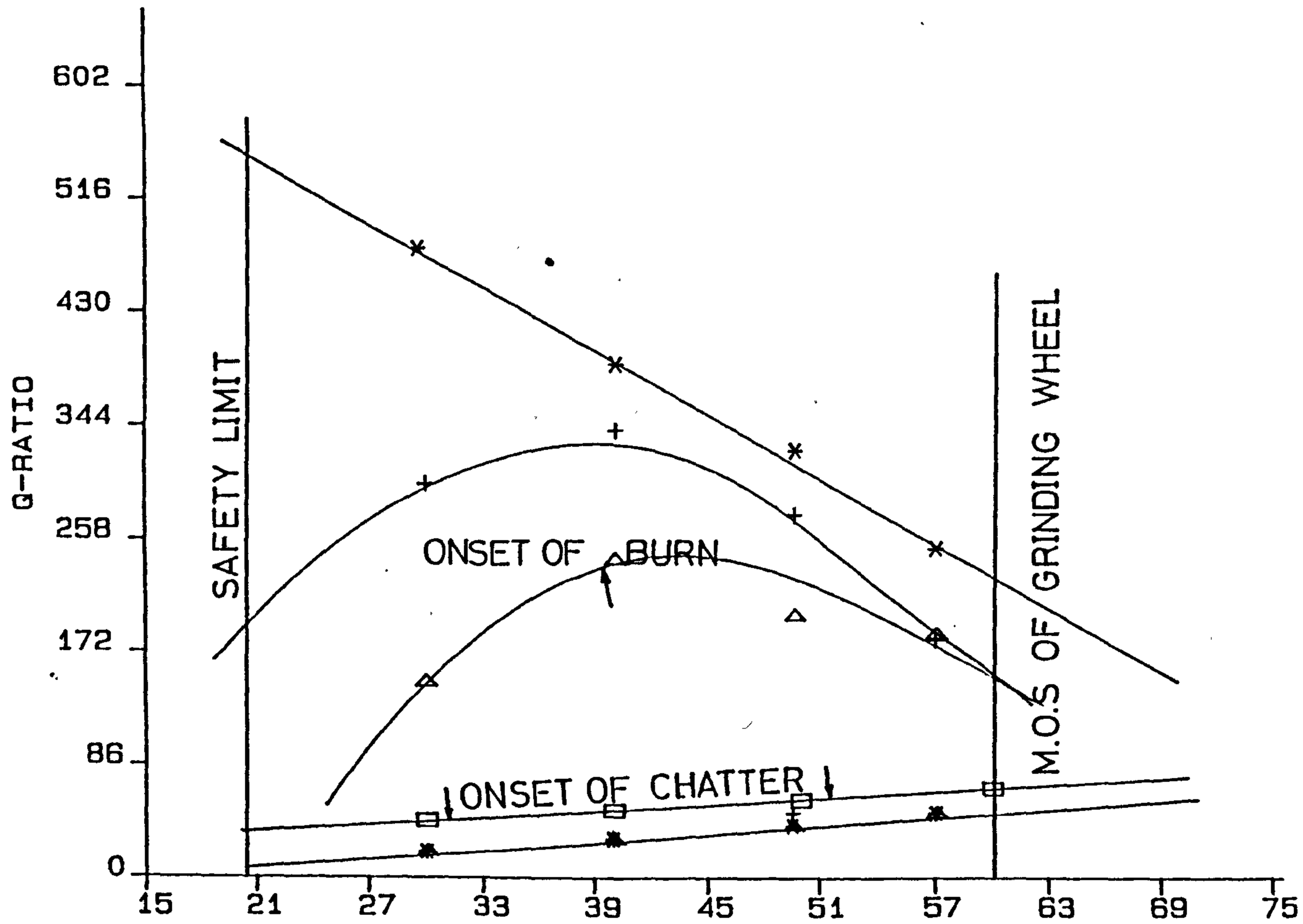

**REFER TO TABLE(S) CI SERIES FOR EXP.L CONDITIONS.

LEGEND

*:- VI = 0.033 MM/S
+:- VI = 0.058 MM/S
△:- VI = 0.088 MM/S
□:- ONSET OF CHATTER

ADDITIONAL DATA

WHEEL - C48 BBT
MATERIAL - CAST IRON

FIG.91

Q-RATIO VS GRINDING WHEEL SPEED

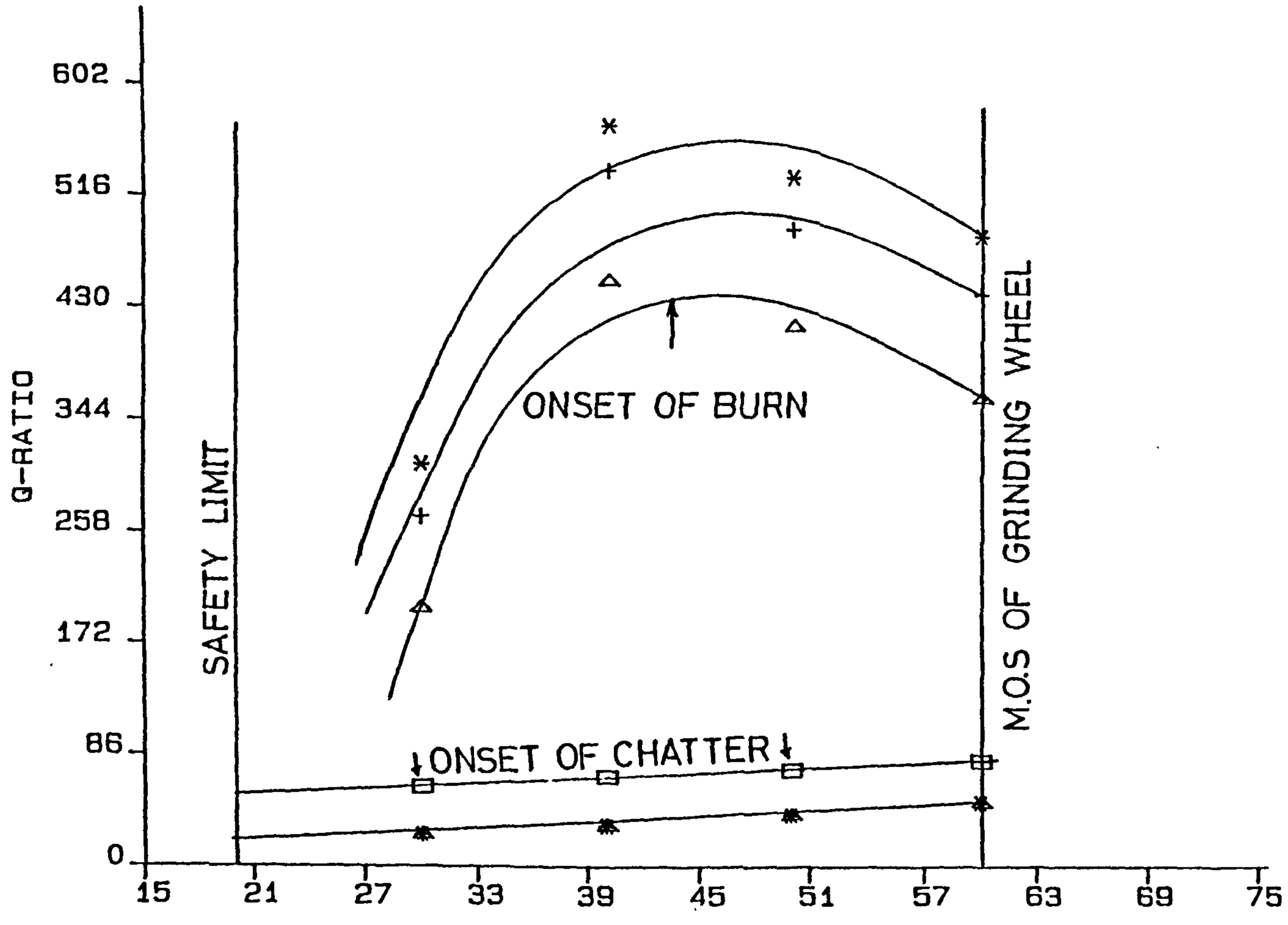

**REFER TO TABLE(S) EN 9 SERIES FOR EXP.L CONDITIONS.

LEGEND

*:- VI = 0.033 MM/S
+:- VI = 0.054 MM/S
△:- VI = 0.086 MM/S
□:- ONSET OF CHATTER

ADDITIONAL DATA

WHEEL - WA60MVRC
MATERIAL - EN 9

FIG.92

PLATES

PLATE 1. HIGH VELOCITY COOLANT STREAM ISSUING FROM THE MANIFOLD COOLANT APPLICATOR.

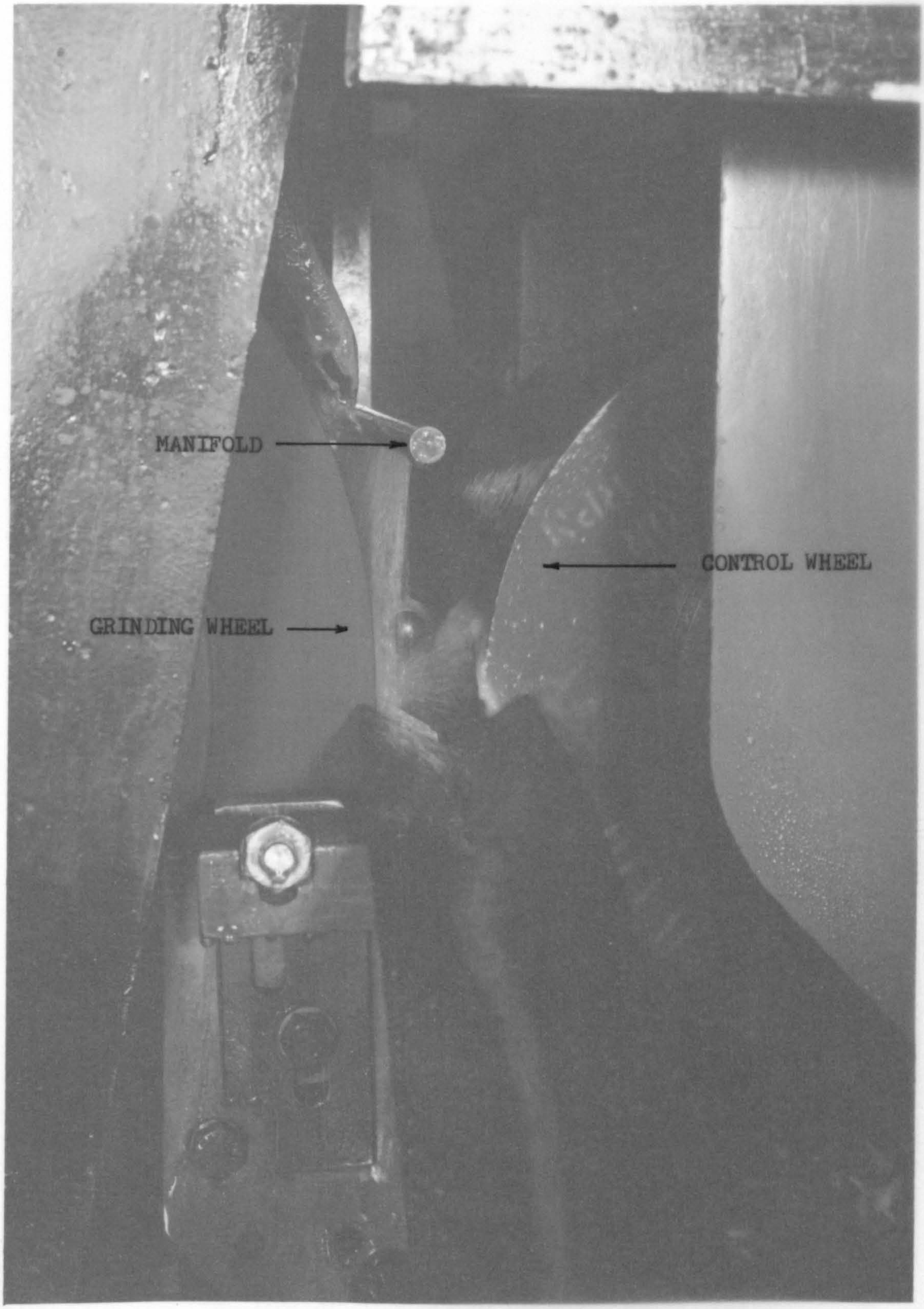

PLATE 1. HIGH VELOCITY COOLANT STREAM ISSUING FROM THE MANIFOLD COOLANT APPLICATOR.

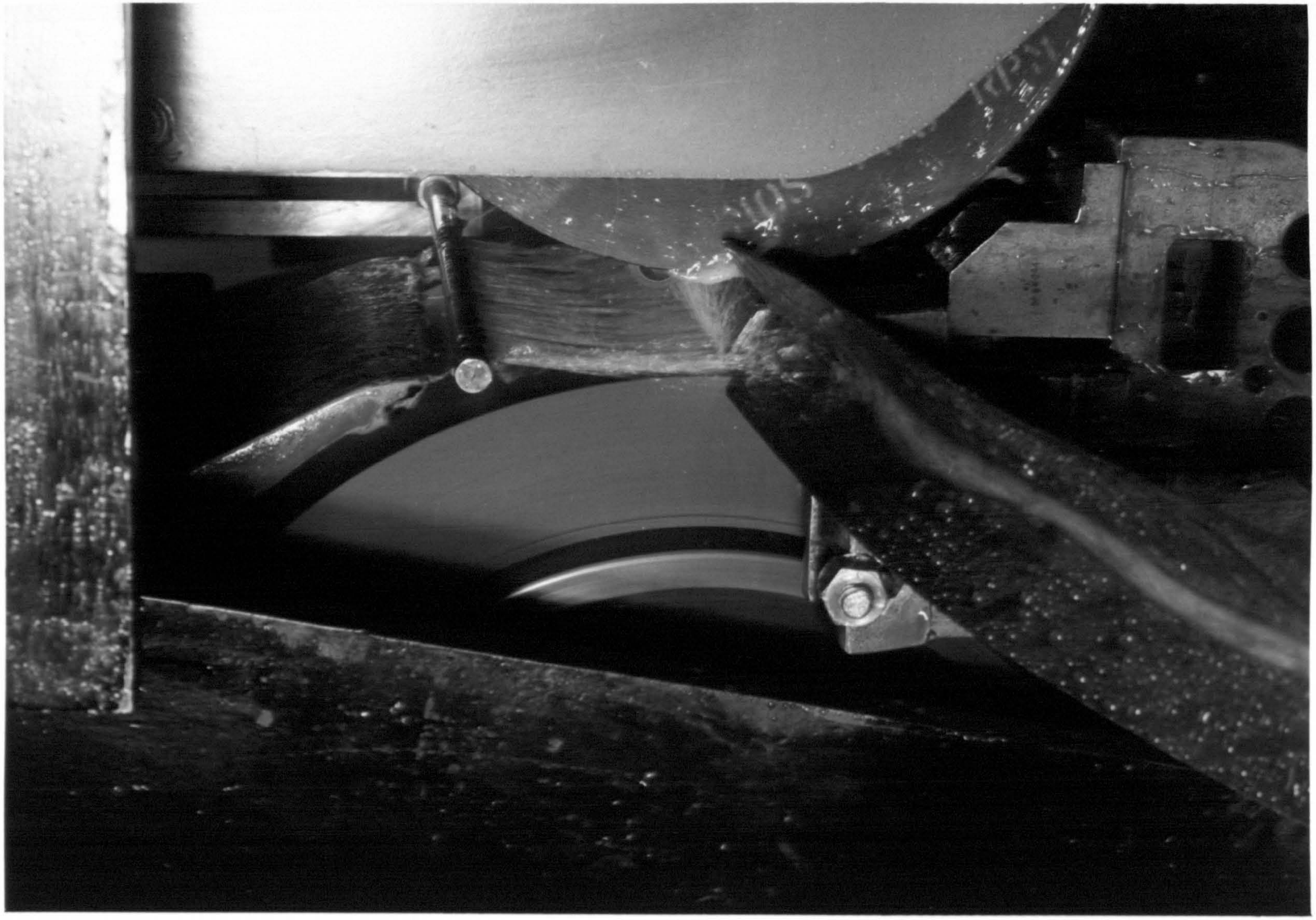

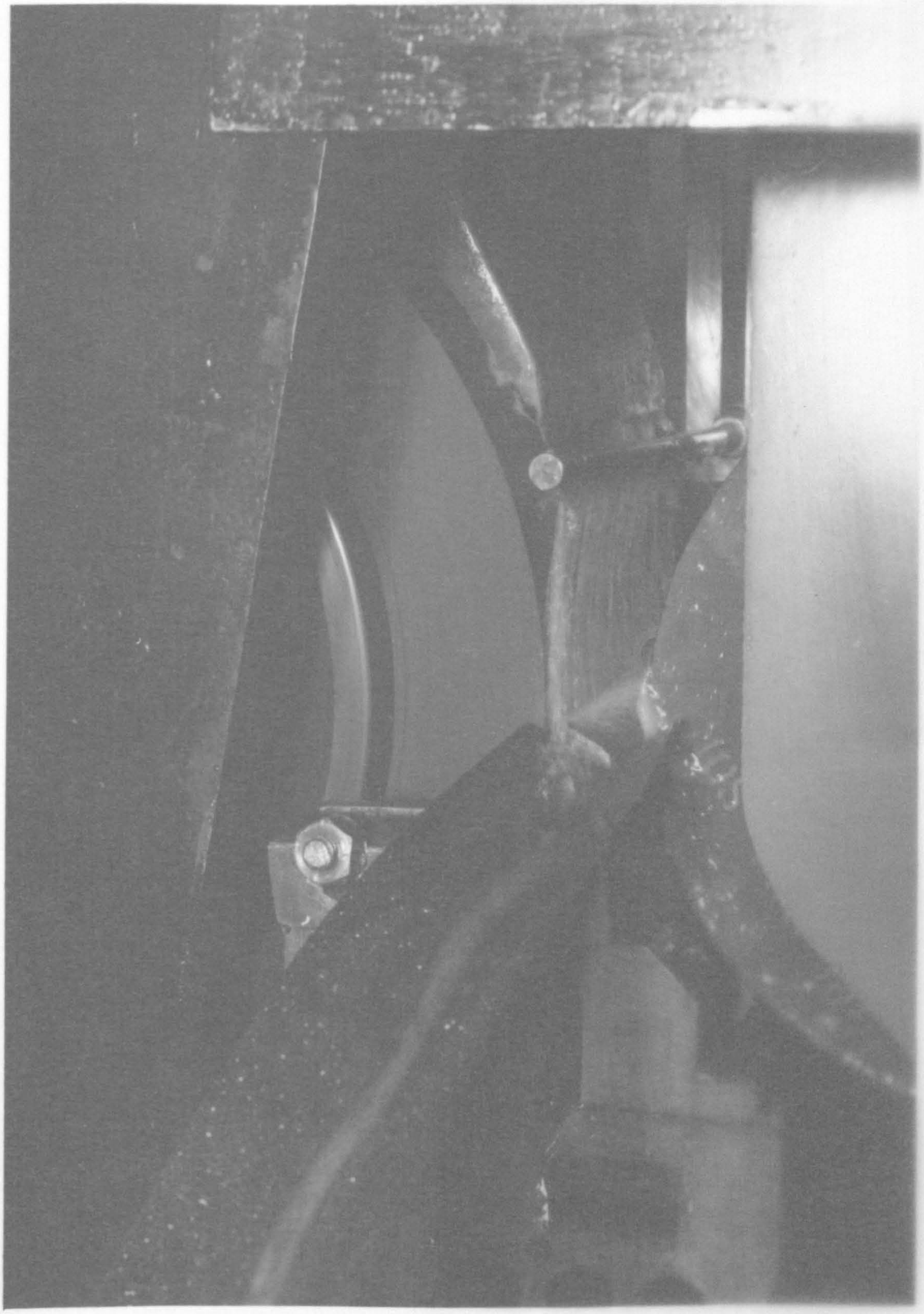

PLATE 2. MANIFOLD DELIVERING A UNIFORM SHEET OF COOLANT ACROSS A WIDE GRINDING WHEEL FACE WIDTH.

PLATE 3. THE MODIFIED CENTRELESS GRINDING MACHINE.

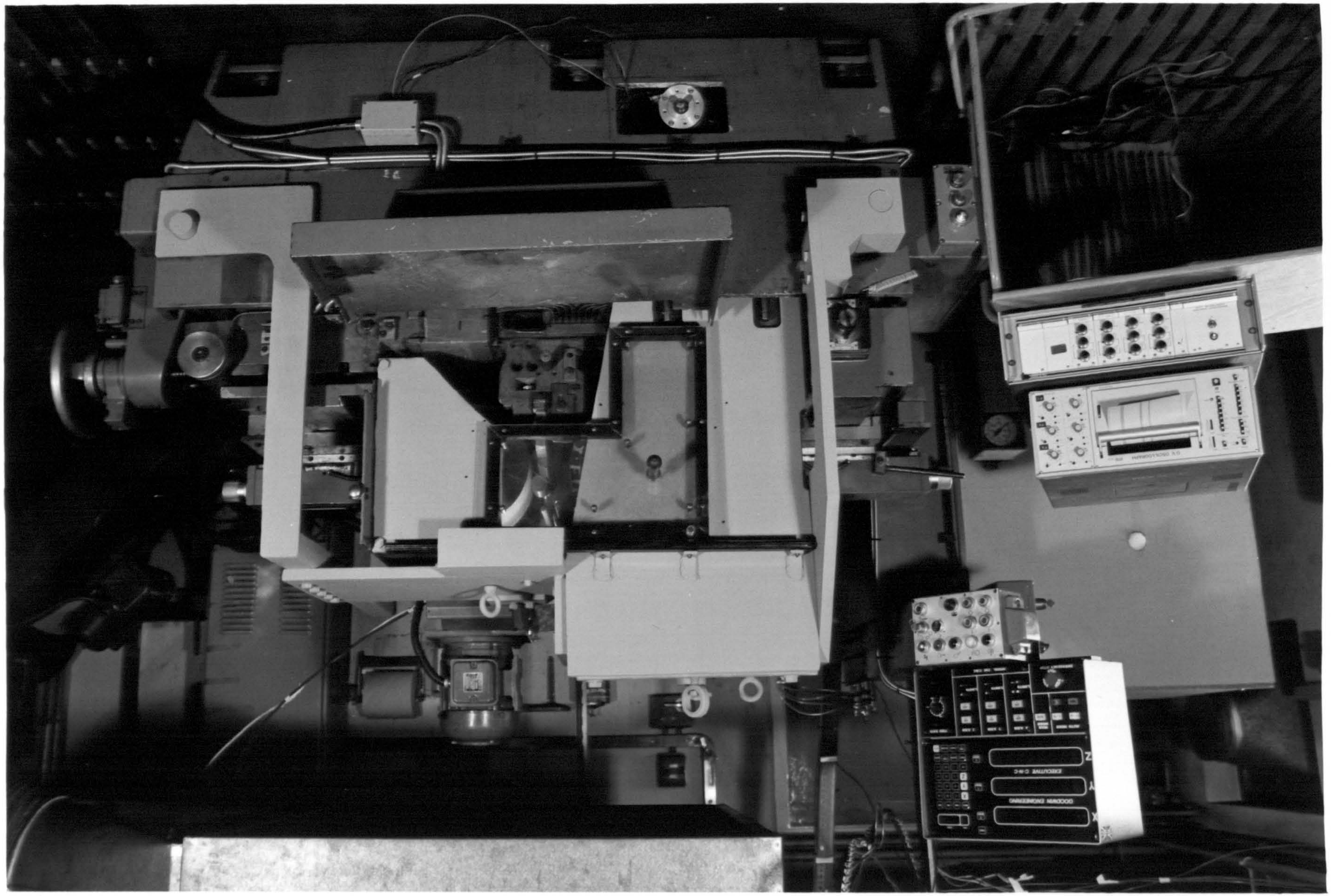

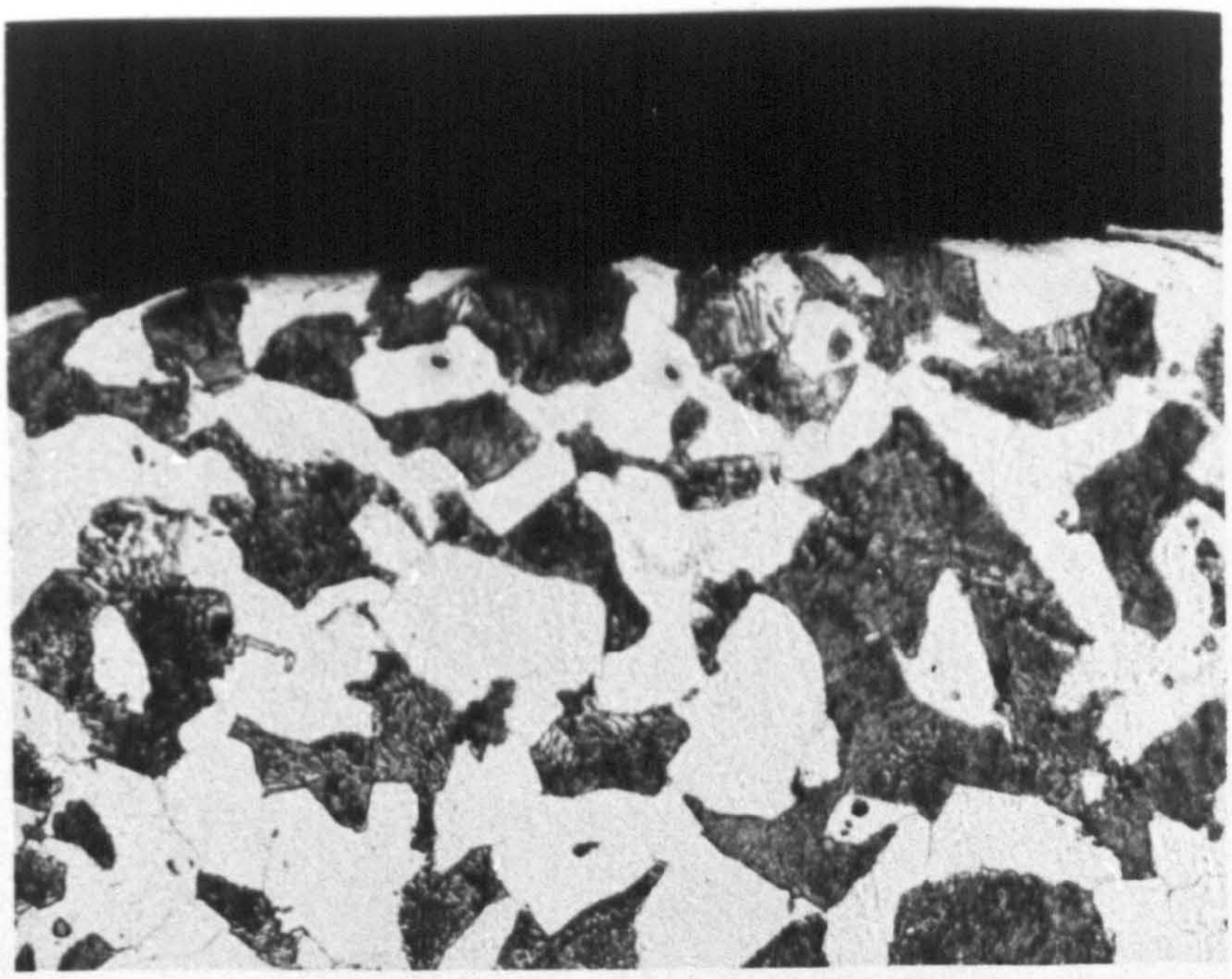

Plate 4. Microstructure at Ground Edge for En9 Steel with 4 Seconds Spark-out.

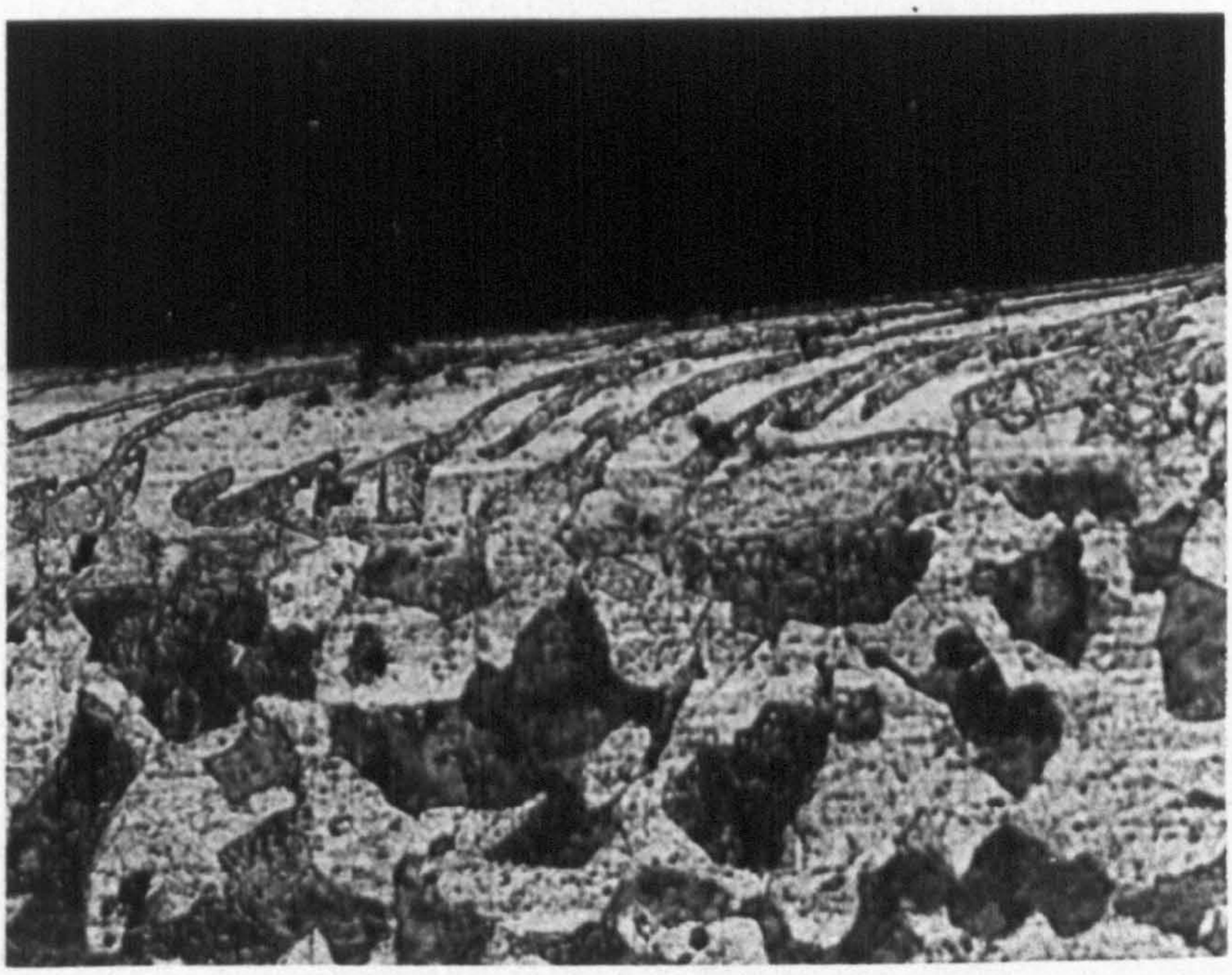

Plate 5. Microstructure of En9 Steel Showing Deformation Layer at Ground Edge - No Spark-out.

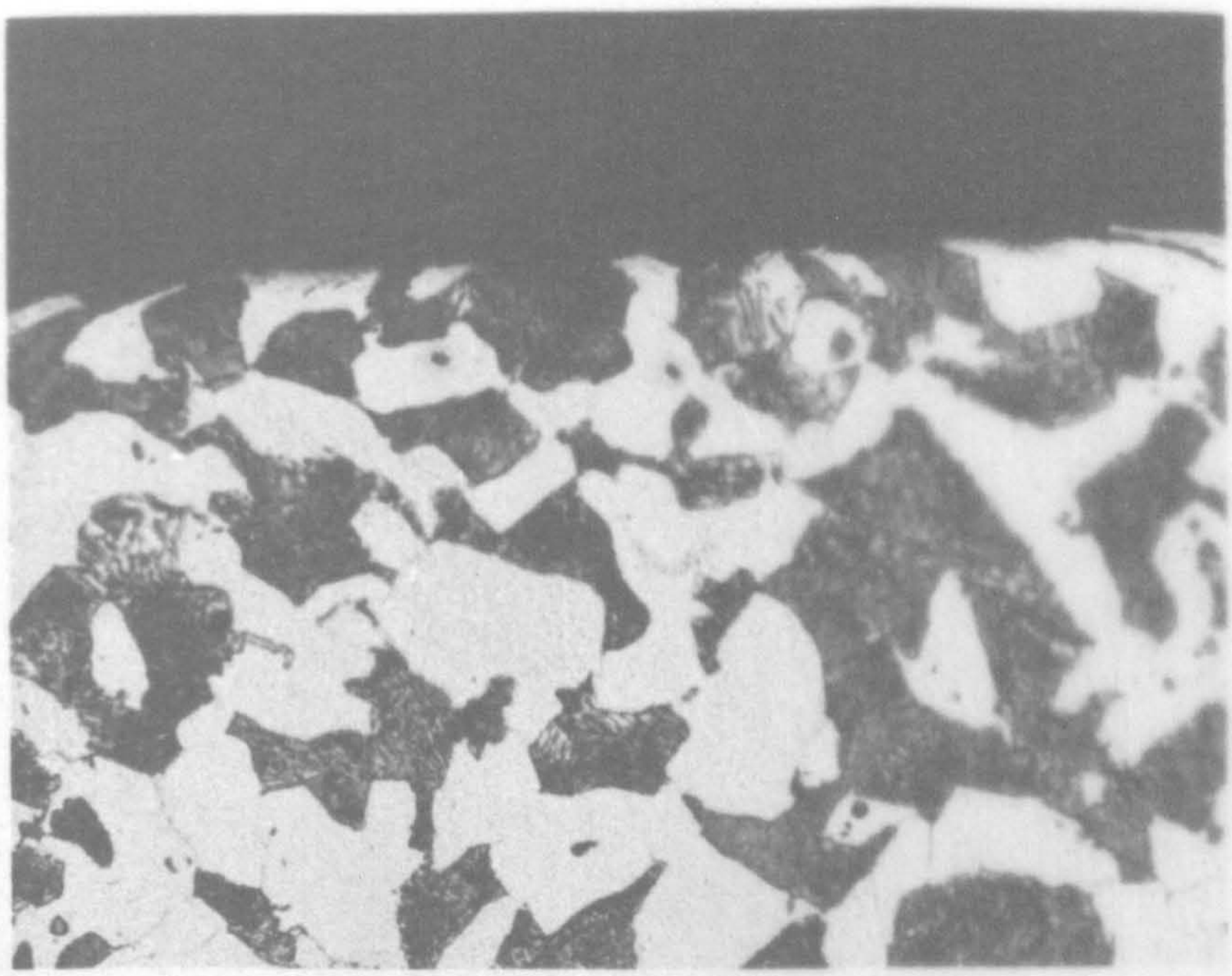

Plate 4. Microstructure at Ground Edge for En9 Steel with 4 Seconds Spark-out.

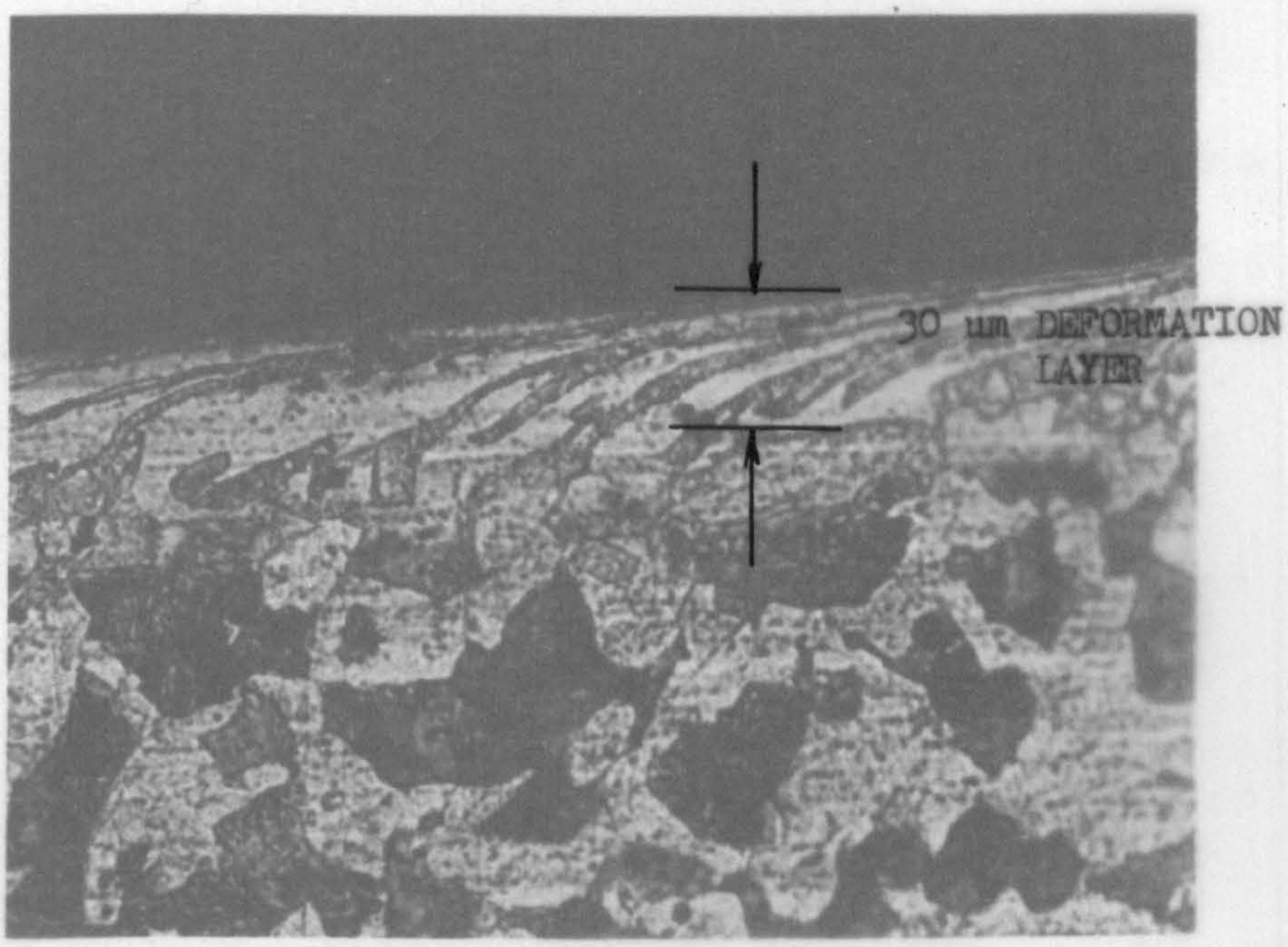

Plate 5. Microstructure of En9 Steel Showing Deformation Layer at Ground Edge - No Spark-out.

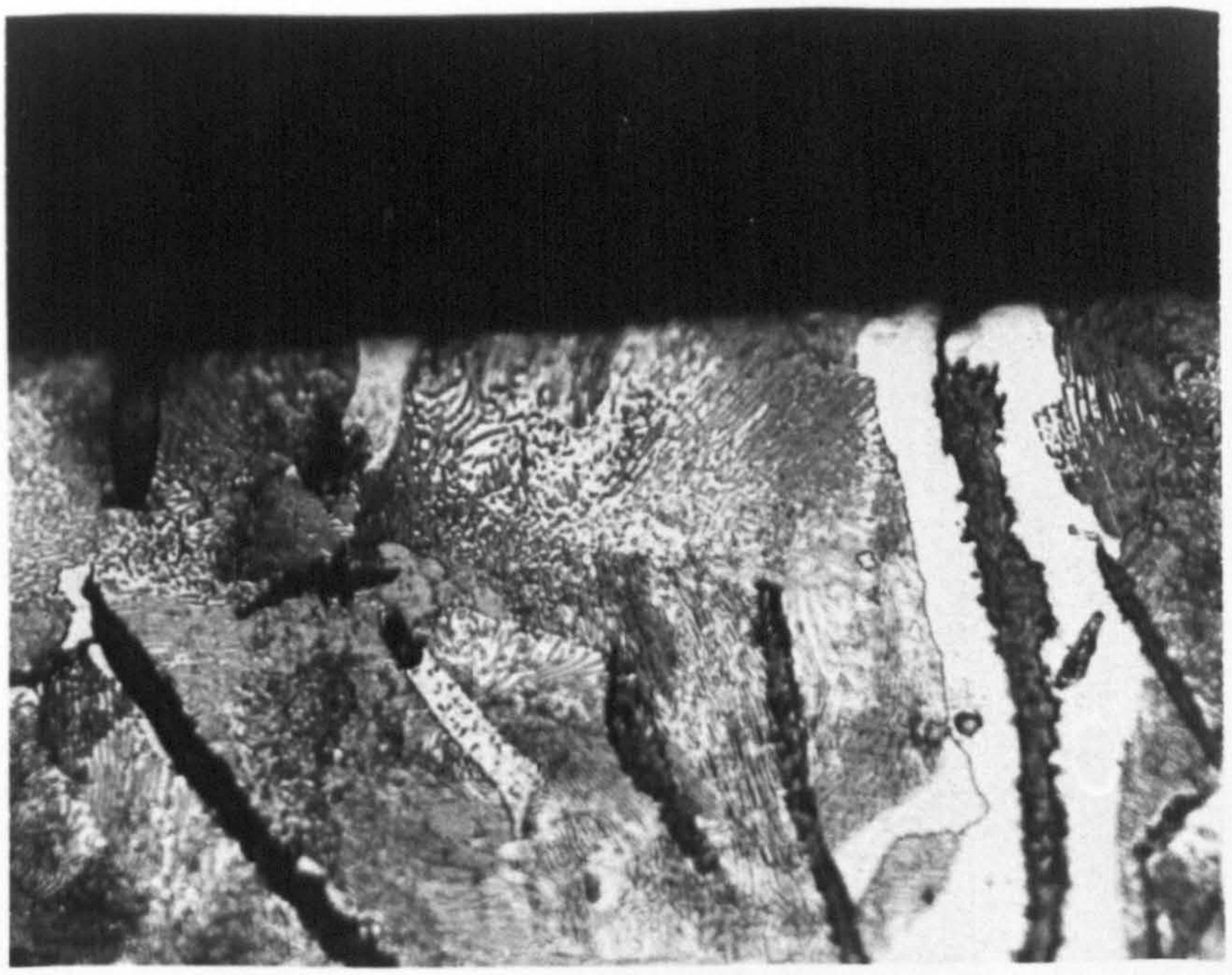

Plate 6. Microstructure of C.I. at Ground Edge with 4 Seconds Spark-out.

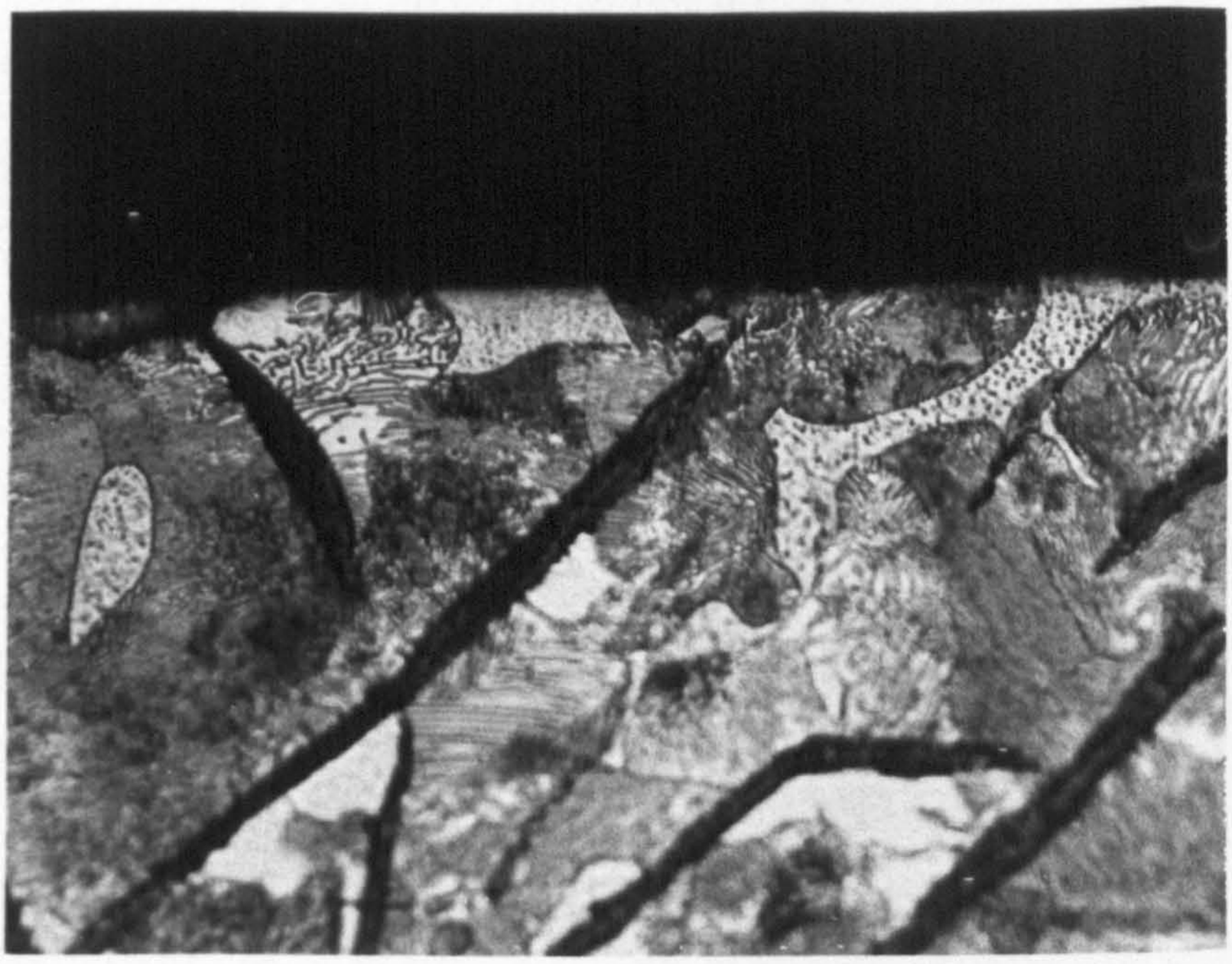

Plate 7. Microstructure of C.I. at Ground Edge without Spark-out - No Deformation Layer.

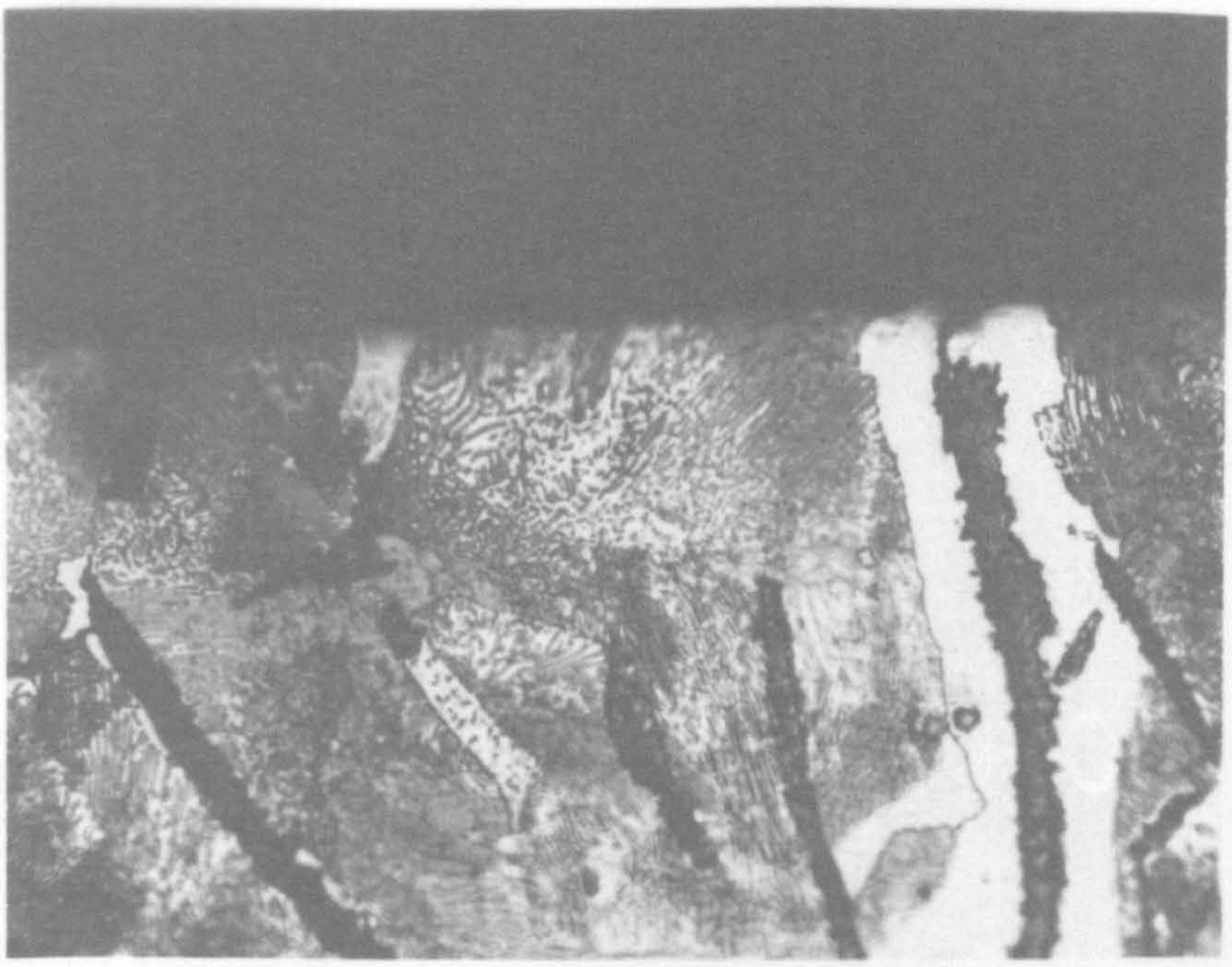

Plate 6. Microstructure of C.I. at Ground Edge with 4 Seconds Spark-out.

Plate 7. Microstructure of C.I. at Ground Edge without Spark-out - No Deformation Layer.

PLATE 8. FORCE TRACES FROM U.V. OSCILLOGRAPH FOR THE THREE MATERIALS GROUND EXPERIMENTALLY.

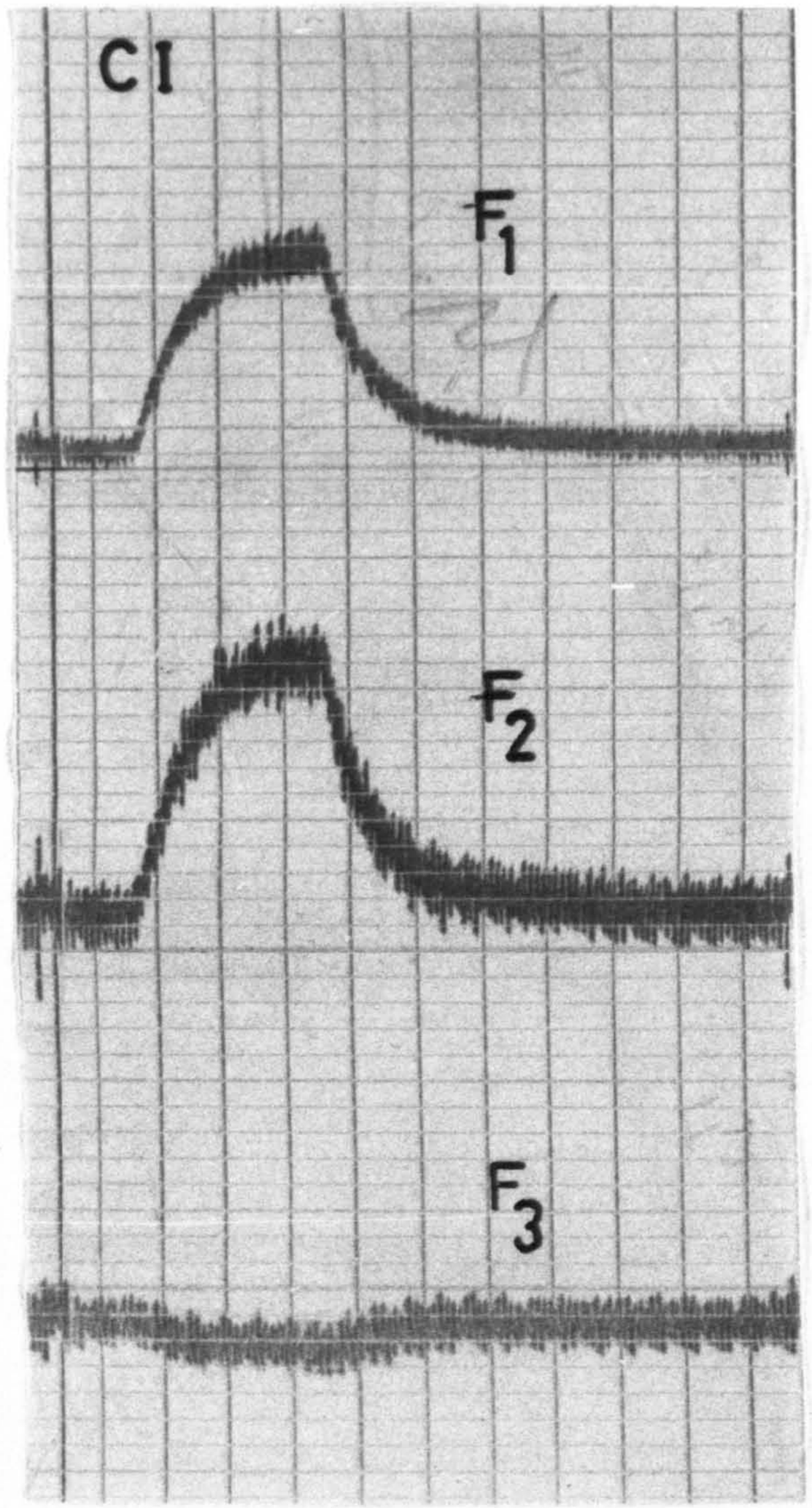
C1
F1
F2
F3

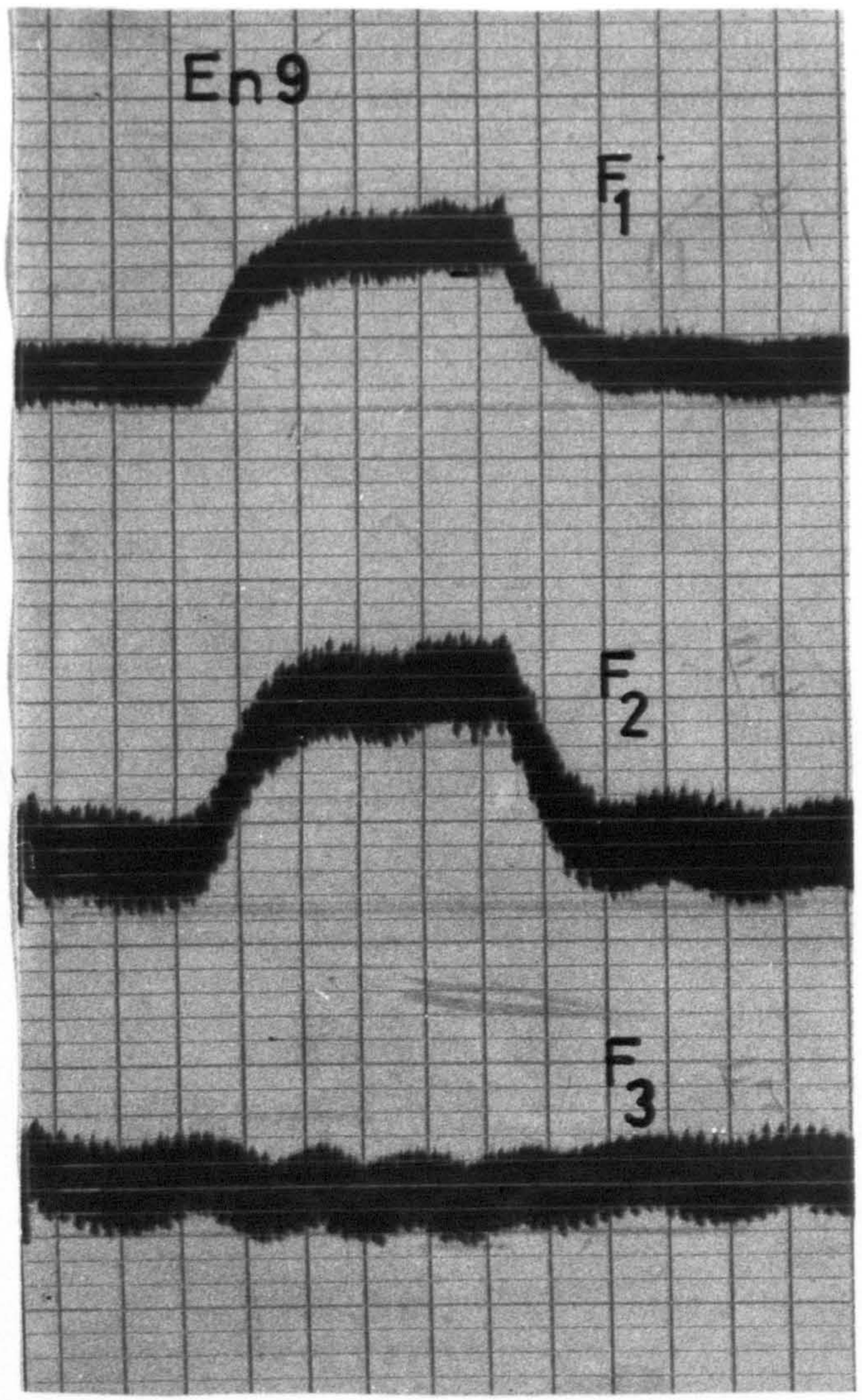
En9
F1
F2
F3

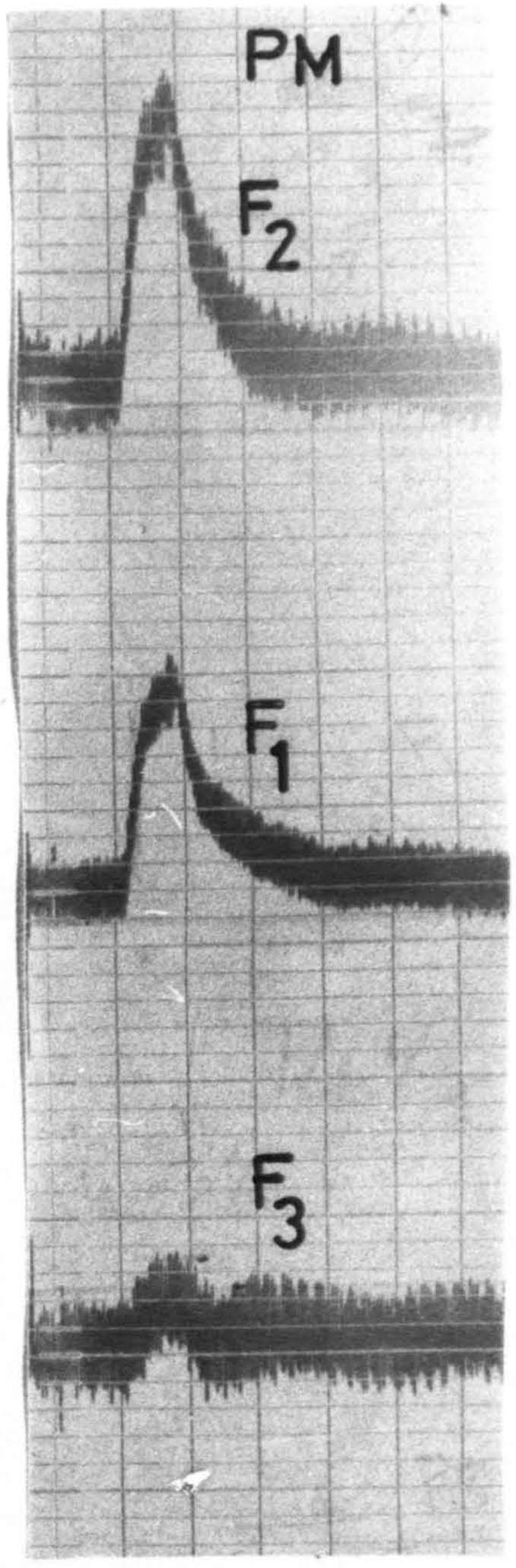
PM
F2
F1
F3

NON-VIOLENT VIBRATION

VIOLENT VIBRATION

PLATE 9. TRACES ILLUSTRATING CHARACTERISTICS OF THE TWO VIBRATION TYPES ENCOUNTERED WHILST GRINDING.

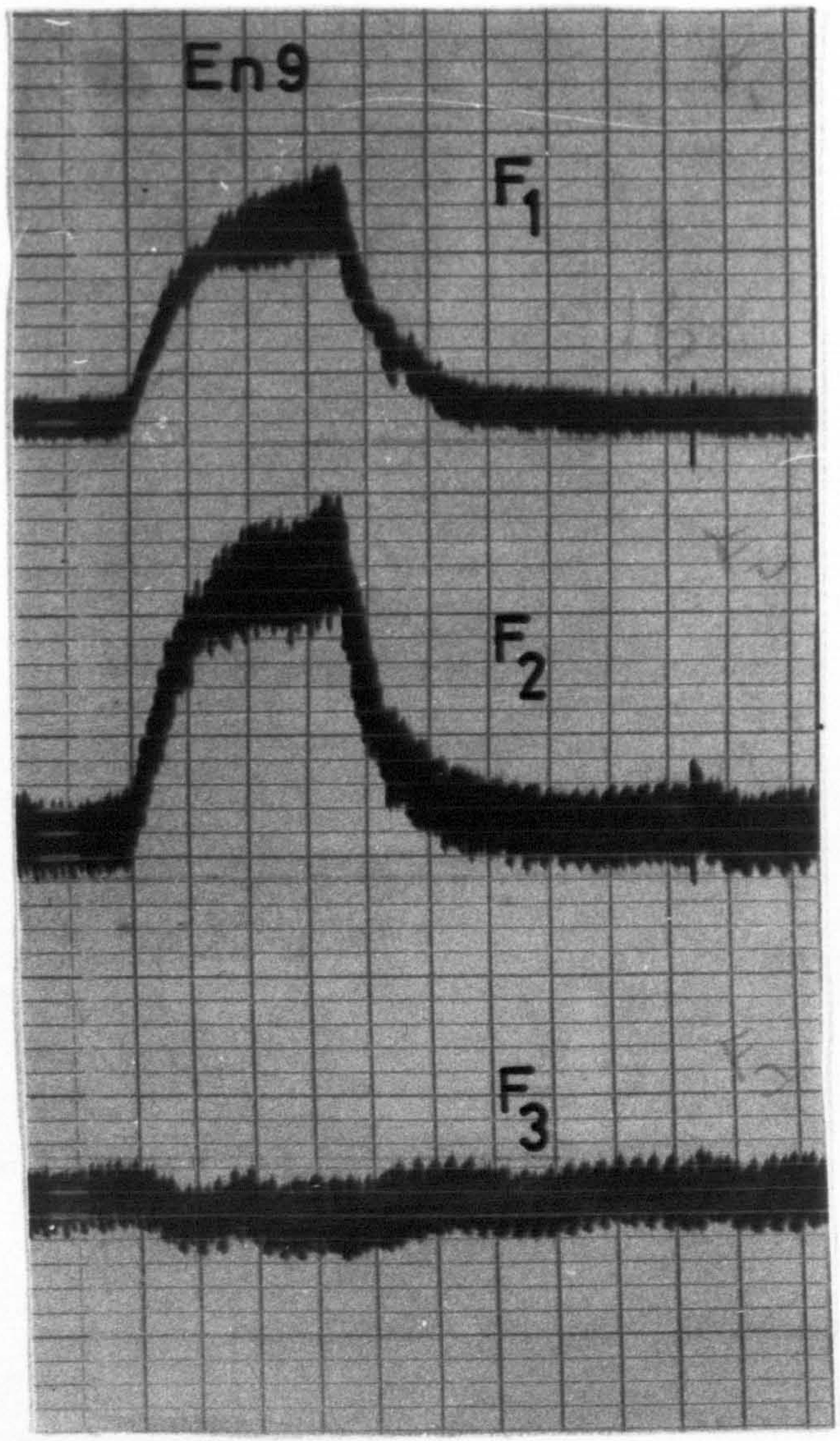
En9
F1
F2
F3

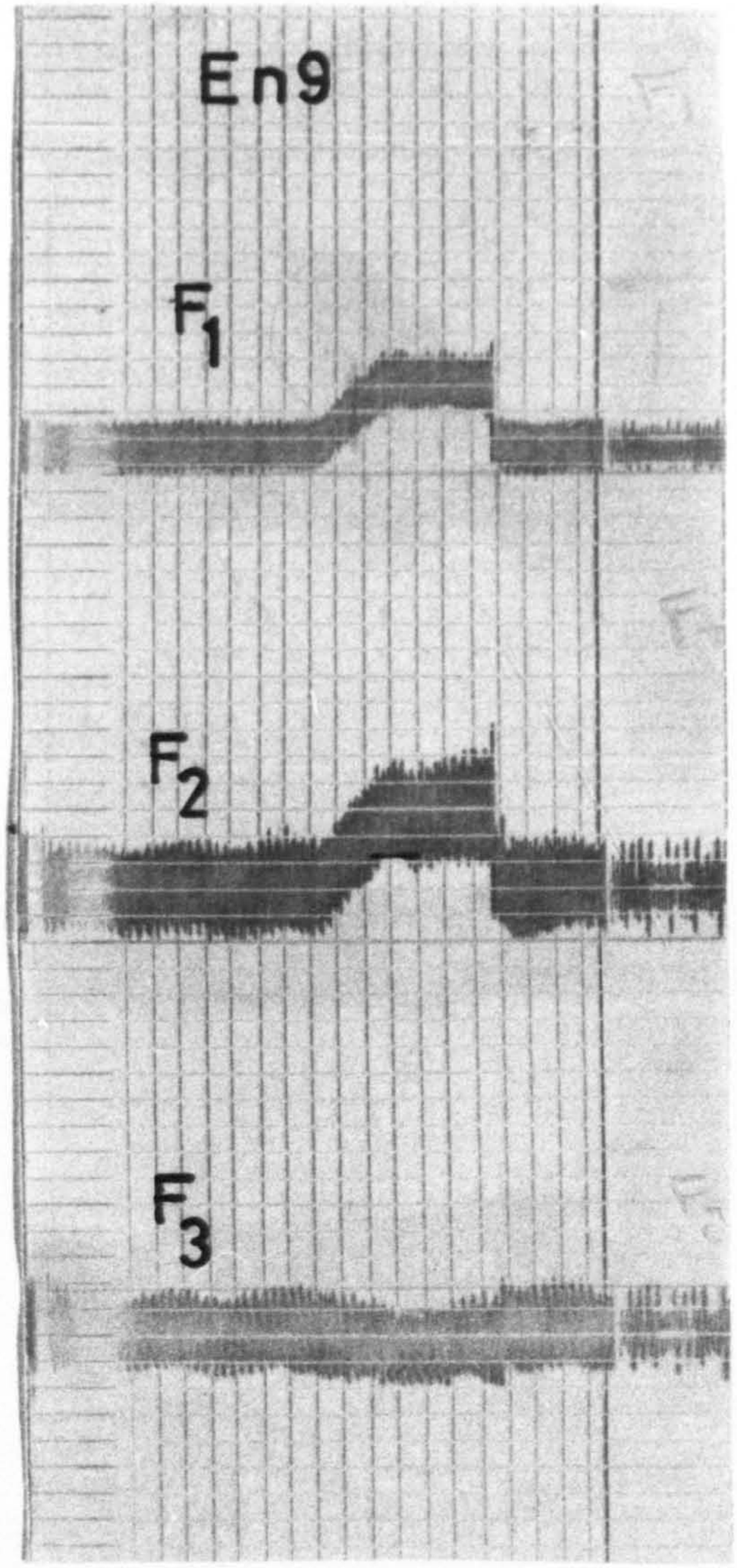
En9
F1
F2
F3

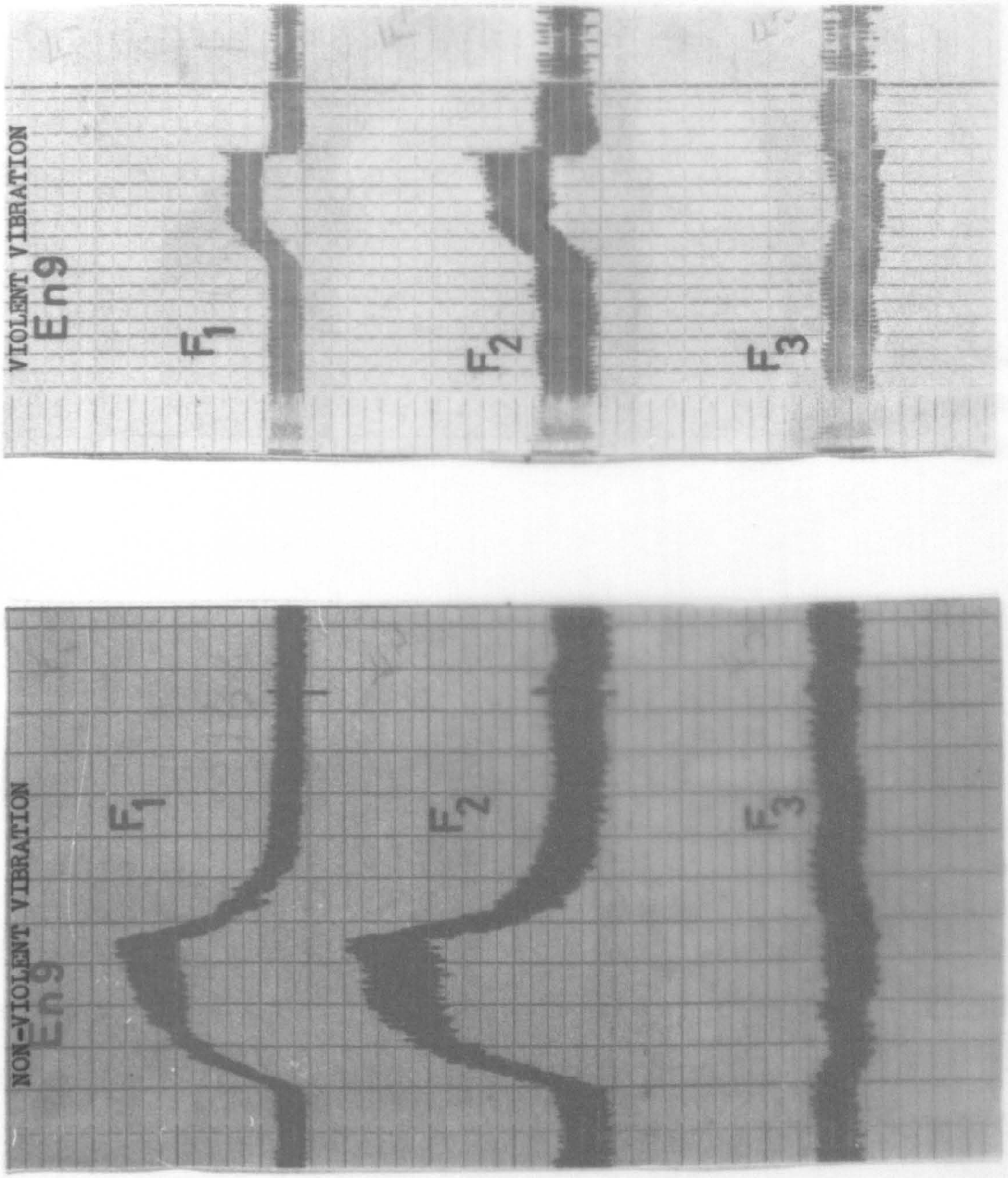

PLATE 9. TRACES ILLUSTRATING CHARACTERISTICS OF THE TWO VIBRATION TYPES ENCOUNTERED WHILST GRINDING.

PLATE 10. IMPROVED MAIN DRIVE TRANSMISSION SYSTEM.

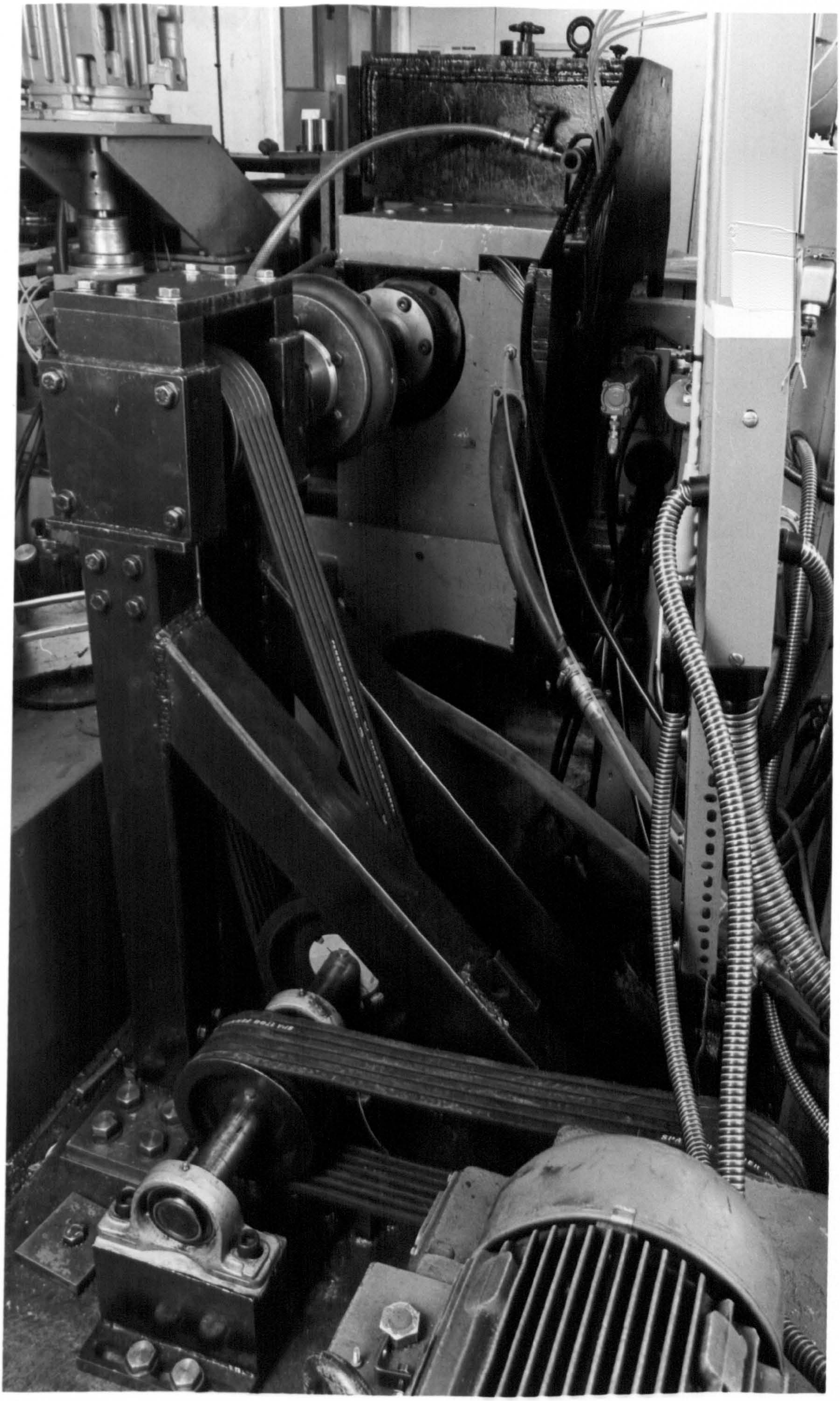

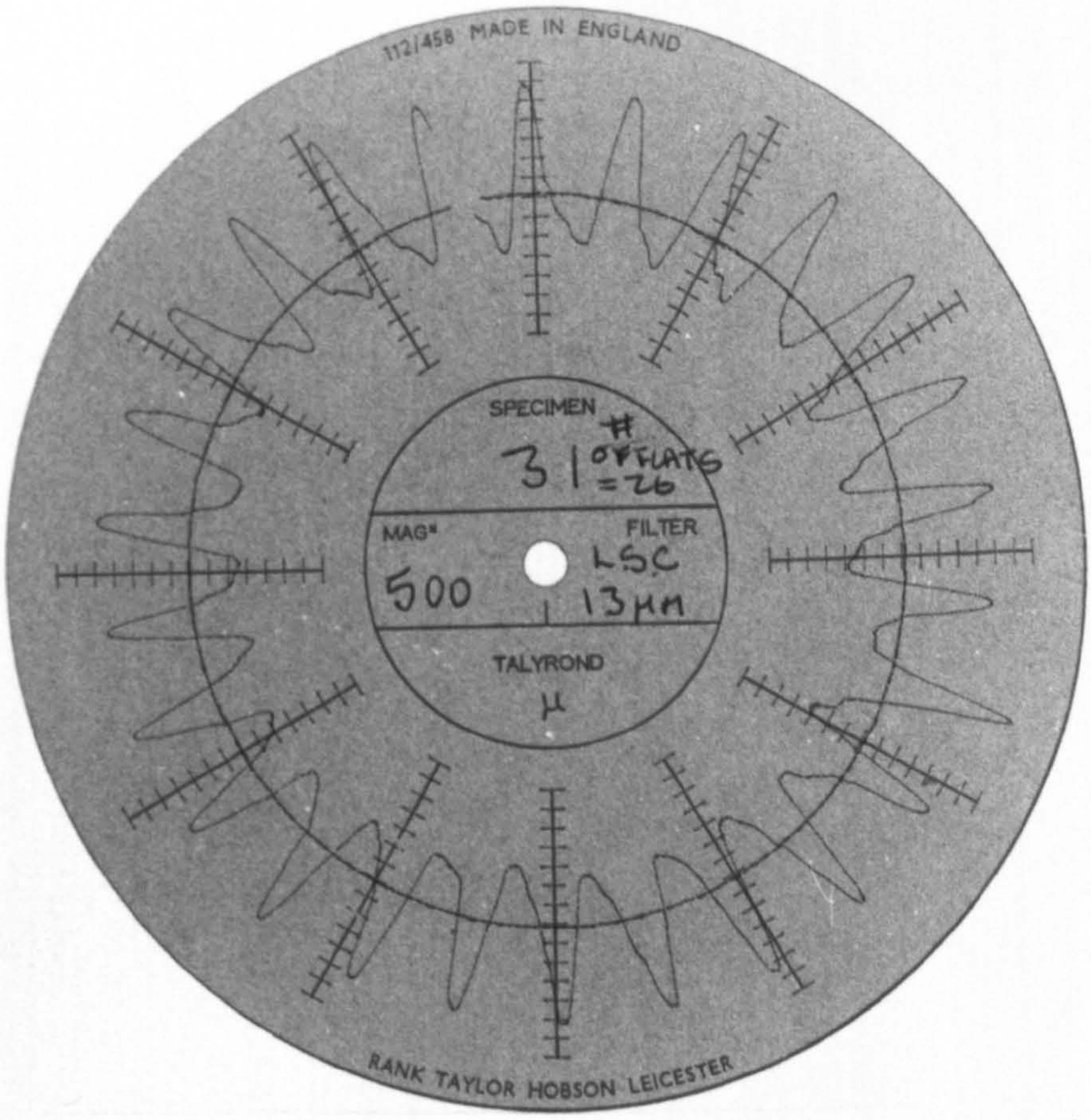

Plate 11a. Talyrond Trace for Chattered Component.

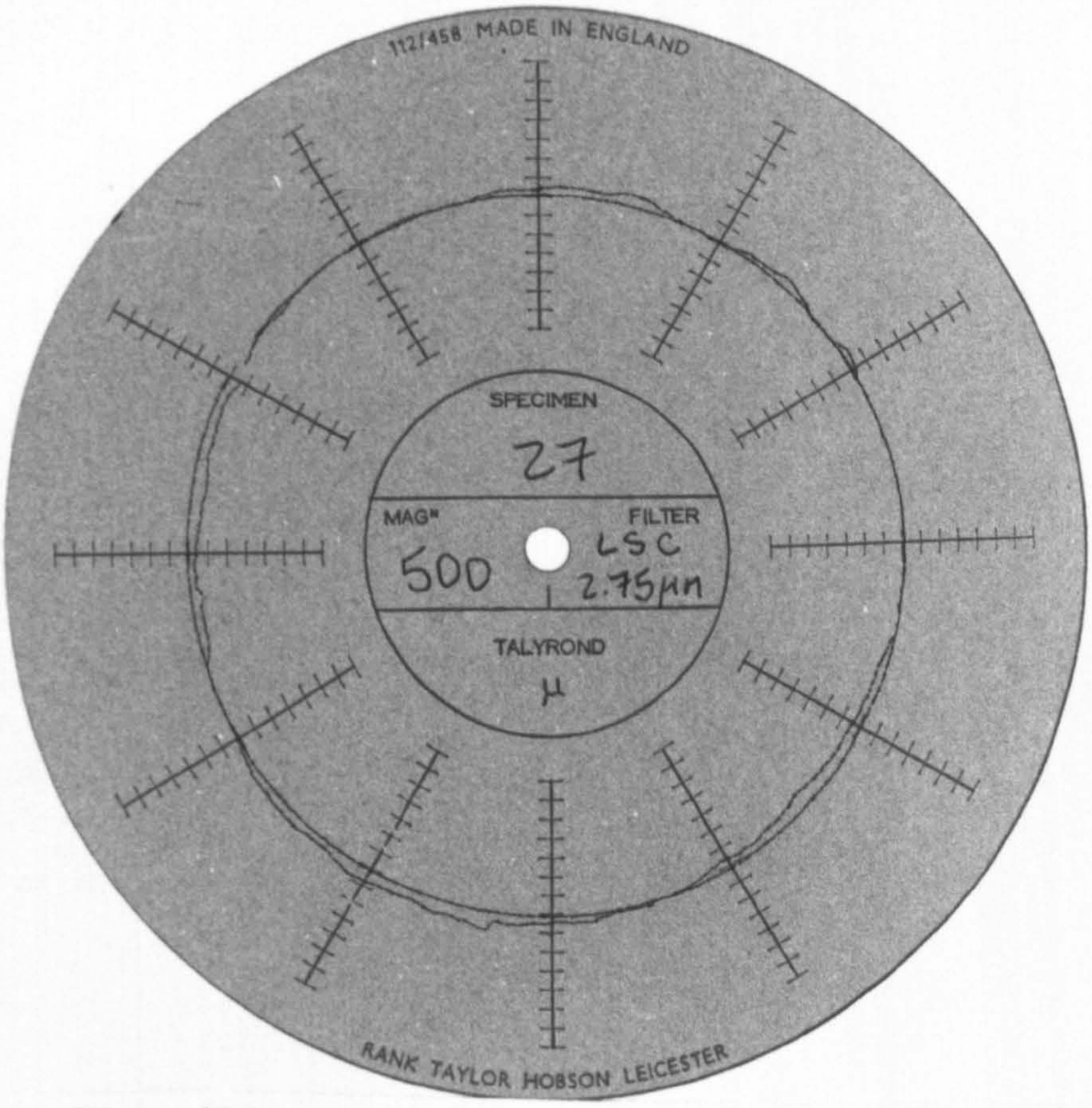

Plate 11b. Talyrond Trace for Non-chattered Component.

PLATE 12. EN 9 SPECIMEN GROUND WITH CHATTER.

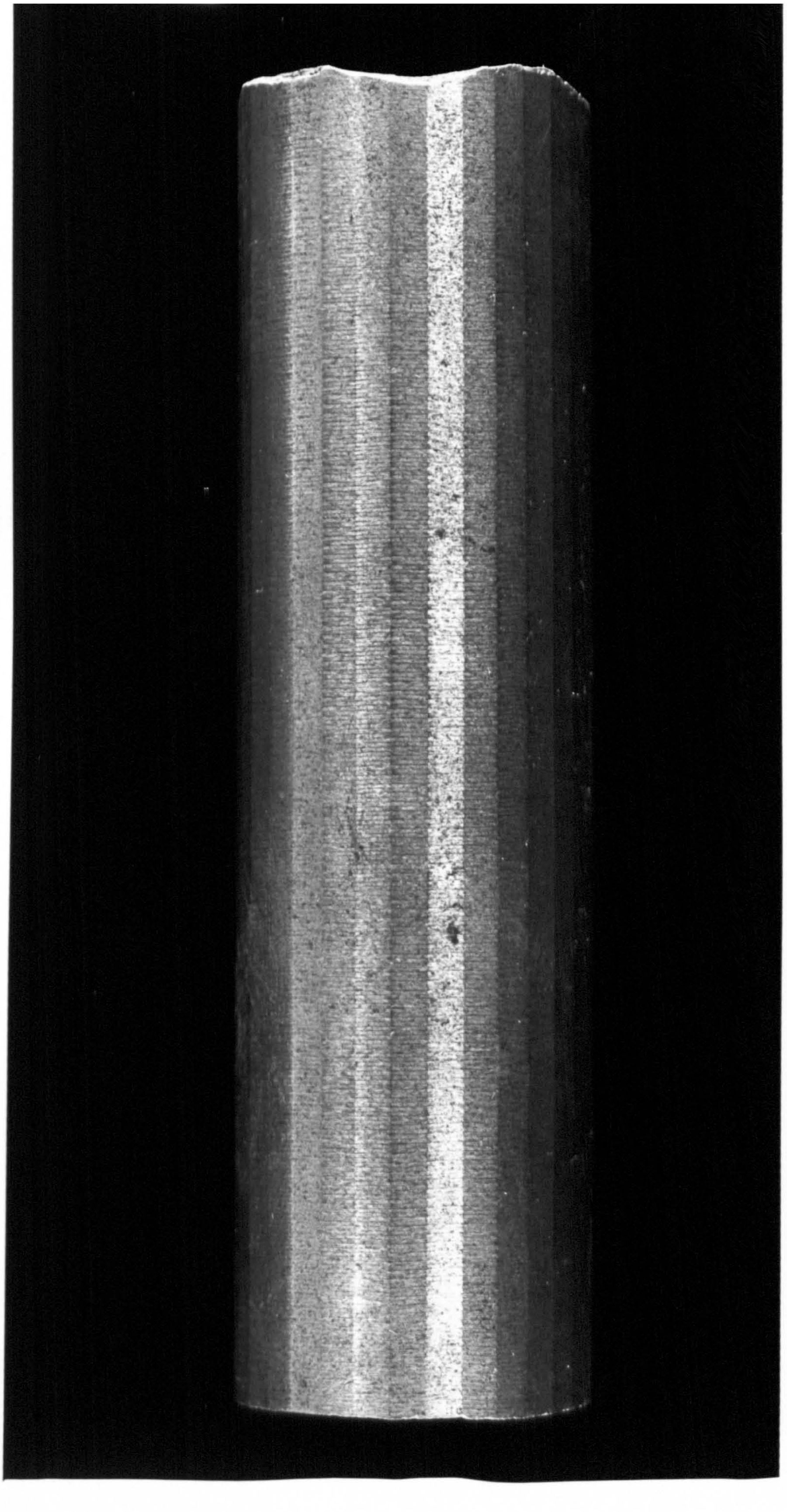

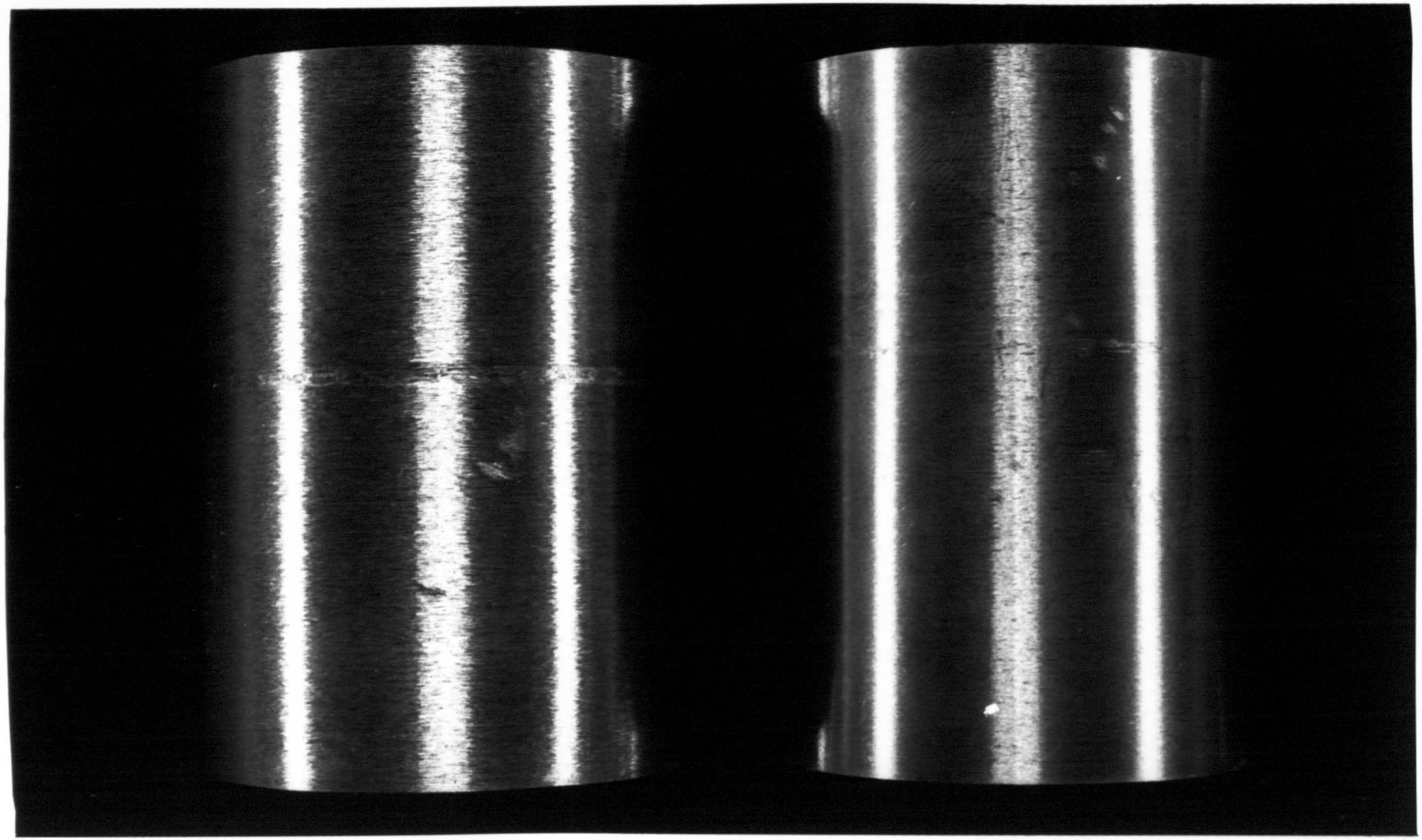

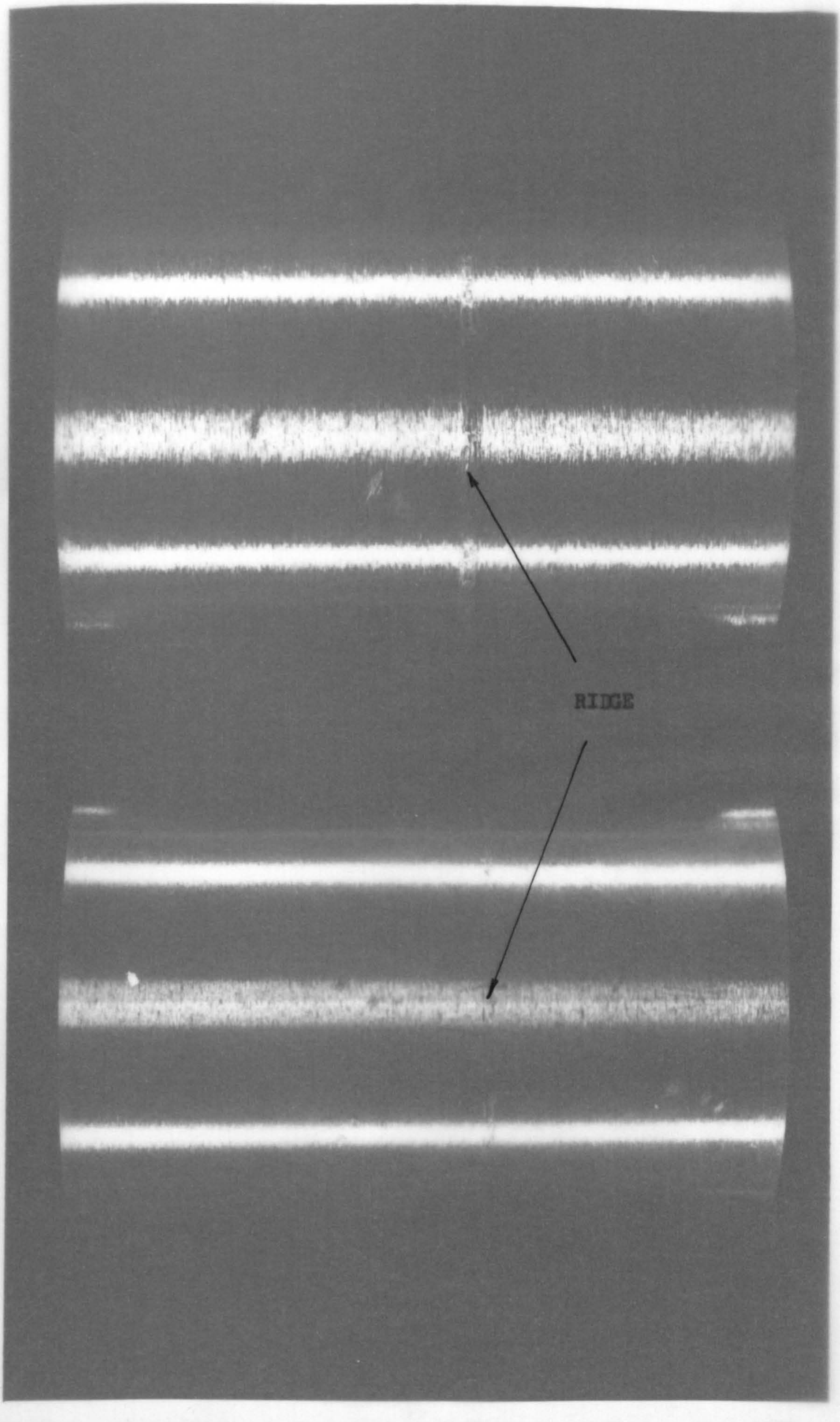

PLATE 13. RIDGE FOUND ON WORKPIECE JUST PRIOR TO CHATTER - EN 9 ONLY.

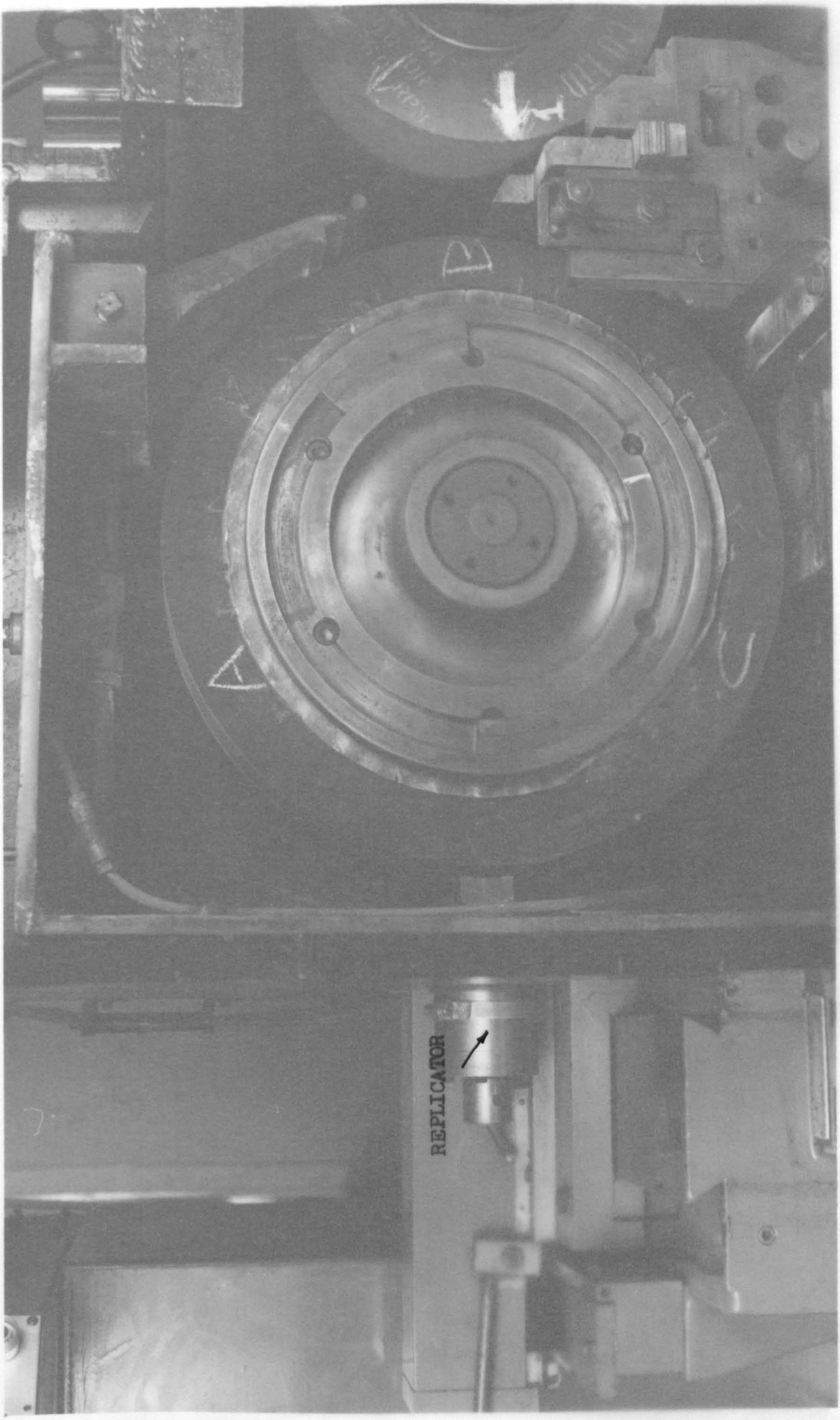

PLATE 14. GRINDING WHEEL SURFACE REPLICATOR FITTED TO THE GRINDING MACHINE.

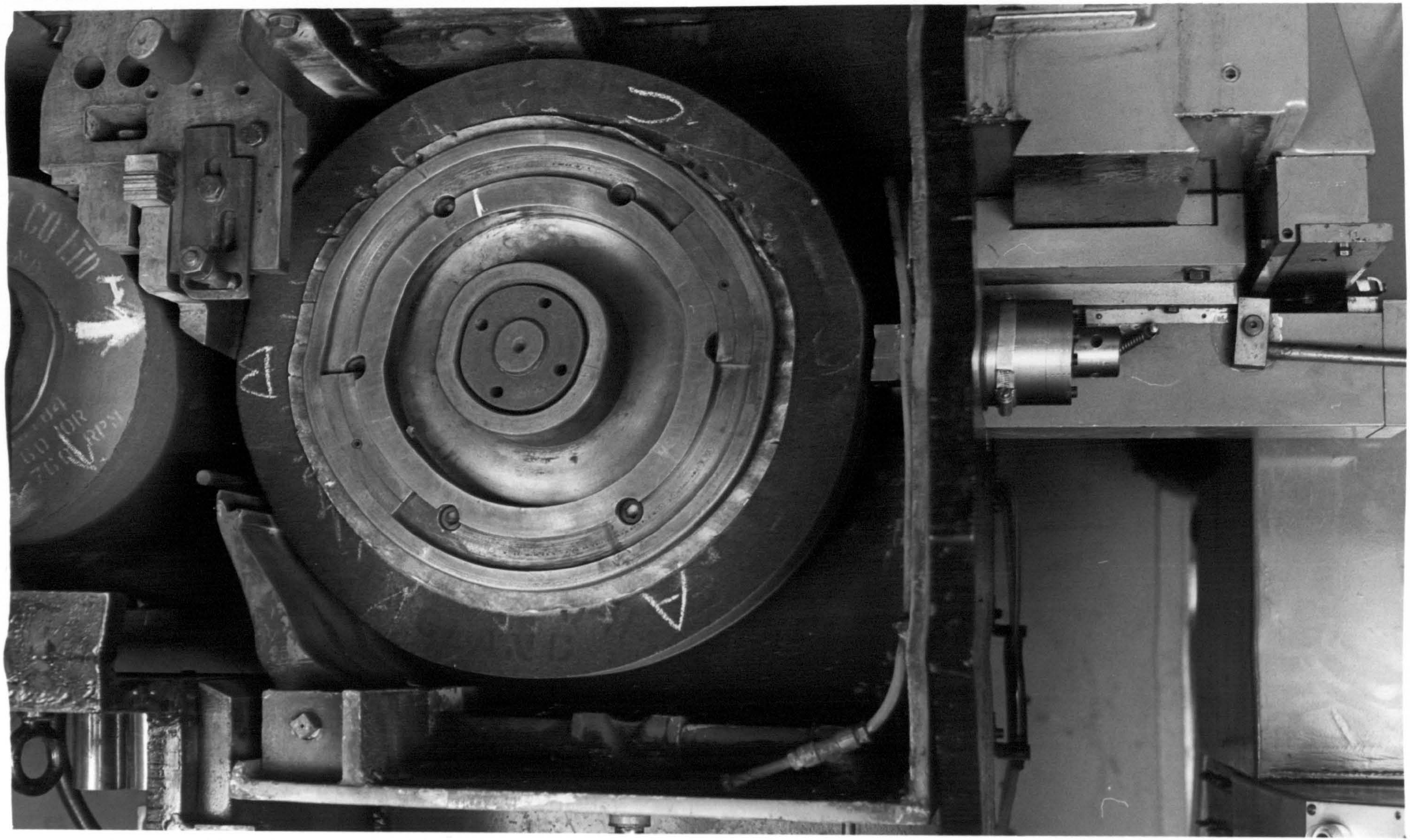

TABLES

Table 1. Sample Transducer Calibration Sheet

Computer Input Data

Trace Amplitudes (mm)	Grinding Wheel Speed (m/s)			
	60	50	40	30
A1a	24	17½	10	5¼
A2a	28¼	24½	15½	8½
A3a	28	21½	13	7½
A1b	20	14	8¼	4½
A2b	25½	20	12½	7
A3b	23	17½	10¼	6¼
A1c	15½	11	6	3½
A2c	20½	16	9½	5½
A3c	18¼	13½	8	4½
B1a	16½	11½	6½	3½
B2a	22	17¼	10½	6
B3a	18½	14½	8½	5½
B1b	12	8¼	5	3
B2b	16½	12	8	4½
B3b	14½	11	7	4¼
B1c	7½	5	3¼	2
B2c	10½	8½	5½	3½
B3c	9¼	7¼	5	3¼
Large calibrating mass, mp = 0.08 kg				
Small calibrating mass, mq = 0.04 kg				
Leverage factor = 1.1				

Computer Output Data

Calibration Values (N/mm)	Grinding Wheel Speed (m/s)			
	60	50	40	30
Trace 1 $\bar{K}1$	20.4	20.18	22.29	23.1
Trace 2 $\bar{K}2$	16.3	14.4	14.25	15.0
Trace 3 $\bar{K}3$	17.6	16.34	17.26	17.4

TABLE 2

SET DATA SHEET

DATE:- 5/79

EXPERIMENT NUMBER:- WFB.1

EXPERIMENT TYPE:- BATCH/~~INDIVIDUAL~~/PLUNGE/~~THRO'FEED~~

1 GRINDING WHEEL Ø X BORE X WIDTH SIZE:- 0.478 × 0.305 × 0.2 GRADE:- WA60MVRC	**2 CONTROL WHEEL** Ø X BORE X WIDTH SIZE:- 0.295 × 0.125 × 0.2 GRADE:- A60 OR
3 COOLANT TYPE:- PURFISOL AGE:- 2 WEEKS DILUTION:- 80/1 FILTER SYSTEM:- HYDROCYCLONE	
4 WORKPIECE BORE:- - HARDNESS:- A/R CONDITION:- NORMALISED MATERIAL SPECIFICATION:- En9 STEEL	
5 MACHINE SETTINGS ℄ h' = 11mm ENDSTOP TYPE:- BALL NOZZLE ARRANGEMENT:- COMBINATION CONTROL TILT:- 0.5° WORKBLADE SIZE:- 20mm WORKBLADE TYPE:- PLUNGE WORKBLADE ANGLE:- 30°	
6 HYDRAULIC OIL TEMP^{c}:- 27 °C	
7 ROOM TEMP^{e} a) START OF RUN:- - b) END OF RUN:- —	

COMMENTS

EXPERIMENT TO INVESTIGATE THE INFLUENCE OF COOLANT SUPPLY TECHNIQUE ON GRINDING FORCES.

TABLE No.3. - Influence of Coolant Supply Technique on Force Levels in Centreless Grinding

SET DATA	Component Number	A	B	C	D	E	F	G	H	Units
	Grinding Wheel Speed	60	60	60	60	60	60	60	60	m/s
	Workpiece Speed	0.5	0.5	0.5	0.5	0.5	0.5	0.5	0.5	m/s
	Q Ratio	120	120	120	120	120	120	120	120	-
	Maximum Metal Removal Rate	6.9	7.9	10.2	16.4	19.2	23.9	24.9	36	$mm^3/mm/s$
FLOOD NOZZLE	Normal Force (F'_n)	3.13	3.79	5.18	6.81	8.77	10.29	11.31	13.26	N/mm
	Tangential Force (F'_t)	1.78	2.1	2.68	3.34	4.34	5.01	5.39	6.25	N/mm
	Ratio (F'_n/F'_t)	1.76	1.8	1.93	2.04	2.02	2.05	2.1	2.12	-
MANIFOLD	Normal Force (F'_n)	2.74	3.4	4.73	6.19	7.89	9.3	10.2	11.8	N/mm
	Tangential Force (F'_t)	1.57	1.92	2.42	3.05	3.91	4.55	5.01	5.76	N/mm
	Ratio (F'_n/F'_t)	1.74	1.74	1.95	2.02	2.01	2.03	2.05	2.05	-

ADDITIONAL INFORMATION

A) Grinding Wheel Grade	WA60MURC	Diameter	0.498 (m)
B) Control Wheel Grade	A60 OR	Diameter	0.294 (m)
C) Workpiece Material	EN9	Condition	Normalised
D) Dressing Lead	0.8 (mm/s)	Diamond Type	Single Point
E) Coolant Type	Purfisoc	Dilution	80:1

Table 4 Sample Data Recording Sheet for En 9 Steel

PROCESS VARIABLES	RECORDED DATA						
Machine Details	Hydraulic supply: 750 PSI @ 27°C			Workblade Type: Plunge			
Coolant Application	Fluid: purfisol 2006/A		Dilution: 200/1	Supply Technique: Combination			
Grinding Wheel Description	Designation: WA60MURC		Diameter: 478 mm				
Control Wheel Description	Designation: A60 OR		Diameter: 295 mm				
Workpiece Description	Material: En 9 Steel		Condition: Normalised				
Component Number	1	2	3	4	5	6	7
Grinding Wheel Speed (m/s)	61	55	50	45	40	35	32
Workpiece Speed (m/s)	0.51	0.46	0.42	0.375	0.333	0.292	0.267
q - ratio (vg/vw)	120	120	120	120	120	120	120
Initial Workpiece Diameter (mm)	44.79	44.79	44.79	44.79	44.79	44.79	44.79
Diameter After Grinding (mm)	44.35	44.35	44.35	44.35	44.35	44.35	44.35
Infeed-rate (mm/s)	0.049	0.049	0.049	0.049	0.049	0.049	0.049
Equivalent Chip Thickness (mm)	114	124	137	153	174	200	214
Surface Roughness (mm)	1'	1.02	1.14	1.15	1.32	1.54	1.75

Table 5 Sample Calculated Results for En 9 Steel

This table complements Table 4

Grinding Parameters	Calculated Data						
Component Number	1	2	3	4	5	6	7
Specific Normal Force (N/mm)	4.58	5.17	5.69	6.29	7.77	9.33	9.82
Specific Tangential Force (N/mm)	2.5	2.66	2.67	2.87	3.74	4.71	4.99
Specific Total Grinding Force (N/mm)	5.22	5.81	6.29	6.73	8.63	10.4	11
Force Ratio (Fn/Ft)	1.83	1.94	2.12	2.12	2.07	1.98	1.95
Maximum Metal Removal Rate ($mm^3/mm/s$)	6.89	6.89	6.89	6.89	6.89	6.89	6.89
Wheel Cutting Ability ($mm^3/N/s$)	1.51	1.33	1.21	1.1	0.89	0.73	0.7
Power to Grind (W/mm)	152	146	133	129	150	164	160
Specific Energy (J/mm^2)	22.1	21	19.6	19	22	23.8	23.2

Table 6 Maximum Undeformed Chip Thickness Expressions of Various Workers

Author(s)		Year	Expression
Alden	[39]	1914	$tc = \frac{lg.vw}{vg} \cdot \sin(\gamma_k + \varphi_k)$
Pahlitzsch Helmerdig	[40]	1943	$tc = 2.lg.\frac{vw}{vg} \cdot \left(\frac{\pi.vi(Dw+Dg)}{vw.Dg}\right)^{\frac{1}{2}}$
Reichenbach Mayer Kalpakcioglu Shaw	[41]	1956	$tc = 2.\left(\frac{vw}{\pi.cp.vg}\right)^{\frac{1}{2}} \cdot \left(\frac{\pi.vi(Dw+Dg)}{vw.Dg}\right)^{\frac{1}{4}}$
Peklenik	[42]	1957	$tc = \frac{\pi.Dw.vi.vw.lg}{vg.lc}$
Opitz Ernst Meyer	[37]	1965	$tc = \frac{\pi.vi.Dw.lg}{vg.lc}$
Okamura Lemmon	[43]	1966	$tc = D.\left(\frac{D.\pi.Dw.vi}{vw} - rw.\frac{1}{4}.\left(\frac{D.rw.A.B+1}{rg}\right).(\gamma_{cs} - \alpha)^2\right)$
Kassen	[44]	1969	$tc = 0.71x\left(\frac{2}{cl.tg.\kappa}\right)^{\frac{1}{3}} \cdot \left(\frac{vw}{vg}\right)^{\frac{1}{3}} \cdot \left(\frac{\pi.Dw.vi}{Dg}\right)^{\frac{1}{3}}$
Werner	[45]	1971	$tc = \frac{1}{(1.2)^p} \cdot \left(\frac{2}{cll.kg}\right)^{\frac{1}{p+1}} \cdot \left(\frac{vw}{vg}\right)^{\frac{1}{p+1}} \cdot \left(\frac{\pi.Dw.vi}{vw.De}\right)^{\frac{1}{2(p+1)}}$
Rowe Stout	[46]	1971	$tc = \frac{2.\pi.Dw.vi.lg}{vg}\sqrt{\frac{vw.(Dw+Ds)}{\pi.Dw.vi.Dg.Dw}}$
Bell Brough Rowe	[38]	1980	$tc = \left(1-\frac{2.\pi.vi.De}{vw.Dg}\right).\left[\frac{ld.vw}{vg}\sqrt{\frac{4.De.\pi.vi}{vw.Dw}} - \frac{\pi.vi.De}{vw} \ldots\ldots\right.$ $\left. \ldots\ldots - \frac{\pi.vi.De}{vw} - \left(\frac{ld.vw}{vg}\right)^2.\frac{1}{Dw}\right] + \frac{\pi.Dw.vi}{vw}.\left(1+\frac{Dw.\pi.vi}{vw.Dg}\right)$

TABLE 7. SAMPLE ANALYSES FOR VARIOUS TC EXPRESSIONS

AUTHOR	EXPRESSION FOR $\bar{t}c$	INFEED-RATE (m/s)			
		0.001	$\bar{t}c$ µm	0.01	$\bar{t}c$ µm
BELL ETAL CASE 1	a) $Rg + hg - Rd$	0.242 - 0.24199612	3.88	0.242 - 0.2419875	12.49
	b) $Rg + hg - Rd$	$0.242 + 0.45\times10^{-6} - 0.24199612$	4.33	$0.242 + 1.55\times10^{-6} - 0.2419875$	14.04
BELL ETAL CASE 2	$\frac{lg\,vw}{vg}\sqrt{\frac{4\,De\,\pi\,vi}{vw.vg}} - \frac{\pi\,vi\,De}{vw}$ .... $+ \frac{\pi\,Dw\,vi}{vw}\left(1 + \frac{Dw\,\pi\,vi}{vw\,Dg}\right)$	$3.886\times10^{-6} - 1.2566\times10^{-4}$ .... $- 3\times10^{-8} + 1.256\times10^{-4}$	3.88	FAILS	-
PAHLITZSCH	$\frac{2.lg\,vw}{vg}\left(\frac{\pi.Dw\,vi}{vw}.\frac{Dg+Dw}{Dw.Dg}\right)^{0.5}$	$\frac{2\times0.002}{60}.\left(\frac{\pi\times0.04\times0.001\times10^{-3}}{36.96}\right)^{0.5}$	3.88	$\frac{2\times0.002}{60}\left(\frac{\pi\times4\times10^{-4}}{36.90}\right)^{0.5}$	12.3
ROWE ETAL	$\frac{2.\pi.Dw\,vi.lg}{vg}\sqrt{\frac{vw}{\pi.Dw\,vi}.\frac{Dg+Dw}{Dw.Dg}}$	$\frac{2\times\pi\times8\times10^{-8}}{60}\sqrt{\frac{10^{-8}}{\pi\times4\times36.96}}$	3.88	$\frac{2\times\pi\times8\times10^{-7}}{60}\sqrt{\frac{10^{-7}}{\pi\times4\times36.96}}$	12.3
PEKLENIK	$\frac{\pi.Dw\,vi.lg}{vg.\bar{t}c}$	$\frac{\pi\times0.04\times0.001\times0.002}{60\times2.193\times10^{-3}}$	1.91	$\frac{\pi\times0.04\times0.01\times0.002}{60\times6.867\times10^{-3}}$	61
OPITZ ETAL	$\frac{\pi.Dw\,vi.lg}{vg.\bar{t}g}$	$\frac{\pi\times0.04\times0.001\times0.002}{60\times2.193\times10^{-3}}$	1.91	$\frac{\pi\times0.04\times0.01\times0.002}{60\times6.867\times10^{-3}}$	61

TABLE 8: Tables of Theoretical Results.

The following tables contain idealised undeformed chip data calculated from the expressions developed in section 3.0. The theoretical results for the undeformed chip thickness were calculated using the expression for variable grit height and separation (3.6); assuming hg, the grit height variation to be zero. For the range of conditions examined, similar values for tc would have been obtained from expression (3.13), the solution for constant grit height and separation.

TABLE I - Effect of Grinding Wheel Speed on the Undeformed Chip Dimensions

Grinding Wheel Speed (m/s)	10	20	30	40	50	60	70
Grinding Wheel Diameter (m)	0.484	0.484	0.484	0.484	0.484	0.484	0.484
Workpiece Diameter (m)	0.04	0.04	0.04	0.04	0.04	0.04	0.04
Distance Ld (m)	0.002	0.002	0.002	0.002	0.002	0.002	0.002
q-ratio (vg/vw)	60						
Workpiece Speed (m/s)	0.17	0.33	0.5	0.67	0.83	1	1.17
Infeed Rate (m/s)	0.0001						
Chip Length (µm)	1652	1185	963	832	747	681	629
Chip Thickness (µm)	3.0	2.09	1.71	1.48	1.31	1.19	1.11
Chip Formation Time (µsec)	165	59.3	32.1	20.8	14.96	11.4	9
Infeed Rate (m/s)	0.0002						
Chip Length (µm)	2337	1677	1362	1176	1057	963	890
Chip Thickness (µm)	4.21	2.98	2.43	2.11	1.87	1.71	1.58
Chip Formation Time (µsec)	234	83.8	45.4	29.4	21.1	16.1	12.7
Infeed Rate (m/s)	0.0003						
Chip Length (µm)	2862	2054	1669	1440	1294	1179	1090
Chip Thickness (µm)	5.16	3.66	2.97	2.58	2.3	2.1	1.94
Chip Formation Time (µsec)	286	102.7	55.6	36	25.9	19.6	15.59

TABLE I - Continued

Infeed Rate (m/s)	0.0004						
Chip Length (µm)	3305	2372	1927	1663	1494	1362	1259
Chip Thickness (µm)	5.97	4.21	3.46	2.99	2.66	2.42	2.25
Chip Formation Time (µsec)	331	118	64.2	41.6	29.9	22.7	18
q-ratio (vg/vw)	90						
Workpiece Speed (m/s)	0.111	0.222	0.333	0.444	0.555	0.666	0.777
Infeed Rate (m/s)	0.0001						
Chip Length (µm)	2045	1446	1180	1022	914	834	772
Chip Thickness (µm)	2.46	1.729	1.41	1.21	1.08	0.99	0.92
Chip Formation Time (µsec)	205	72.3	39.4	25.5	18.3	13.9	11
Infeed Rate (m/s)	0.0002						
Chip Length (µm)	2892	2045	1669	1446	1292	1180	1092
Chip Thickness (µm)	3.45	2.46	2	1.72	1.54	1.41	1.29
Chip Formation Time (µsec)	289	102	55.6	36.2	25.8	19.6	15.6
Infeed Rate (m/s)	0.0003						
Chip Length (µm)	3542	2505	2045	1771	1583	1445	1338
Chip Thickness (µm)	4.22	2.99	2.46	2.13	1.89	1.73	1.59
Chip Formation Time (µsec)	354	125	68.1	44.3	31.6	24.0	19.1
Infeed Rate (m/s)	0.0004						
Chip Length (µm)	4090	2892	2361	2044	1829	1668	1544
Chip Thickness (µm)	4.87	3.45	2.82	2.46	2.19	2.00	1.84
Chip Formation Time (µsec)	409	144.6	78.7	51.1	36.6	27.8	22.1

TABLE I - Continued

q-ratio (vg/vw)	120						
Workpiece Speed (m/s)	0.08	0.167	0.25	0.33	0.417	0.5	0.583
Infeed Rate (m/s)	0.0001						
Chip Length (µm)	2409	1667	1362	1185	1054	963	892
Chip Thickness (µm)	2.12	1.51	1.22	1.05	0.94	0.86	0.79
Chip Formation Time (µsec)	241	83.4	45.4	29.6	21.1	16	12.7
Infeed Rate (m/s)	0.0002						
Chip Length (µm)	3407	2358	1927	1676	1491	1362	1261
Chip Thickness (µm)	2.99	2.11	1.74	1.5	1.33	1.22	1.13
Chip Formation Time (µsec)	341	118	64.2	41.9	29.8	22.7	18
Infeed Rate (m/s)	0.0003						
Chip Length (µm)	4172	2888	2360	2054	1828	1665	1544
Chip Thickness (µm)	3.65	2.59	2.12	1.84	1.66	1.51	1.38
Chip Formation Time (µsec)	417	144	78.7	51.4	36.6	27.8	22.1
Infeed Rate (m/s)	0.0004						
Chip Length (µm)	4818	3335	2726	2372	2110	1927	1784
Chip Thickness (µm)	4.21	2.99	2.44	2.11	1.89	1.74	1.61
Chip Formation Time (µsec)	482	166	90.9	59.3	42.2	32.1	25.5
q-ratio (vg/vw)	180						
Workpiece Speed (m/s)	0.055	0.111	0.166	0.222	0.277	0.333	0.388
Infeed Rate (m/s)	0.0001						
Chip Length (µm)	2905	2045	1672	1445	1294	1180	1092
Chip Thickness (µm)	1.72	1.22	0.99	0.86	0.78	0.71	0.65
Chip Formation Time (µsec)	2.90	102	55.7	36.1	25.8	19.6	15.6

TABLE I - Continued

Infeed Rate (m/s)	0.0002						
Chip Length (μm)	4108	2905	2365	2045	1831	1669	1543
Chip Thickness (μm)	2.44	1.73	1.41	1.22	1.08	0.99	0.93
Chip Formation Time (μsec)	410	145	78.8	51.1	36.6	27.8	22.1
Infeed Rate (m/s)	0.0003						
Chip Length (μm)	5032	3542	2888	2505	2242	2045	1890
Chip Thickness (μm)	2.97	2.11	1.72	1.44	1.34	1.25	1.13
Chip Formation Time (μsec)	503	177	96.2	62.6	44.8	34.1	27.0
Infeed Rate (m/s)	0.0004						
Chip Length (μm)	5810	4090	3345	2892	2589	2362	2182
Chip Thickness (μm)	3.42	2.43	1.99	1.73	1.55	1.41	1.31
Chip Formation Time (μsec)	58.1	204	111	72	51.8	39.4	31.3

TABLE II - Effect of the Infeed Rate on the Undeformed Chip Dimensions

Infeed Rate (mm/s)	0.05	0.1	0.15	0.2	0.25	0.3	0.35
Grinding Wheel Diameter (m)	0.484	0.484	0.484	0.484	0.484	0.484	0.484
Workpiece Diameter (m)	0.04	0.04	0.04	0.04	0.04	0.04	0.04
Distance Ld (m)	0.002	0.002	0.002	0.002	0.002	0.002	0.002
Grinding Wheel Speed (m/s)	30	30	30	30	30	30	30
Workpiece Speed (m/s)	0.5						
q-ratio (vg/vw)	60						
Chip Length (µm)	681	965	1180	1362	1523	1669	1803
Chip Thickness (µm)	1.2	1.71	2.1	2.42	2.71	2.99	3.24
Chip Formation Time (µsec)	22.7	32.1	39.6	45.4	50.8	55.6	60.0
Workpiece Speed (m/s)	0.333						
q-ratio (vg/vw)	90						
Chip Length (µm)	835	1181	1446	1669	1867	2045	2209
Chip Thickness (µm)	0.99	1.4	1.73	2.00	2.241	2.46	2.67
Chip Formation Time (µsec)	27.8	39.4	48.2	55.6	62.2	68.2	73.6
Workpiece Speed (m/s)	0.3						
q-ratio (vg/vw)	100						
Chip Length (µm)	879	1244	1524	1759	1967	2154	2327
Chip Thickness (µm)	0.94	1.33	1.63	1.88	2.14	2.32	2.5
Chip Formation Time (µsec)	29.3	41.4	50.7	58.6	65.6	71.8	77.6
Workpiece Speed (m/s)	0.25						
q-ratio (vg/vw)	120						
Chip Length (m)	964	1363	1669	1927	2155	2360	2549
Chip Thickness (m)	0.86	1.22	1.51	1.74	1.96	2.11	2.28
Chip Formation Time (sec)	32.1	45.4	55.6	64.2	71.8	78.6	8.49

TABLE II - Continued

Workpiece Speed (m/s)	0.2						
q-ratio (vg/vw)	150						
Chip Length (μm)	1077	1524	1866	2155	2409	2639	2850
Chip Thickness (μm)	0.77	1.09	1.36	158	1.73	1.9	2.04
Chip Formation Time (μsec)	35.9	50.7	62.2	71.8	80.3	87.9	95.0
Workpiece Speed (m/s)	0.167						
q-ratio (vg/vw)	180						
Chip Length (μm)	1179	1667	2042	2358	2636	2888	3119
Chip Thickness (μm)	0.70	0.99	1.25	1.45	1.58	1.73	1.86
Chip Formation Time (μsec)	39.3	55.6	68.0	78.6	87.9	96.2	1.04
Workpiece Speed (m/s)	0.15						
q-ratio (vg/vw)	200						
Chip Length (μm)	1240	1759	2154	2488	2782	3047	3291
Chip Thickness (μm)	0.67	0.94	1.18	1.34	1.5	1.64	1.77
Chip Formation Time (μsec)	41.5	58.6	71.8	82.9	92.7	101.6	109.7
Grinding Wheel Speed (m/s)	45						
Workpiece Speed (m/s)	0.75						
q-ratio (vg/vw)	60						
Chip Length (μm)	556	787	963	1113	1244	1362	1471
Chip Thickness (μm)	0.97	1.39	1.71	1.98	2.21	2.42	2.62
Chip Formation Time (μsec)	12.4	17.5	21.4	24.7	27.6	30.3	32.7
Workpiece Speed (m/s)	0.5						
q-ratio (vg/vw)	90						
Chip Length (μm)	681	964	1180	1362	1524	1669	1803
Chip Thickness (μm)	0.81	1.14	1.41	1.62	1.83	2.00	2.16
Chip Formation Time (μsec)	15.1	21.4	26.2	30.3	33.9	37.1	40.1

TABLE II - Continued

Workpiece Speed (m/s)	0.45						
q-ratio (vg/vw)	100						
Chip Length (µm)	718	1016	1244	1436	1606	1759	1900
Chip Thickness (µm)	0.77	1.09	1.33	1.54	1.74	1.90	2.06
Chip Formation Time (µsec)	15.96	22.6	27.6	31.9	35.7	39.1	42.2
Workpiece Speed (m/s)	0.375						
q-ratio (vg/vw)	120						
Chip Length (µm)	786	1113	1362	1573	1759	1927	2081
Chip Thickness (µm)	0.70	0.99	1.22	1.41	1.59	1.74	1.89
Chip Formation Time (µsec)	17.5	24.7	30.2	34.9	39.1	42.8	46.3
Workpiece Speed (m/s)	0.3						
q-ratio (vg/vw)	150						
Chip Length (µm)	879	1244	1523	1759	1967	2154	2327
Chip Thickness (µm)	0.63	0.89	1.09	1.28	1.41	1.55	1.67
Chip Formation Time (µsec)	19.5	27.6	33.9	39.1	43.7	47.9	51.7
Workpiece Speed (m/s)	0.25						
q-ratio (vg/vw)	180						
Chip Length (µm)	963	1363	1669	1927	2155	2360	2549
Chip Thickness (µm)	0.58	0.81	0.99	1.18	1.29	1.41	1.52
Chip Formation Time (µsec)	21.4	30.3	37.1	42.8	47.9	52.4	56.6
Workpiece Speed (m/s)	0.225						
q-ratio (vg/vw)	200						
Chip Length (µm)	1016	1436	1759	2031	2271	2488	2687
Chip Thickness (µm)	0.54	0.76	0.95	1.09	1.22	1.34	1.44
Chip Formation Time (µsec)	22.6	31.9	39.1	45.1	50.5	55.3	59.7

TABLE II - Continued

Grinding Wheel Speed (m/s)	60						
Workpiece Speed (m/s)	1						
q-ratio (vg/vw)	60						
Chip Length (µm)	481	681	834	963	1077	1180	1275
Chip Thickness (µm)	0.84	1.19	1.47	1.71	1.91	2.09	2.26
Chip Formation Time (µsec)	8.03	11.4	13.9	16.0	17.9	19.6	21.2
Workpiece Speed (m/s)	0.666						
q-ratio (vg/vw)	90						
Chip Length (µm)	590	834	1022	1181	1320	1446	1562
Chip Thickness (µm)	0.696	0.99	1.21	1.4	1.58	1.72	1.88
Chip Formation Time (µsec)	9.8	13.9	17.0	19.7	22.0	24.1	26.0
Workpiece Speed (m/s)	0.6						
q-ratio (vg/vw)	100						
Chip Length (µm)	622	879	1077	1244	1390	1523	1646
Chip Thickness (µm)	0.66	0.94	1.15	1.33	1.49	1.63	1.78
Chip Formation Time (µsec)	10.3	14.7	17.9	20.7	23.2	25.4	27.4
Workpiece Speed (m/s)	0.5						
q-ratio (vg/vw)	120						
Chip Length (µm)	681	963	1180	1363	1524	1669	1803
Chip Thickness (µm)	0.61	0.86	1.05	1.23	1.38	1.51	1.603
Chip Formation Time (µsec)	11.3	16.1	19.7	22.7	25.4	27.8	30.0
Workpiece Speed (m/s)	0.40						
q-ratio (vg/vw)	150						
Chip Length (µm)	761	1077	1319	1524	1703	1866	2016
Chip Thickness (µm)	0.54	0.77	0.94	1.09	1.24	1.36	1.48
Chip Formation Time (µsec)	12.69	17.9	21.9	25.4	28.4	31.1	33.5

TABLE II - Continued

Workpiece Speed (m/s)	0.333						
q-ratio (vg/vw)	180						
Chip Length (μm)	835	1180	1446	1669	1867	2045	2209
Chip Thickness (μm)	0.49	0.70	0.86	0.99	1.13	1.34	1.35
Chip Formation Time (μsec)	13.9	19.7	24.1	27.8	31.1	34.1	36.81
Workpiece Speed (m/s)	0.3						
q-ratio (vg/vw)	200						
Chip Length (μm)	879	1244	1524	1759	1966	2154	2327
Chip Thickness (μm)	0.47	0.66	0.83	0.96	1.06	1.22	1.25
Chip Formation Time (μsec)	14.6	20.7	25.4	29.3	32.8	35.9	38.8

TABLE III - Effect of High Infeed Rate on Undeformed Chip Parameters

Grinding Wheel Speed (m/s)	10	20	30	40	50	60	70
Grinding Wheel Diameter (m)	0.484	0.484	0.484	0.484	0.484	0.484	0.484
Workpiece Diameter (m)	0.04	0.04	0.04	0.04	0.04	0.04	0.04
Distance Ld (m)	0.002	0.002	0.002	0.002	0.002	0.002	0.002
Infeed Rate (m/s)	0.001	0.001	0.001	0.001	0.001	0.001	0.001
q-ratio (vg/vw)	60						
Workpiece Speed (m/s)	0.17	0.33	0.5	0.67	0.83	1	1.17
Chip Length (µm)	5226	3750	3047	2632	2365	2155	1992
Chip Thickness (µm)	9.39	6.67	5.44	4.71	4.22	3.85	3.56
Chip Formation Time (µsec)	522	188	102	65.8	47.3	35.9	28.5
q-ratio (vg/vw)	90						
Workpiece Speed (m/s)	0.111	0.222	0.333	0.444	0.555	0.666	0.777
Chip Length (µm)	6467	4573	3734	3233	2892	2640	2444
Chip Thickness (µm)	7.64	5.44	4.45	3.86	3.45	3.15	2.92
Chip Formation Time (µsec)	647	228	124	80.8	57.8	44	34.9
q-ratio (vg/vw)	120						
Workpiece Speed (m/s)	0.08	0.167	0.25	0.33	0.417	0.5	0.583
Chip Length (µm)	7618	5270	4309	3750	3336	3047	2822
Chip Thickness (µm)	6.58	4.7	3.85	3.34	2.99	2.73	2.53
Chip Formation Time (µsec)	762	264	144	93.8	66.7	50.7	40.3
q-ratio (vg/vw)	180						
Workpiece Speed (m/s)	0.055	0.111	0.166	0.222	0.277	0.333	0.388
Chip Length (µm)	9188	6467	5288	4573	4094	3734	3459
Chip Thickness (µm)	5.31	3.82	3.13	2.72	2.44	2.23	2.1
Chip Formation Time (µsec)	919	323	176	114	81.8	62.2	49.4

TABLE III - Continued

q-ratio (vg/vw)	200						
Workpiece Speed (m/s)	0.05	0.1	0.15	0.2	0.25	0.3	0.35
Chip Length (µm)	9636	6814	5564	4818	4309	3934	3642
Chip Thickness (µm)	5.03	3.62	2.97	2.58	2.31	2.11	1.96
Chip Formation Time (µsec)	964	341	185	121	86.2	65.6	52

q-ratio (vg/vw)	250						
Workpiece Speed (m/s)	0.04	0.08	0.12	0.16	0.2	0.24	0.28
Chip Length (µm)	10774	7618	6220	5386	4818	4398	4072
Chip Thickness (µm)	4.44	3.22	2.65	2.30	2.07	1.88	1.75
Chip Formation Time (µsec)	1077	381	207	134	96.4	73.3	58.17

Table 9 Maximum Undeformed Chip Length Expressions of Various Workers

Author		Year	Expression
Alden	[39]	1914	$lc = \frac{\nu . T . \sin(A+B) . vw}{n . \pi . Dw . vi}$
Pahlitzsch Helmerdig	[40]	1943	$lc = \sqrt{De . \pi . Dw . vi / vw}$
Reichenbach Mayer Kalpakcioglu Shaw	[41]	1956	$lc = \sqrt{\frac{Dg . T . Dw . vi}{\left(1 + \frac{Dg}{Dw}\right) . vw}} . \left(1 + \frac{vw}{vg}\right)$
Peklenik	[42]	1957	$lc = \frac{lg . vw}{vg} + \sqrt{\frac{De . T . Dw . vi}{vw}}$
Opitz Ernst Meyer	[37]	1965	$lc = \frac{lg . vw}{vg} + \sqrt{\frac{De . T . Dw . vi}{vw}}$
Okamura Lemmon	[43]	1966	None available
Kassen	[44]	1969	$lc = \frac{lg . vw}{vg} + \sqrt{\frac{De . T . Dw . vi}{vw}}$
Werner	[45]	1971	$lc = \sqrt{\frac{De . T . Dw . vi}{vw}}$
Rowe Stout	[46]	1971	$lc = \frac{lg . vw}{vg} + \sqrt{\frac{De . T . Dw . vi}{vw}}$.
Bell Brough Rowe	[38]	1980	$lc = \sqrt{\frac{De . T . Dw . vi}{vw}}$

Table 10 Sample Analyses for Various Chip Length Expressions

Author	Expression for lc	Infeed Rate (m/s)			
		0.001	lc(mm)	0.01	lc(mm)
Bell et al	$\sqrt{\frac{De.\pi.Dw.vi}{vw}}$	$\sqrt{\frac{36.95x\ x0.04x0.001}{1000\ x\ 1}}$	2155	$\sqrt{\frac{36.95x\ x0.04x0.01}{1000\ x\ 1}}$	6814
Pahlitzsch	$\sqrt{\frac{De.\pi.Dw.vi}{vw}}$	$\sqrt{\frac{36.95x\ x0.04x0.001}{1000\ x\ 1}}$	2155	$\sqrt{\frac{36.95x\ x0.04x0.01}{1000\ x\ 1}}$	6814
Rowe et al	$\frac{lg.vw}{vg} + \sqrt{\frac{De.\pi.Dw.vi}{vw}}$	$\frac{0.002x1}{60} + \sqrt{\frac{36.95x\ x0.04x0.001}{1000\ x\ 1}}$	2188	$\frac{0.002x1}{60} + \sqrt{\frac{36.95x\ x0.04x0.01}{1000\ x\ 1}}$	6847
Peklenik	$\frac{lg.vw}{vg} + \sqrt{\frac{De.\pi.Dw.vi}{vw}}$	$\frac{0.002x1}{60} + \sqrt{\frac{36.95x\ x0.04x0.001}{1000\ x\ 1}}$	2188	$\frac{0.002x1}{60} + \sqrt{\frac{36.95x\ x0.04x0.01}{1000\ x\ 1}}$	6847
Opitz et al	$\frac{lg.vw}{vg} + \sqrt{\frac{De.\pi.Dw.vi}{vw}}$	$\frac{0.002x1}{60} + \sqrt{\frac{36.95x\ x0.04x0.001}{1000\ x\ 1}}$	2188	$\frac{0.002x1}{60} + \sqrt{\frac{36.95x\ x0.04x0.01}{1000\ x\ 1}}$	6847

TABLE 11a

SET DATA SHEET

DATE:- 4/82

EXPERIMENT NUMBER:- CI/6L

EXPERIMENT TYPE:- BATCH/~~INCREMENTAL~~/PLUNGE/~~THROUGH-FEED~~

1	GRINDING WHEEL	2 CONTROL WHEEL	COMMENTS
	∅ X BORE X WIDTH SIZE:- 0.467×0.305×0.2	∅ X BORE X WIDTH SIZE:- 0.286×0125×0.2	GRINDING WHEEL SPEED = 50 m/s q-ratio = 170 INFEED-RATE = VARIOUS
	GRADE:- C46 BBT	GRADE:- A60 OR	
3	COOLANT	TYPE:- PURFISOL AGE:- 3 MONTHS	
	DILUTION:- 80/1	FILTER SYSTEM:- HYDROCYCLONE	
4	WORKPIECE	BORE:- — HARDNESS:- A/R	
	CONDITION:- AS CAST	MATERIAL SPECIFICATION:- CAST IRON	
5	MACHINE SETTINGS	℄ h' = 11 mm	
	ENDSTOP TYPE:- BALL NOZZLE ARRANGEMENT:- MANIFOLD CONTROL TILT:- 0.5° WORKBLADE SIZE:- 20 mm WORKBLADE TYPE:- PLUNGE WORKBLADE ANGLE:- 30°		
6	HYDRAULIC OIL TEMP^{C}:- 27 °C		
7	ROOM TEMP^{e} a) START OF RUN:- b) END OF RUN:-		

Table 11b Sample Computer Input Data Sheet for Cast Iorn

Component Number	1	2	3	4
Calibration Value Trace 1 K1 (N/mm)	18.25	18.25	18.25	18.25
Calibration Value Trace 2 K2 (N/mm)	24.97	27.97	24.97	24.97
Calibration Value Trace 3 K3 (N/mm)	16.64	16.64	16.64	16.64
Control Wheel Diameter (m)	0.286	0.286	0.286	0.286
Grinding Wheel Diameter (m)	0.469	0.469	0.469	0.469
Grinding Wheel Speed (m/s)	50	50	50	50
Trace 1 Deflection (mm)	8	10	13	22.5
Trace 2 Deflection (mm)	4.5	6	8	13
Trace 3 Deflection (mm)	2	2	3	4
Initial Workpiece Diameter (mm)	47.78	47.77	47.79	47.8
Diameter of Workpiece After Grinding (mm)	47.32	47.32	47.32	47.32
Length of Workpiece (mm)	70	70	69	70
Infeed Rate (mm/s)	0.057	0.092	0.139	0.349
Motor Idle Current (Amps)	18	18	18	18
Maximum Grinding Current (Amps)	52	67	79	128
Idle Voltage (Volts)	266	265	265	264
Maximum Grinding Voltage (Volts)	279	281	280	278
Surface Roughness (mm)	0.99	1.2	1.57	2.34
Workpiece Speed (m/s)	0.299	0.299	0.299	0.299

TABLE 13a. Incidence of Violent Vibrations when Grinding En9 Steel**

Grinding Wheel Speed (m/s)	20	30	40		50			60		
q-ratio	14	20	20		30	42	50	40	50	60
Number of Workpiece Waves	20	20	18	20	20	20	20	20	20	16
Integer Values Coincident with Troughs on Stability Chart	20	20	20		20	20	20	20	20	-
Frequency of Workpiece Waves (Hz)	198	204	237	263	224	160	134	210	161	108
Nearest Natural Frequency of the Machine (Hz)	189	189	189	189	189	157	136	189	157	108
Rotational Speed of Grinding Wheel, Ng (rev/sec)	13.2	19.6	26.3		32.8			39.6		
Rotational Speed of Workpiece Nw (rev/sec)	9.88	10.2	13.15		11.2	7.98	6.7	10.5	8.04	6.77
Ng/Nw	1.33	1.92	2		2.93	4.11	4.89	3.77	4.9	5.85

TABLE 13b. Incidence of Violent Vibration when Grinding Cast Iron**

Grinding Wheel Speed (m/s)	30			40			50		60		
q-ratio	20	30	40	30	40	50	40	80	50	70	80
Number of Workpiece Waves	20	16	22	20	16	20	24	26	26	20	22
	22	20	-	24	-	20	26	-	26	-	26
				26	-	-					
Interger Values Coincident with Troughs on Stability Chart	20	-	22	20	-	20	24	26	26	20	22
	22	20	-	24	-	20	26	-	26	-	26
				26	-	-					
Frequency of Workpiece Waves (Hz)	207	111	114	184	111	111	205	111	211	116	112
	228	138	-	221	-	111	222	-	211	-	132
				240	-	-					
Nearest Natural Frequency of the Machine (Hz)	189	108	108	189	108	108	189	108	189	108	108
	189	136	-	189	-	108	189	-	189	-	136
				189	-	-					
Rotational Speed of Grinding Wheel, Ng (rev/sec)	19.6			26.3			32.8		39.6		
Rotational Speed of Workpiece Nw (rev/sec)	10.37	6.92	5.18	9.22	6.93	5.54	8.51	4.28	8.13	5.3	5.08
Ng/Nw	1.89	2.93	3.78	2.85	3.8	4.75	3.83	7.66	4.87	6.83	7.8

TABLE 13c. Incidence of Non-Violent Vibrations when Grinding En9 Steel**

Grinding Wheel Speed (m/s)	30			40				50		
q-ratio	248	292*	409	512	295	541	-	254	375	500
	258	353	445	569	501	613	-	329	402	-
Number of Workpiece Waves	30	22	18	32	32	32	-	56	19	26
	22	26	18	20	17	28	-	40	32	-
Integer Values Coincident with Troughs on Stability Chart	30	22	18	32	32	32	-	-	-	26
	22	26	18	20	-	28	-	-	32	-
~~Frequency of Workpiece Waves (Hz)~~	25	15	9	13	21	16	-	72	17	17
	17	15	8	7	9	12	-	40	26	-
Nearest Natural Frequency of the Machine (Hz)	27	27	27	27	27	27	-	72	27	27
	27	27	27	27	27	27	-	27	27	-
Rotational Speed of Grinding Wheel, Ng (rev/sec)	19.6				26.3			32.8		
Rotational Speed of Workpiece Nw, (rev/sec)	0.81	0.69	0.5	0.4	0.67	0.49	-	1.29	0.88	0.66
	0.78	0.58	0.46	0.36	0.53	0.43	-	1.0	0.81	-
Ng/Nw	24.2	28	39.4	49.4	39.5	54.1	-	25.4	37.4	49.9
	25.1	34	42.8	54.9	50	61.3	-	32.8	40.5	-

**Alternative Main Drive Transmission Fitted.